

The University of Nottingham

UNITED KINGDOM · CHINA · MALAYSIA

Development of bioactive electrospun scaffolds to support granulation tissue formation in non-healing wounds.

A thesis submitted to the University of Nottingham for the degree of

Doctor of Philosophy

Annesi Giacaman

September 2017

Supervisors: Felicity R.A.J. Rose, Cameron Alexander,

David Pritchard.

School of Pharmacy
Nottingham, United Kingdom

Abstract

Wound healing is a complex and coordinated response where the skin repairs itself. It can be divided into four phases: inflammation, proliferation, maturation and remodelling. The prolongation or failure of one of these phases may result in a chronic wound condition due to a healing delay or a non-healing wound. Failure of wound healing is an unsolved and significant public health problem, associated with economic and human costs. However, skin tissue regeneration may provide therapies which enhance wound healing. Despite the fact that a variety of scaffolds have been fabricated for wound healing, an increasingly aging and diabetic (as major risk factor for non-healing wounds) population is now creating a further extensive demand for new regenerative products.

The first body of research examined in the present thesis evaluated the effects of propolis and its compounds, quercetin, rutin, and artepillin C on fibroblast proliferation and migration rates. In order to investigate this, cytotoxicity, membrane disruption, and *in vitro* scratch experiments were conducted. However, findings showed that there is not a compelling argument to pursue the use of propolis and its isolated components related to cell migration and proliferation; as a result, another natural product, *Lucilia sericata* maggot excretion/secretion (*L. sericata* maggot E/S) was investigated.

The second and third bodies of research have involved the development of electrospun polycaprolactone (PCL) scaffolds in the micron scale range (2-14 μm) to allow good fibroblast infiltration. *In vitro* biocompatibility and infiltration behaviour of 3T3 GFP dermal

fibroblasts, as an exemplar cell type on electrospun PCL scaffolds, were investigated. Additionally, synthesis of polycapolactone-poly(ethylene glycol)–block copolymer (PCL-b-PEG) was included in this study, where it was hypothesized that PCL-b-PEG containing scaffolds may enhance degradation, wettability, and cell-compatibility as previous research has reported. Caprolactone-poly(ethylene glycol) block copolymer were blended with commercial caprolactone (PCL-b-PEG/PCL) and electrospun scaffolds were developed and fully characterised. Selected scaffolds (PCL and PCL-b-PEG/PCL with an average fibre diameter of 4 μm) were compared in terms of: i) *in vitro* biocompatibility and cell infiltration, ii) mechanical properties, iii) physiochemical properties, iv) degradation rate, and v) porosity. The generated evidence suggested that PCL-b-PEG/PCL electrospun scaffolds with an average fibre diameter of 4 μm, with a porosity of~70% (mCT), average pore size of 40 μm and a Young's modulus of ~9 MPa possess suitable properties to enhance the fibroblasts' (murine and human) growth. In addition, PCL-b-PEG/PCL scaffolds allowed significantly higher fibroblast migration (60% after 5 days) compared with PCL scaffolds (40%).

The third and fourth bodies of research focused on scaffolds as a platform for *Lucilia sericata* maggot excretion/secretion release as bioactive molecule for wound healing. The protein models (lysozyme and avidin) and the *Lucilia sericata* maggot excretion/secretion were absorbed onto the PCL, H-PCL and PCL-b-PEG/PCL scaffolds with and without cationic polymer poly (trimethylamino) ethyl methacrylate hydrochloride-block-Poly(N-(2-hydroxypropyl)methacrylamide

($PTMAEMA_{33}$-b-$PHPMA_{180}$) modification. The comparison of the release profiles of avidin from PCL, H-PCL and PCL-b-PEG/PCL scaffolds with and without out cationic polymer treatment showed that the release of avidin from cation polymer modified scaffolds, tend to exhibit zero order kinetics and is not time dependent. Meanwhile, scaffolds without cationic treatment showed a greater and prolonged burst release (first 6 h). Also, the release profile of lysozyme (smaller protein than avidin) shows that lysozyme released from PCL, H-PCL and PCL-b-PEG/PCL scaffolds without cationic polymer treatment was lower than the release from non-modified scaffolds. In addition, it was found that the bioactivity of lysozyme was not statistically reduced by the cationic modification of the scaffold surface.

Finally, *L. sericata* maggot E/S was incorporated more efficiently on cationically modified PCL-b-PEG/PCL scaffolds than on scaffolds without cationic polymer. The loading and release of *L. sericata* maggot E/S from electrospun scaffolds has not been reported before. The release profiles of *L. sericata* maggot E/S revealed that the burst release and the cumulative release of *L. sericata* maggot E/S was significantly lower when cationic polymer was incorporated into the scaffolds. After 21 days, cumulative amount of released *L. sericata* maggot E/S was ~14 µg/mL from cationicallly modified scaffolds. No statistical differences were found between materials. In addition, the protease activity of *Lucilia sericata* maggot E/S was preserved when PCL-b-PEG/PCL and cationically modified PCL-b-PEG/PCL scaffolds were used as release platform.

The present research addressed the challenge of generating bioactive electrospun scaffolds for skin wound healing. The approach combined the fabrication of scaffolds that provide a structural stability to cell to grow and facilitate infiltration. Furthermore, the idea that the scaffolds can be used as a release platform for therapeutic molecules from *L. sericata* maggot E/S for skin wound healing was investigated. The evidence presented here supports its novelty as a potential strategy for skin regeneration.

Acknowledgments

The present work has been supported by a grant from 'Comisión Nacional de Investigación Científica y Tecnológica de Chile'. Special thanks to Ioanna Styliari and Vincenzo Taresco for all their support in the synthesis and characterization of PCL-PEG copolymer. To Marta Alvares Paino for her help in the synthesis and characterization of the cationic polymer and much more. I want to extend my gratitude to Elisabetta, Pritesh, Meena, Gizem and Inchira who always offered me their help.

This work was proof reading by Yulia Balogh and Profesor Kanti Bhoola.

I would like to thanks all the technicians and member of staffs in CBS and Boot buildings.

I want to thanks God for giving me this great opportunity. A special thanks to my husband, for all his love and support when everything was hard. I am very happy and proud to be your wife. Thanks to my daughter Sofia and Valentina for be patient and compressive when mum was away. My gratitude is extended to my mum Sylvia who every year spend some time in England caring of my children. To my sister Belen for supporting me financially and spiritually. In general to all my extended family; my dad Eduardo, my sister Nadia and my brother Israel. Thanks to Tim and Jensine kitchen, Clow family, Wise family, Gwen and Millie, thanks for being our family, for trusting us and give more than anyone. You are part of our hearts. To my best friends Gizem, Elisabetta and Marta. You make this journey easier with your

supporting words, your kindness and good friendship, we had a great time together. Thanks are extended to my supervisors Felicity Rose, Cameron Alexander, and David Pritchard for your support and good leading.

Poster presentation relevant to thesis:

- A. Giacaman, V. Taresco, I. Styliari, I. Aldala, D. Pritchard, A. Cameron F.R.A.J. Rose. Tissue Engineering International and Regenerative Medicine Society (TERMIS) - EU Conference. *Electrospun Scaffolds with potential application in skin wound healing and drug delivery*. June 24-28, 2017, Sweden.
- A. Giacaman, D. Pritchard, A. Cameron, F.R.A.J. Rose. International Pharm. Tech. Conference, 2016. Poster presentation and oral presentation in EHDA Network Meeting. *Development of a 3D electrospun scaffold of PCL/ PEG5000-b-PCL to support granulation tissue formation in non-healing skin wound*. November the 4Th, Leicester, UK.
- A. Giacaman, D. Pritchard, A. Cameron, F.R.A.J. Rose. 7th APS International PharmSci Conference, 2016. *Development of a 3D electrospun scaffold of PCL/ PEG5000-b-PCL to support granulation tissue formation in non-healing skin wound*. September 5-7, Glasgow, Scotland.
- A. Giacaman, D. Pritchard, A. Cameron, F.R.A.J. Rose. Electrospinning Principles, Practices and Possibilities, 2015. *Development of a 3D electrospun scaffold of poly(ε-caprolactone) for the treatment of skin wound healing*. London, UK.
- A. Giacaman, D. Pritchard, A. Cameron, F.R.A.J. Rose. TCES (Tissue and Cell Engineering Society annual meeting), 2015. *Biological active compound from Green propolis for wound healing*. July 19-21, Southampton, UK.

List of abbreviations

Abbreviation	Definition
g	Atmospheric gravitational acceleration
rpm	Revolutions per minute
kV	Kilovolts
KDa	kilodalton
Pa	Pascal
Pa s	Pascal-second
A	Ampere
MPa	Mega pascal
3D	Three dimensional
3T3	NIH Swiss mouse embryonic fibroblasts
BJ6	Human dermal fibroblast
GFP	Green fluorescent protein
EGF	Epidermal growth factor
PDGF	Platelet dermal growth factor
TGFβ	Transforming growth factor
TNFα	Tumour necrosis factor alpha
VEGF	Vascular endothelial growth factor
FGF	Fibroblast growth factor
PMN	Polymorphonuclear
ECM	Extracellular matrix
PI	Propidium Iodine
HOE	Hoechst
NHS	National Health Service

FDA	Food and Drug Administration
DMEM	Dulbecco's Minimum Essential Media
HBBS	Hank's Balance Salt Solution
PBS	Phosphate-buffered saline
FCS	Foetal calf serum
DMSO	Dimethyl sulfoxide
PCL	Polycaprolactone
PEG	Polyethylene glycol
HEAMA	Hydroxyethylmethacrylate
PTMAEMA	N-(2-hydroxypropyl) methacrylamide
SD	Standard deviation
SEM	Mean
SEM	Scanning electron microscope
mCT	Micro computed tomography
NMR	Nuclear magnetic resonance
GPC	Gel permeation chromatography
UV	Ultraviolet (light)
w/w	Weight/weight
Đ	Polydispersity
M_n	Number averages molecular weight
Mw	Weigh average molecular weight

Table of contents

Abstract i
Acknowledgments v
List of abbreviations viii
Table of contents x
List of figures xxiii
CHAPTER 1 Introduction 1
1.1 Wound healing phase regulation 1
1.1.1 Haemostasis 3
1.1.2 Inflammation 3
1.1.3 Proliferation 4
1.1.3.i Angiogenesis 5
1.1.3.ii Granulation tissue 5
1.1.4 Remodelling 5
1.2 Impaired healing 6
1.2.1 Impaired wound healing in diabetic foot ulcers (DFUs) 7
1.2.1.i Vascularity 7
1.2.1.ii Neuropathy 8
1.2.1.iii Infections 8
1.2.1.iv Cellular and molecular abnormalities 9
1.3 Impaired wound healing is a significant public health problem 10
1.4 Clinical approaches and technological advances to correct impaired healing 11
1.4.1 Debridement 11
1.4.2 Wound dressings 12
1.4.2.i Modern dressing 12
1.4.2.ii Advanced wound dressing 15
1.4.2.ii.a Skin substitute 15
1.4.2.ii.b Natural and synthetic polymeric dressing 16
1.4.3 Other approaches to reverse wound healing impairment 20
1.4.3.i Growth factors 20
1.4.3.ii Stem cells 20
1.4.3.iii Antimicrobial agents 21
1.4.3.iv Natural products 22
1.5 Aims and Objectives 22
CHAPTER 2 Material and methods 24
2.1 General chemical and reagents 24
2.2 General methods 24
2.2.1 Mammalian cell maintenance 24
2.2.2 Standard curve for NIH-3T3, GFP-3T3 mouse fibroblasts and BJ6 human fibroblasts 25
2.2.3 AlamarBlue® assay 26
2.2.4 Scratch assay-Time-lapse microscopy 27
2.3 Chemical and methodology for chapter 3- searching for therapeutic molecules for enhancing granulation tissue and wound healing 28
2.3.1 Chemical and reagents 29
2.3.1.i Green Propolis 29
2.3.1.i.a Chemical analysis of propolis extract (conducted by the company) 29
2.3.2 Evaluation of propolis and its compounds as a potential candidate for wound healing 30
2.3.2.i Propolis/quercetin/rutin/artepillin C test solutions for cytotoxicity, membrane integrity and scratch assays 30
2.3.2.ii Seeding procedures for cytotoxicity assay, membrane integrity and scratch assays. 31

2.3.2.iii Cytotoxicity assay (24/48 h) of propolis/ quercetin/rutin/artepillin C 31
2.3.2.iv Hoechst (HOE) and Propidium iodide (PI) double staining for 3T3 membrane integrity evaluation 32
2.3.2.v *In vitro* scratch assay–time lapse microscopy.....34
2.4 Chemical and methodology for chapter 4 Development and characterization of Poly (ε-caprolactone) (PCL) and PCL-b-PEG/PCL electrospun scaffolds.....34
2.4.1 Chemical and reagents 34
2.4.2 Synthesis and purification of PCL-b-PEG copolymers 35
2.4.2.i Characterization of PCL-PEG copolymers 36
2.4.2.i.a Nuclear magnetic resonance analysis (^{1}H NMR) 36
2.4.2.i.b Gel permeation chromatography (GPC) 36
2.4.3 Characterization of polymeric solutions 37
2.4.3.i Viscosity.....37
2.4.3.ii Conductivity 37
2.4.4 Electrospinning set up 37
2.4.5 Characterization of the electrospun scaffolds.....39
2.4.5.i Scaffold morphology (SEM), fibre diameter analysis and thickness 39
2.4.5.ii Porosity and pore size 39
2.4.5.iii Water Contact Angle (WCA) measurements.....40
2.4.5.iv Mechanical properties/uniaxial tensile test 41
2.4.5.v *In vitro* degradation studies 42
2.4.6 Biological evaluation of the scaffolds 42
2.4.6.i Scaffold preparation 42
2.4.6.ii Cell viability 43
2.4.6.iii Cell morphology and cell-scaffold interaction analysis ...44
2.4.6.iv Cell infiltration 45
2.5 Chemicals and methodology for chapters 5 and 6-loading and release studies of proteins and *L. sericata* maggot E/S from PCL, H-PCL and PCL-b-PEG/PCL scaffolds (with/without cationic modification) 46
2.5.1 Chemical and reagents 46
2.5.2 Wet chemical surface modification 47
2.5.3 Scaffold materials.....47
2.5.4 Proteins used for adsorption and release studies 48
2.5.5 Protein loading efficiency studies. 49
2.5.6 Quantification of proteins by modified Bradford Assay 50
2.5.7 Quantification of proteins by fluorescence.....51
2.5.8 Release of proteins 52
2.5.9 Relative bioactivity of lysozyme.....52
2.5.10 Relative bioactivity of *L. sericata* maggot E/S.....53
2.5.11 Synthesis of PTMAEMA-b-PHPMA 54
2.5.12 Synthesis of Fluorescein-labelled $PTMAEMA_{33}$-b-$PHPMA_{180}$ copolymer. 57
2.5.12.i Characterization of $PTMAEMA_{33}$-b-$PHPMA_{180}$ copolymers..58
2.5.12.i.a Gel permeation chromatography (GPC) and nuclear magnetic resonance (NMR) analysis of $PTMAEMA_{33}$-b-$PHPMA_{180}$ polymers.....58
2.5.12.i.b Determination of the maximum emission and excitation wavelengths of $PTMAEMA_{33}$-b-$PHPMA_{180}$ 58
2.5.13 Effects of cationic PTMAEMA and $PTMAEMA_{33}$-b-$PHPMA_{180}$ polymers on murine fibroblast metabolic activity. 59
2.5.14 Surface modification of PCL, H-PCL and PCL-b-PEG scaffolds with cationic ($PTMAEMA_{33}$-b-$PHPMA_{180)}$ copolymers. 59

2.5.15 Assessing the influence of *L. sericata* maggot E/S from controlled release scaffolds on fibroblast motility in an *in vitro* scratch assay 60
2.5.16 Statistical analysis 61
CHAPTER 3 Searching for therapeutic molecules for enhancing granulation tissue and wound healing 62
3.1 Naturally-derived molecules that have wound healing properties..62
3.2 Propolis as a wound healing candidate 63
3.2.1 Green propolis and its compounds 66
3.2.2 Biological activities and mechanism of action of propolis.....68
3.2.2.i Antimicrobial activity 68
3.2.2.ii Anticarcinogenic activity.....69
3.2.2.iii Anti-inflammatory activity 70
3.2.2.iv Wound healing.....72
3.2.3 Limitations in the use of propolis 74
3.3 Aims and objectives.....75
3.4 Results and discussion 77
3.4.1.i AlamarBlue® assay of propolis and its compounds (24/48h) using 3T3 culture media (2% *(v/v)* FCS concentration).....77
3.4.2 Membrane integrity assay.....87
3.4.3 Assessment of wound closure following exposure to propolis and its compounds 99
3.5 Conclusions 113
CHAPTER 4 Development and characterization of Poly (ε-caprolactone) (PCL) and PCL-b-PEG/PCL electrospun scaffolds . 114
4.1 Skin tissue engineering 114
4.1.1 Scaffolds and fabrication 115
4.1.1.i Requirement for a functional scaffold 115
4.1.1.ii Electrospinning 116
4.2 Aims and objectives.....121
4.3 Results and discussion 123
4.3.1 Characterization of PCL-b-PEG/PCL polymer (NMR and GPC) 123
4.3.2 Characterization of PCL solution prior electrospinning.....125
4.3.3 Characterization of PCL-b-PEG solutions and its blends with PCL (PCL-b-PEG/PCL) prior to electrospinning 130
4.3.4 Geometrical evaluation of PCL electrospun scaffolds.....134
4.3.4.i Fabrication and morphology analysis (SEM) 134
4.3.5 Biological evaluation of PCL scaffolds 143
4.3.5.i Cell metabolic activity 143
4.3.5.ii Cell morphology and cell-scaffold interactions 146
4.3.5.iii Cell infiltration 149
4.3.6 Geometrical evaluation of PCL-b-PEG and its blends PCL-b-PEG/PCL scaffolds ratios 40:60; 50: 50 and 60:40. 153
4.3.6.i Fabrication and morphology analysis (SEM) 153
4.3.7 Fabrication of electrospun scaffolds based on PCL-b-PEG/ PCL blends at a ratio 40:60 (15 % *w/w*).....155
4.3.8 Biological evaluation of fibrous scaffolds of different fibre diameter fabricated from PCL-b PEG/PCL 40:60 (15% *w/w*) blend..157
4.3.8.i Cellular metabolic activity.....157
4.3.8.ii Cell morphology and cell-scaffold interactions 159
4.3.9 Porosity and thickness evaluation of electrospun scaffolds .162
4.3.9.i Evaluation of PCL electrospun scaffolds porosity 162
4.3.9.ii Evaluation of PCL electrospun scaffolds thickness 165

4.3.9.iii Porosity, pore size and thickness evaluation of the two selected types of scaffolds produced (PCL alone and PCL-b-PEG/PCL 40:60 (15% *w/w*)) 167
4.3.10 Physicochemical evacuation of PCL electrospun scaffolds 170
4.3.10.i Contact angle measurements of PCL electrsopun scaffolds 170
4.3.10.ii Water Contact Angle (WCA) measurements of the two selected types of scaffolds produced (PCL alone and PCL-b-PEG/PCL 40:60 (15% *w/w*)) 173
4.3.11 Mechanical properties evaluation of PCL scaffolds 175
4.3.11.i Mechanical properties of PCL alone and PCL-b-PEG/PCL 40:60 (15% *w/w*) scaffolds 178
4.3.11.ii *In vitro* degradation studies of PCL alone and PCL-b-PEG/ PCL 40:60 (15% *w/w*) scaffolds 181
4.3.11.iii Cell proliferation 3T3 and BJ6 comparison between PCL and PCL-b-PEG/PCL scaffolds 184
4.3.11.iv Cell infiltration 186
Summary table with results 188
4.4 Conclusions 190
CHAPTER 5 Loading and release of model and therapeutic proteins on PCL and PCL-b-PEG/PCL scaffolds 192
5.1 Active wound dressing 192
5.1.1 Requirements of the active dressing 192
5.2 Scaffolds as a platform for protein release 193
5.2.1 The method used for drug-loading onto electrospun scaffolds 193
5.2.2 Mechanism of protein release 194
5.2.3 Factors affecting loading and release of drugs: 194
5.3 *Lucilia sericata* maggot excretion/secretion as therapeutic molecule for wound healing 195
5.3.1 Mechanism of actions of *Lucilia sericata* maggot excretion/secretion. 196
5.4 Aims and objectives: 198
5.5 Results and discussion 200
5.5.1 Wet chemical surface modification prior protein absorption 200
5.5.2 Avidin–fluorescein (AVI-FITC) conjugate loading on PCL and H-PCL and PCL-b-PEG/PCL scaffolds 203
5.5.3 Avidin–fluorescein (AVI-FITC) conjugate release from PCL and H-PCL and PCL-b-PEG/PCL scaffolds 206
5.5.4 Lysozyme–rhodamine B (LYZ-RB) conjugate loading on PCL and H-PCL and PCL-b-PEG/PCL scaffolds 209
5.5.5 Lysozyme-rhodamine B (LYZ-RB) conjugate release from PCL and H-PCL and PCL-b-PEG/PCL scaffolds 214
5.5.6 The bioactivity of lysozyme after release 219
5.5.7 *Lucilia sericata* maggot excretion/secretion loading on PCL and H-PCL and PCL-b-PEG/PCL scaffolds 221
5.5.8 *Lucilia sericata* maggot excretion/secretion release from PCL and H-PCL and PCL-b-PEG/PCL scaffolds 224
5.5.9 Bioactivity of *L. sericata* maggot excretion/secretion, after release 229
5.5.10 Activity of *L. sericata* maggot ES from controlled release scaffolds on fibroblast motility-*in vitro* scratch assay 230
5.6 Conclusions 233

CHAPTER 6 Surface modification of PCL and PCL-b-PEG/PCL with cationic polymers 235
6.1 Cationic polymers 235
6.1.1 Applications of cationic polymers 235
6.1.2 Interaction between cationic polymers and the surface of scaffolds, and between cationic polymers and proteins 236
6.1.3 Incorporation of cationic polymers at scaffolds surfaces 237
6.2 Aim and objectives 238
6.3 Results and Discussion 240
6.3.1 Synthesis of $PTMAEMA_{33}$-b-$PHPMA_{180}$ polymers 240
6.3.1.i Characterizations of $PTMAEMA_{33}$-b-$PHPMA_{180}$ polymers 241
6.3.1.ii Absorbance, emission and excitation spectra of FITC conjugated- $PTMAEMA_{33}$-b-$PHPMA_{180}$ polymer 243
6.3.2 Cytotoxicity of $PTMAEMA_{33}$ and $PTMAEMA_{33}$-b-$PHPMA_{180}$ cationic polymers on murine fibroblasts. 245
6.3.3 Modification of PCL, H-PCL and PCL-b-PEG/PCL surface scaffolds using cationic polymer $PTMAEMA_{33}$-b-$PHPMA_{180}$. 248
6.3.4 Loading of avidin-rhodamine (AVI-RB) on the cationically modified surface of PCL, H-PCL and PCL-b-PEG/PCL scaffolds 251
6.3.5 Avidin (AVI-RB) release from the cationically modified surface of PCL, H-PCL and PCL-b-PEG/PCL scaffolds 254
6.3.6 Loading of Lysozyme-rhodamine B (LYZ-RB) on the cationically modified surface of PCL, H-PCL and PCL-b-PEG/PCL scaffolds 258
6.3.7 Release of Lysozyme-rhodamine B from the cationically modified surface of PCL, H-PCL and PCL-b-PEG/PCL scaffolds 261
6.3.8 The bioactivity of Lysozyme-rhodamine B (LYZ-RB) after its release from the scaffolds 266
6.3.9 The loading of *Lucilia sericata* maggot excretion/secretion on the cationic polymeric modified surface of PCL, H-PCL and PCL-b-PEG/PCL scaffolds 268
6.3.10 The release of *L. sericata* maggot ES from the cationically modified PCL, H-PCL and PCL-b-PEG/PCL scaffolds 270
6.3.11 The activity of *Lucilia sericata* maggot excretion/secretion after release 276
6.4 Conclusions 278
CHAPTER 7 Conclusions and Future work 281
7.1 Future work 288
References 291
Appendix 319

List of figures

Figure 1.1 – The diagram above shows the phases of wound healing..... 2
Figure 1.2 - Schematic approach development of electrospun scaffolds.. .23
Figure 2.1 - Synthesis scheme of PCL-b-PEG copolymer.....35
Figure 2.2 - Synthesis of $PTMAEMA_{33}$-b-$PHPMA_{180}$-.....55
Figure 3.1 – Chemical structure of some green propolis compounds. 67
Figure 3.2 – Schematic of propolis as a wound healing candidate.....76
Figure 3.3 – AlamarBlue® assay after 24 h and after 48 h. The effect of propolis on fibroblast metabolic. 77
Figure 3.4 - AlamarBlue® assay 24 h and after 48 h. The effect of quercetin on fibroblast metabolic activity. 81
Figure 3.5 - AlamarBlue® assay after 24 h and after 48 h. The effect rutin upon fibroblast viability. 83
Figure 3.6 - AlamarBlue® assay after 24 h and after 48 h. The effect artepillin C on fibroblast metabolic activity. 85
Figure 3.7 - Membrane integrity assay. Hoechst /Propidium Iodine double stain. Cell was cultured by 48 h with propolis.. 88
Figure 3.8 - Membrane integrity assay. Hoechst /Propidium Iodine double stain. Cell was cultured by 48 h with quercetin.. 91
Figure 3.9 - Membrane integrity assay. Hoechst /Propidium Iodine double stain. Cell was cultured by 48 h with rutin.....94
Figure 3.10 - Membrane integrity assay. Hoechst /Propidium Iodine double stain. Cell was cultured by 48 h with artepillin C.. 97
Figure 3.11 - Effect of Green propolis on fibroblast migration-*in vitro* scratch assay.. 100
Figure 3.12 - Effect of propolis on fibroblast migration-*in vitro* scratch assay. % of covering scratch.....101
Figure 3.13 - Effect of quercetin on fibroblast migration-*in vitro* scratch assay.. 103
Figure 3.14 - Effect of quercetin on fibroblast migration-*in vitro* scratch assay % of covering scratch.....104
Figure 3.15 - Effect of rutin on fibroblast migration-*in vitro* scratch. 106
Figure 3.16 - Effect of rutin on fibroblast migration-*in vitro* scratch assay. % of covering scratch.....107
Figure 3.17 - Effect of artepillin C on fibroblast migration-*in vitro* scratch assay. 109
Figure 3.18 - Effect of artepillin C on fibroblast migration-*in vitro* scratch assay % of covering scratch.....110
Figure 4.1 Schematic representation of the electrospinning setup.. 117
Figure 4.2 - Representative NMR of PCL-b- PEG polymer after its purification. 124
Figure 4.3- Viscosity curves showing the shear behaviour for different concentrations of Poly(caprolactone) 126
Figure 4.4 - Viscosity curves showing the shear behaviour for the different concentrations and ratios of the mixture PCL and PCL-b-PEG blends.....131
Figure 4.5 - Representative scanning electron micrographs of PCL electrospun microfibres 135
Figure 4.6 - Effect of flow rate on fibre morphology and diameter: scanning electron microscopy of PCL scaffolds 137
Figure 4.7 - Effect of voltage on fibre diameter. Scanning electron microscopy of PCL scaffolds.....139
Figure 4.8 - Effect of PCL solution concentration and solvent on fibre diameter.....141
Figure 4.9 - Fluorescence readings of metabolic activity of 3T3 GFP fibroblasts cultured on PCL scaffolds.....144

Figure 4.10 - Phase contrast and fluorescence merged images of fibroblast 3T3 GFP attached to the different PCL scaffolds.. 147
Figure 4.11 - Confocal images of GFP 3T3 fibroblasts cultured on PCL scaffolds.. 148
Figure 4.12 – Confocal microscope z-stack images of 3T3 GFP fibroblasts seeded onto the PCL microfibrous scaffolds. 151
Figure 4.13 - Confocal microscope z-stack images of 3T3 GFP fibroblasts seeded onto the PCL microfibrous scaffolds. 152
Figure 4.14 – Representative SEM micrographs of PCL-PEG scaffolds and blended PCL-b-PEG/PCL scaffolds.....154
Figure 4.15 - SEM micrographs of PCL-PEG/PCL 40:60 scaffolds 156
Figure 4.16 - 3T3 metabolic activity was assessed using Alamar Blue™. Fluorescence readings of metabolic activity of 3T3 GFP fibroblasts cultured on PCL-b-PEG/PCL 40:60 15% w/w scaffolds.....158
Figure 4.17 -SEM images and phase contrast from 3T3 fibroblast on PCL-b-PEG/PCL scaffolds. 160
Figure 4.18 - Confocal images of PCL-b-PEG/PCL scaffolds with different average of fibre diameters. 161
Figure 4.19 - Porosity of PCL scaffolds.....163
Figure 4.20 - PCL scaffold thickness.. 166
Figure 4.21 - Porosity of PCL and PCL-b-PEG/PCL scaffolds. 167
Figure 4.22 – PCL and PCL-PEG/PCL scaffold thickness.. 169
Figure 4.23 - Advancing and receding water contact angles of PCL electrospun scaffolds. 170
Figure 4.24 - Comparing PCL and PCL-b-PEG/PCL with their respective advancing and static contact angles.. 174
Figure 4.25 - Stress-strain curves of PCL scaffolds with different fibre diameters 176
Figure 4.26 - Stress-strain curves of PCL and PCL-PEG/PCL scaffolds with average fibre diameter ~4 μm.. 179
Figure 4.27 - Degradation rate study of PCL and PCL-b-PEG/PCL scaffolds 182
Figure 4.28 - Alamar Blue™ metabolic activity of 3T3 GFP fibroblasts cultured on PCL and PCL-b-PEG/PCL scaffolds, over 12 days. 185
Figure 4.29 - A) Confocal microscope z-stack images of 3T3 GFP fibroblasts seeded on PCL and PCL-b-PEG/PCL micro fibrous scaffolds. 187
Figure 5.1 - Schematic approach of protein loading on electrospun scaffolds. 199
Figure 5.2 - Representative micrographs of NaOH modified PCL fibre scaffolds 201
Figure 5.3 - Avidin-fluorescein conjugate protein (AVI-FITC) adsorbed onto PCL, H-PCL and PCL-b-PEG/PCL fibre scaffolds.....204
Figure 5.4 - Avidin-fluorescein conjugate protein (AVI-FITC) adsorbed onto PCL and H-PCL fibres scaffolds. 207
Figure 5.5 - Lysozyme-rhodamine B conjugate protein (LYZ-RB) adsorption on PCL and H-PCL fibre scaffolds.....210
Figure 5.6 - Comparison between AVI-FITC and LYZ-RB loading percentages on PCL, H-PCL and PCL-b-PEG/PCL fibrous scaffolds. 212
Figure 5.7 - Lysozyme-rhodamine B conjugate protein (LYZ-RB) adsorbed onto PCL, H-PCL, PCL-b-PEG/PCL fibres scaffolds.. 215
Figure 5.8 - Comparison between AVI-FITC and LYZ-RB release profiles from PCL, H-PCL and PCL-b-PEG/PCL scaffolds. 218
Figure 5.9 - Lysozyme bioactivity following release from the scaffold. ..220
Figure 5.10 - *L. sericata* maggot E/S-NHS rhodamine conjugate protein absorbed onto PCL, H-PCL and PCL-b-PEG/PCL scaffolds. 222

Figure 5.11 - Comparative analysis of *L. sericata* maggot E/S, avidin and lysozyme loading onto PCL, H-PCL and PCL-b-PEG/PCL fibrous scaffolds. 223
Figure 5.12 - *L. sericata* Maggot E/S-rhodamine B conjugate protein absorbed on PCL, H-PCL and PCL-b-PEG/PCL scaffolds.....225
Figure 5.13 – Comparative release profile of avidin, lysozyme and L. sericata maggot E/S from PCL, H-PCL and PCL-b-PEG/PCL scaffolds.....228
Figure 5.14 - Relative *L. sericata* maggot E/S activity. 229
Figure 5.15 - *In vitro* scratch assay to evaluate different fraction of *L. sericata* maggot E/S released from PCL, H-PCL and PCL-b-PEG/PCL scaffolds. 232
Figure 6.1 - Schemetic approach of protein loading 239
Figure 6.3 - NMR of $PTMAEMA_{33}$ –b-$PHPMA_{180.}$ polymer after its purification. $PTMAEMA_{33}$ –b-$PHPMA_{180.}$ ^{1}H NMR.....242
Figure 6.2 - NMR of $PTMAEMA_{33}$ polymer. ^{1}H NMR.....242
Figure 6.4 – A) absorbance spectrum of FITC conjugated $PTMAEMA_{33}$-b-$PHPMA_{180}$ polymer B) Fluorescence emission and excitation spectrum of $PTMAEMA_{33}$-b-$PHPMA_{180}$ polymer. 244
Figure 6.5 - Cytotoxicity of $PTMAEMA_{33}$ and PTMAEMA33-b-PHPMA180 on fibroblast 246
Figure 6.6 - Cationic polymer-fluorescent conjugate protein (PTMAEMA-FITC) absorbed into PCL, H-PCL and PCL-b-PEG/PCL scaffolds.....249
Figure 6.7 - Avidin-rhodamine protein (AVI-RB) absorbed into PCL, H-PCL and PCL-b-PEG/PCL scaffolds. 252
Figure 6.8 - Avidin-rhodamine release profiles from PCL, H-PCL and PCL-b-PEG/PCL scaffolds 255
Figure 6.9 - Comparison between AVI-RB release profile from PCL, H-PCL scaffolds and PCL-b-PEG/PCL with and witout ationic polymer treament. 257
Figure 6.10 - Lysozyme-rhodamine B conjugate protein (LYZ-RB) absorbed on cationically modified PCL, H-PCL and PCL-b-PEG/PCL scaffolds.. 259
Figure 6.11 - Lysozyme-rhodamine release profiles from PCL, H-PCL and PCL-b-PEG/PCL scaffolds.....262
Figure 6.12 - Comparison between LZ-RB release profile from PCL, H-PCL scaffolds and PCL-b-PEG/PCL with and witout ationic polymer treament. 264
Figure 6.13 - Relative lysozyme activity.....266
Figure 6.14 - *L. sericata* maggot E/S-NHS Rho fluorescein conjugate protein absorbed into cationically modified PCL, H-PCL and PCL-b-PEG/PCL scaffolds.. 269
Figure 6.15 - *L. sericata* maggot E/S -rhodamine release profiles from PCL, H-PCL and PCL-b-PEG/PCL scaffolds 271
Figure 6.16 – Comparision of L. sericata maggot E/S-rhodamine release profiles from PCL, H-PCL and PCL-b-PEG/PCL scaffolds with and without cationic polymeric 273
Figure 6.17 - Relative protease activity from *L. sericata* maggot E/S. *L. sericata* maggot E/S release pooled fraction from PCL, H-PCL and PCL-b-PEG/PCL scaffolds with and without cationic treatment. 277

CHAPTER 1 Introduction

1.1 Wound healing phase regulation

In normal skin, the epidermis creates a natural and effective physical barrier against the external environment (Evans et al., 2013). The epidermis is divided into four or five layers (depending on the region of the body) where the stratum corneum is the outermost layer and its main function is to regulate the exchange of substances through the skin (Baroni et al., 2012). The epidermal barrier is semipermeable, and it can be altered by different external and internal stimuli such as: climate, physical stressors, and a number of skin and systemic diseases (Darlenski et al., 2011).

A wound involves the loss of epithelial continuity and integrity. Therefore, it is essential that the homeostasis is re-established to avoid fluid loss and infection (Greaves et al., 2013, Eming et al., 2007). In normal physiological conditions, injury to the skin initiates a complex cascade of biochemical and cellular events with the purpose of re-establishing the integrity of the skin and repairing the injured tissue (Wu et al., 2007).

The wound healing process is a complex and overlapping cascade of events which can be classified into four distinct phases: i) haemostasis, ii) inflammation, iii) proliferation and iv) remodelling (Sonnemann and Bement, 2011). Figure 1.1 shows the main events and key cells involved in each of the four phases.

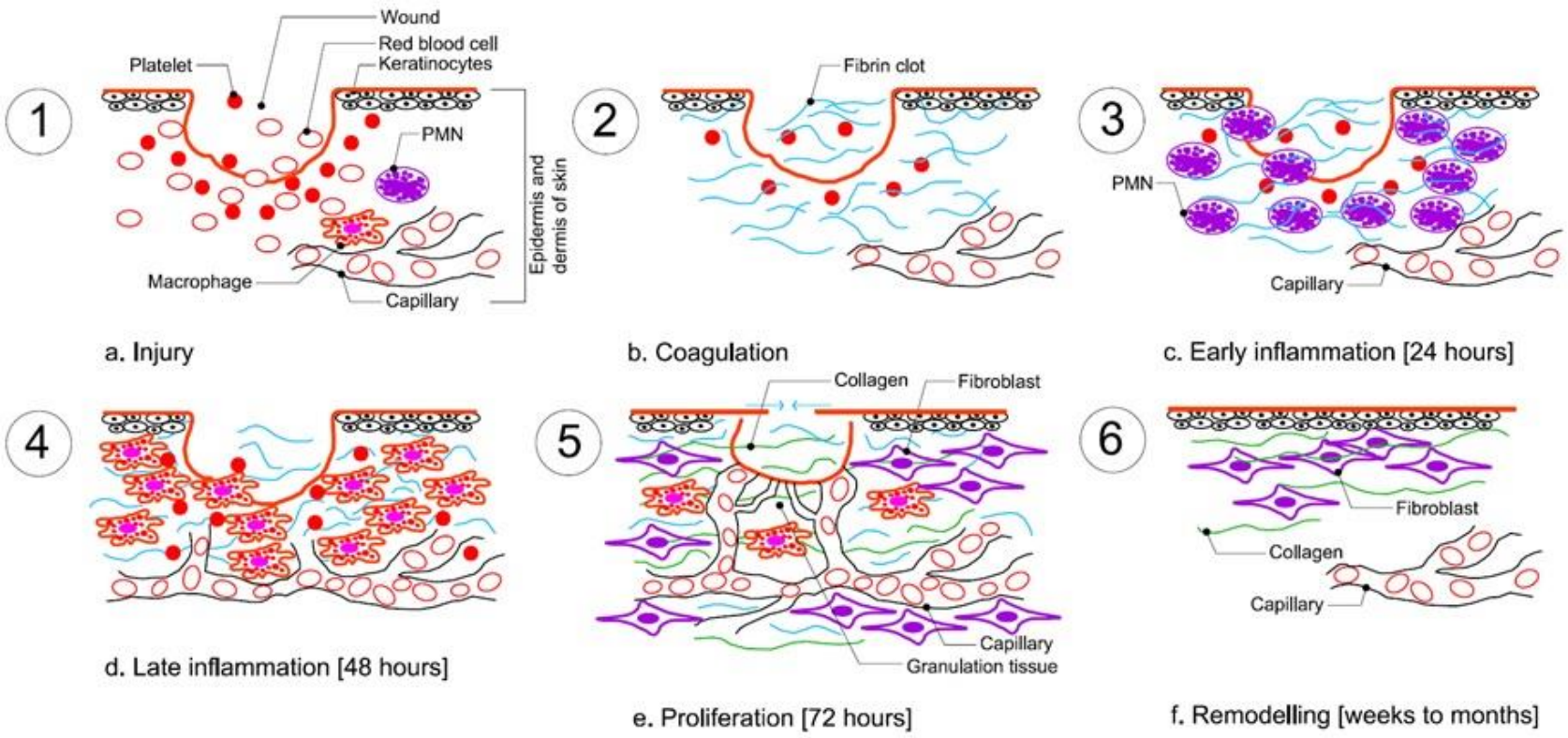


Figure 1.1 – The diagram above shows the phases of wound healing. 1) Wound immediately after injury. Blood vessels are damaged which increase PMNs, neutrophils, and platelet infiltration in the wound side 2) coagulation happens when platelets are aggregated with fibrin forming a fibrin clot 3) platelets begin to release growth factor including PDGF and TGF which attract PMNs to wound area 4) After 48 h PMNs are replaced by macrophages which remove the debris, release growth factors and begin to re-establish the extracellular matrix 5) at 72 h fibroblasts begin to synthesise collagen induced by growth factors 6) Remodelling may take weeks to months. Adapted from (Sonnemann and Bement, 2011).

1.1.1 Haemostasis

The haemostasis phase is the repairing process that is initiated immediately after injury. During this phase there is fibrin clot formation followed by the local release of cytokines and growth factors (Reinke and Sorg, 2012). Coagulation is a very important event in order to maintain haemostasis and wound protection. An injury causes the disruption of blood vessels and subsequently the exposure of subendothelial collagen to platelets. This results in the aggregation and activation of a coagulation cascade. Fibrin, fibronectin, vitronectin, thrombospondin and aggregated platelets combine to form a blood clot. The main functions of a clot are reduction of blood loss, protection of the wound against bacteria, serving as a scaffold for cells, and to acting as a reservoir for growth factors which may be required in the later phases of wound healing (Falanga, 2005, Golebiewska and Poole, 2014).

1.1.2 Inflammation

The inflammatory phase is characterised by an increase of vascular permeability, cellular migration from the circulation to the wound site, and wound debridement (Demidova-Rice et al., 2012b).

The early inflammation stage occurs approximately 24 h after injury. During this time the aggregated platelets in the blood clot begin to release cytokines and growth factors. These include platelet-derived growth factor (PDGF) and transforming growth factor β (TGF-β). The main function of these growth factors is to attract polymorphonuclear

cells (PMNs) to the wound site which release important chemical signals to begin the inflammation phase (Baum and Arpey, 2005). After 48 h, macrophages replace PMNs as the principal inflammatory cell. Macrophages are phagocytic cells whose function is to remove debris from the wound (Sonnemann and Bement, 2011, Harper et al., 2014) and to release growth factors such as PDGF and epidermal growth factor (EGF) for the stimulation of angiogenesis and granulation tissue formation (Harper et al., 2014).

1.1.3 Proliferation

The proliferation phase begins about 72 h after injury is induced (Beanes et al., 2003). In this phase, the essential events are the synthesis of collagen (an important extra cellular matrix (ECM) protein), angiogenesis, proliferation and migration of fibroblasts, endothelial cells and keratinocytes (Falanga, 2005). The release of several cytokines and growth factors such as, PDGF, TGF-β and connective tissue growth factor (CTGF) stimulates the migration of fibroblasts (Delavary et al., 2011). The main role of fibroblasts is the production of permanent ECM and growth factors. Fibroblasts produce collagen and proteoglycans; they also release growth factors such as the platelet-derived growth factor (PDGF) and vascular endothelial growth factor (VEGF) which enhance granulation tissue formation and reepithelization during the proliferative phase (Demidova-Rice et al., 2012b).

1.1.3.i Angiogenesis

In addition, endothelial cells proliferate and start to form new capillaries, a process known as angiogenesis (Caiado et al., 2011). Angiogenesis re-establishes the supply of oxygen and nutrients in an effective way to achieve wound closure. It is regulated by several cytokines and growth factors (Bauer et al., 2005), such as vascular endothelial growth factor (VEGF), fibroblast growth factor (FGF), angiopoietin and TGF-β (Greaves et al., 2013).

1.1.3.ii Granulation tissue

By this time, the morphology of the wound has changed. This is attributed to the replacement of the provisional ECM by granulation tissue. The formation of granulation tissue is clinical evidence of wound closure (Iizaka et al., 2011). Granulation tissue is bright red and granular in appearance due to the invasion of capillaries. The cellular components of this tissue are: fibroblasts, blood cells and macrophages, which produce a significant amount of growth factors and cytokines (Barrientos et al., 2014, Behm et al., 2012).

Keratinocytes cross the granulation tissue from opposite sides of the wound in order to re-establish contact. This process is known as contact guidance and it is part of the re-epithelialisation process (Kroeze et al., 2011).

1.1.4 Remodelling

This phase is characterized by the deposition of connective tissue, scar formation and wound contraction. This process could be

completed weeks to months after the initial injury has occurred depending of the wound type and its size (Schreml et al., 2010). The wound appearance changes over time. It has been observed that the wound begins to strengthen as its thickness decreases. This is as a result of the increase in the proportion of collagen type I while collagen type III, proteoglycans, and water content decrease during the remodelling process (Baum and Arpey, 2005). Even if the collagen synthesis slows down after about three weeks, the reorganization can continue for months after injury (Reinke and Sorg, 2012).

The wound starts to contract approximately 7 days after injury. Important cells in this process include myofibroblasts, whose cytoskeletal structures are different to resting/quiescent fibroblasts because they contain α-smooth muscle actin. It is known that myofibroblasts have an important role in the wound contraction phase because they synthesize ECM components such as collagen type I and III, playing a mechanical function. When re-epithelization is finished, myofibroblasts disappear (Baum and Arpey, 2005, Sonnemann and Bement, 2011).

1.2 Impaired healing

There are two contrasting clinical problems associated with the failure of wound healing. The first one is called excessive healing, which is characterized by the excessive deposition of connective tissue. It may lead to a pathological condition called fibrosis (i.e. keloids and hypertrophic scar formation) (Grieb et al., 2011). The second one is

characterized by a lack of connective tissue deposition which may lead to a chronic condition (i.e. diabetic foot ulcer) (Diegelmann and Evans, 2004).

The prolongation or failure of one of the previously described phases may result in a delay in healing or a non-healing wound (Wu et al., 2007), leading to a chronic wound condition. Chronic wounds are those that, under standard medical treatment, do not heal completely after 30 days. Additionally, it is also common to find periods of healing which are interrupted by stationary phases in which the wound does not improve (Moroz and Deffune, 2013).

Local factors such as foreign bodies, infections, venous sufficiency and oxygenation may affect wound healing. Systemic factors such as advanced age, gender, malnutrition, disease (e.i diabetes), smoking and medication may also alter the normal healing process (Guo and DiPietro, 2010a).

1.2.1 Impaired wound healing in diabetic foot ulcers (DFUs)

The combination of both, local and systemic factors are the cause of impaired healing in diabetic ulcers. They include neuropathy, vascular deficiency, infections, cell and molecular abnormalities (Falanga, 2005, Berlanga-Acosta et al., 2012).

1.2.1.i Vascularity

Diabetic patients frequently suffer from macrovascular and microvascular deficiencies which are characterized by the reduction

in the size of small-blood vessels, and the thickening of their basal membrane (Hile and Veves, 2005). As a result, leucocyte migration is reduced contributing to increased risk of infection. Moreover, the blood flow is maldistributed causing prolonged hypoxia (oxygen deprivation). A sustained hypoxia can induce apoptosis, cell arrest, and oxidative stress. The hypoxia mechanism alters the redox stage of complex I, II and III of the electron transport chain generating reactive oxygen species (ROS). (Demidova-Rice et al., 2012b, Demidova-Rice et al., 2012a, Tafani et al., 2016).

1.2.1.ii Neuropathy

Neuropathy problems are closely linked with vascularity deficiency. Blood flow reduction results in morphological and physiological changes of nerves (Tecilazich et al., 2012); sensory, motor and autonomic nerve fibres become defective. Under this sensory deficit, diabetic patients frequently tend to develop ulcers caused by trauma and pressure (Tesfaye and Selvarajah, 2012).

1.2.1.iii Infections

Infections are severe complications to wound healing, which may lead to amputations and morbidity in diabetic patients (Tiwari et al., 2014). The most common complication caused by the infection of a diabetic foot ulcer is osteomyelitis. The figures indicate that between 44-68% of patients admitted to hospital with infected diabetic ulcers have osteomyelitis, increasing the risk of amputation threefold (La Fontaine et al., 2014).

Wound infections have been related to an overproduction of interleukin-8 (IL-8) and other inflammatory cytokines that inhibit keratinocyte proliferation (Kraft et al., 2014). Moreover, colonization by bacteria can lead to a disastrous and persistent inflammatory response, forming a fragile granulation tissue and damage of the extra cellular matrix (ECM) which finally retards the wound healing process (Kraft et al., 2014, Liao et al., 2009).

1.2.1.iv Cellular and molecular abnormalities

There are hundreds of physiological factors that contribute to the impaired wound healing capacity of diabetic ulcers (Brem and Tomic-Canic, 2007). In general, isolated fibroblasts from diabetic ulcers have shown deficiency in growth factor release and a poor proliferative response (Falanga, 2005). Biopsies from the non-healing edge of diabetic ulcers revealed overexpression of c-myc and β-catenin, two biomarkers indicating impaired wound healing. It has been reported that these biomarkers were associated with the inhibition of keratinocyte migration and the alteration of their differentiation (Liao et al., 2009).

In addition, the increase of protease expression and high levels of reactive oxygen species (ROS), pro-inflammatory cytokines and metalloproteases (MMPs) cause damage of ECM proteins (Eming et al., 2007). All these disordered events contribute to ECM degradation which leads to re-epithelization delay, angiogenesis, and neovascularization impairment (McLennan et al., 2006, Greaves et al., 2013).

1.3 Impaired wound healing is a significant public health problem

Wound healing failures remain as an unsolved and significant public health problem worldwide due to the associated economic and human costs (Driver et al., 2010, Andrews et al., 2015). The National Health Service (NHS) in the United Kingdom spent in 2010-2011 an estimated £639 million–£662 million on the treatment of chronic diabetic foot ulceration in England (Kerr, 2012).

Dressings, community nurse visits, and hospitalization contribute to the cost of wound care (Kerr, 2012). The estimated cost of dressing between 2010 and 2011 was £185 and the cost of healthcare professionals was £525 over a 24-week period (Jeffcoate et al., 2009). The total expenditure in admitted patients with foot ulceration which include minor and major amputation was estimated at £257 million in 2010-11. Any delay or prolongation in the normal tissue response to injury has a significant impact in length of hospital stay increasing the cost (Posnett et al., 2009).

Not least important is the human cost for patients with chronic wounds. The costs have been quantified in pain, distress, anxiety, and complication associated with prolonged hospital stays, chronic morbidity or death. All of them have an important negative impact in the quality of life of the patients and their families (Kerr, 2012).

1.4 Clinical approaches and technological advances to correct impaired healing

Effective wound management must evaluate the desirable function and the clinical significance of the dressing or clinical procedure in order to achieve successful wound healing in a reasonable time (Boateng et al., 2008, Andrews et al., 2015). The following sections describe the wound management which consider: debridement, alternatives of dressing for moisture balance and control of infection.

1.4.1 Debridement

Debridement is the removal of devitalized tissue and pathogens from the area surrounding the wound (Sohrabi and Russell, 2014). Naturally, debridement is conducted via autolytic processes, where macrophages and endogenous proteolytic enzymes play an important role (Gray et al., 2011). In chronic wounds the lack of natural debridement causes the formation of necrotic tissue which covers the wound. This increases the length of the inflammatory phase and risk of infection leading to impaired wound healing (Brem and Tomic-Canic, 2007). Clinicians use different types of debridement which include: surgical removal, wound irrigation, enzymatic biological therapies, and rehydration by changing dressings (Boateng et al., 2008). Surgical removal uses a scalpel, scissors and sometimes local anaesthesia (Sohrabi and Russell, 2014). Wound irrigation delivers fluid (saline or antiseptic solution) via a nozzle under sufficient pressure to remove necrotic tissue (Leaper, 2011). Some enzymes

available for debridement are bacterial collagenase, papain (from papaya fruit), DNAse and fibrinolysin which are applied to the wound bed and combine with the enzymes in the body removing devitalized tissue (Vijaykumar et al., 2011). In addition, *Lucilia sericata* maggot is an organism which is applied directly to the wound; secreted enzymes and subsequent action by the maggots debrides and promotes wound healing (Telford et al., 2011, Horobin et al., 2005).

1.4.2 Wound dressings

Dressings have been classified over the years according to their functions (debridement, occlusive, absorbent, antimicrobial) or the type of material used to produce those (Table 1.1)(Moura et al., 2011, Boateng et al., 2008).

1.4.2.i Modern dressing

Modern dressings have been developed to improve the clinical outcome achieved compared to traditional ones (Boateng et al., 2008) such as cotton wool, gauzes and tulles (Jones, 2005). These have been replaced by modern dressing due to the discovery of more cost effective alternatives (Schmitz et al., 2014). Depending on the kind of wound, clinicians evaluate the appropriate dressing to be used in order to maintain optimum conditions for wound healing. They include hydrogels, hydrocolloids, foams, and calcium alginates amongst others (Abdelrahman and Newton, 2011). Nevertheless, there are certain concerns that some types of dressing may promote microbial proliferation (Skórkowska-Telichowska et al., 2013).

Table 1.1 - Examples of the most common wound dressings used to treat chronic wounds. Extract from (Abdelrahman and Newton, 2011).

Type of dressing	Commercial examples	Indications	Advantages	Disadvantages
Hydrocolloids (occlusive or semi-occlusive)	Cutinova® Thin (Beiersdorf-Jobst), DuoDerm® CGF (ConvaTec), RepliCare® (Smith & Nephew, Inc.), Restore® Wound Care Dressing (Hollister)	Wounds with light to moderate exudate i.e pressure ulcers and venous ulcers	No pain on removal Absorbent	Fluid trapping increases the risk of infection Malodours
Alginates (hydrophilic)	Algisite® (Smith & Nephew), Kaltostat® (ConvaTec), Tegagen® HG or HI (3M Health Care), Comfeel SeaSorb® (Coloplast AS), AlgiDERM (Bard),	For diabetic ulcers with moderate to heavy exudate	Non-toxic Highly absorbent Non-traumatic removal Preserve granulation tissue Painless Biodegradable	Could delay the wound healing process by over-dehydration
Hydrogels (non-occlusive)	Granugel® (ConvaTec), Intrasite Gel (Smith & Nephew) Purilon Gel® (Coloplast) Aquaflo™ (Covidien)	For chronic wounds with light to moderate exudate Non-infected wounds	Improves re-epithelization	Overhydrates Skin maceration Bacterial proliferation

Semi-permeable film	Tegaderm film®(3M), Mepitel film® (Molnlycke) Oposite flexigrid (smith and nephew)	Non-infected wounds Non-deep or cavity wound Minimal exudate	Transparent Easy to check wound	Fluid trapping Limited ability to absorb Skin maceration Bacterial proliferation
Foam	Aquacel® foam (Covantec), Mepilex® Lite (Molnlycke), kendall ™foam.	Non-dry scars Non-cavity wounds For pressure ulcers	Prevents bacterial infections and loss of fluid Highly absorbent	Malodour

1.4.2.ii Advanced wound dressing

Recent advances in wound healing technologies have been used to develop more effective wound healing treatments (La Fontaine et al., 2014). These include a skin substitute, and natural and synthetic polymer–based dressings (Moura et al., 2013, Andrews et al., 2015).

1.4.2.ii.a Skin substitute

Skin substitutes have been created to accelerate wound healing. They include artificial epidermal, dermal, and composite layers of skin. Two types of matrix have been used: acellular matrices (i.e. Integra™) and cell-based matrices (i.e Apligraft™). The matrices used are made of collagen and glycosaminoglycans (Boateng et al., 2008). Although a large number of approaches have been tried to make an adequate skin substitute, many of these have led to graft rejection caused by the immune reaction of the patient, antigenicity, and pathogen transfer from cell or animal proteins (Alrubaiy and Al-Rubaiy, 2009). Also, the high production costs associated with the use of artificial skin grafts are considered a drawback in their clinical adoption. Although nowadays there are around two dozen skin substitutes in the USA and European markets (only Dermagraft® in UK), the availability and patient access is not extensively offered in hospitals for all the reasons pointed out before (Metcalfe and Ferguson, 2007, Nyame et al., 2014).

1.4.2.ii.b Natural and synthetic polymeric dressing

Different synthetic and natural-based polymeric dressings for wound healing treatment have been developed more recently. Some of them have been tested in animal models and others in humans (Moura et al., 2011). Table 1.2 shows some examples of natural / synthetic polymers, bioactive substances, and the main results of the most recent studies within which they have been used (Moura et al., 2013).

- **Natural polymers**

These are obtained from sources such as polysaccharides or proteins. They can include chitosan and its derivatives, alginate, silk, hyaluronic acid, collagen and fibrin (Moura et al., 2013). These materials have the advantage of being biodegradable and a biomimetic of ECM. In biological terms, these polymers have the ability to interact with cells and support their proliferation, differentiation, survival and cell migration (Malafaya et al., 2007, Sell et al., 2010). Only alginate has been reported to have an inconsistent biocompatibility which is dependent on its viscosity and hence the mannuronate/guluronate content (Tam et al., 2011).

In spite of the advantages pointed out, biological variation from plant or animal sources could be difficult to standardize between different batches which may limit their application. Moreover, polymers such as collagen, which are isolated from xenogeneic tissue, have the risk of transmitting pathogens to the donor. Even if the recombinant human collagen eliminates the risk of the immunogenic response and the risks of potential pathogen contamination, this technology presents a high cost (Malafaya et al., 2007).

- **Synthetic polymers**

Synthetic polymers are fabricated through chemical processes which lead to a wide variety of structural and functional materials. Examples of the main synthetic polymers used in wound healing applications include poly (vinyl alcohol) (PVA), poly (ethylene glycol) (PEG), polyurethanes (PU), poly (vinyl pyrrolidone) (PVP) and polyesters. An important advantage of using synthetic polymers is that the risk of transmitting infections is greatly reduced in comparison to the use of some natural polymers. In addition, synthetic polymers can be tuned to enhance specific properties such as mechanical strength, shape and biodegradation rate. Comparatively, synthetic polymers are often cheaper than natural polymers because they can be produced in large-scales and with minimal post-synthetic processing (Armentano et al., 2010). Synthetic biomaterials such as polyglycolic acid and polyester derivatives are hydrolytically degradable (Baldwin and Kiick, 2010). However, there can also be problems with certain synthetic polymers due to poor cell-recognition motifs and high overall hydrophobicity of their surfaces which can denature proteins. Nevertheless, poly(lactic acid) (PLA) and poly(glycolic acid) (PGA) have been reported to be biocompatible and have the approval for the US Food and Drug Administration (FDA) for clinical use (Armentano et al., 2010). A lot of research is now focused on the synthesis of more clinically relevant biocompatible polymers (Baldwin and Kiick, 2010).

Table 1.2 - Examples of polymers uses for wound healing treatment.

Polymers	Bioactive substances incorporated	Model	Results	References
Natural				
Chitosan	Acetyglucosamine oligomers	Human diabetic	Reduction of wound size and the enhancing of reepithelization	(Ben-Shalom et al., 2012)
	Neurotensin	Diabetic mice	Increase in fibroblast migration and collagen production. Improved wound healing. Reduces inflammatory infiltrated	(Moura et al., 2014)
Cellulose	Silver nanoparticles	*In-vitro* assay	Activity against *Escherichia coli*, *Staphylococcus aureus* and *Pseudomona aeruginosa*.	(Wu et al., 2014)
	Polyhexamethylase biguanide (PHMB)	Human with chronic wound	Inhibits bacteria proliferation. Reduces necrosis and improves wound healing	(Serafica et al., 2010)
Collagen	----	Human patient with DFUs	Stimulates granulation tissue formation	(Iorio et al., 2011)
	Propolis	Dermal burn rodent	Improved cicatrisation	(de Almeida et al., 2013)

Hyaluronic acid	Arginine and EGF (epidermal growth factor)	Rats	Reduction of wound size. Enhances reepithelization and induces early inflammation.	(Matsumoto and Kuroyanagi, 2010)
Silk	*Aloe vera* extract	Diabetic rat	Enhances wound healing	(Inpanya et al., 2012)
Synthetic				
PVA (poly (vinyl alcohol))	Neomycin	Rats	Antibacterial activity against Gram + and Gram – bacteria	(Nitanan et al., 2013)
PEG (poly (ethylene glycol)	Growth factors	Rats	Enhanced collagen deposition and exhibit a shorter healing time compared with the control	(Huang et al., 2011, Armentano et al., 2010)
PVP (poly (vinyl pyrrolidone))	Oxide nitric (NO)	Diabetic rat	Improved wound healing by promoting epithelization	(Matsumoto and Kuroyanagi, 2010)
PU (Polyurethanes)	Propolis	*In vitro*	Enhanced relative metabolic activity (%) and antibacterial capacity	(Kim et al., 2014a)
Polyesters (i.e poly(lactic acid) (PLA), poly(glycolic acid) (PGA), poly(ε-caprolactone PCL)	Curcumin Growth factor	Diabetic mice Diabetic mice	Improved wound healing rate Enhanced reepithelization and fibroblast proliferation. Improved rate of wound closure	(Merrell et al., 2009) (Chu et al., 2010)

1.4.3 Other approaches to reverse wound healing impairment

Alternative approaches for the treatment of chronic wounds include the use of bioactive substances (La Fontaine et al., 2014) such as antimicrobial agents, growth factors, stem cells, gene therapy and natural products, as summarised below (Moura et al., 2011).

1.4.3.i Growth factors

Recombinant human platelet-derived growth factor (rhPDGF-BB or becaplermin) and epidermal growth factor (EGF) have shown promise in aiding wound healing by improving wound closure by accelerating reepithelialisation of venous ulcers and diabetic foot ulcers (Gowda et al., 2013). However, it is difficult to use growth factors as therapeutics due to their instability *in vivo* (they are rapidly degraded by various proteases found in the body) and their high costs (Chen et al., 2010). Moreover, the majority of clinical trials have been poorly effective when the using soluble growth factors alone. However, beneficial therapeutic effects of growth factors have been reported when delivery platforms helping to control their release and prevent their degradation have been used (Lee et al., 2011).

1.4.3.ii Stem cells

Mesenchymal stem cells and adipose-derived stem cells have shown therapeutic potential in improving wound healing by promoting wound closure and stimulating the production of matrix compounds (Amos et al., 2010, Lin et al., 2013). Mesenchymal stem cells have been

transdifferentiated into endothelial cells and keratinocytes *in vitro* under defined conditions and adipose-derived stem cells have shown differentiated *in situ* into endothelial cells that promote angiogenesis (Lin et al., 2013, Jackson et al., 2012). This technology represents a real advancement in the field of wound healing. Despite this, it has yet to be scaled up in industry due to the cost associated, the time required, the risk of contamination and the lack of knowledge of the precise mechanisms involved in how MSCs improves wound healing. In fact, it remains unknown how MSCs respond *in vivo*, how the target cells are affected and how the microenvironments, such as ischemia and oxidative stress, may alter the MSCs phenotype. These are some of the limitations of this therapy (Yolanda et al., 2014, Hocking and Gibran, 2010).

1.4.3.iii Antimicrobial agents

Infection is one of the most common reasons for impaired wound healing (section 1.2.1 iii). In order to reduce or combat the risk of infection, some antimicrobial agents have been incorporated into dressings (Tanaka et al., 2005, Oliveira et al., 2016). These include silver and antibiotics such as tetracycline, gentamicin, and ofloxacin. Although these agents protect against infection, silver dressings have been reported to cause a cytotoxic effect on fibroblasts and keratinocytes (Cho Lee et al., 2005, Fong and Wood, 2006). In addition, samples from chronic wounds showed bacterial resistance to antibiotics (Ng, 2010).

1.4.3.iv Natural products

Some investigations have considered natural products as bioactive substances to promote wound healing. There has been considerable amount of research into *Calendula officinalis* (Duran et al., 2004, Parente et al., 2012), *Aloe vera* (Somboonwong et al., 2000), green tea extracts (QIN et al., 2010), maggot secretions (Horobin et al., 2005, Smith et al., 2006, Britland et al., 2011) and honey (Molan, 2006, Sarhan and Azzazy, 2017). However, as previously pointed out, the use of natural sources has the limitation of batch-batch variation in the sample collection, production and processing (Yun et al., 2012).

1.5 Aims and Objectives

Several technical advances have been developed in order to improve the management of wound healing and subsequent clinical outcome. However, there is still a need to consider new candidates to reduce infection, enhance the presence of granulation tissue, eliminate disease transfer, and reduce cytotoxicity towards the newly formed and previously existing tissue. On the basis of the observations and background already presented above it is hypothesized that a 3D electrospun scaffold loaded with therapeutic biomolecules have a beneficial effect on granular tissue formation by i) providing a structural support for fibroblasts to grow ii) allowing fibroblast infiltration and iii) as a platform for the release of therapeutic molecules.

The main aims of this work were (Figure 1.2):

- To create bioactive electrospun scaffolds with suitable properties to support fibroblasts' growth and infiltration.
- Evaluate bioactive molecules and investigate their therapeutic action for application in wound healing.
- Asses the loading and release profiles of therapeutic molecules from electrospun scaffolds for wound healing.

This investigation aims to develop an electrospun scaffold that allows dermal fibroblast proliferation and infiltration. Despite the fact that a variety of scaffolds have been fabricated for wound healing, the demand for skin regeneration strategies persist (Chong et al., 2007a, Andrews et al., 2015). The proposal of this research combined the idea of the fabrication of scaffolds that provide a structural stability to cell-growth and migration. As a result, the appropriate scaffold will be taken forward for further studies related to the absorption of therapeutic biomolecules and their release to enhance tissue granulation. For this reason, it is believed that the proposal is novel and provides a strategy to better support skin wound healing.

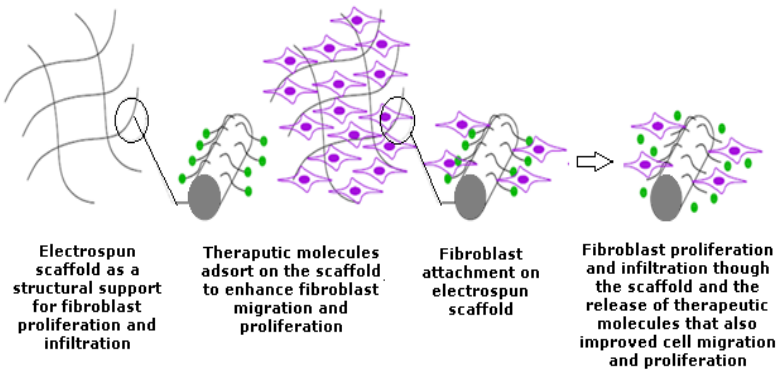


Figure 1.2 - Schematic approach. Electrospun scaffolds will be developed with suitable properties to allow cell proliferation and infiltration. Though post modification, therapeutic molecules will be adsorbed that may potentially enhance wound healing, using the scaffold as well as platform for biomolecules release.

CHAPTER 2 Material and methods

2.1 General chemical and reagents

AlamarBlue® reagent (Life technologies, Fisher scientific). Hank's balanced salt solutions (HBSS) 1X with calcium and magnesium without phenol red (Thermo Scientific Hyclone, Fisher Scientific). Dulbecco's Modified Eagle Media (Gibco) (Invitrogen™ LTD), Phosphate buffered saline (PBS) (Fisher scientific). The following were obtained from Sigma Aldrich: Foetal calf serum (FCS), Antibiotic/antimycotic solution (10,000 units/ml penicillin G, 10 mg/ml streptomycin sulphate and 25 µg/ml amphotericin), Trypsin, Dimethyl sulfoxide (DMSO) (Scientific laboratory), paraformaldehyde, fluoromount™ aqueous mounting media, ethanol denaturized.

2.2 General methods

2.2.1 Mammalian cell maintenance

NIH 3T3, GFP-3T3 mouse embryo fibroblast cells and BJ6 foreskin human fibroblast cells were provided by Dr. James Dixon (University of Nottingham) and were previously purchased from ECACC. Cell procedures were carried out in aseptic conditions. Fibroblasts were cultured in DMEM supplemented with foetal calf serum (FCS) 10% (*v/v*) which was named as 'fibroblast culture media'. Alternatively, culture media were prepared by reducing foetal calf serum (FCS) to 5% (*v/v*) and 2% (*v/v*). They were called '5%-starvation culture

media' and '2%-starvation culture media' respectively. Cells were maintained at 37°C, 5% CO_2 in air at 95% relative humidity (RH). Cells were expanded in tissue culture flasks (T75, Costar Corning). When they reached 80-90% confluency the media was removed, and the cells were trypsinized with 3 mL trypsin-EDTA solution. The trypsinization reaction was quenched by adding 7 mL of 'fibroblast culture media'. The cells were then collected and centrifuged at 200 x g for 5 min at 25°C.

Cell counts were conducted in a Neubauer improved haemocytometer. Subsequently, cells were seeded in 24 well cell culture plates with the number of cells varying with each experiment performed.

Alternatively, cell stocks were stored by preserving them in 10% (*v/v*) dimethyl sulfoxide (DMSO) in 90% (*v/v*) FCS and frozen for 24 h at-80°C. Vials were then transferred into liquid nitrogen for long term storage.

2.2.2 Standard curve for NIH-3T3, GFP-3T3 mouse fibroblasts and BJ6 human fibroblasts

Serial dilutions of NIH-3T3, GFP-3T3 and Bj6 fibroblasts were prepared using 'fibroblast culture media' and an initial cell stock solution of $2x10^6$ cell/mL. Aliquots (500 µL) of each serial dilution were transferred to each well of a 24 well tissue culture plates in triplicate. Cells were incubated for a period of 3 h (to allow cell attachment), with an AlamarBlue® assay performed to determine relative fluorescence units at the individual cell numbers. Standard

curves were generated for each experiment. Statistical regression analyses were performed.

2.2.3 AlamarBlue® assay

The AlamarBlue® assay is based on cell growth and cellular metabolic activity. AlamarBlue® is comprised of resazurin (7-Hydroxy-3H-phenoxazin-3-one 10-oxide), a non-fluorescence blue dye which is reduced in the mitochondria by metabolically active cells to resorufin, ultimately fluorescing which can be detected in the red channel (Rampersad, 2012). Metabolic activity of cells is often well correlated with the number of cells and their proliferation rate (Kühn et al., 2013).

In order to perform the AlamarBlue® assay, each well was washed three times with HBSS (without phenol red) to remove any remaining culture media. AlamarBlue® assay was carried out by adding 1 mL of filtrated (0.22 µm Millipore filter) AlamarBlue® solution 10% (*v/v*) (diluted in HBSS without phenol red) into each well and incubated for 90 min at 37°C. Aliquots (200 µL) from the samples were then transferred into a 96 well non-tissue culture treated plate and relative fluorescence units measured in a plate reader (Tecan Infinite M200, Reading), set at an excitation wavelength range of 530-560 nm and emission at 590 nm.

Observed relative fluorescence units were plotted as relative metabolic activity which was calculated as the ratio of the relative fluorescence units reading of the treatment (T) to the relative fluorescence units mean of its control (C). The ratio was calculated

after subtracting the relative fluorescence units (base line) before propolis treatment.

$$Relative\ metabolic\ activity(\%) = \frac{Relative\ fluorescence\ units\ (T)}{Relative\ fluorescence\ units\ (C)}\ x\ 100$$

2.2.4 Scratch assay-Time-lapse microscopy

A scratch assay is the most common approaches for evaluating collective cell migration due to its simplicity in allowing visualization of cell migration (Kramer et al., 2013). These assays were performed with the aim of determining the effects of a bioactive molecule upon NIH-3T3 fibroblasts migration. This method involved the creation of a scratch in a cell monolayer (confluent culture) and monitoring cell migration regularly at fixed periods of time or until the scratch closes (Liang et al., 2007).

An *in vitro* scratch assay was performed by using a stock cell concentration of 300,000 cells/mL; aliquots (500 µL) were transferred to each well of a 24 well tissue culture plates (150,000 cells in each well). One mL of 'fibroblast culture media' was added to the cells and incubated at 37ºC, 5% CO_2 in air, 95% relative humidity (RH) for 24 h. 'Fibroblast culture media' was replaced by '5%-starvation culture media'. Cells were incubated for an additional 24 h until confluence. The media was then removed, and wells were washed twice with PBS. A scratch in the cell monolayer was created with a p10 pipette tip with any debris removed with PBS.

A volume of 1 mL of test and control (C) solutions were transferred into each well and the cell migration rate was measured over 72 h.

After the scratches were done, the well plate was sealed with laboratory film and a needle was inserted between the bottom and the lid of the well plate. The needle was connected to a plastic hose, which lead to a cylinder with a mix of 5% CO_2 and 10% oxygen/nitrogen.

An inverted LEICA DMRBE microscope with an integrated automated camera and self-contained, incubator/control chamber was used. The temperature was set at 37°C. The camera was set to capture bright field images at 3 points per hours. The objective len was set at a magnification of 10x. The avi video format was converted to JPEG images using Free video to JPG convert software (DVDVideoSoft). An analysis of the % area coverage was done using the same procedure as described above. The images were processed using ImageJ software 1.48 v (National Institutes of Health). The results were plotted by using the following equation:

$$\% \text{ covering scratch} = 100\text{-}\left(\frac{Af}{Ai} x 100\right)$$

Where Af is final area and Ai is initial area.

2.3 Chemical and methodology for chapter 3- searching for therapeutic molecules for enhancing granulation tissue and wound healing

To prove the hypothesized that propolis and its compounds (quercetin, rutin and artepillin C) may have a beneficial effect on

wound healing by enhancing fibroblast proliferation and migration. Cytotoxicity assays, membrane disruption assays and migration assays were carried out.

2.3.1 Chemical and reagents

Propidium iodide solution 1.0 mg/mL in water, quercetin powder, rutin powder, Triton® x-100. Hoechst pentahydrate (bis-benzimide), 10 mg/mL solution (Life technologies). L-ascorbic acid (Scientific laboratory supplies). Artepillin C powder was provided by Wako pure chemical,10 mg.

2.3.1.i Green Propolis

Water soluble extra-green propolis powder 100% extract (PWSE), was provided by Apis Flora Co (Ribeirão Preto, São Paulo, Brazil). This extract was prepared by pooling different propolis samples from several geographical areas located in Brazil to generate one working batch of propolis. Chemical characterization and chromatographic profiling was provided by Apis Flora Co (see appendix).

2.3.1.i.a Chemical analysis of propolis extract (conducted by the company)

Total Flavonoids (as quercetin):	43.1 mg/g
Artepillin C:	44.1mg/g
Total Phenol (as tannic acid):	167.4mg/g
Heavy Metals (Hg, As, Pb, Cd):	Below detection limit

2.3.2 Evaluation of propolis and its compounds as a potential candidate for wound healing

In order to evaluate the effect of propolis and its components quercetin, rutin and artepillin C on NIH-3T3 fibroblasts metabolic activity and migration; AlamarBlue® assays, membrane integrity and scratch assays were performed.

2.3.2.i Propolis/quercetin/rutin/artepillin C test solutions for cytotoxicity, membrane integrity and scratch assays

Stock solutions and test solutions of propolis and its compounds were preparing as describe in Table 2.1.

Table 2.1-Preparation and final concentration of propolis/quercetin/rutin/artepillin C solutions.

	Propolis	**Quercetin**	**Rutin**	**Artepillin C**
Solvent for preparation of stock	Deionised water	Dimethyl sulfoxide (DMSO)	DMSO	DMSO
solutions Conc. stock solutions	100 mg/mL	0.1 M	0.1 M	0.65 M
Preparation of test solutions	Dilution of stock solutions using 2%-starvation culture media or *. Stock solutions of quercetin, rutin and artepillin C were prepared using 2%-starvation culture media, adding 30 µM of ascorbic acid (to avoid oxidation). Solutions were filtered using filter unit 0.45 µm (MCE membrane)			
Conc. Test solutions	187-2.9 µg/mL	100-1 µM	100-1 µM	100-1 µM
Control solutions	1 mL of deionised water with 2%-starvation culture media	1 mL of DMSO 0.001% (*v/v*) with 2%-starvation culture media and 30 µM ascorbic acid.		

*Culture media DMEM was supplemented with foetal calf serum (FCS) concentration 2% (*v/v*) and 5 mL antibiotic/antimycotic.

2.3.2.ii Seeding procedures for cytotoxicity assay, membrane integrity and scratch assays.

For this purpose, 60,000 cells were transferred to each well of a 24 well tissue culture plate and maintained at 37°C, 5% CO_2 in air at 95% relative humidity (RH) for 24 h. Initially, cells were suspended in fibroblast culture media, 3 h later it was changed to '5%-starvation culture media' with cultures maintained at 37°C, 5% CO_2 in air 95% relative humidity (RH) for 24 h. After a period of 24 h, '5%-starvation culture media' was replaced and propolis/quercetin/rutin and artepillin C test and control solutions with '2%-starvation culture media' were added. This procedure was used to evaluate the cytotoxicity (section 2.3.2.iii) of propolis and its compounds on fibroblasts and 3T3 membrane integrity evaluation (section 2.3.2 iv). For scratch assays the number of cells seeded was increased to 150,000 cells/well (section 2.2.4).

2.3.2.iii Cytotoxicity assay (24/48 h) of propolis/ quercetin/rutin/artepillin C

In order to evaluate the cytotoxicity effect of propolis and its components quercetin, rutin and artepillin C on NIH-3T3 fibroblasts metabolic activity, AlamarBlue® assays were performed as described in section 2.2.3. Propolis/quercetin/rutin and artepillin C test and control solution were prepared as described above (section 2.3.2.i). Fibroblasts were seeded as described in section 2.3.2.ii. The AlamarBlue® assay was performed prior to exposure to propolis or its compounds, 24 h and 48 h after drug application. After AlamarBlue®

assays were carried out at time 0 (24 h post seeding), cells were washed three times with HBSS (without phenol red) to remove the AlamarBlue® reagent and replaced with '2%-starvation culture media' for a period of 1 h. After that propolis/quercetin/rutin/artepillin C test or control solutions were transferred to the wells in triplicate and maintained for 24 h when the AlamarBlue® assay was performed (24 h post treatment). The solutions were replaced with fresh solutions (same condition) and, after 48 h (post treatment), the solutions were removed and the AlamarBlue® assay was repeated in the same conditions as previously mentioned. Observed relative fluorescence units were plotted as relative metabolic activity as was explained in section 2.2.3.

2.3.2.iv Hoechst (HOE) and Propidium iodide (PI) double staining for 3T3 membrane integrity evaluation

This double staining assay distinguished between normal cells and dead cells using fluorescence microscopy. Hoechst (HOE) is a blue fluorescence dye, which can enter the cell and interact with DNA (excitation/ max emission is at 352/461 nm). Since, HOE stains dead and live cells, cells with condensed chromatin (apoptotic cell) appear brighter than viable cells. On the other hand, PI is a red-fluorescence dye (excitation/ max emission 535/617 nm), which only stains cells with loss of membrane integrity (Akiyama et al., 2002, Perez-Vizcaino et al., 2006). The working solution of HOE (40 µg/µL) and PI (20 µg/µL) were prepared by diluting stock solutions in PBS.

NIH-3T3 fibroblasts were seeded as described in section 2.3.2.ii. Then, different concentrations of propolis (187, 46.8 and 2.9 µg/mL), quercetin (100,10 and 1 µM) rutin (200,100,10 and 1 µM) and artepillin C (100,10 and 1 µM) were added using '2%-starvation culture media'. As a positive control, triton 0.5% (*w/v*) was used to kill the cells. Cells were maintained under treatment for 48 h. After that, the media was removed carefully and 200 µL of each stain; Hoechst and PI concentration (40 and 20 µg/mL respectively) were added into each well. The cells were incubated at 37°C in 5% CO*2* in air 95% relative humidity (RH) for 30 min. After that, cells were fixed with 3.7% of formaldehyde solution for 15 min at 37°C inside of a CO_2 incubator Finally, plates were imaged using an inverted fluorescence microscope, Leica DM IRB. This experiment was carried out by exciting each sample within the green (515-560 nm) and UV (340-380 nm) excitation range. Images were taken using a digital QICAM fast 1394 camera, and using QIC capture/pro software, in three different fields of view for each concentration. These experiments were conducted in triplicate. Cell membrane integrity evaluation was quantified by counting cells manually and computer-assisted cell counting using ImageJ software, (National Institutes of Health) (Andrabi et al., 2006). The results were plotted as percentages of PI positive cells as (Perez-Vizcaino et al., 2006) described.

$$PI\ \%\ of\ positive\ cell = \frac{number\ of\ cell\ Pi\ positive}{number\ of\ total\ cells\ (Hoeschst\ positive\ cells)} \times 100$$

2.3.2.v *In vitro* scratch assay–time lapse microscopy

Analysis of propolis and its components upon NIH-3T3 fibroblasts migration was conducted by *in vitro* scratch assay as described in section 2.2.4.

Propolis/quercetin/rutin/artepillin C test and control solutions were prepared as described in section 2.3.2.i. A volume of 1 mL of propolis/quercetin/ rutin/artepillin C test (T) or control (C) solutions was transferred into each well and the cell migration rate was measured over 72 h using time-lapse microscopy as described in section 2.2.4.

2.4 Chemical and methodology for chapter 4 Development and characterization of Poly (ε-caprolactone) (PCL) and PCL-b-PEG/PCL electrospun scaffolds

2.4.1 Chemical and reagents

Poly (ε-caprolactone) (PCL) (M_n=80.000g mol^{-1}), $CDCl_3$. Monomethoxy poly(ethylene glycol) (mPEG) (M_n=5000 g mol^{-1}), ε-caprolactone (CL) and 1,5,7-Triazabicyclo[4.4.0]dec-5-ene (TBD) were purchased and used as received and were stored in a nitrogen atmosphere. Solvents chloroform, methanol and dichloromethane were laboratory reagent grade (Life technologies, Fisher scientific,). Hoechst pentahydrate (bis-benzimide) solution (Life technologies, UK).

2.4.2 Synthesis and purification of PCL-b-PEG copolymers

PEG-PCL diblock copolymers were prepared by ring-opening polymerization of ε-CL initiated by mPEG 5 KDa using 1,5,7 triazabicyclo[4.4.0]dec-5-ene (TBD) as the catalyst (Figure 2.1). The PCL-PEG copolymer was synthesized as follows: 0.806 g of mPEG (Mn= 5 KDa, x 0.16 mmoles), 9.194 g (80.55 mmoles) of ε-CL, and 0.224 g of TBD (1.65 mmoles) were added into a round-bottom flask under a dry nitrogen atmosphere. The temperature of the reaction system was maintained at 110°C for 1.5 h. The PCL-b-PEG copolymer obtained was precipitated in cold methanol and then the resultant solid was centrifuged at 1600 x g for 5 min at 1°C. The copolymer was dissolved in methanol, sonicated and re-precipitated in cold methanol. Subsequently, cold methanol was used to remove any remaining monomer and catalyst and the purified copolymers were stored in air and at room temperature overnight to remove any traces of solvent prior to NMR analysis.

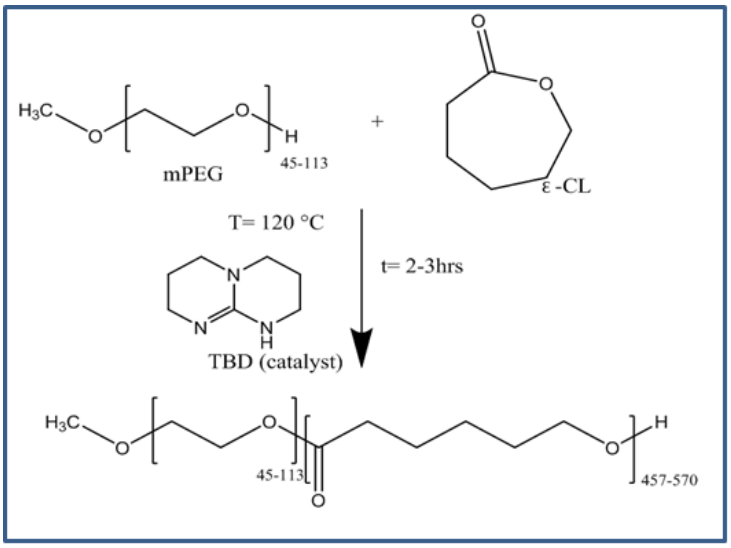


Figure 2.1 - Synthesis scheme of PCL-b-PEG copolymer

2.4.2.i Characterization of PCL-PEG copolymers

2.4.2.i.a Nuclear magnetic resonance analysis (^{1}H NMR)

^{1}H NMR spectra were recorded on a Bruker 400 MHz spectrometer using deuterated-chloroform as the solvent. Chemical shifts are expressed in parts per million (δ) downfield from the internal standard, tetramethylsilane. ^{1}H NMR was also used to estimate the molar mass (M_n) and the length of the caprolactone block in the copolymers. The molecular weight was calculated by assigning an integral value of three, corresponding with the three protons at the CH_3 of the PEG at 3.40 ppm and comparing with the integral for the ester CH_2 groups at 4.10 ppm of the caprolactone main chain. This latter signal was used to evaluate the length of the hydrophobic chain by comparison with the ester peak of the first unit bonds to the PEG chain at 4.25 ppm.

2.4.2.i.b Gel permeation chromatography (GPC)

Gel permeation chromatography (GPC) was carried out using a PL50 Polymer Laboratories system, employing 2 Polymer Laboratories Mixed Bed (D) columns at 30°C, using chloroform as the mobile phase, flow rate 1 mL/min, and with a refractive index detector. Polystyrene standards (Mw range: 482400-162 g mol^{-1}) were used to calibrate the SEC.

2.4.3 Characterization of polymeric solutions

In order to assess the polymeric solutions for electrospinning, rheological characterization of PCL, PCL-b-PEG and PCL-b-PEG/PCL solutions was conducted.

2.4.3.i Viscosity

To evaluate the polymeric solutions, rheology measurements were conducted using an MCR301 rheometer (Anton Paar) with a cone–plate measuring system (CP25-1), at a constant temperature of 25°C, and a sample volume of approximately 1 mL.

2.4.3.ii Conductivity

Conductivity of the polymeric solution was measured at 25°C using a Seven compact ™ S230 conductivity meter and Inlab 720 conductivity probe (Mettler-Toledo AG). The probe was calibrated using a buffer standard solutions of 1413 µS/cm at 25°C.

2.4.4 Electrospinning set up

Electrospinning was carried out in an electrospinning apparatus EC-CLI (spinning chamber and climate control unit) (IME Technologies). It was used to electrospin three different electrospun scaffolds a) PCL b) PCL-PEG copolymer and d) a blend of PCL-PEG/PCL. The electrospinning conditions for PCL scaffold: scaffolds were electrospun using PCL (Mn=80.000 g mol^{-1}) solution of different concentrations (15, 10, 7, 8, 4 *w/w*%) prepared in chloroform and chloroform:

methanol. Table 4.4, Table 4.5, Table 4.6 and Table 4.7 (chapter 4) summarise the solution and processing variables. A total of 74 different scaffold morphologies were produced and a representative set of examples is shown.

The PCL-PEG copolymer was synthesised and scaffolds were made using batch 1 and 4 (approximately Mn=57.000 g mol^{-1}). Solutions of PCL-PEG copolymer were prepared using chloroform, chloroform: methanol (3:1) and dichloromethane. A total of 24 different scaffolds were made. However, PCL-b-PEG solutions formed beads and non-uniform small fibres with an average of 0.1±0.1 μm. Consequently, in order to obtain homogenous and larger fibres, PCL-b-PEG was blended with PCL (80.000 mol^{-1}) and dissolved in chloroform. Table 4.8 and table 4.9 show the electrospinning processing conditions. A total of 29 different scaffolds were made.

In general, polymeric solutions were dissolved overnight at room temperature and clear solutions were taken up in a 5 mL syringe using a capillary tube spinneret of 0.6 mm inner diameter which was set up vertically. A climate-controlled electrospinning machine (IME technologies) was set at a temperature of 20°C and a relative humidity of 44%. Rotating drum collector module EM-RDC and the rotating target collector (EM-RTC) were used to collect the fibre mats.

2.4.5 Characterization of the electrospun scaffolds

2.4.5.i Scaffold morphology (SEM), fibre diameter analysis and thickness

To assess the morphology of the fibres and their diameter distribution, SEM images were taken with an FEI- XL30 (tungsten filament) scanning electron microscope (Philips). An accelerating voltage of 10 kV and 20 mm for working distance were used. Prior to analysis, samples were fully dried at room temperature for 1 week and then coated using a gold blazer sputter coater for 5 minutes (Leica EM SCD005). The diameter of individual fibres were measured by using imageJ software (National Institutes of Health). A total of five images (at 3000 x mag) from five random fields were used for a total of 100 measurements. In addition, thickness measurements of the selected scaffolds were carried out by freezing scaffold samples at -80°C and after 24 h, a cross section of the samples was excised using a cold scalpel blade. Samples were oriented tangentially to the surface of the SEM sample holder and coated using a gold sputter coater for 5 minutes (Leica EM SCD005. Three different areas were analysed to estimate the average thickness of the scaffold.

2.4.5.iiPorosity and pore size

Porosity of the electrospun scaffolds was assessed through two different methods.

a) **Gravimetric method:** porosity was calculated using the fallowing equation (Yang et al., 2008):

$$\varepsilon = 1 - \left[\frac{\delta\ scaffold}{\delta\ material}\right] x100\%$$

Where $\delta\, scaffold$ is the density of the scaffold, calculated as the ratio of mass and volume of the scaffold. Scaffolds with a diameter of 8 mm (n=3) were weighed in a microbalance. Scaffold thicknesses, length and width were estimated with a micro-calliper and then thicknesses were confirmed through SEM images. For $\delta\, material$ (material density), the density of PCL was used (1.145 g/cm^3).

b) Microcomputer tomography (microCT): to examine the porosity of the scaffolds, the samples were set vertically inside of a straw and fixed in the top side with blue glue (Blu-tack). The X-ray source was set at 50 kV and 800 μA. The samples were scanned using a micro-CT (Skyscan 1174). The images were binarized with a threshold range 22 to 255 (gray values). A misalignment of -5 to+5 was used. Three-dimensional measurements and structural analyses were performed with custom software CTAn (Bruker software). NRecon (Bruker software) was used to reconstruct 2D slices (horizontal to the sample). In addition, the pore- size of a) PCL, b) PCL-b-PEG and c) PCL-b-PEG/PCL scaffolds was evaluated.

2.4.5.iii Water Contact Angle (WCA) measurements

Water Contact Angles of liquids on the electrospun scaffolds were measured using a modular CAM 200 optical contact angle meter (KSV Instruments Ltd.) equipped with a camera (JAi®). The sessile drop method was performed using deionised water in a 2 mL luer-lock syringe. Furthermore, rectangular areas (3x1.5 cm) of the scaffolds

were fixed with double sided tape to glass cover slips; 3 pieces of the same scaffold were analysed and measurements were repeated at least 3 times. A 5 µL water droplet was dropped onto the surface of each scaffold and sequential images were recorded. From these images a water contact angle was calculated using image J.

Additionally, in order to evaluate the wettability of the scaffolds, assuming they may have a rough or chemically heterogeneous surface, water contact angle measurements were carried out in advancing (θa) and receding (θr) mode. First of all, the needle deposited a small amount of deionised water on the surface of the scaffold. The needle was retained inside the drop while more liquid was slowly added, increasing the drop size until it reached a saturation point. To measure the receding water contact angle the opposite procedure was carried out (i.e the drop was receding by pumping the water out from the drop). The angle (θr) was measured just before the drop became detached from the scaffold surface (Korhonen et al., 2013). A further calculation of hysteresis (H) was conducted as is follows:

$$H = \theta a - \theta r$$

2.4.5.iv Mechanical properties/uniaxial tensile test

Mechanical properties of electrospun fibrous scaffolds were determined with a uniaxial testing machine (TA-HD Plus Texture Analyser). A 5 Kg load cell under a cross-head speed of 10 mm/min at room temperature was used. All scaffolds were cut in a rectangular shape with dimensions of 15×10 mm. The thicknesses of samples were measured with a digital calliper having a precision of 1 µm and

confirmed with SEM measurements. At least five samples were tested for each sample. Only the scaffolds that had broken in the centre were considered for statistical analysis.

Young's modulus, the yield point, the elongation at break and ultimate tensile strength were evaluated.

2.4.5.v *In vitro* degradation studies

Measurement of degradation rate *in vitro* was conducted for a selection of PCL and PCL-b-PEG/PCL scaffolds. To elucidate the effect of scaffold degradation, 8 mm scaffolds (n=3) were immersed in PBS prior to weighing them on a microbalance.

The scaffolds were maintained in a glassware vial containing 5 mL of PBS during agitation at 30 rpm, 37 °C during 1 h. After that time, the scaffolds were washed with deionised water, blotted with a Whatman® filter paper and vacuum dried at 25°C overnight. Then the scaffolds were reweighed, returned to the vials and 5 mL of fresh PBS was added. The same procedure was repeated regularly (0, 1,2,3 and then 5,7,9,11 and 12 months). Additionally, selected samples were taken at time point of 0, 2 months, 5 months and 12 months for SEM analysis and at time point 0, 5 months and 12 months for GPC analysis.

2.4.6 Biological evaluation of the scaffolds

2.4.6.i Scaffold preparation

To prepare scaffolds for mammalian cell culture, circles with a diameter of 8 mm from random areas of the selected scaffold were

taken. Scaffolds were sterilised using a UV lamp (CL-1000 UV crosslinker) for 10 min at power 200 (x 100 μJ/cm^2). Later, scaffolds were immersed with 1 mL of culture media ('fibroblast culture media'). Scaffolds were maintained at 37°C, 5% CO_2 in air at 95% relative humidity (RH) for 24 h.

2.4.6.ii Cell viability

To prepare scaffolds for cell culture, circles with a diameter of 8 mm from random areas of the electrospun mat were taken. The scaffolds were sterilised using a UV lamp for 10 min. Later, the scaffolds were fixed to the bottom with a small quantity of aquarium sealant glue (King British) and immersed in 1 mL of cell culture media. Furthermore, the scaffolds were maintained at 37°C, 5% CO_2 in air at 95% relative humidity (RH) for 24 h.

To investigate fibroblast viability on the scaffolds, *in vitro* analysis was conducted by seeding 60,000 cells/well (in aliquots of 500 μL) on the prepared scaffolds in a 24 non-tissue culture treated plates (see section 2.3.2 ii). The metabolic activity of the fibroblasts on each scaffold was determined by performing the AlamarBlue® assay (see section 2.2.3) after 6 hours, 3 days, 6 days, 9 days and 12 days post seeding. BJ6 foreskin human fibroblast were evaluated until 15 days. The scaffolds were transferred to new 24 non-tissue culture treated plates before carrying out the AlamarBlue® assay to avoid measuring cells attached to the bottom of the well plate. In addition, each well was washed three times with Hanks' balanced salt solution (Sigma) to remove unattached and dead cells. The AlamarBlue® assay was

carried out by adding 1 mL of AlamarBlue® solution 10% (*v/v*) (diluted in Hanks' balanced salt solution) into each well and incubating for 60 min at 37°C. Aliquots (200 µL) from the samples were then transferred into a 96 well non-tissue culture treated plate. Relative fluorescence units were measured in a plate reader, set at an excitation wavelength of 560 nm and emission at 590 nm.

2.4.6.iii Cell morphology and cell-scaffold interaction analysis

In order to evaluate the morphology of the cells adherent on the scaffolds, confocal laser microscopy imaging was performed. A total of 60,000 cells/well (in aliquots of 500 µL) were seeded on the scaffolds and after 5 days of culture (37°C, 5% CO_2 in air), specimens were collected. The scaffolds were rinsed three time with PBS for 3 min each time and then fixed with paraformaldehyde 3.7% (in PBS) for 10 min at room temperature. Later, the cells were stained with Hoechst and incubated for 30 min at 37°C. Finally, the samples were mounted in fluorescence mounting media and the cells were visualized using laser scanning confocal microscopy (LSCM;Zeiss, LSM 880).

To visualize the interactions between cells and fibres, phase contrast images were taken and in addition SEM was carried out after 5 days of culture. Specimens were collected and processed on day 5 following procedures as previously reported by . The scaffolds were rinsed with PBS and then fixed with 3.7% paraformaldehyde for 30 min at 4°C. Later, the constructs were dehydrated using an ethanol

gradient (20-100) and stored at room temperature overnight to dry. Finally, the samples were sputter-coated with gold for 5 min and observed by SEM. Additional analyses were conducted for PCL-b-PEG based scaffolds considering cell morphology analysis at day 5 and day 12.

2.4.6.iv Cell infiltration

To determine the level of cell penetration into the scaffolds after of 5 days of cell culture, z-stacked confocal microscopy analysis was carried out. Different planes were obtained of stained cells growing on and in the scaffolds. Laser excitation at 405 nm and 488 nm was used, and sequential imaging of Hoechst (blue) and GFP (green fluorescent protein) was performed. The parameters used were as follows: pinhole set to 1 Airy unit, pixel dwell time: 0.26 µs, 5 µm plane thickness.

The infiltration depth (%) of the fibroblasts was calculated by estimating the maximum distance (microns) migrated by fibroblasts from the top to the bottom into the scaffolds (visualization on Z-stack) and using the total distance, the thickness of the scaffolds estimated by SEM (section 2.4.5 i) (Lim et al., 2010, Wang et al., 2013, Zhang et al., 2005b).

$$Infiltration\ deph\ (\%) = \frac{\text{Max. distance migrated (µm)}}{Tickness\ (\mu m)}\ x100$$

2.5 Chemicals and methodology for chapters 5 and 6- loading and release studies of proteins and *L. sericata* maggot E/S from PCL, H-PCL and PCL-b-PEG/PCL scaffolds (with/without cationic modification)

2.5.1 Chemical and reagents

Llysozyme- rhodamine B (NANOCS). Avidin-fluorescein conjugate (Sigma-Aldrich). For cationically modified scaffolds (chapter 6) lysozyme-rhodamine B protein, *Lucilia sericata* maggot excretion/secretion (*L. sericata* maggot E/S*)* modified with NHS and Avidin-rhodamine (Vector laboratories) were used.

Nine vials of *L. sericata* maggot E/S were produced as described by (Horobin et al., 2003) in Professor D. Pritchard's laboratory (University of Nottingham) generation 5, date 26.07.12. NHS-rhodamine (Thermo scientific).

The following reagents were supplied by Sigma: Trimethyl aminoethyl methacrylate (TMAEMA) , RAFT agent 4-Cyanopentanoic acid dithiobenzoate (CAPADB) , initiator 4,4'-Azobis(4-cyanovaleric acid) V-501, 1-ethyl-3-(3-dimethylaminopropyl) carbodiimide hydrochloride (EDC), sulfo-N-hydroxysulfosuccinemide (NHSS), N-(2-Hydroxypropyl) methacrylamide (HPMA) (it was synthesized by Nora Francini in Professor Cameron Alexander's laboratory (University of Nottingham)(Francini et al., 2015).

2.5.2 Wet chemical surface modification

The surface of biodegradable aliphatic polyester electrospun scaffolds can be partially hydrolysed though acidic or alkaline treatment, which is a widely used method to incorporate new chemical functionality and to improve the wettability of the material (Yoo et al., 2009). In order to obtain a more reactive surface, by exposing carboxyl and hydroxyl groups on the PCL fibres, circles of 8 mm of scaffolds were immersed in NaOH solution. The PCL scaffolds were immersed at different concentrations of NaOH solutions at 0.5 M and 1M at 37°C and under agitation on a roller mixer. Different incubation times of 3 h, 6 h and 12 h respectively, were evaluated.

After incubation in basic conditions, the scaffolds were washed 3 times with deionised water and dried for48 h in a vacuum oven at 25 °C. After that, PCL scaffolds were taken for SEM, contact angle and GPC analysis.

2.5.3 Scaffold materials

PCL, H-PCL and PCL-b-PEG/PCL electrospun scaffolds with an average fibre diameter ~4 microns (Chapter 4) were selected to be used as a platform for protein release (chapter 5 and 6). Also, experiments were carried out using PCL scaffolds pre-treated with alkaline solutions; these are known as H-PCL (PCL hydrolysed with NaOH).

PCL, H-PCL and PCL-b-PEG/PCL scaffolds with similar weight ~800 µg were cut into circles with a diameter of 8 mm and stored in dry conditions, at room temperature (inside of a sealed bag) until used.

Additionally, PCL, H-PCL and PCL-b-PEG/PCL scaffolds were modified using a cationic polymer $PTMAEMA_{33}$-b-$PHPMA_{180}$ (chapter 6).

2.5.4 Proteins used for adsorption and release studies

In order to study the adsorption efficiency of proteins on PCL, H-PCL and PCL-b-PEG/PCL and on cationically modified PCL, H-PCL and PCL-b-PEG/PCL scaffolds, albumin, lysozyme, and avidin were used as model proteins. However, after preliminary tests, albumin was not studied further because of the quantity of bubbles that caused disruption during fluorescence measurements.

Lysozyme is a protein with a relatively simple structure with 129 amino acids. It possesses a net positive charge of +9 at pH 7.0 (PI:11) (Ganguli et al., 2009). Lysozyme- rhodamine B labelled was used immediately after being dissolved, avoiding thaw and freezing cycles.

Avidin is a medium molecular-weight protein (66 KDa) and it is a highly glycosylated protein, with a PI:10-10.5 and estimated cationic charge density of 16 (Liao et al., 2005). An avidin-fluorescein conjugate was immediately used after being dissolved, avoiding thaw and freezing cycles. Additionally, avidin–rhodamine, was used to carry out experiments on catatonically modified scaffolds (chapter 6).

Nine vials of *L. sericata* maggot E/S were produced as described by (Horobin et al., 2003), in Professor D. Pritchard's laboratory (The University of Nottingham) generation 5, date 26.07.12 were used in this study.

Part of the *L. sericata* maggot E/S material was used for labelling with NHS-rhodamine. NHS-rhodamine were dissolved in DMSO by stirring for one hour in the dark. Then, this solution was added under agitation to *L. sericata* maggot E/S solution and incubated for 1 hour at room temperature. Non-reacted NHS-rhodamine was removed by dialysis using a membrane with 3.5 K MWCO (SnakeSkin™ dialysis tubing Thermo Scientific) against deionised water for 4 days at 25°C.

2.5.5 Protein loading efficiency studies.

PCL and PCL-b-PEG/PCL scaffolds (with and without cationically modification) with similar weight ~800 µg. The scaffolds were sterilised using a UV lamp for 10 min. The initial concentration of adsorbed protein was quantified by fluorescence and confirmed by the Bradford assay. Then, the scaffolds were fixed to the bottom of the vial with a small quantity of aquarium sealant glue and fully immersed in 1 mL of the protein solution. The scaffolds were checked regularly to guarantee the sink condition of the scaffolds at all times.

The scaffolds and protein solutions were incubated in an environmental incubator at 37°C in constant agitation. Aliquots of the supernatant were taken after 3 h, 6 h and 24 h post incubation. Fluorescence microscopy was used to qualitatively determine protein-labels on the scaffolds at initial points (immediately after the addition of the protein solution), and after 3 h, 6 h and 24 hours.

The amount of protein loaded on the scaffolds was determined indirectly by measuring the protein concentration in the supernatant, at different time points (after 3, 6, 12 and 24 hours). The following

equation was used to calculate the absorption efficiency (AE). AE estimates the percentage of drug that was successfully **adsorbed** onto the scaffolds (Nanjwade et al., 2011).

$$AE = \frac{protein\ added - free\ unabsorbed\ protein}{protein\ added}\ x100$$

The loading efficiency of proteins was also assessed through a direct method. The scaffolds were dissolved in 0.5 mL of chloroform, sonicated for 15 min and 1 mL of PBS added. The samples were maintained in glass vials under agitation for 3 h at room temperature and protected from light. Chloroform was allowed to evaporate at room temperature. The solution was centrifuged at 15,000 x g at 4°C for 15 min and the supernatant collected for protein quantification (sections 2.5.6 and 2.5.7). This methodology was modified from (Kim et al., 2014b), who used a mixture of water and hexane ratio 1:2 rather than chloroform.

2.5.6 Quantification of proteins by modified Bradford Assay

In order to evaluate the quantity of protein adsorbed and released from scaffolds, the Bradford assay was performed (Bradford, 1976). Bradford analysis was conducted by diluting 2.5-fold the Bradford reagent (Bio-Rad) in deionized water which was used the same day. Calibration curves were carried out by using known concentrations of bovine serum albumin (BSA) prepared from a serial dilution of 1 mg/mL BSA in deionised water (i.e the same diluent as the samples; final concentrations 1–50 µg/mL).

To assess the protein concentration of unknown samples and diluted samples (factors of dilution 10x, 5x and 2x) were prepared. A 100 µL aliquot of each sample (including a blank sample of deionised water) was transferred to a multiwell plate and 100 µL Bradford reagent added (total volume 200 µL). The samples were mixed and absorbance at 590 and 450 nm was measured by using a plate reader. The measurement was carried out each time within 60 min of colour development. The calibration curves were prepared by dividing the absorbance values 590/450. The protein concentration of the unknown samples were estimated by interpolation on the linear equation of the calibration curve as it was described by (Ernst and Zor, 2010).

2.5.7 Quantification of proteins by fluorescence

In order to evaluate the concentration of protein absorbed and released from the scaffolds, UV-spectroscopy measurements were performed. Relative fluorescence units (RFU) were determined in a plate reader.

Aliquots of 150 µL of each sample were added to a black flat bottom non-treated 96 well plate in triplicate. To measure the avidin-FITC conjugate at the wavelengths used were Ex/Em 494/518nm; for the avidin-rhodamine conjugate measurements were taken at Ex/Em 544/576 nm. The Lysozyme–Rhodamine B conjugate was measured at Ex/Em 544/576 and the *L. sericata* maggot E/S-NHS rhodamine conjugate at Ex/Em 552/575 nm.

2.5.8 Release of proteins

In order to evaluate the release profile of avidin, lysozyme and *L. sericata* maggot E/S from PCL and PCL-b-PEG/PCL scaffolds, with and without cationically modification, scaffolds were washed 3 times with deionised water in order to remove excess protein and dried in a vacuum oven at 25°C for 48 h.

For the release studies, protein loaded-scaffolds were immersed in 1 mL PBS (pH 7.4). The samples were maintained under agitation at 37°C 5% CO_2 in air for 21 days. At each time point (30 min, 1 h, 2 h,3 h, 4 h,5 h,6 h,12 h 24 h, day 2, day 3, day 4, day 5 day 6, day 9, day 12, day 15, day 18 day 21) 1 mL was removed and replaced with fresh; the samples were stored at -20°C for further protein quantification and activity estimation.

The results of release assays were express as cumulative release % as function of time. Cumulative release % was calculated using the following equation (Ji et al., 2010):

$$Cumulative\ release\ \% = 100x\ \frac{Mt}{M\infty}$$

Where Mt is the amount of protein released at time t and $M\infty$ is the total amount of protein adsorbed onto the scaffolds.

2.5.9 Relative bioactivity of lysozyme

The relative bioactivity of lysozyme was determined by using EnzChek® Lysozyme assay kit, which measures lysozyme activity in a solution. The assay measures the lysozyme activity against *Micrococcus lysodeikticus* through lysis of the cell wall as described

by Liao et al. (2001). Briefly, the bioactivity of the individual samples was determined using a calibration curve constructed using a fresh lysozyme standard. The relative biological activity of lysozyme at each time point is expressed in reference to the lysozyme amount detected initially (t0). This test used a lysozyme substrate, *Micrococcus lysodeikticus* fluorescein conjugates and lysozyme from chicken egg white. Lysozyme action acts on *Micrococcus lysodeikticus* fluorescein conjugates, releasing fluorescein. Since fluorescence intensity increases proportionally to lysozyme activity, this can be detected by using a fluorescence microplate-reader at Ex/EM 494/518 nm and the activity of unknown samples determined from a standard curve.

2.5.10 Relative bioactivity of *L. sericata* maggot E/S

One of the most important aspects of drug incorporation and release of a biological is to retain the bioactivity throughout the entire process (Buschle-Diller et al., 2007). As a result, in order to evaluate the bioactivity of *L. sericata* maggot E/S after release, all the aliquots at the different time points were pooled (to ensure sufficient protein was collected to be above the minimum detection limits of the assay). The samples were concentrated using an ultrafiltration device (Vivaspin, GE Healthcare Bio-Science AB) with a MWCO membrane of 3000 Da and centrifugation at 4000 rpm for 30 min at 4°C. The volume of each sample was adjusted to 1mL and stored at 4°C for next day analysis.

The bioactivity of the *L. sericata* maggot E/S was assessed using a Protease Fluorescent Detection Kit (Sigma Aldrich), which allows the detection of serine, cysteine, metallo, and aspartic protease activity. The protease fluorescence kits detect the activity of proteases by using a FITC-casein substrate. The action of the proteases is the cleavage of the casein-FITC bond releasing free FITC which can be detected (Twining, 1984).

2.5.11 Synthesis of PTMAEMA-b-PHPMA

Poly (trimethylamino)ethylmethacrylate hydrochloride) (PTMAEMA. HCl) with a theoretical chain length of 30 monomer units was synthesized by reversible addition–fragmentation chain transfer (RAFT) polymerization (Figure 2.2). The monomer trimethylaminoethylmethacrylate hydrochloride (TMAEMA) (10 g, 0.048 mol) was polymerised by using 4-Cyano-4-(phenylcarbonothioylthio) pentanoic acid (0.45 g, 0.0016 mol) as chain transfer agent and 4,4'-Azobis(4-cyanovaleric acid) (V-501) (0.09 g, 0.0003 mol) as initiator in a molar ratio of 30:1:0.2, respectively. For that, the TMAEMA monomer was placed in a Schlenk tube and chain transfer agent CPADB previously dissolved in 5 mL of methanol and 34 mL of acetate buffer (1 M, pH 5.2) were then added. The mixture was degassed with argon for at least 30 min. Then, V-501 initiator dissolved in methanol (5 mL) was added and degassed for 5 min. The reaction started after immersion of the flask in an oil bath at 70°C. Samples were taken at 0, 20, 35, 90, 120 min and monomer conversion was followed by ^{1}H NMR analysis in DMSO.

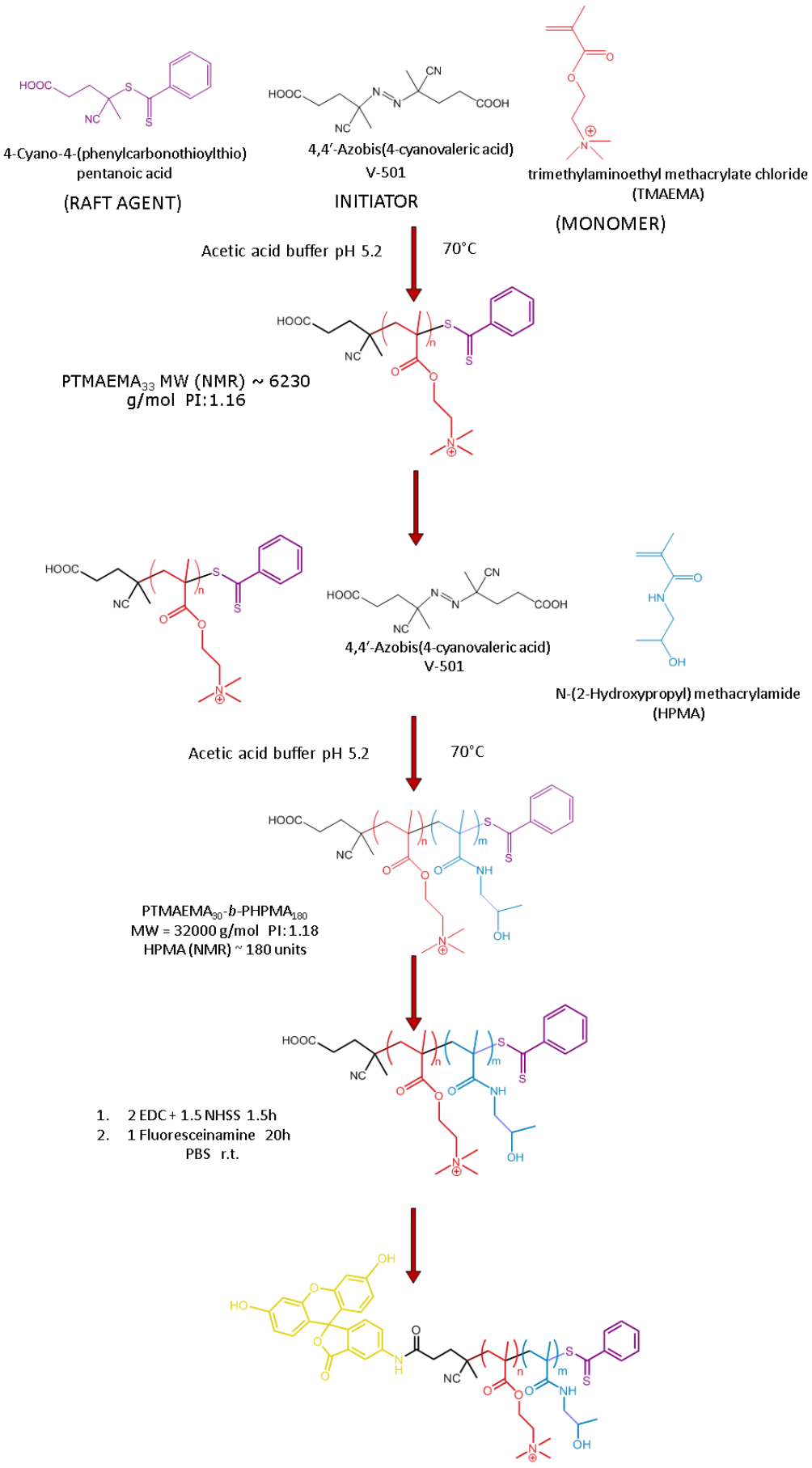


Figure 2.2 - Synthesis of fluorescein-conjugated $PTMAEMA_{33}$-b-$PHPMA_{180}$- using reversible addition–fragmentation chain transfer (RAFT) polymerization techniques.

The reaction was stopped after 120 min by cooling down and opening the tube to the air. Purified polymer was obtained after precipitation in acetone and re-precipitation in THF. Molecular weight and molecular weight distributions of the final polymer were analysed by ^{1}H NMR and GPC. A M_n (NMR) of 6230 g/mol and Đ of 1.16 were determined, corresponding to a degree of polymerisation of 33 units p(TMAEMA)$_{33}$.

PTMAEMA$_{33}$ (r=1) was then used as macroinitiator for the copolymerisation of N-(2-hydroxypropyl) methacrylamide (HPMA)(r=100). PTMAEMA$_{33}$ (1.0 g, 0.16 mmol) and HPMA (2.3 g, 16 mmol) were dissolved in acetate buffer (1 M, pH 5.2) (4.6 mL) and degassed under N_2 for 20 min. Initiator V-501 (0.009 g, 0.03 mmol) was added to the mixture and mixture degassed for 5 minutes. Reaction was started by immersion in an oil bath set at 72°C. Samples were taken at 0, 15, 40, 70, 130, 175, 225 min and monomer conversion analysed by ^{1}H NMR in DMSO. The reaction was stopped after 4 h and 30 min and the polymer was precipitated in THF twice. Monomer composition in the final copolymer was obtained by NMR analysis. The signal at 4.4 ppm corresponding to CH_2 from TMAEMA was used as reference and signal at 3.9 ppm corresponding to C*H* from HPMA was used to estimate monomer units of the HPMA block. Signals between 7.4-8.0 ppm corresponds to aromatic protons (C_6H_5) of RAFT chain transfer agent and were used as reference. Signal between 0.5-1.5 ppm corresponding to TMAEMA methyl group (CH_3) was used to calculate units of TMAEMA monomer in the final polymer. Calculated polymerisation degree for HPMA block was 180

units corresponding to a total M_n (NMR) of 32000 g/mol. In addition, from PTMAEMA-b-PHPMA signal at 4.5 ppm corresponding to CH_2 protons close to the acrylate of TPMAEMA was used as reference. Signal at 3.85 ppm corresponding to CH group of HPMA was used to calculate units of HPMA monomer in the final copolymer. Polydispersity of the final $PTMAEMA_{33}$-b-$PHPMA_{180}$ copolymer was 1.26 as determined by GPC analysis.

2.5.12 Synthesis of Fluorescein-labelled $PTMAEMA_{33}$-b-$PHPMA_{180}$ copolymer.

Once $PTMAEMA_{33}$-b-$PHPMA_{180}$ polymer was synthesized and characterised, fluorescein dye was incorporated by using the widespread EDC/NHS coupling method, according to previous work (Levere et al., 2013). One equivalent of $PTMAEMA_{33}$-$PHMA_{180}$ (0.5 g, 0.016mmmol), 2 equivalents of 1-ethyl-3-(3-dimethylaminopropyl) carbodiimide hydrochloride EDC (0.006 g,0.031 mmol) and 1.5 equivalents of sulfo-N-hydroxysulfosuccinimide (NHSSS) (0.005 g, 0.023 mmol) were dissolved in PBS pH 7 and left reacted for 1.5 h. Then 1 equivalent (0.0054) of 4-aminofluorescein (0.005 g, 0.016 mmol) dissolved in 10 mL of PBS pH 7 was added. Reaction was maintained for 20 h at room temperature. Polymer labelled with fluorescein was dialysed for 3 days against deionised water to remove unreacted reagents.

2.5.12.i Characterization of $PTMAEMA_{33}$-b-$PHPMA_{180}$ copolymers

2.5.12.i.a Gel permeation chromatography (GPC) and nuclear magnetic resonance (NMR) analysis of $PTMAEMA_{33}$-b-$PHPMA_{180}$ polymers.

In order to determine molecular weight (Mn, Mw) and the polydispersity (Đ) of $PTMAEMA_{33}$-b-$PHPMA_{180}$ polymers gel permeation chromatography (GPC) and nuclear magnetic resonance (NMR) analysis were performed. GPC was carried out using a PL50 Polymer Laboratories system, employing 2 mixed bed (D) columns at 30°C and equipped with a refractive index detector. PBS pH 7.4 was used as the mobile phase at a flow rate of 1 mL/min. GPC system was calibrated with polyvinylpyrrolidone standards (M_w range: 482400-162 g/ mol).

^{1}H NMR spectra was recorded on a Bruker 400 MHz spectrometer in d_6-DMSO. Chemical shifts were expressed in parts per million (δ) downfield from the internal standard, tetramethylsilane. ^{1}H NMR was exploited to estimate the NMR molecular weight and the length of the purified $PTMAHEMA_{33}$ and $PTMAEMA_{33}$-b-$PHPMA_{180}$ polymers.

2.5.12.i.b Determination of the maximum emission and excitation wavelengths of $PTMAEMA_{33}$-b-$PHPMA_{180}$

In order to evaluate the range of absorption and emission of the polymer 5 mg of $PTMAEMA_{33}$-b-$PHPMA_{180}$ polymer was dissolved in 5 mL of deionised water with a final concentration of 1 mg/mL. Then, an absorbance scan between 250-750 nm was carried out. Maximum

absorption and emission wavelengths were observed at λex 450 nm, λem 518 nm, respectively.

2.5.13 Effects of cationic PTMAEMA and $PTMAEMA_{33}$-b-$PHPMA_{180}$ polymers on murine fibroblast metabolic activity.

Stock solutions of 1 mg/mL of $TMAEMA_{33}$ and $PTMAEMA_{33}$-b-$PHPMA_{180}$ were prepared in deionised water. Serial dilutions were performed diluting $TMAEMA_{33}$ and $PTMAEMA_{33}$-b-$PHPMA_{180}$ polymers in a concentration range of 500,200,100,50,20,10 and 5 μg/mL and control with media using DMEM and 2% *w/w* and 10% *w/w* of FCS.

Cell were transferred to each well of a 24 well tissue culture plate (60,000 cells in each well) as described in section 2.3.2.ii. The AlamarBlue® assay was used to measure the metabolic activity of the cells before and after 24 h the treatment with $TMAEMA_{33}$ and $PTMAEMA_{33}$-b-$PHPMA_{180}$ solutions (AlamarBlue® procedures were described in section 2.2.3.

2.5.14 Surface modification of PCL, H-PCL and PCL-b-PEG scaffolds with cationic ($PTMAEMA_{33}$-b-$PHPMA_{180}$) copolymers.

Fluorescein-conjugated $PTMAEMA_{33}$-b-$PHPMA_{180}$ polymers were used to modify the surface of PCL, H-PCL and PCL-b-PEG/PCL scaffolds.

A stock solution of Fluorescein-conjugated $PTMAEMA_{33}$-b-$PHPMA_{180}$ polymers with a concentration of 1 mg/mL was dissolved in deionised

water. Then 1 mL of polymeric solution concentration 200 µg/mL was added to a vial, which contain the different scaffolds PCL, H-PCL and PCL-b-PEG. The scaffolds and cationic polymeric solutions were incubated in an environmental incubator at 37°C in constant agitation for 24 h.

The amount of cationic polymer loaded onto the scaffolds was determined indirectly by measuring the fluorescein concentration in the supernatant, at different time points (after 3, 6, 12 and 24 hours) (Prabaharan et al., 2007). The fluorescence of the supernatant was measured with a TECAN microplate reader at Ex/Em 450/518 nm before and after polymer interaction with the scaffolds. Calibration curves were performed at each time point using serial dilutions of fluorescein from 2000 to 0 µg/mL in PBS. Loading efficiency was calculated as described in section 2.5.5.

2.5.15 Assessing the influence of *L. sericata* maggot E/S from controlled release scaffolds on fibroblast motility in an *in vitro* scratch assay.

The influence of *L. sericata* maggot E/S on the motility of fibroblasts was assessed by an *in vitro* scratch assay in the presence of the different released-aliquots of *L. sericata* maggot E/S. The protease activity from the aliquots of *L. sericata* maggot E/S was measured, and samples with the highest protease activity were selected. The scratch assay was performed on a 24 well plate coated with human fibronectin (Human Fibronectin Cellware). A scratch was made in a cell monolayer (confluent culture) as described in section 2.2.4.

DMEM containing *L. sericata* maggot E/S (1 mL) was added to each well and time–lapse microscopy was set for 3 days. After that period, the closure of the *in vitro* scratch wound was evaluated in the same way as described in section 2.2.4.

2.5.16 Statistical analysis

All data were expressed as mean±SD. Experiments were carried out in triplicate for a minimum of n=3 individual experiments, unless otherwise stated. To analyse significant differences for the performed tests, a one way-ANOVA Tukey's multiple comparison post-hoc test was carried out (unless otherwise stated). Statistical analysis of data presented here was performed using Prism (GraphPad Prism6, San Diego CA). Significant differences were determined at $P \leq 0.05$. P values were expressed as the follows: ns for $P > 0.05$, * for $P \leq 0.05$, ** $P \leq 0.01$, *** $P \leq 0.001$, **** $P \leq 0.0001$. For fibre diameter analysis, one hundred measurements were taken using ImageJ software (National Institutes of Health) and statistical analysis performed by analysing frequency distribution and non-linear regression (Log Gaussian) using Prism (GraphPad Prism6).

CHAPTER 3 Searching for therapeutic molecules for enhancing granulation tissue and wound healing

3.1 Naturally-derived biomolecules that have wound healing properties

Researchers have considered the use of natural products as bioactive substances for wound healing (Lindblad, 2008). Some examples of these are honey (Visavadia et al., 2008), curcumin (Gong et al., 2013), *Aloe vera* (Takzare et al., 2009), *Lucilia sericata* maggot excretion/secretion (*L. sericata* maggot E/S) (Horobin et al., 2005, Telford et al., 2010) and propolis resinous material which is produced and used by bees (McLennan et al., 2008). Honey is one of the most studied natural products and has been adopted for use in clinical practices (Al-Waili et al., 2011). It has been reported that honey showed a positive effect on wound closure when tested in animal models and clinical trials (Al-Waili et al., 2011). Honey's action on wound healing was mainly due to its antioxidant capacity that reduce free radical species and its antibacterial activity (Mandal and Mandal, 2011). Honey dressing can be found in the market as Medihoney® (USA) and Mesitran® (Netherlands) (Mphande et al., 2007). Curcumin is another natural component which can be extracted from the herb turmeric. Studies have shown the efficacy of curcumin promoting wound healing in diabetic animals (Kant et al., 2014).

Early studies on *Aloe vera* came to the conclusion that although it has promising effect promoting wound healing further studies need to be done to probe its clinical efficacy (Maenthaisong et al., 2007). More recently studies using animal model have shown that rats treated with *Aloe vera* exhibited a faster wound contraction (Oryan et al., 2010) (Takzare et al., 2009).

Considerable amount of researches into this field has been done from 2000 (Duran et al., 2004, Parente et al., 2012, Somboonwong et al., 2000, QIN et al., 2010). However, the use of natural product s has the limitation of batch-batch variation in the sample collection, production and processing (Yun et al., 2012, Lindblad, 2008).

This literature review will focus on propolis as potential candidate for promoting wound healing.

3.2 Propolis as a wound healing candidate

Propolis is described as a resinous material which is produced and used by *Apis mellifera L*. bees to protect their hives from bacterial and fungal infections and to preserve aseptic conditions in the place where their queen will lay her eggs. Worker bees collect propolis from the exudates of trees, buds, and other plant components. After collection, bees modify propolis by adding their saliva and wax (Daleprane and Abdalla, 2013). Propolis has been used as a medicine to treat wounds by Egyptians, Romans, and Greeks for centuries. However, the use of propolis was reduced in the Middle Ages and it wasn't until the last century when propolis was rediscovered and studies about its chemical composition began (Kuropatnicki et al.,

2013). Propolis is a natural and complex substance containing around 300 different components (Bankova, 2005). The chemical composition, and as a consequence, biological activity of propolis varies depending on the local plant source, climate and other geographical factors (Berretta et al., 2012a, Berretta et al., 2012b, Isidorov et al., 2014, Cheng et al., 2013, Popova et al., 2010). The different types of propolis which have been reported in the literature are presented in the Table 3.1.

Table 3.1 - The main compounds of five types of propolis and their biological actions.

Type of propolis	Geographical area	Source	Chemical composition	Main biological actions	references
Poplar	Europe, Asia (including China)	Poplar tree	P-coumaric acid mainly artepellin c and baccharin High levels of flavonoids and phenolic acids.	Antioxidant, anti-inflammatory and antidiabetic effect *in vitro* and *in vivo*	(Wang et al., 2014a)
Green	Brazil	*Baccharis dracunculifolia*	Dipertenes, p-counmaric acid mainly Artepillin C, flavonoids such as quercetin and Kaempferol	Antiulcer, anti-inflammatory and antibacterial effect	(Cheung et al., 2011)
Red	Northeast cost of Brazil, China, Mexico, Venezuela and Cuba	Clusia sorobiculata, clusia minor and major and dalbergia ecastophyllum	Isoflavonoids, flavonoids terpenes, chalcones, pterocarpans	Antimicrobial, anti-inflammatory and analgesic effect	(López et al., 2014)
Mediterranean	Greece	---	Dipertenes	Antimicrobial	(Popova et al., 2010)
South America	Chile, Argentine	---	Flavonoids such as quercetin and phenolics	Antioxidant	(Russo et al., 2004, Castro et al., 2014)

3.2.1 Green propolis and its compounds

Green propolis comes from the southeast of Brazil, one of the major suppliers of propolis in the world (López et al., 2014). The main plant source is *Baccharis dracunculifolia* (alecrim plants). This propolis is one of the most studied in term of its composition and biological activity (Sawaya et al., 2011). A variety of methods have been used to identify and quantify green propolis compounds. Some of these include: i) chromatographic analysis (i.e reverse phase High Performance Liquid Chromatography (HPLC)) and ii) direct insertion probe mass spectrometry (Sawaya et al., 2011). In general terms, raw green propolis consists of 50% of resin and balsam (polyphenolic and flavonoid fraction), 30% of wax (wax and fatty acids), 10% of aromatic and essential oils (volatiles), 5% of pollen (protein and amino acids) and 5% of other substances (organic and minerals (Farooqui and Farooqui, 2012). The contents and concentration of phenolic and flavonoids of green propolis will vary depending of the sample (batch) and the solvent used in the extraction (Righi et al., 2013). Major phenolic and flavonoids contents of a ethanolic extract analysed by HPLC has shown that green propolis is constituted by artepillin C 3.3% (*w/w*), p-coumaric acid 0.63% (*w/w*), trans-cinnamic acid 0.05% (*w/w*), chlorogenic acid 0.21% (*w/w*), caffeine acid 0.04% (*w/w*), kaempferol 0.08% (*w/w*), kaempferide 0.63% (*w/w*) and isosakuranetin 0.12% (*w/w*) (de Funari et al., 2007), quercetin and rutin (qualitative identification)(Cheung et al., 2011, Righi et al., 2013) (Figure 3.1).

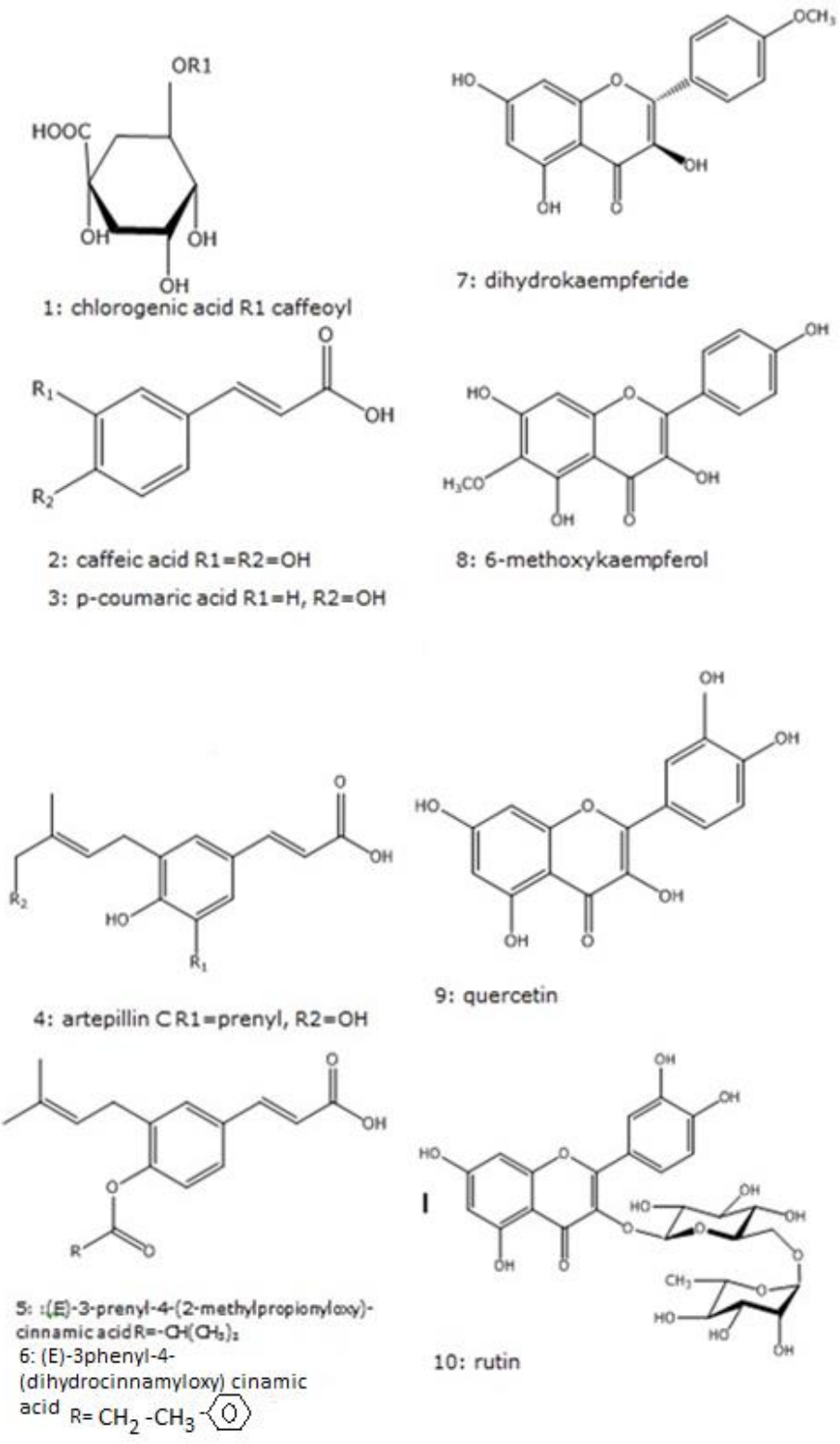


Figure 3.1 – Chemical structure of some green propolis compounds. Adapted from (Toreti et al., 2013)

3.2.2 Biological activities and mechanism of action of propolis

The main biological activities of propolis include: i) analgesic/anaesthetic properties (Kamburoglu and Özen, 2011), ii) immunomodulatory effects (McLennan et al., 2008, Barroso et al., 2012, Hori et al., 2013), iii) antibacterial properties, iv) fungicidal properties (Drago et al., 2007, Dota et al., 2011), v) anticarcinogenic effects (Daleprane and Abdalla, 2013, Umthong et al., 2011, Russo et al., 2004)) and vi) wound healing effects (Sehn et al., 2009, Olczyk et al., 2013b, Kozma, 2013).

Although there are a significant number of studies on the biological activity of propolis, its mechanisms of action are not yet fully understood (Berretta et al., 2012a). The active molecule in which propolis performs these actions is still under debate (Hori et al., 2013).

3.2.2.i Antimicrobial activity

There are many studies confirming that different propolis extracts have a strong, synergic (Kucharzewski et al., 2013) and dose dependent (Bonvehí and Gutiérrez, 2012) antimicrobial activity against Gram-positive and Gram-negative bacteria and fungi (Bonvehí and Gutiérrez, 2012, Kucharzewski et al., 2013). Propolis has shown a noticeable response against Gram positive bacteria (Silva et al., 2012), including *Staphylococous aureus*, the most common pathogen in diabetic foot osteomyelitis (Elamurugan et al., 2011). Some authors (Souza et al., 2014, Silva et al., 2012) highlight

that Gram negative bacteria are less sensitive to propolis action and it is necessary to use a higher propolis concentration to observe bacteriostatic or bactericidal effects (Orsi et al., 2012). The possible explanation for this difference is that propolis acts upon the Gram positive bacterial, inhibiting cell wall synthesis, DNA gyrase, and ATP production (Silva et al., 2012). Gram negative bacteria have an outer membrane which may delay and/or inhibit the penetration of propolis and hence confers resistance (Silva et al., 2012). Studies suggest (Cushnie and Lamb, 2005, Lotfy, 2006) that the antimicrobial activity of propolis relates to its rich composition of flavonoids and caffeic acid phenethyl ester (CAPE) compounds. The action mechanism of propolis against fungi has been studied in *Saccharomyces cerevisiae* which have been used as a model of a eukaryote organisms (de Castro et al., 2011). These studies conclude that green propolis is able to control *Candida albicans* infections and also to induce programmed cell death (apoptosis) and necrosis through the regulation of *cytochrome c* and *metacaspase YCA1* genes. In addition, propolis is able to interrupt the following biological processes: the electron transport chain, oxidative stress mechanisms, autophagy and cellular responses to lack of nutrients (starvation) (de Castro et al., 2011).

3.2.2.ii Anticarcinogenic activity

In the recent years, most of the studies of propolis and its compounds have been focussed in propolis as a potential anticancer drug. Propolis has been shown to contain compound(s) with anti-proliferative activity *in vitro* when tested on cancer cell lines. Higher

concentrations of propolis (50-150 µg/mL) inhibit tumour cell growth. Although the mechanism of action of propolis is not fully understood, recently researches have associated the anticarcinogenic activity of propolis with the capacity of scavenging free radicals which is probably correlated with phenolic constituents (da Silva Frozza et al., 2013b, Umthong et al., 2011).

In addition, Valente et al. (2011) and da Silva Frozza et al. (2013) showed that propolis reduced the viability of cancer cells through induction of DNA damage and at the same time has a protective action upon primary cells. The literature suggests the selective effect of propolis may be correlated with higher proliferative index of malignant cells compared with normal cells (da Silva Frozza et al., 2013b). It is thought that propolis may have a selective antiproliferative activity. This could highlight propolis as a potential anti-cancer candidate.

3.2.2.iii Anti-inflammatory activity

The inflammation process is important in a number of pathologic conditions including venous ulcers and chronic diabetic ulcers (Búfalo et al., 2013). Mast cells are found in connective tissue and they are originated from hematopoietic stem cells. Mast cells are present in all wound healing phases. The main function of these cells is to release inflammatory mediators in areas of acute inflammation (Ng, 2010).

The effect of propolis was compared to dexamethasone, a glucocorticoid used as an immunosuppressive and anti-inflammatory

drug. It was found that propolis reduced inflammation more effectively than dexamethasone by decreasing the number of mast cells, inhibiting histamine release, prostaglandin E2 production and hydrolysis of arachidonic acid (Barroso et al., 2012). It was suggested that the mechanism of action was due to caffeic acid phenethyl ester (CAPE) and artepillin C (ARC) constituents of propolis inhibit nitric oxide and prostaglandin E2 production by inhibiting nuclear factor Kappa B (NF-κB) activity (Paulino et al., 2008).

In addition, propolis has been shown to up regulate toll-like receptor (TLRs: TLR 2 and TLR4) expression and inhibit production of pro-inflammatory cytokines such as IL-6 and IL-1β in macrophages. Whilst TNF-α and IL-10 (anti-inflammatory cytokine) production were enhanced at lower concentrations of propolis (Búfalo et al., 2014).

Moreover, it has been reported that CAPE inhibits arachidonic acid hydrolysis, and as a result, the production of prostaglandin E2 and the release of histamine by mast cells is inhibited (Barroso et al., 2012). Recently, it has been reported that artepillin C inhibits iNOS and COX-2 activity. Both enzymes are produced in the inflammation site and act synergistically, promoting an overproduction of inflammatory mediators (Sakthivel and Guruvayoorappan, 2013). iNOS is an enzyme which synthesizes nitric oxide from L-Arginine. The increasing expression of iNOS causes damage to the cells via formation of NO-reactive species. Artepillin C inhibits iNOS gene expression and thereby reduces NO levels (Sakthivel and Guruvayoorappan, 2013).

3.2.2.iv Wound healing

According to *in vivo* pre-clinical studies and histopathology evaluations (Sehn et al., 2009, McLennan et al., 2008, Berretta et al., 2012a), propolis has been reported to improve the early formation of granulation tissue, enhancing reepithelialisation, accelerating wound healing, enhancing anti-inflammatory response (Berretta et al., 2012a) and avoiding a number of septic complications (Kucharzewski et al., 2013, Sehn et al., 2009).

The first systematic study which showed the effect of propolis in a diabetic rodent model was done by (McLennan et al., 2008). The study evaluated the morphology of the wound by analysing animal skin biopsies, cellular content and myeloperoxidase activity (MPOa) (via blood vessel density measurement). The results revealed that interfollicular distances were not improved by propolis treatment, since the mechanism of action is not through wound contraction, but via re-epithelization. The number of blood vessels observed was not affected by the use of propolis. This point seems controversial because more recently pre-clinical studies lead by (Berretta et al., 2012a) pointed out that a large number of new blood vessels are present in the histological sections of propolis-treated wounds. However, despite this disagreement from both studies, authors did agree on the beneficial anti-inflammatory action of propolis and concluded that the wound healing processes can be improved by the use of propolis (McLennan et al., 2006, McLennan et al., 2008, Berretta et al., 2012a). In addition, it is known that the wound healing process involves sulphated glycosaminoglycan (GAGS) such

as, dermatan sulfates (DS), chondroitin (CS), heparin (H), heparan sulfates (Bishayee et al.), and keratan sulfates (KS). (Olczyk et al., 2013a) observed that during the initial phase of wound healing, treatment with propolis induced the accumulation of GAGS at the wound site. GAGs bind to PDGF, FGF-2 and FGF-7 growth factors preventing their degradation by proteolysis. These growth factors play a crucial role in wound reepithelialisation and granulation. Moreover, propolis has been shown to aid ECM (extracellular matrix) formation via enhancing the deposition of collagen fibres and causing an increase in the thickness of the epidermal layer on the wound site (Berretta et al., 2012a). A recent pilot clinical study in 24 patients with diabetic foot ulcers demonstrated that topical applications of propolis were well tolerated, and wound healing rates were improved considerably in the treated group. Bacterial colonization was reduced, and MMP-9 levels decreased significantly (rapid response) in the patient group treated with propolis. They concluded that propolis has a role in promoting the healing of diabetic ulcers (Henshaw et al., 2014).

In addition, it has been reported that CAPE (propolis compound) improved wound healing by enhancing keratinocyte proliferation/migration and the differentiation of myofibroblasts (Moura et al., 2011, de Almeida et al., 2013, Sen et al., 2009, Olczyk et al., 2013a).

In conclusion, the wound healing action of propolis remains unclear and controversial because of the difficulties in identifying and understanding the role of the individual bioactive components that

make up propolis and due to the poor understanding of the propolis-mediated mechanisms involved in wound healing (Sehn et al., 2009).

3.2.3 Limitations in the use of propolis

Some limitations that should be taken into account for the future use of propolis as a wound healing agent are: i) the variability in propolis chemical composition, and ii) the complexity of its composition and pharmacology. The variability of compounds and its concentration are dependent on the plant source, weather and season. As a result studies among different types of propolis cannot be simply extrapolated and batch to batch variation should be considered (Berretta et al., 2012a). Furthermore, the purification of isolated compounds is difficult and linking one compound to a specific biological activity remains a challenge. Some compounds exert biological action independently while others act synergistically (Zhang et al., 2014, Daleprane and Abdalla, 2013, Bankova, 2005). In fact, some authors have pointed out that the mix of propolis components such as flavonoids, hydroxyl acids, and sesquiterpenes may have a synergistic effect on biological activities (Vardar-Ünlü et al., 2008); therefore, the total extract may act as an "active principle" (Hori et al., 2013).

3.3 Aims and objectives

Therapeutic molecules used for wound healing need to have anti-inflammatory properties, enhance deposition of extracellular matrix compounds, possess antimicrobial effects, and enhance granulation tissue formation in which the migration of fibroblast is the pivotal step.

On the basis of the observations and background already presented above it was hypothesized that propolis and its compounds (quercetin, rutin and artepillin C) may have a beneficial effect on wound healing by i) regulating the inflammation process, ii) enhancing fibroblast proliferation and migration and iii) controlling wound infections (see Figure 3.2).

Despite the fact that propolis has been reported to have anti-inflammatory and antimicrobial properties, the motogenic effect of propolis and its compounds upon fibroblasts has not yet been investigated.

This chapter addresses the second point ii) and investigates the effect of propolis and its compounds on fibroblast proliferation and migration rates. The focus here was to evaluate propolis and its main compounds quercetin, rutin and artepillin C, as potential candidates for wound healing management.

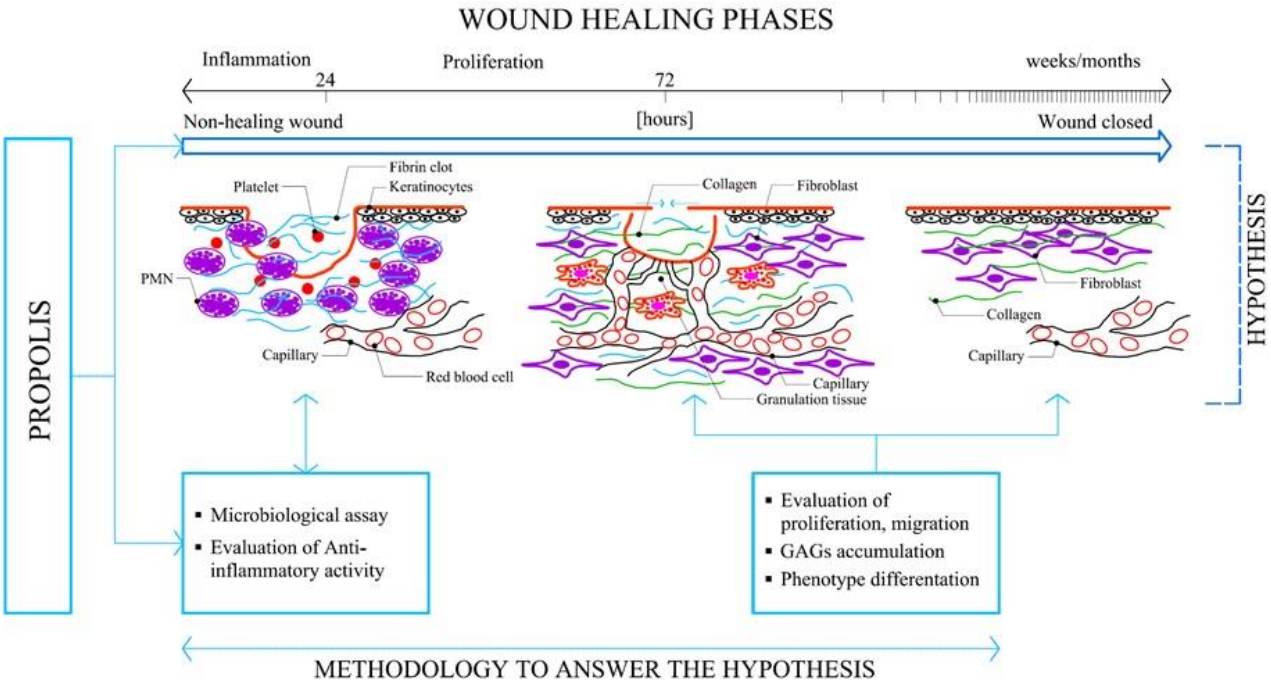


Figure 3.2 – Schematic illustrating hypothesis that shows how propolis will be tested as a wound healing candidate. It is hypothesised that propolis have a) antimicrobial, b) anti-inflammatory actions, c) enhanced GAGS accumulation, d) cell phenotype differentiation, e) enhance fibroblast proliferation and f) fibroblast migration. Where the last two actions e) and f) are a pivotal requirement for a wound healing candidate.

The main aims of this work were to:

- Assess the cytotoxic effect of propolis and its constituents (quercetin, rutin and artepillin C), on mammalian fibroblasts using AlamarBlue® assay and membrane integrity assay by double staining with Propidium iodide and Hoechst.
- Examine the influence of propolis and its compounds on fibroblast migration using *in vitro* wound scratch and Boyden chamber assays.

This investigation aims to create an innovative alternative for wound healing through the evaluation of potential natural agents like propolis and their main bioactive constituents.

3.4 Results and discussion

3.4.1.i AlamarBlue® assay of propolis and its compounds (24/48h) using 3T3 culture media (2% *(v/v)* FCS concentration)

Figure 3.3 shows relative metabolic activity (%) versus the following propolis concentrations 187, 93.5, 46.8, 23.3, 11.7, 5.8, and 2.9 (µg/mL) compared to the control (without propolis) over a period of 24 h (Figure 3.3-A) and 48 h (Figure 3.3-B) of treatment.

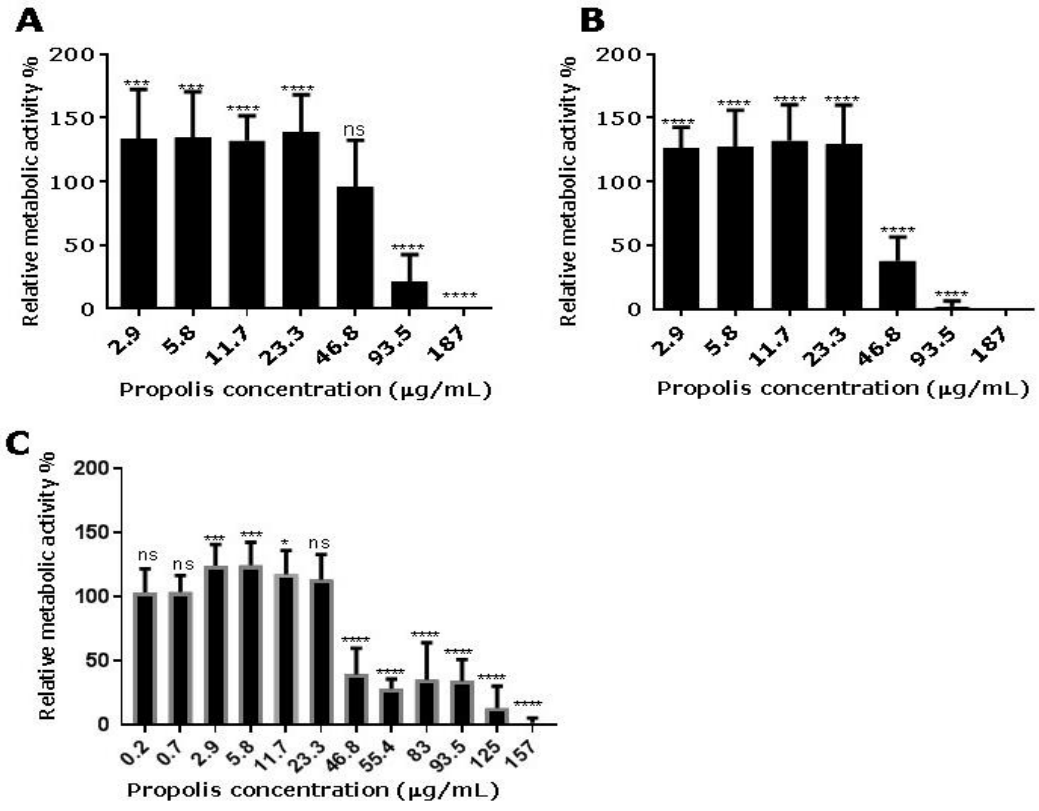


Figure 3.3 – AlamarBlue® assay after 24 h (Fig –A) and after 48 h (Fig-B). Figures show the effect of propolis on fibroblast metabolic activity in the concentration–range of 187-2.9 µg/mL with 2% -starvation culture media (DMEM supplemented with FCS 2% (*v/v*)), three independent experiments carried out in triplicate (means±SD). Fig-C shows the effect of propolis after 48 h including additional concentration-range. Five independent experiments carried out in triplicate (means±SD).

Overall, the results show that the cytotoxic effect of propolis was more prominent at 48 h than 24 h post treatment. Cells exposed to propolis at a concentration of 46.8 µg/mL at 48 h showed a percentage of relative metabolic activity (%) reduced to lower than 40% of the control while that at 24 h, at the same concentration of propolis, was around 100%. Also, at a concentration of 93.5 µg/mL, at 24 h relative metabolic activity (%) is around 20% while at 48 h this percentage decreased to approximately 2%. In terms of statistical significance, at 24 h and at a concentration of 46.8 µg/mL there was no significant inhibition or enhancement of relative metabolic activity (%) whilst at 48 h, cell metabolic activity is significantly inhibited. These results suggest that propolis has a time-dependent effect upon fibroblast viability. These results are in agreement with previous investigations (Valente et al., 2011, de Funari et al., 2007, da Silva Frozza et al., 2013a) which pointed out that propolis has a time-dependent effect on relative metabolic activity (%). (Bufalo et al., 2009) pointed out that the effects of propolis were more prominent after 24 h of exposure which supports the findings of this study where cytotoxicity at higher concentrations of propolis (187 µg/mL) were seen after 24 h whereas at lower concentrations (46.8 µg/mL), cytotoxicity was only seen following 48 hours exposure.

Furthermore, additional propolis solutions were prepared, expanding the concentration-range as follow: 187, 125, 93.5, 83, 55.4, 46.8, 23.3, 11.7, 5.8, 2.9, 0.7, 0.2 µg/mL and a control (the diluent without propolis). Figure 3.3-C reveals the effect of propolis on 3T3 fibroblast

cells over 48 h using these additional propolis solutions. A minimum of 5 independent experiments were performed in triplicate. The data showed that higher propolis concentrations, between 46.8 µg/mL to 187 µg/mL, had an extremely significant ($p < 0.0001$) inhibitory effect on relative metabolic activity (%) compared to the cells exposed to the control sample. At 187 µg/mL propolis, only ~ 2% of cells remained metabolically active. In contrast, cells exposed to propolis concentrations 2.9 to 5.8 µg/mL showed to significantly enhanced 3T3 fibroblast metabolic activity ($p < 0.0001$), reaching values around 120% of the control. The percentage of relative metabolic activity (%) exceeded 100% because the data were normalized to mean control values. In the concentration range of 0.7 to 0.2 µg/mL propolis, no statistical significance in terms of relative metabolic activity (%) was found when compared with the control.

In the work reported here, propolis showed a dose-dependent cytotoxic effect on the 3T3 fibroblasts; an enhancing effect on relative metabolic activity (%) at lower concentrations of (2.9 and 5.8 µg/mL), while higher concentrations (83-187 µg/mL) were cytotoxic. The effect of propolis on fibroblast metabolic activity was time dependent; over 48 h post treatment effects were more prominent than 24 h of treatment.

These results were in agreement with those obtained by (de Funari et al., 2007) who evaluated the effect of another green propolis sample on in NIH-3T3 fibroblasts. *In vitro* studies, revealed that propolis concentrations ranging from 31.25 to 125 µg/mL led to cell death while lower concentrations of propolis (between 7.8 and 2.9 µg/mL)

revealed no significant effect upon relative metabolic activity (%) (de Funari et al., 2007). There are however a limited number of publications reporting non-cytotoxic effect at low concentrations on fibroblasts. To date, most studies of propolis are focussing as a potential anticancer drug; i.e. evaluation of cytotoxicity effect on malignant cell types and understanding the mechanism of its action using a concentration range up to 100 µg/mL. The cytotoxic effect of higher concentrations of propolis on mammalian cells reported here were in agreement with (Carvalho et al.) (2014) and (Barbarić et al., 2011) who showed a similar effect when propolis was tested on malignant cells. The findings showed that higher concentrations of propolis (around 76 µg/mL) significantly inhibit malignant cell proliferation due to the synergistic action of phenolic acid and flavonoids contained in propolis which lead to cell death via apoptosis.

Figure 3.4 reveals the effect of commercial quercetin (Sigma), one of the bioactive compounds of propolis, upon 3T3 fibroblast metabolic activity. Cells were treated with quercetin concentrations of 100, 30, 10, 3, and 1 (µM) and compared to the control (without quercetin) over a period of 24 h (Figure 3.4-A) and 48 h (Figure 3.4-B) of treatment.

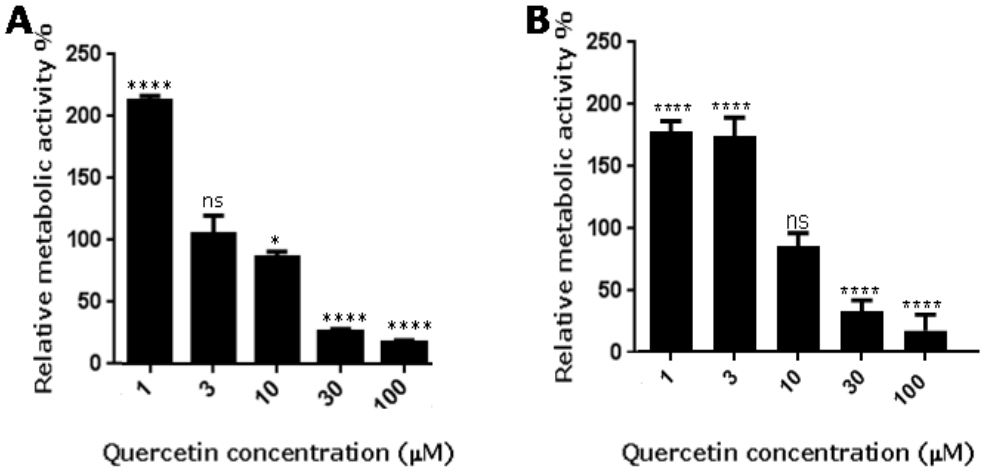


Figure 3.4 - AlamarBlue® assay 24 h (Fig –A) and after 48 h (Fig-B). Figures show the effect quercetin on fibroblast metabolic activity in the concentration–range of 1-100 µM with 2%-starvation culture media. Five independent experiments carried out in triplicate (means±SD).

Overall, quercetin affects relative metabolic activity (%) in a dose-dependent manner. Higher concentrations (100 and 30 μM) of quercetin had an extremely significant ($p \leq 0.0001$) detrimental effect upon the relative metabolic activity (17% and 35% respectively) of the fibroblasts. By contrast, lower concentrations (1 and 3 μM) of quercetin did show a significant enhancement of relative metabolic activity (%) ($p, \leq 0.0001$), metabolic activity exceed 180% over 48 h under quercetin treatment

The results show that the effect of quercetin upon fibroblasts metabolic activity was more prominent at 48 h than 24 h, at lower concentration. Fibroblasts exposed to quercetin at a concentration of 3 μM showed substantially increased in metabolic activity from 100% to 180% after 48 h. Oppositely, concentrations of 30-100 μM of quercetin showed a detrimental effect on metabolic activity over 24 h and 48 h of treatment. Metabolic activity values were under 25% over this period of time. Previous studies using quercetin found that concentrations of up to 25 μM had cytotoxic effect and could activate different signal transduction pathways such as receptor-mediated signalling and module oestrogen receptor alpha (ER-a)-mediated cell cycle arrest and an anti-proliferative effect through p-38 kinase and caspase-3 activation (Bulzomi et al., 2012, Bishayee et al., 2013).

Figure 3.5 shows the effect of commercial rutin (Sigma), an analogue of quercetin, upon 3T3 fibroblast metabolic. Rutin was tested at concentrations of 200, 100, 30, 10, 3, and 1 (μM) and compared to the control (without rutin) over a period of 24 h (Figure 3.5-A) and 48 h (Figure 3.5-B) treatment.

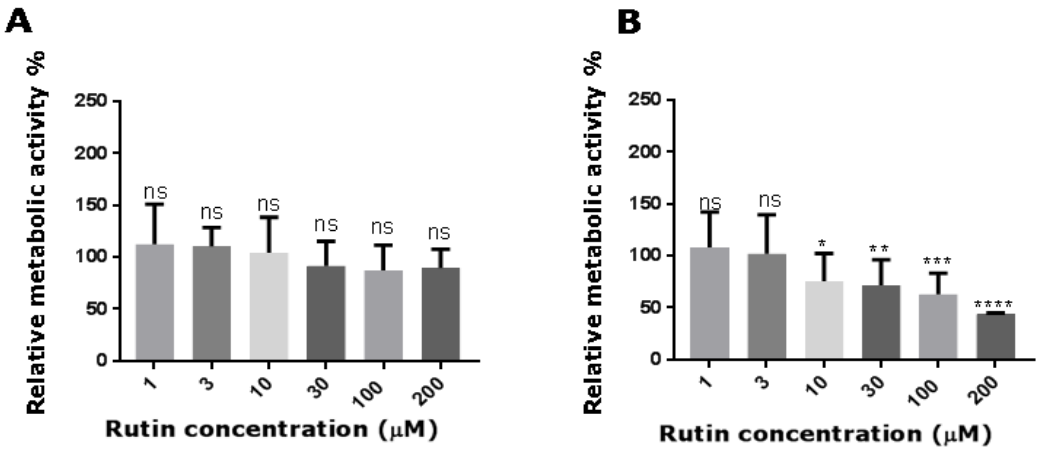


Figure 3.5 - AlamarBlue® assay after 24 h (Fig –A) and after 48 h (Fig-B). Figures show the effect rutin upon fibroblast viability in the concentration–range of 1-100 μM with 2%-starvation culture media. Five independent experiments carried out in triplicate (means±SD).

Overall, rutin did not show any statistically significant beneficial or detrimental effect upon the metabolic activity of the fibroblasts after 24 h of treatment. In general, after 48 h rutin effects fibroblast metabolic activity in a dose-dependent manner. Rutin concentration from 10 μM to 200 μM cause a detrimental effect on the metabolic activity of the fibroblasts. Statistical significance values vary from $p \leq 0.05$ (10 μM) to $P \leq 0.0001$ (200 μM) and metabolic activity decreased from 76% (10 μM) to 44% (200 μM) (Figure 3.5).

Rutin, is a flavonol glycosides present in propolis that is claimed to have multiple pharmacological activities (Chua, 2013), such as wound healing properties (Tran et al., 2011). For this reason, the cytotoxic effect of rutin upon murine fibroblast over 48 h was tested by measuring metabolic activity. The findings reported here revealed a dose dependent manner to inhibit fibroblast metabolic activity. Rutin concentration from 10-200 µM had an unfavourable effect, decreasing metabolic activity. In general, the results presented here are in agreement with the findings reported by (ben Sghaier et al., 2016) who indicated that rutin inhibits cell viability in a dose-dependent manner (*in vitro*) and different cell types have a different sensitivity. For instance, human lung cancer cell (a549) were inhibited at rutin concentrations from 31.25 µM while other cancer cell lines such as colon (HT29 and Caco-2) were inhibited using higher concentration of rutin (388 and 559 µM respectively). On the contrary, *in vitro* studies of rutin-chitosan hydrogel reported by (Tran et al., 2011) showed that rutin concentration of 144 µM enhanced proliferation of L929 mouse fibroblasts.

Finally, Figure 3.6 reveals the effect of commercial artepillin C (ARC), one of the major bioactive compounds of green propolis (from Brazil), upon 3T3 fibroblast metabolic. Artepillin C concentrations was tested at concentrations of 100, 50, 30, 10, 3, and 1 (μM) and compared to the control (without ARC) over a period of 24 h (Figure 3.6-A) and 48 h of treatment (Figure 3.6-B).

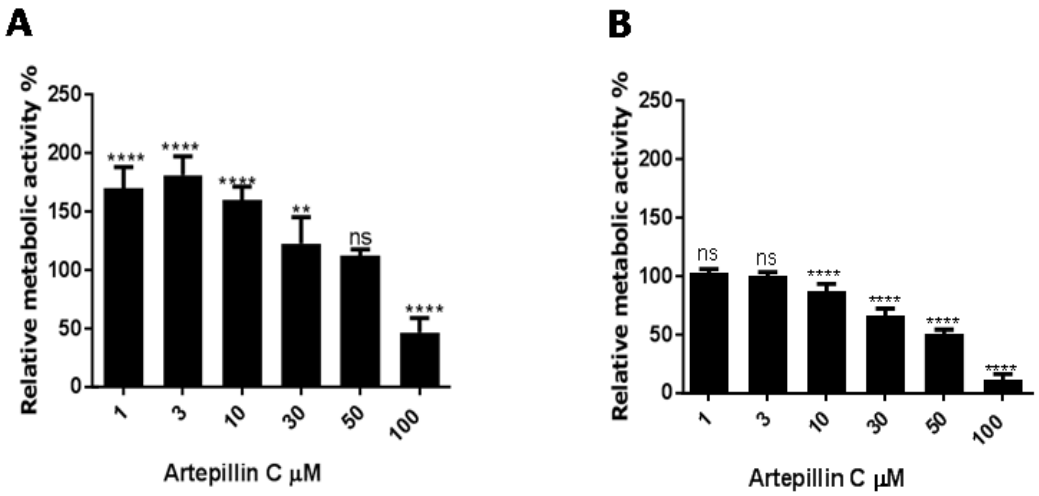


Figure 3.6 - AlamarBlue® assay after 24 h (Fig –A) and after 48 h (Fig-B). Figures show the effect artepillin C on fibroblast metabolic activity in the concentration–range of 1-100 μM with 2%-starvation culture media. Three independent experiments carried out in triplicate (means±SD).

On the whole, artepillin C (ARC) showed to affected fibroblast metabolic activity in a dose depended-manner. The enhancing in relative metabolic activity % was significant ($p \leq 0.0001$) for lower concentration of ARC (1-10 μM) after 24 h treatment, reaching values between 180-160% from ARC concentration 1-10 μM. Fibroblast metabolic activity significantly decreased ($p \leq 0.0001$), reaching values of 47% at 100 μM of ARC treatment. After 48 h of treatment, fibroblast metabolic activity continued being affected in a dose-dependent manner. Higher concentrations (100 to 10 μM) of ARC showed a significant ($p \leq 0.0001$) detrimental effect upon fibroblast

relative metabolic activity reducing values from 87% (10 µM) to 12% (100 µM). By contrast, lower concentrations (1 and 3 µM) of ARC did not significantly ($p>0.05$) enhance relative metabolic activity (%) over 48 h of treatment

Overall, these results showed that the detrimental effect of higher concentrations of ARC on fibroblasts was more prominent over 48 h of treatment. Unexpectedly, the observed beneficial effect in metabolic activity of fibroblast at lower concentration of ARC at 24 h decayed over 48 h of treatment. Artepillin C is a phenolic acid exclusively found in Green propolis, with. similar effects as CAPE from European propolis (Wadhwa et al., 2016). Overall, the results from artepillin C show clearly that at concentrations 10-100 µM this compound has a prominent inhibition effect on fibroblasts' metabolic activity (after 48 h of treatment). Moreover, artepillin C has showed to inhibit cell growth in a dose-dependent manner by entry to the cell cycle arrest G_o/G_1 (Shimizu et al., 2005 , Kumazaki et al., 2014).

3.4.2 Membrane integrity assay

The effect of propolis and its compounds quercetin, rutin and artepillin C, upon cell membrane integrity was evaluated by double cell staining using Propidium Iodide and Hoechst. Figure 3.7-A shows a membrane integrity assay conducted by incubating cells with 3 different concentrations of propolis: 187, 46.8 and 2.9 µg/mL and additional positive (Triton) and negative ('2%-starvation culture media') controls for 48 h. Figure 3.7-B shows percentages of PI positive cells exposed to three different concentration of propolis with their respective controls. The graph reveals that the differences between the concentrations of propolis at 2.9 ug/mL, 46.8 ug/mL and control were not statically significant. The percentage of PI positive cells was around 30%. Contrary to this, cells exposed to higher concentrations of propolis (187 µg/mL) exhibited around 73% of PI positive cells. Cells exposed to Triton also exhibited a higher percentage of PI positive cells, over 100% (cell counting images analysis). Figure 3.7-C shows the effect of propolis concentrations 187, 46.8 and 2.9 µg/mL in term of cell number by measuring cell stains with Hoechst. It was observed the cell number is reduced in a dose–dependent manner. Higher propolis concentration (46.8 and 187 µg/mL) did show a significant detrimental effect upon fibroblasts number.

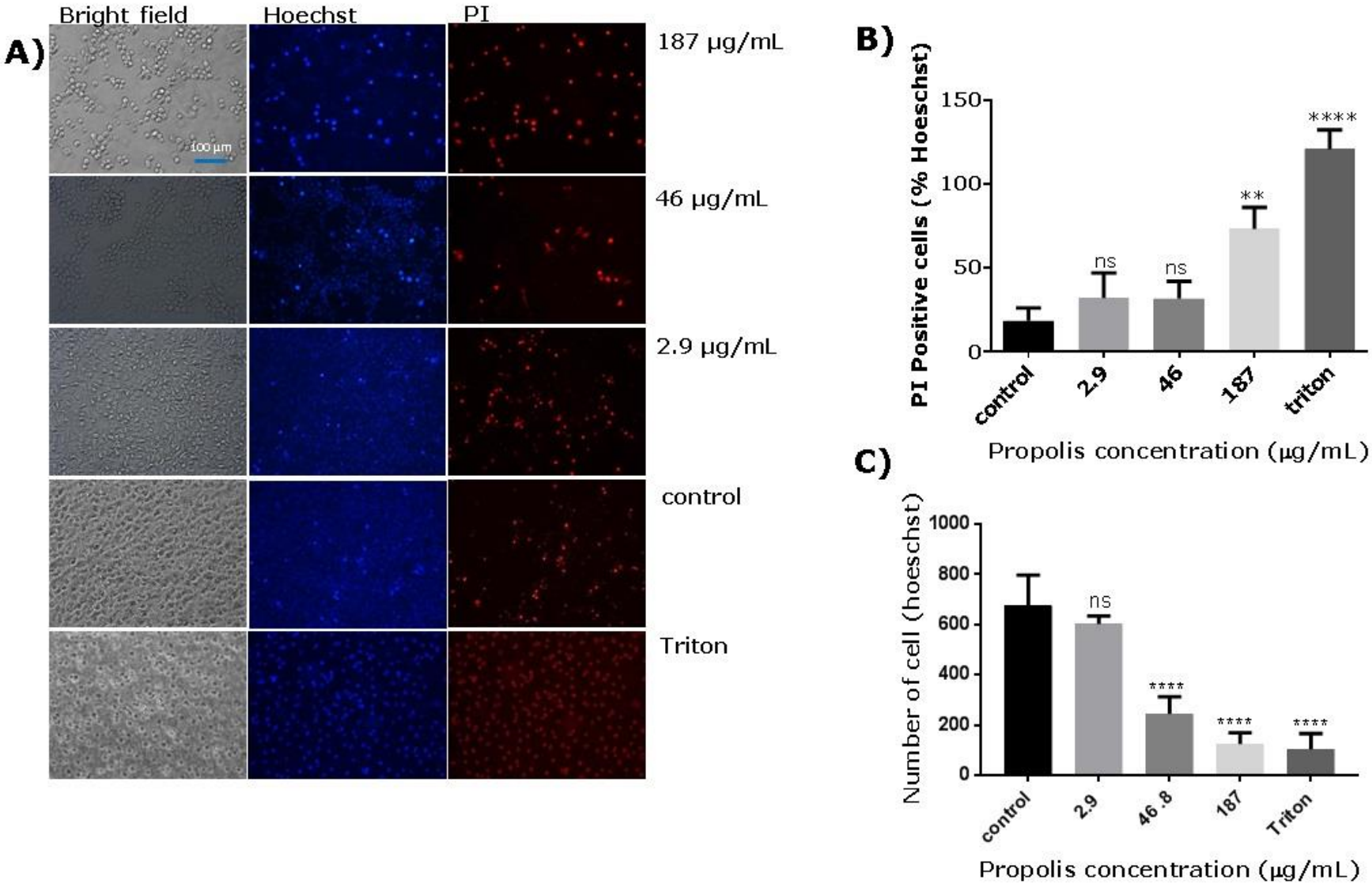


Figure 3.7 - Membrane integrity assay. Hoechst /Propidium Iodine double stain. (Fig-A) Cell was cultured by 48 h with propolis. Fluorescence microscopy (Magnification, ×10) bars 100 µm bright field, cells with Hoechst and cell stained with PI at the same view. Cell double stained indicated cell death. (Fig-B). Show PI positive cell (% Hoechst) using image cell counting after 48 h of propolis treatment. Three independent experiments carried out in triplicate (means±SD).

The resulted presented here are very similar to the ones obtained by measuring metabolic activity thought AlamarBlue® assay. Both assays showed that propolis affects metabolic activity and cell numbers in a dose dependent manner. Membrane integrity assay confirmed that higher concentrations of propolis (187 µg/mL) exerted a toxic effect, leading to cell death and inhibition of cell numbers.

A possible explanation for the cytotoxic effect upon fibroblast cells shown here and supported from previous studies may be explained by the fact that propolis has the capacity to interfere in the cell cycle. Studies of the cell cycle phase distribution using flow cytometry revealed that exposing cells to a propolis extract induced G2/M arrest in B16F10 cells (musculus skin melanoma) prior to DNA damage inducing apoptosis (Novak et al., 2014). In addition, propolis decreased cell proliferation and supressed invasion and migration by blocking specific signalling pathways (i.e β-catenin, c-myc, NF-κB and some intermediary of the PI3K/AKT pathway), increasing apoptosis and inhibiting angiogenesis (Chan et al., 2013).

Figure 3.8-A shows a membrane integrity assay conducted by incubating cells with 3 different concentrations of quercetin (100, 10 and 1 μM). It was noticed that control cells and fibroblast exposed to lower concentration of quercetin (1μM) were well attached and spread on the plate surface maintaining cell to cell contact. In comparison, the fibroblasts exposed to a higher concentration of quercetin (10-100 μM) were more spherical and there were no visible cell-cell contacts.

Fibroblasts exposed to lower concentrations of quercetin (1-10 μM) exceeded percentages of PI positive cells by 10% and no statistical significance regarding their control was found. Contrary to this, cells exposed to higher concentrations of quercetin (100 uM) exhibited 64% of PI positive cells. Cells exposed to Triton also exhibited a higher percentage of PI positive cells, 95% (cell counting images analysis) (Figure 3.8-B). Figure 3.8-C shows the number of total cells exposed to three different concentrations of quercetin (100, 10 and 1 μM) with their respective controls. The graph reveals no significant difference in terms of the numbers of cells between quercetin concentration 1 μM and its control (~600 number of cells). The number of total cells was significantly reduced when quercetin concentration was increased from 10 to 100 μM, reaching values from 200 to 60 number of cells respectively. Comparing the effect of quercetin on fibroblast metabolic activity % and cell number (double stained assays) it was noticed that both assays showed a detrimental effect on fibroblasts at quercetin concentration from 10-100 μM while lower quercetin concentration exerted no detrimental effect on cells.

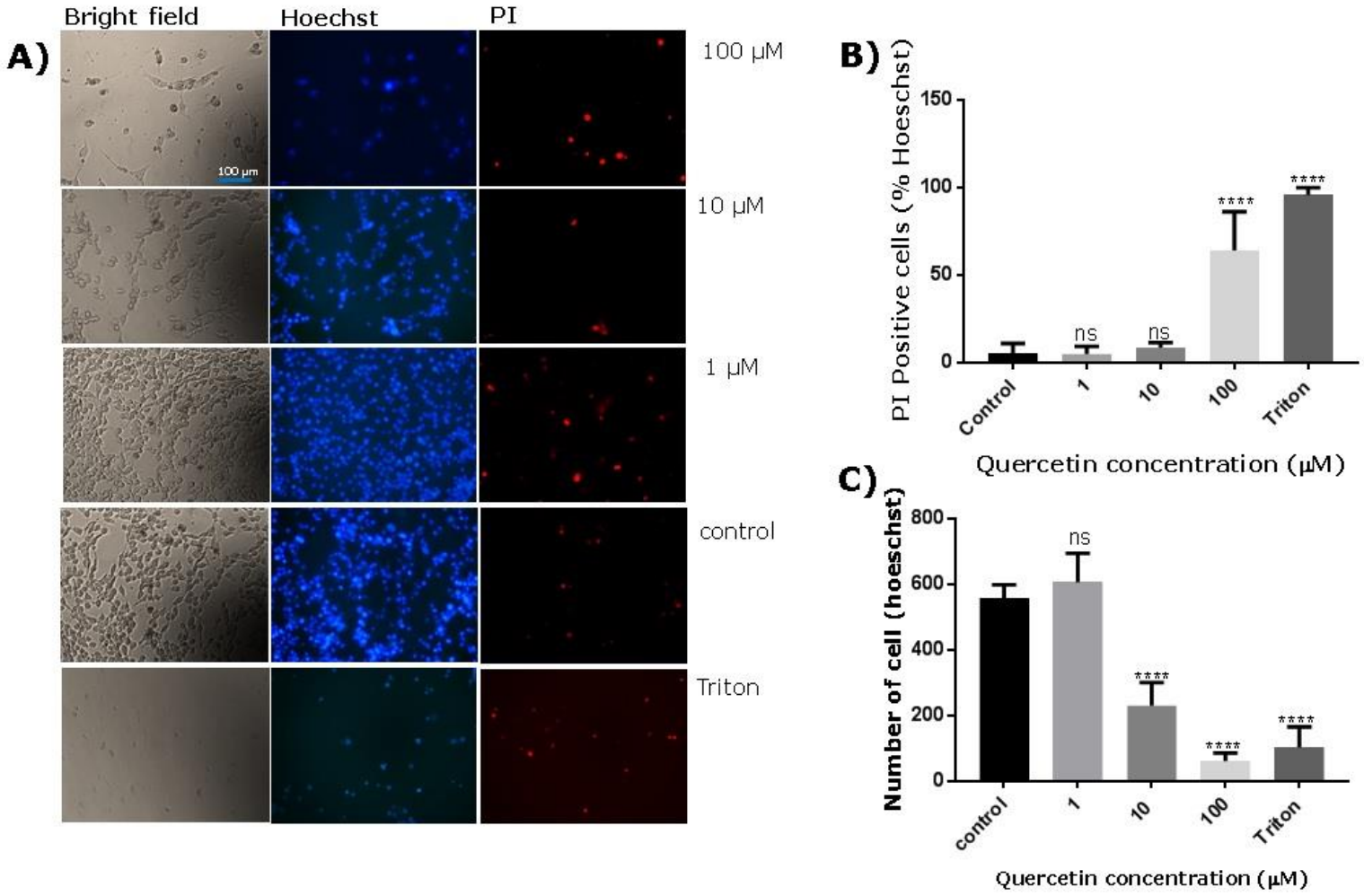


Figure 3.8 - Membrane integrity assay. Hoechst /Propidium Iodine double stain. (Fig-A) Cell was cultured by 48 h with quercetin. Fluorescence microscopy (Magnification, ×10) bars 100 µm bright field, cells with Hoechst and cell stained with PI at the same view. Cell double stained indicated cell death. (Fig-B) Show PI positive cell (% Hoechst) using image cell counting after 48 h of quercetin treatment. (Fig-C). Total cell number stained with Hoechst and measured using image counting. Two independent experiments carried out in triplicate (means±SD).

In the present report, membrane integrity assay confirmed that higher concentration of quercetin (100 μM) increased cellular damage and reduced cell viability. A similar dose–dependent cytotoxic effect was observed by (Borska et al., 2012) and (Bulzomi et al., 2012) in cancer cell lines (e.g., breast, prostate and gastric). Also, quercetin has been reported to induce changes in cell morphology, nucleosome fragmentation and cell detachment from the substrate (Bishayee et al., 2013).

Figure 3.9- A shows a membrane integrity assay conducted by incubating cells with 4 different concentrations of rutin (200, 100, 10 and 1 μM). Overall, at bright field observation, control fibroblasts had an elongated flattened form and some cell-to-cell contact was observed. In contrast, fibroblasts exposed to rutin concentrations from 1-100 μM appeared more spherical. In samples exposed to 100 μM of rutin cellular debris was noticed. Also it is interesting that at the highest rutin concentration of 200 μM fibroblasts presented similar features as the control. Figure 3.9-B fibroblasts exposed to concentrations of rutin from 1-200 μM exceeded percentages of PI positive cells around 10% and no statistical significance regarding their control was found. Unexpectedly, PI positive cells % at concentration 100 μM was equal to the rest of the sample regardless of the debris found in those samples. Cells exposed to Triton exhibited a higher percentage of PI positive cells, 95%. Figure 3.9-C shows the number of total cells exposed to four different concentrations of rutin with their respective controls. No significant difference was found in terms of number of cells between rutin concentration (1-200μM) and its control. Comparing the effect of these four concentrations of rutin upon murine fibroblast metabolic activity and cell number, it is clear that fibroblast metabolic activity is significantly affected after 48 h of rutin treatment from concentrations 10-200 μM, while the numbers of cell did not reveal a significant reduction.

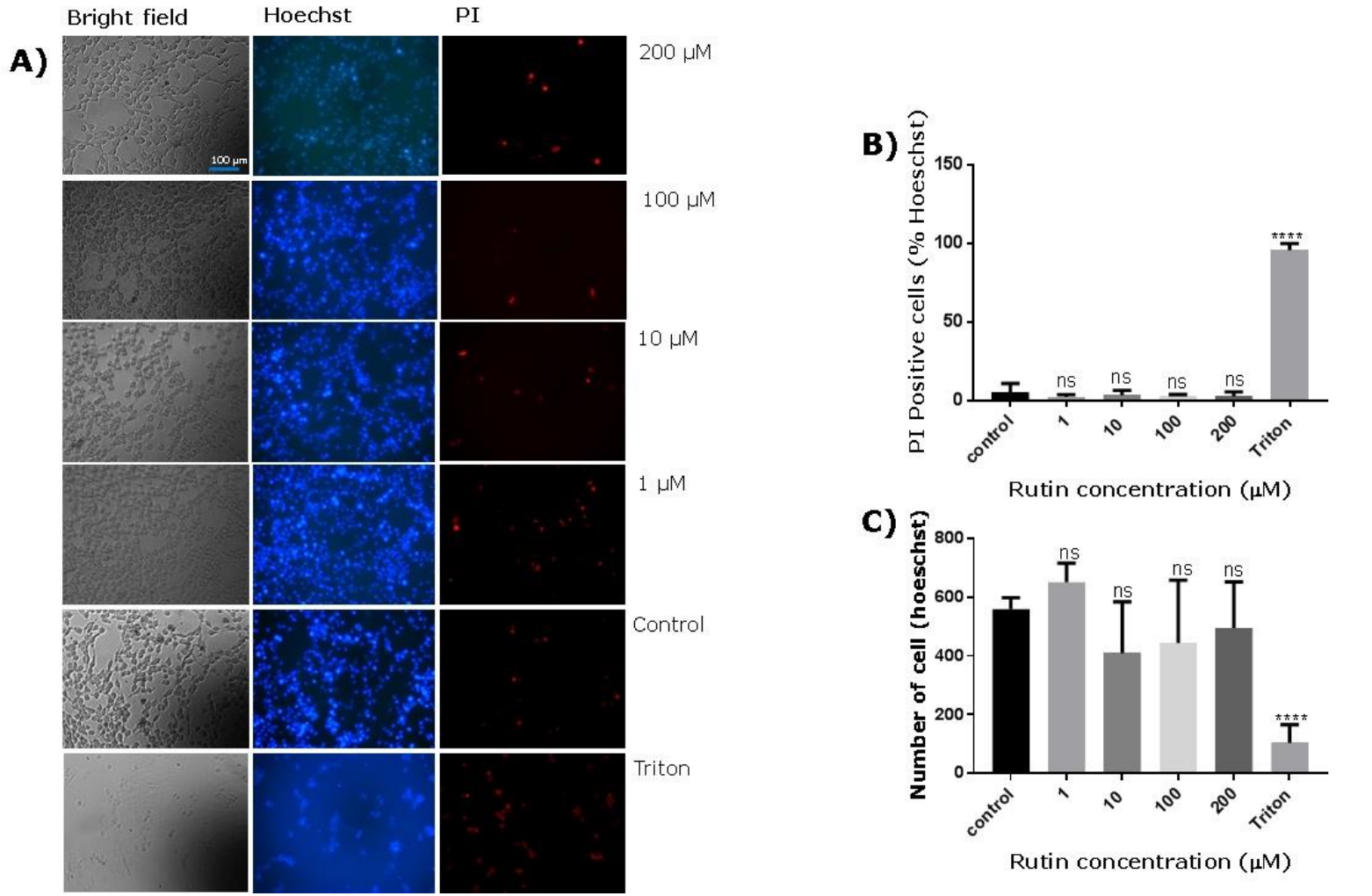


Figure 3.9 - Membrane integrity assay. Hoechst /Propidium Iodine double stain. (Fig-A) Cell was cultured by 48 h with rutin. Fluorescence microscopy (Magnification, ×10) bars 100 µm bright field, cells with Hoechst and cell stained with PI at the same view. Cell double stained indicated cell death. (Fig-B) Show PI positive cell (% Hoechst) using image cell counting after 48 h of rutin treatment. (Fig-C). Total cell number stained with Hoechst and measured using image counting. Two independent experiments carried out in triplicate (means±SD).

Moreover, membrane integrity assay presented here did not reveal any significant cell damage (% of positive PI cells), including exposition of fibroblast to high concentration of rutin (100-200 µM). These results seem to disagree with the metabolic activity result (AlamarBlue®). A possible explanation for this inconsistency between assays, is the fact that AlamarBlue® assay measures cell metabolic activity while double stain HOE and PI assay measures the total number of cells and damaged cells in a death late stage (PI positive cells). While metabolic activity was reduced by the action of rutin, cell membrane damage was not detected perhaps due to the cells having been in an early apoptotic stage and not being permeable to PI (Warnes, 2016).

On the whole, quercetin has showed a more potent effect upon fibroblasts reducing metabolic activity to under 50% and damaging the membrane at doses between10-100 µM while rutin inhibited metabolic activity at higher range of doses 100-200 µM. Also the percentage of metabolic activity did not go below 50% when the fibroblasts were exposed to rutin, and not significant cell damage was revealed. Regarding this point, previous studies show that rutin (quercetin3-O-rutoside) and quercetin are chemically analogue. The additional glucoside group in rutin (rutoside) has been reported to attenuate the apoptotic activities compared with quercetin (Chow et al., 2005).

Figure 3.10- A shows a membrane integrity assay conducted to test 3 selected concentrations of artepillin C (100, 10 and 1 μM). Overall, at bright field observation, control fibroblasts and cells exposed to artepillin C (ARC) concentration 1 μM did not show any evidence of detrimental effect upon fibroblast, a normal phenotype as well cell-to-cell contact was observed. By contrary, fibroblasts exposed to ARC concentrations from 10-100 μM appeared more spherical. In addition, the same cells were stained with PI indicating that the cell membrane was damaged. Figure 3.10-B fibroblasts exposed to concentrations of ARC 1-10 μM exceed percentages of PI positive cells around 1% and no statistical significance regarding their control was found. A significant increase on PI positive cells was found when cells were exposed to ARC concentration 10-100 μM, reaching values PI % of 7 and 20% respectively.

Figure 3.10-C reveals that the total number of cells decreased in a dose-dependent manner. The lowest concentration did not have a significant effect on cell number (ns) compared with its control. Fibroblasts exposed to ARC 10 μM did not show any significant detrimental effect on cell numbers compared with its control. On the contrary, ARC concentrations of 100 μM had a significantly detrimental effect on fibroblast numbers, decreasing the total number cells to 200.

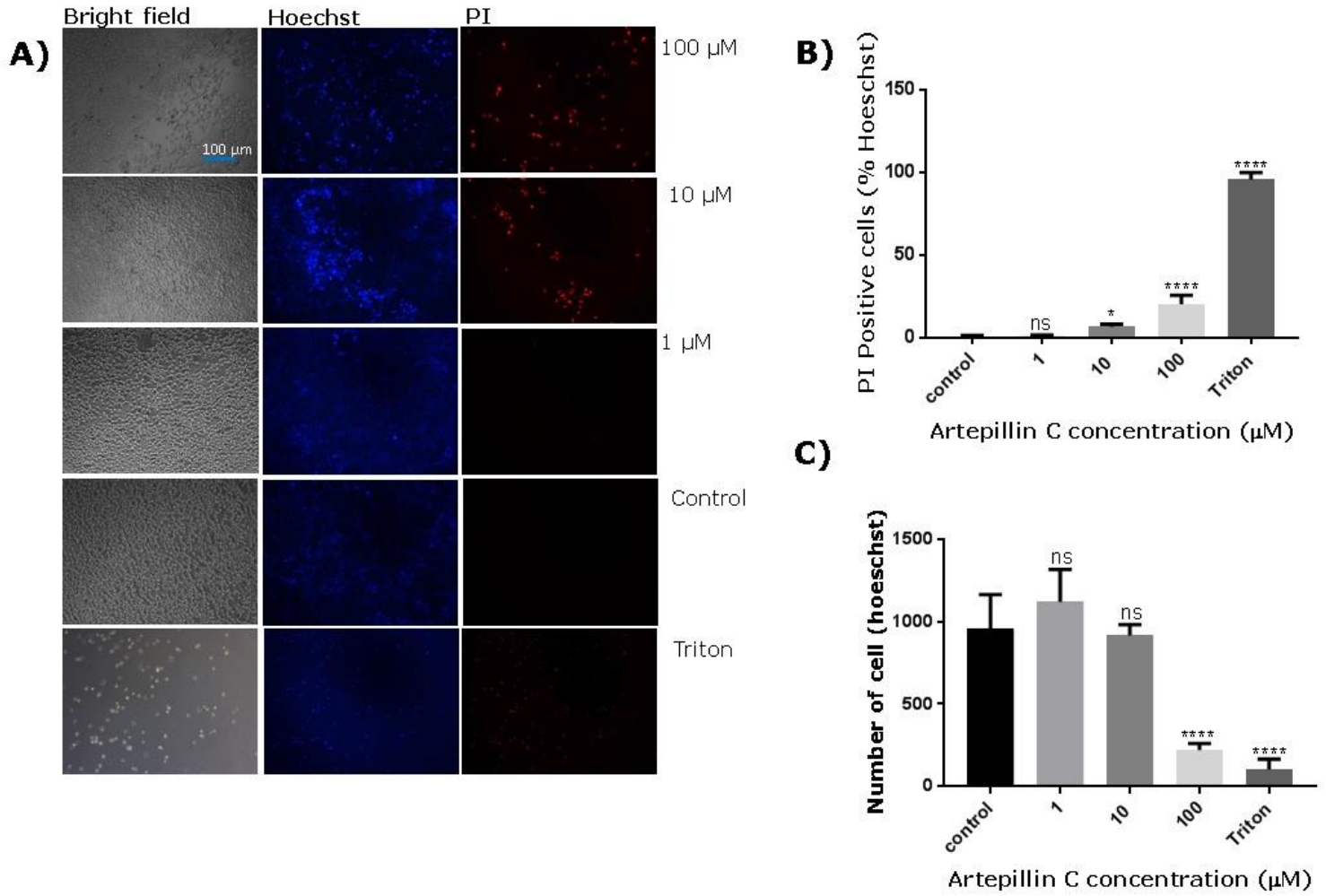


Figure 3.10 - Membrane integrity assay. Hoechst /Propidium Iodine double stain. (Fig-A) Cell was cultured by 48 h with artepillin C. Fluorescence microscopy (Magnification, ×10) bars 100 µm bright field, cells with Hoechst and cell stained with PI at the same view. Cell double stained indicated cell death. (Fig-B) Show PI positive cell (% Hoechst) using image cell counting after 48 h of artepillin C treatment. (Fig-C). Total cell number stained with Hoechst and measured using image counting. Two independent experiments carried out in triplicate (means±SD).

Comparing the effect of artepillin C on murine fibroblast metabolic activity % measured with number of cells, it was noticed that metabolic activity was unfavourable 48 h of artepillin C (10-100 μM) treatment while the number of cells was reduced, and membrane integrity affected at 100 μM.

Membrane integrity revealed that ARC concentration of 100 μM conduced the cells to death and reduced their number. Supporting this finding the literature has reported that ARC concentration from 3-50 μM, had inhibitory effect upon endothelial cells in a concentration-dependent manner and so exerted an anti-angiogenesis effect (Messerli et al., 2009). Rutin and quercetin exert an anti-cancer action by decreasing ROS production, which protects cells from damage caused for oxidative stress. The same flavonoids has been reported to block cell cycle, inducing apoptosis and caspase3 activity as well as the inhibition of VEGF factor production (ben Sghaier et al., 2016). At the same time, (Messerli et al., 2009) suggested that ARC block Pak1 signalling. Early evidence showed that ARC prevents oxidative damage by suppressing membrane lipid peroxidation and oxidation of intracellular DNA (Shimizu et al., 2004).

.

3.4.3 Assessment of wound closure following exposure to propolis and its compounds

Figure 3.11 shows the effect of green propolis on fibroblast migration using scratch assays and time-lapse microscopy. Figure 3.12 shows quantitative analysis of images, showing the percentage of the scratch covered after 9 h, 24 h, and 48 h. The data showed that propolis has a time and dose-dependent effect on NIH- 3T3 fibroblast migration. After 9 h post scratch, higher and lower concentrations of propolis did not show significant enhancement or inhibition on cell migration (Figure 3.12-A). In terms of scratch covering %, all samples showed a wound closed under 15%. Figure 3.12–B shows the effect of propolis on cell migration over 24 h. The action of propolis from 2.9-187 µg/mL upon fibroblast migration was not statistically significant. Figure 3.12-C shows the effect of propolis on fibroblast migration after 48 h of treatment. Exposure to propolis at lower concentrations (11.7-2.9 µg/mL) did not significantly enhance cell migration. By contrary, exposure to higher concentrations of propolis (187-93.5. µg/mL) significantly inhibited cell migration ($p \leq 0.01$).

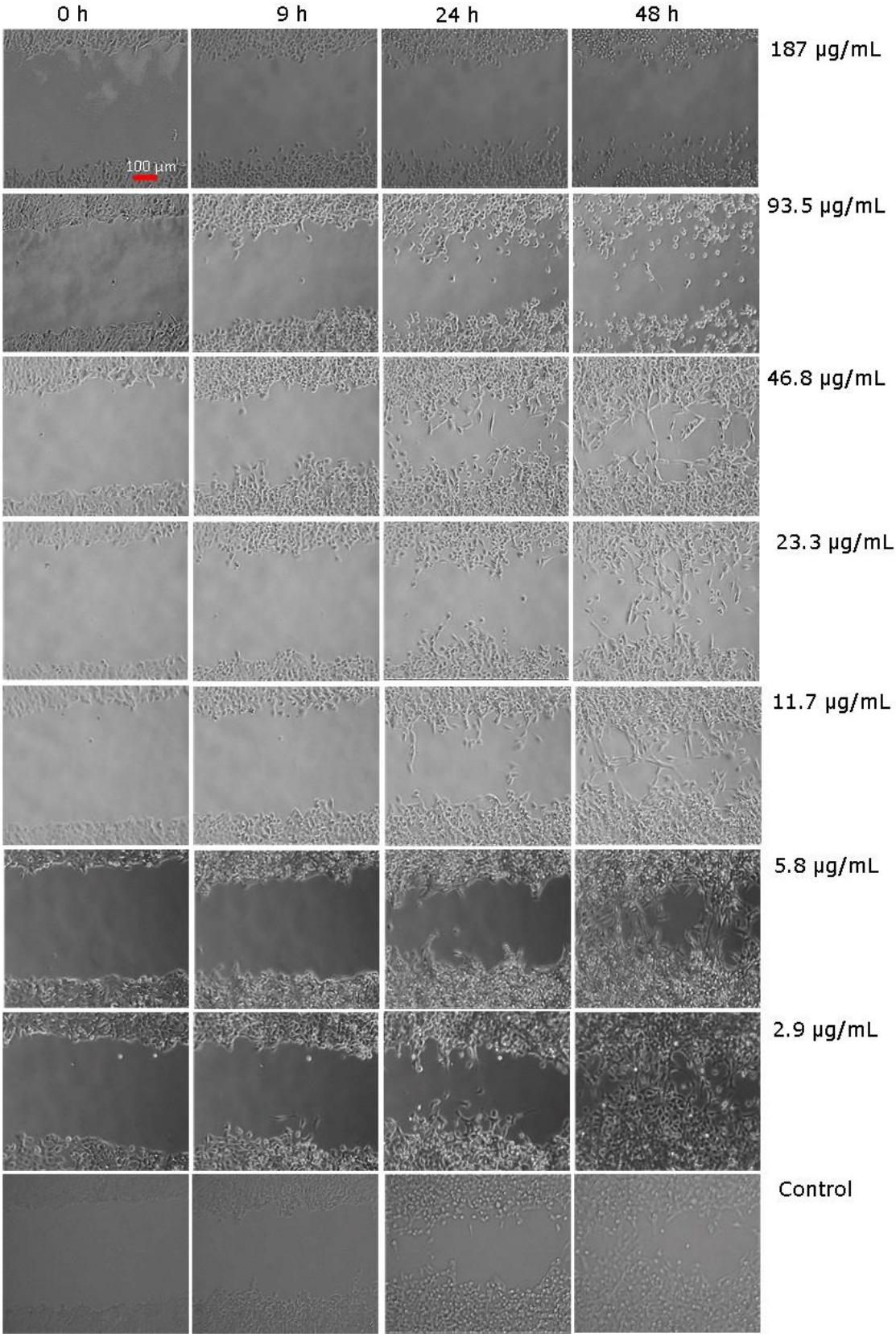


Figure 3.11 - Effect of Green propolis 187-2.9 µg/mL concentrations on fibroblast migration-*in vitro* scratch assay. Fig. Shows phase contrast micrographs taken using time-lapse microscopy during 48 h (Magnification, ×10) bars 100 µm**.**

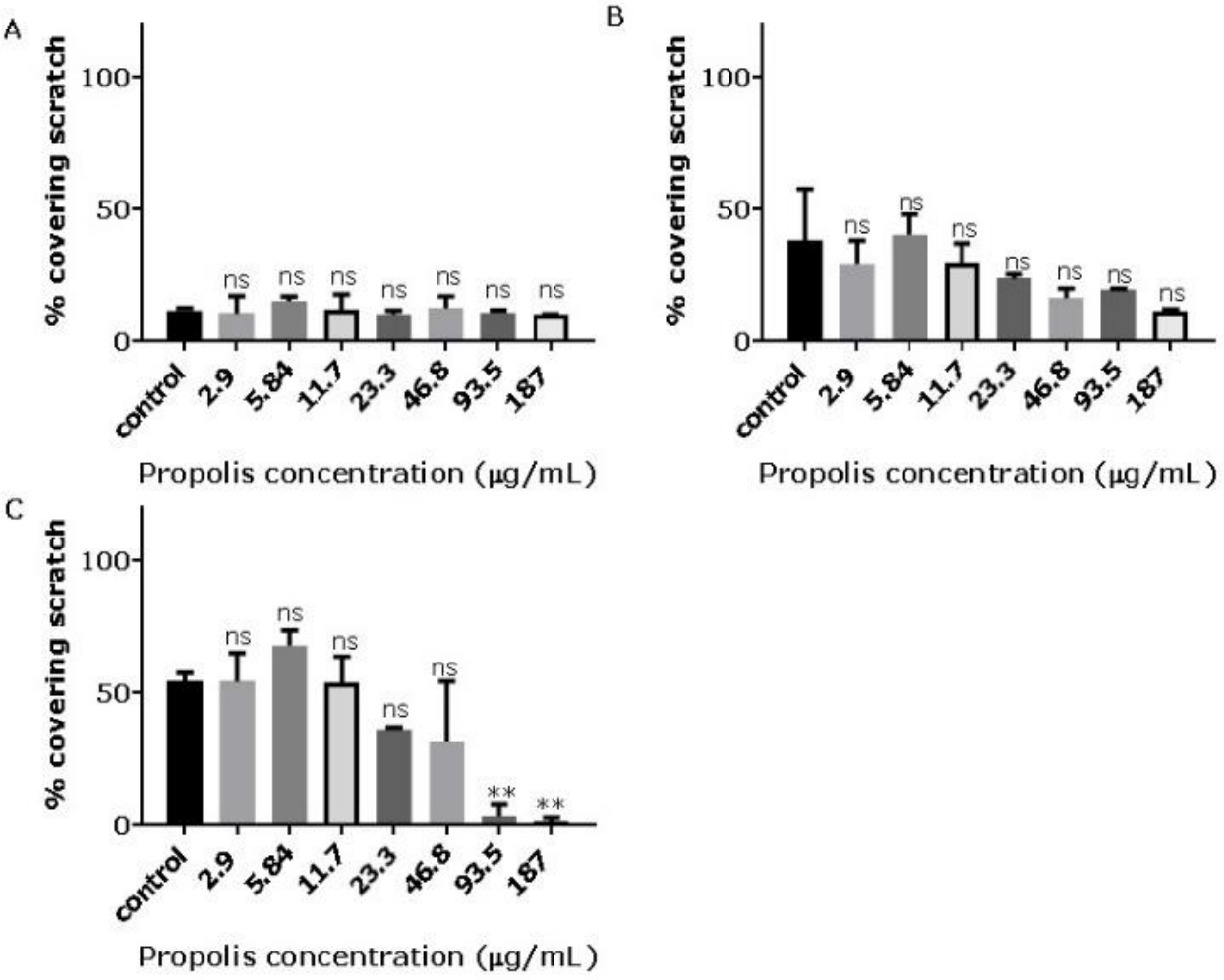


Figure 3.12 - Effect of propolis on fibroblast migration-*in vitro* scratch assay. Fig A- shows the % of covering scratch after 9h. B) after 24h C) 48h post scratch wound using time-lapse microscopy. Percentage of covering. Three independent experiments carried out in triplicate (means±SD).

Figure 3.13 shows the effect of commercial quercetin on fibroblast migration using scratch assays and time-lapse microscopy. Figure 3.14 shows the percentage of the scratch covered after 9 h, 24 h, and 48 h. After 9 h post scratch, only higher concentration of quercetin 30 and 100 μM exceed significant inhibition action against cell migration reaching values of 14 and 7% respectively, lower than theirs control which had 20% of covered area (Figure 3.14-A). Figure 3.14-B shows the effect of quercetin after 24 h post scratch. Lower concentrations of quercetin (1-10 μM) did not show significant enhancements on cell migration. In contrast, fibroblasts exposed to quercetin concentrations of 30-100 μM exerted a significant detrimental effect upon cell migration ($p \leq 0.05$ and $p \leq 0.0001$), reaching wound closure values between 30-10%. Figure 3.14-C shows the effect of quercetin upon fibroblast migration after 48 h. Exposure to quercetin at lower concentrations (1-3 μM) did not significantly enhance cell migration. Quercetin concentrations of 10 μM did not inhibit cell migration significantly while at concentrations of 30-100 μM the inhibition was statistically significant ($p \leq 0.0001$).

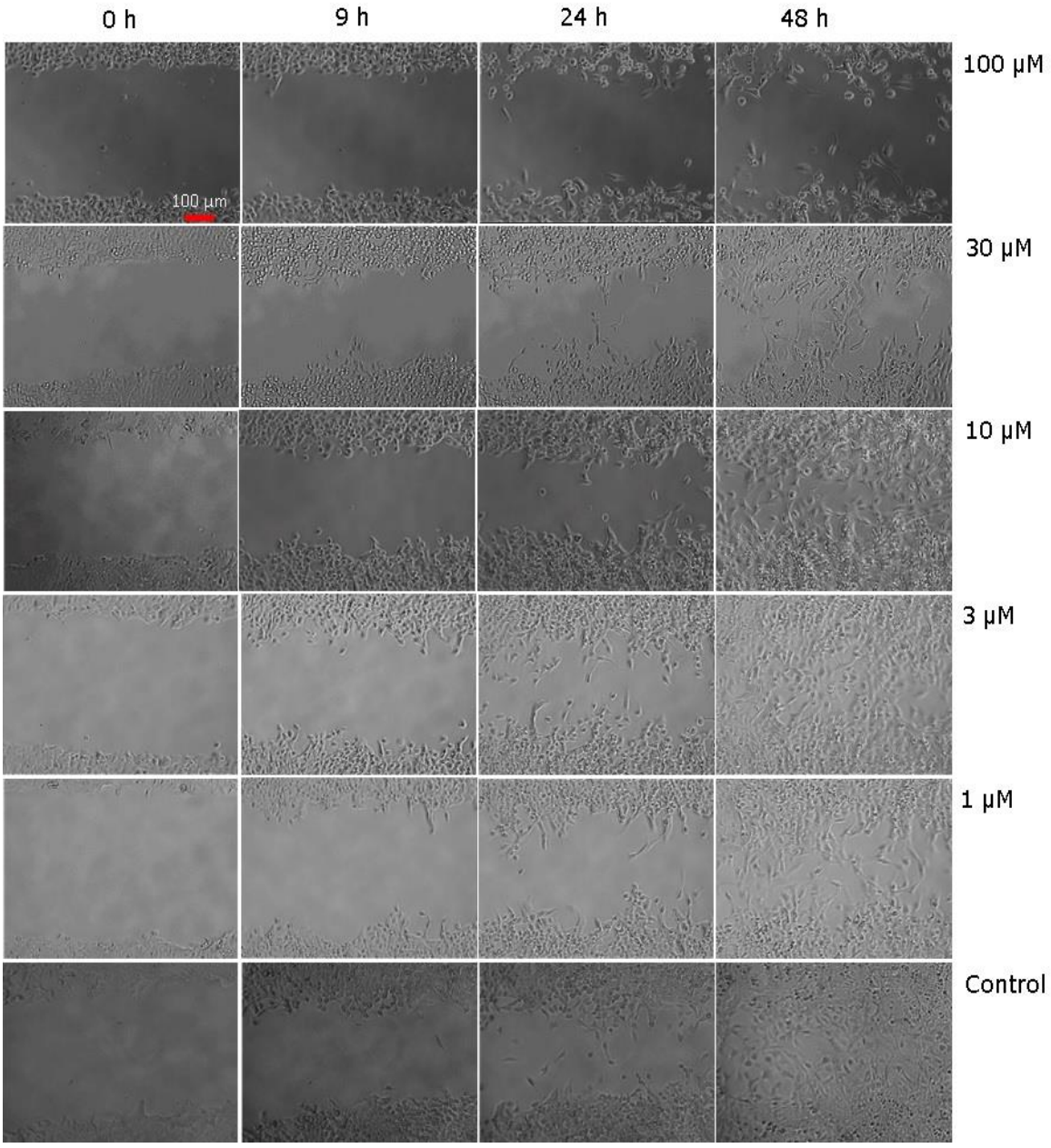


Figure 3.13 - Effect of quercetin 100-1 µM concentrations on fibroblast migration-*in vitro* scratch assay. Fig. Shows phase contrast micrographs taken using time-lapse microscopy during 48 h (Magnification, ×10) bars 100 µm.

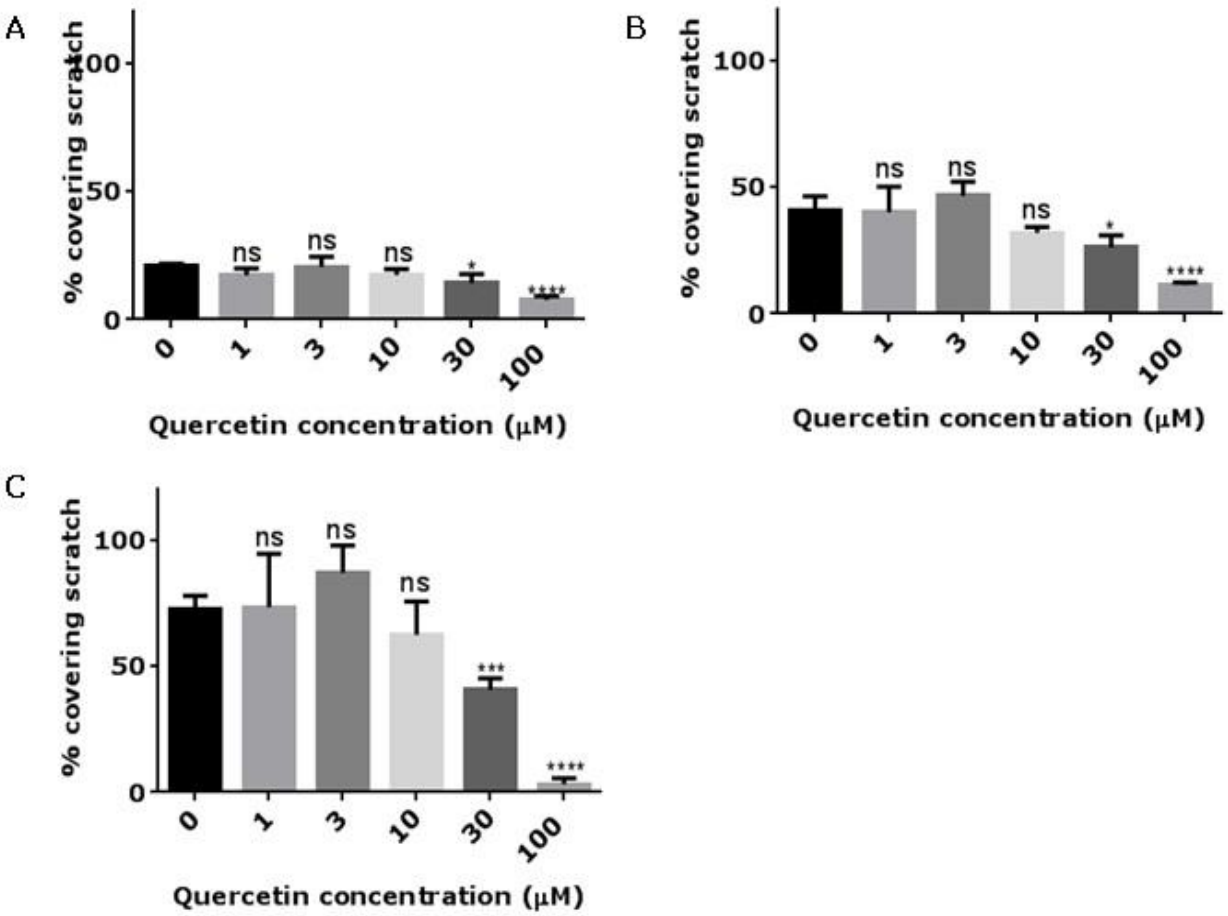


Figure 3.14 - Effect of quercetin on fibroblast migration-*in vitro* scratch assay. Fig A- shows the % of covering scratch after 9h. B) After 24h C) 48 h post scratch wound using time-lapse microscopy. Three independent experiments carried out in triplicate (means±SD).

Figure 3.15 shows the effect of commercial rutin on fibroblast migration using scratch assay and time-lapse microscopy. Overall, the covering area did not show differences between rutin concentration 1 μM and control. In addition, the fibroblasts exposed to higher concentrations of rutin gradually reduced the covering area of the scratch. Figure 3.16-A depicts a quantitative analysis of images, showing the percentage of the scratch covered after 9 h, 24 h, and 48 h. It is noticed that, after 9 h post scratch, the fibroblasts exposed to rutin concentrations (1-200 μM) were not affected negatively nor were they enhanced in terms of their migration. After 24 h of post scratch, lower concentrations of rutin (1 and 3 μM) did not show significant enhancement or inhibition on cell migration. In terms of percentage of scratch covering, samples had covered ~20%. The fibroblast exposed to rutin concentrations of 10 and 100 μM exerted a significant ($p \leq 0.01$) detrimental action upon cell migration, reaching values from 15-10% of wound closure which was lower than theirs control (32% covered) (Figure 3.16-B). Figure 3.16-C shows the effect of rutin on fibroblast migration after 48 h of treatment. Exposure to rutin at lower concentrations of 1 μM did not significantly enhance cell migration. The fibroblasts exposed to rutin concentrations between 3-200 μM exerted a dose-dependent detrimental effect in terms of the migration, reaching values between 47-24% of covering scratch.

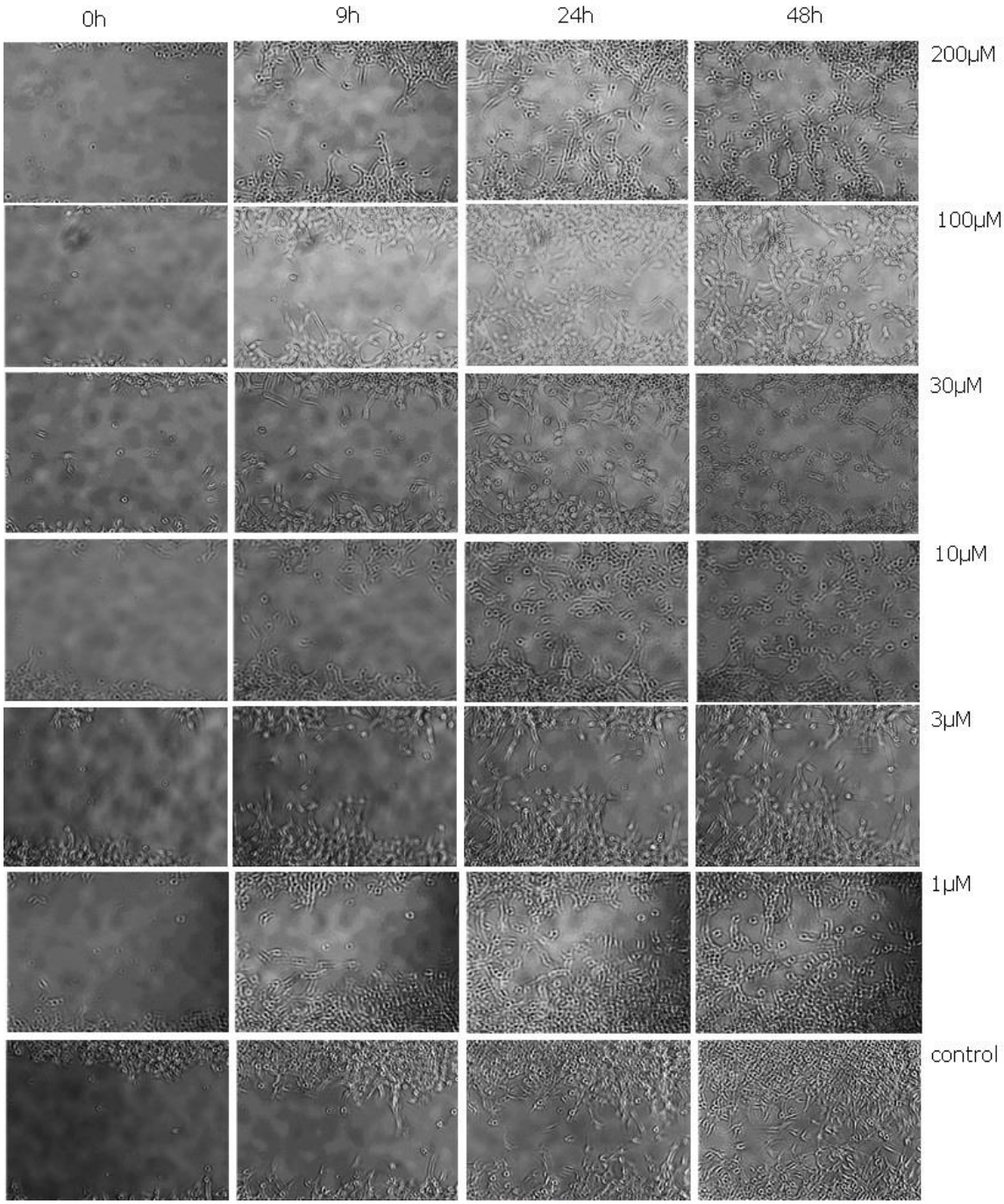


Figure 3.15 - Effect of rutin 200-1 µM concentrations on fibroblast migration-*in vitro* scratch assay. Fig. Shows phase contrast micrographs taken using time-lapse microscopy during 48 h (Magnification, ×10) bars 100 µm, a minimum of n=3 experiments.

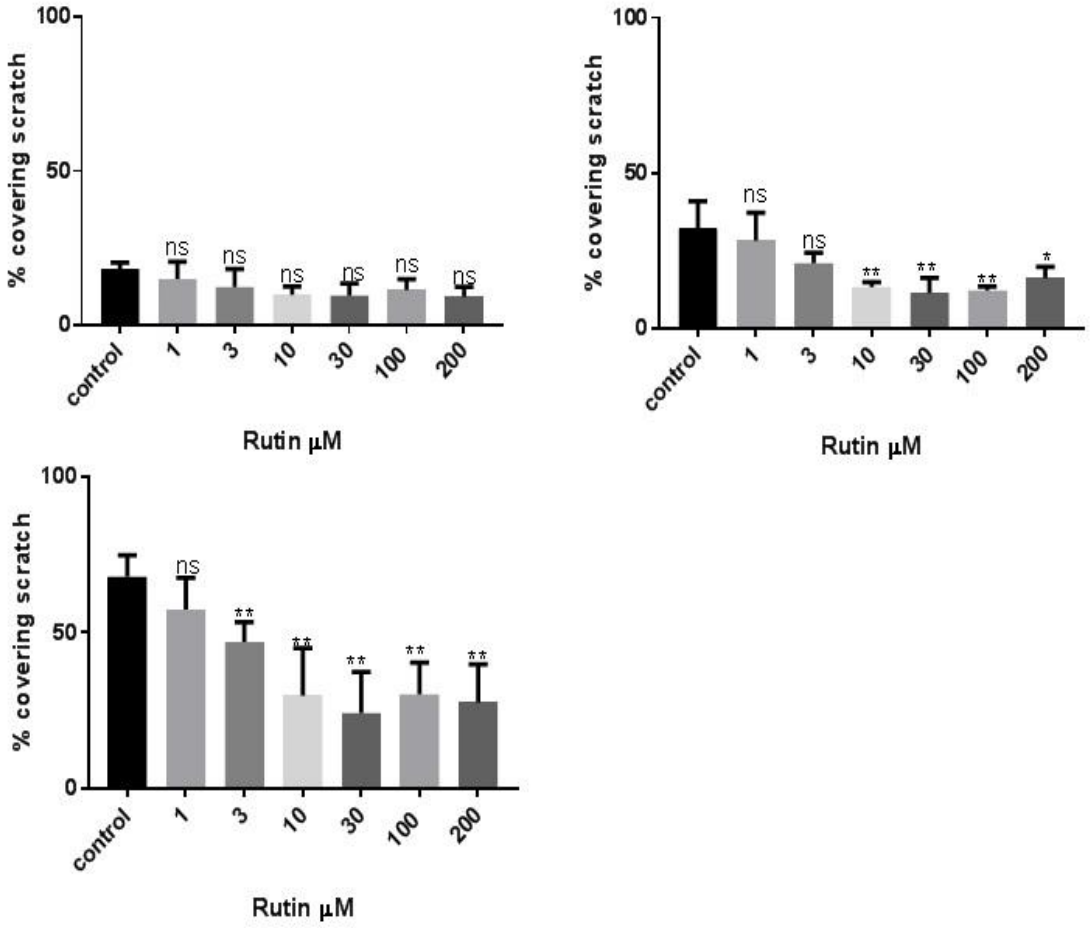


Figure 3.16 - Effect of rutin on fibroblast migration-*in vitro* scratch assay. Fig A- shows the % of covering scratch after 9h. B) After 24h C) 48h post scratch wound using time lapse microscopy. Percentage of covering. Three independent experiments carried out in triplicate (means±SD).

Figure 3.17 shows the effect of commercial artepillin C (ARC), on fibroblast migration. On the whole, analyses of images revealed that ARC concentration 1 μM had similar impact on fibroblast migration as its control. In contrast, ARC concentration 3-100 μM had a detrimental effect on cell migration. Figure 3.18 shows the percentage of the scratch covered after 9 h, 24 h, and 48 h. After 9 h post scratch, no statistical significance was found between the fibroblasts exposed to ARC concentration (1-100 μM) and their controls (Figure 3.18–A). Figure 3.18-B shows the effect of artepillin C (ARC) upon fibroblast migration after 24 h post treatment. Concentrations of artepillin C 1 μM showed a significantly enhancement in cell migration compared to their control ($p \leq 0.05$). In term of covering scratch %, fibroblast covered 50% at ARC concentration 1 μM which represented higher values than its control (35% of covered area). Fibroblasts exposed to ARC concentrations 33-100 μM exerted a not significant detrimental action upon cell migration. Figure 3.18-C shows the effect of ARC upon fibroblast migration after 48 h of treatment. Exposure to ARC concentrations 1 μM significantly enhanced cell migration ($p \leq 0.05$), reaching values of covering scratch of 70%. In addition, the concentration of ARC 3 μM had a significant ($p \leq 0.05$) negative impacted on cell migration, decreasing the value of covering area to 46%. Higher concentrations of ARC from 10-100 μM exerted a significant detrimental effect upon cell migration ($p \leq 0.001$ and $p \leq 0.0001$ respectively), reaching values of covering area of 48% at 10 μM and 16% at 100 μM.

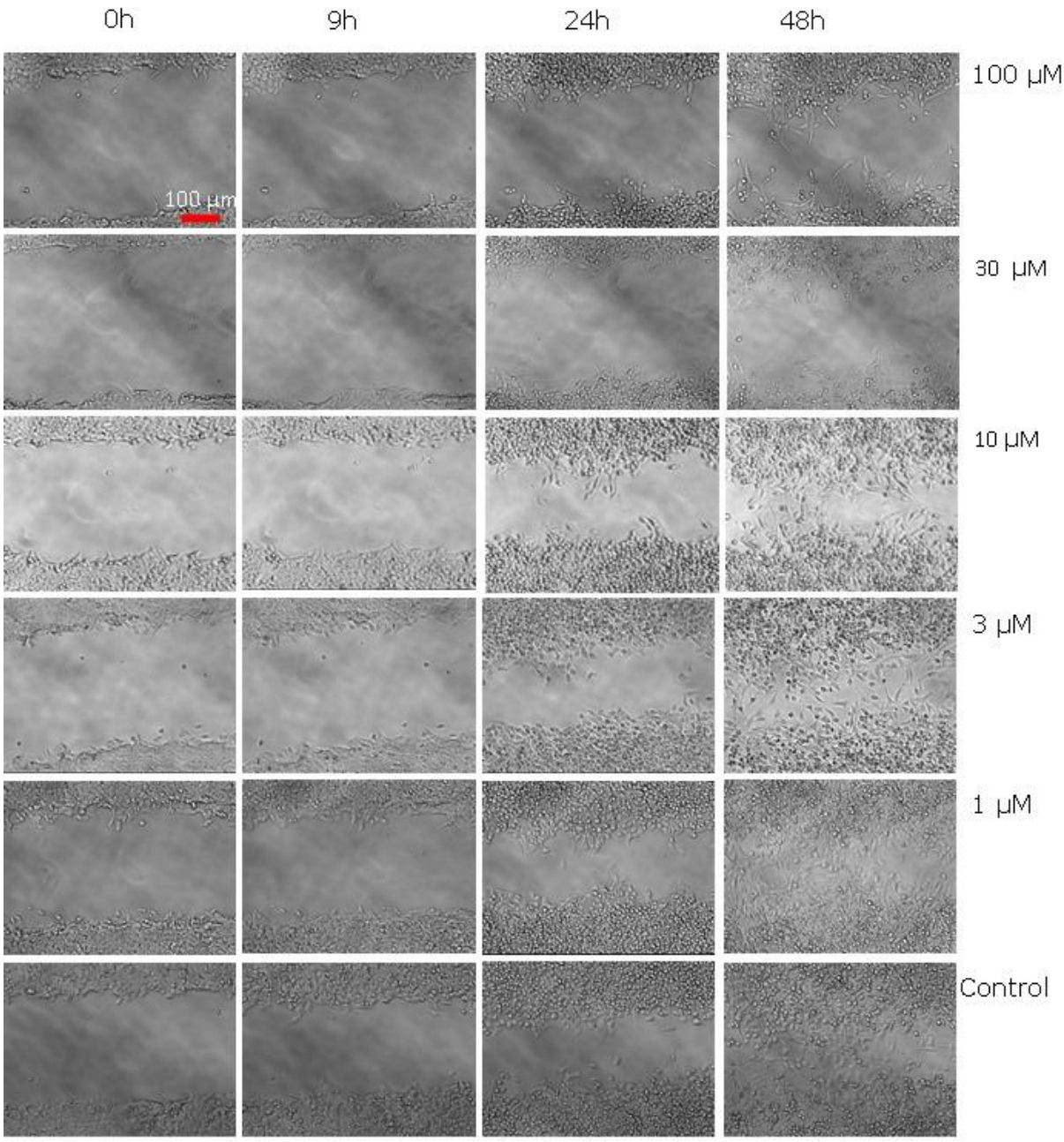


Figure 3.17 - Effect of artepillin C 100-1 µM concentrations on fibroblast migration-*in vitro* scratch assay. Fig. Shows phase contrast micrographs taken using time lapse during 48 h (Magnification, ×10) bars 100 µm.

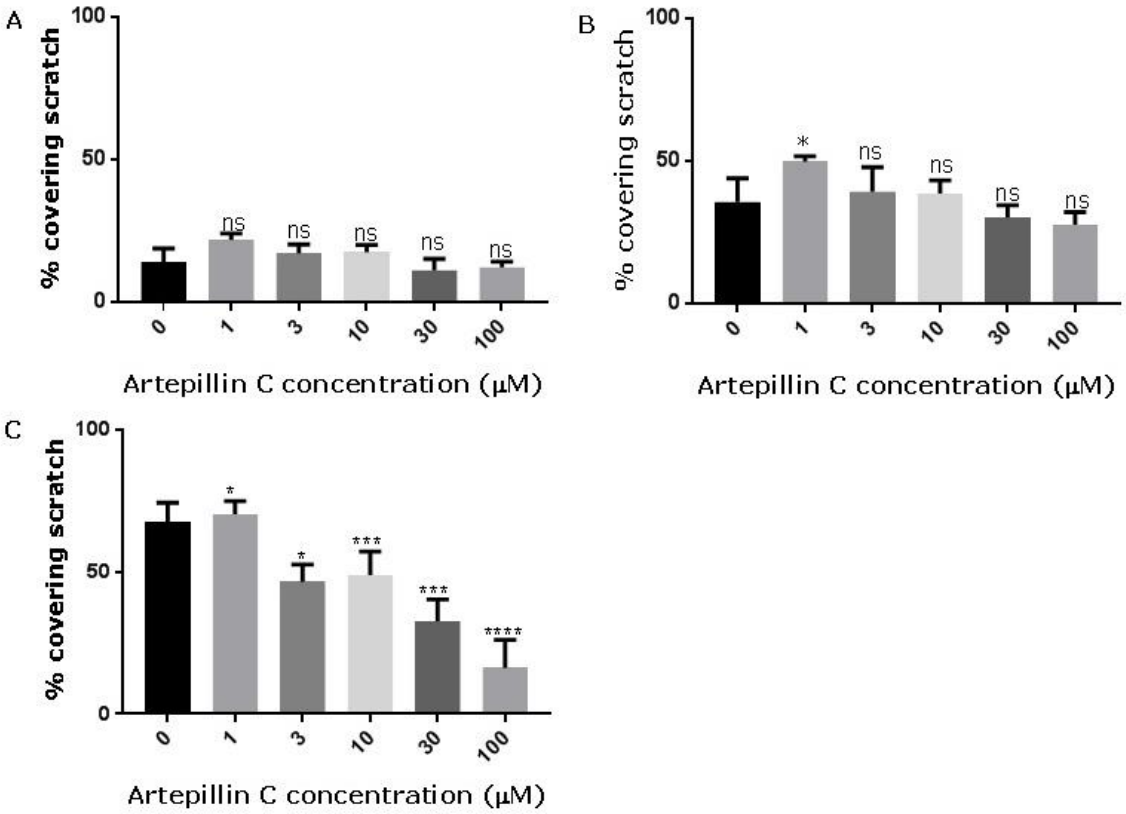


Figure 3.18 - Effect of artepillin C on fibroblast migration-*in vitro* scratch assay. Fig A- shows the % of covering scratch after 9h. B) After 24h C) 48h post scratch wound using time-lapse microscopy. Percentage of covering. Three independent experiments carried out in triplicate (means±SD).

Table 3.2 Summary of the main results of the influence of propolis and its compounds on fibroblast metabolic activity and migration.

	Concentration	AlamarBlue® assay- Metabolic activity	Double stain- membrane integrity assay	Cell migration- wound scratch assay
Propolis µg/mL	2.9	√√√	ND	ns
	5.8	√√√	ND	ns
	11.7	√	ND	ns
	23.3	ns	ND	ns
	46.8	ϕϕϕ	ns	ns
	93.5	ϕϕϕ	ND	ϕϕϕϕ
	187	C	ϕϕϕϕ	ϕϕϕϕ
Quercetin µM	1	√√√√	ns	ns
	3	√√√√	ND	ns
	10	ns	ns	ns
	30	ϕϕϕ	ND	ϕϕϕ
	100	ϕϕϕϕ	ϕϕϕϕ	ϕϕϕϕ
Rutin /µM	1	ns	ns	ns
	3	ns	ND	ϕϕ
	10	ϕϕ	ns	ϕϕϕ
	30	ϕϕ	ND	ϕϕϕ
	100	ϕϕ	ns	ϕϕϕ
	200	ϕϕϕ	ns	ϕϕϕ
Artepillin C /µM	1	ns	ns	√
	3	ns	ND	ϕϕ
	10	ϕϕ	ns	ϕϕ
	30	ϕϕ	ND	ϕϕϕ
	100	ϕϕϕϕ	ns	ϕϕϕ

√: represent enhancement of fibroblast proliferation (compared with control)/no visible dame of cell membrane/enhancement of fibroblast migration.

ns: no significant effect

ϕ: represent inhibition of fibroblast proliferation (compared with control)/ damage of cell membrane/inhibition of fibroblast migration.

C: complete inhibition

ND: not done

Propolis is a natural compound produced and used by bees to protect their hives against infections (Kuropatnicki et al., 2013). (Bankova, 2005) was one of the first to point out the necessity to conduct evaluations of propolis based on bioassay-guided chemical analysis. This is a means of evaluating the biological activity combined with qualitative and quantitative analysis of the major compounds in a particular propolis sample. In recent years, a number of publications have reported the biological activity of CAPE, artepillin C, quercetin, cinnamic acid and other compounds found in propolis including anti-inflammatory, anticancer and antimicrobial activity. However, the literature did not has never before reported the effect of propolis on fibroblast migration as a pivotal step to enhance granulation tissue formation and wound healing (Baum and Arpey, 2005) and this is the novelty of the work presented in this chapter.

3.5 Conclusions

In this project it was hypothesized that propolis and its main compounds quercetin, rutin and artepillin C may have a beneficial effect on wound healing by i) regulating the inflammation process, ii) enhancing granulation tissue formation, and iii) controlling wound infections. This study focused on the second point and aimed to evaluate the influence of propolis and its compound (quercetin, rutin and artepillin C) on fibroblast metabolic activity and cell migration essential for granulation tissue formation.

Cytotoxicity assays revealed that propolis enhanced relative metabolic activity (%) at concentrations 2.9- 11.7 µg/mL, and at higher concentrations a cytotoxic effect was observed. Higher concentrations of quercetin, rutin and artepillin c (100-30 µM) showed the same cytotoxic effect. Additionally, no evidence was found that propolis and its compounds significantly enhanced NIH-3T3 fibroblast migration *in vitro*. It needs to be considered that propolis may positively influence wound healing through different pathways, which require further investigation. For example, propolis may aid wound healing by controlling the inflammatory response and infection.

Finally, there is not a compelling argument to pursue the use of propolis and its isolated components related to cell migration and proliferation; another natural product (*Lucilia sericata* maggot excretion/secretion) will be investigated. The ultimate aim will be the development of a bioactive wound dressing that effectively promotes fibroblast migration.

CHAPTER 4 Development and characterization of Poly (ε-caprolactone) (PCL) and PCL-b-PEG/PCL electrospun scaffolds

4.1 Skin tissue engineering

Failure of wound healing is an unsolved and significant public health problem, associated with economic and human costs (Guo and DiPietro, 2010b, Driver et al., 2010). Skin tissue regeneration may provide therapies which enhance wound contraction, inhibit infection, control inflammation and maintain the moisture balance of the wound bed (Boateng et al., 2008). Three common strategies used by tissue engineering are: a) cell-based therapies (Tenenhaus et al., 2016), b) scaffold-cell constructs and c) tissue induction factor therapy (Leppiniemi and Hytönen, 2016).

A large number of materials for skin wound regeneration have been investigated. Advanced wound dressings include skin substitutes, and natural and synthetic polymer-based dressings (Moura et al., 2013). Specifically, skin substitutes can be acellular matrices (i.e Integra™) or cell-based matrices (i.e Apligraf™)(Boughton and Mclennan, 2013). There are two dozen skin substitutes available on the American and European markets (Nyame et al., 2014). The main disadvantages of the use of skin substitutes are: i) graft rejection caused by immune reaction, concerns about transmission of pathogens from cell or animal proteins, and ii) the high cost of production (Boughton and Mclennan, 2013).

4.1.1 Scaffolds and fabrication

Three-dimensional electrospun scaffolds are widely used for tissue engineering strategies, including skin regeneration (Cai et al., 2013, Sheikh et al., 2014, Gigliobianco et al., 2015, Bye et al., 2014).

Scaffolds are 3-D, solid and highly porous structures that serves as a substitute for the native extracellular matrix by providing temporary support for cells (Khorshidi et al., 2016).

4.1.1.i Requirement for a functional scaffold

At a cellular level, a biodegradable, non-toxic material that supports cell adhesion, fibroblast proliferation and infiltration is desirable (Boateng et al., 2008, Karahaliloğlu et al., 2014).

Fibre diameter and porosity of scaffolds are critical features in tissue regeneration because cell attachment, infiltration, proliferation and differentiation depends upon them (Chen et al., 2009). It has been reported that fibroblasts prefer scaffolds with a fibre diameter in the micron scale ~ 4-10 μm as these scaffolds allow fibroblasts to penetrate into fibres, resulting in a multilayer coverage (Lowery et al., 2010, Farrugia et al., 2013, Powell and Boyce, 2009, Kempf et al., 2011). The majority of investigations have focused on the development of 3D scaffold nanofibrous scale (less or equal to 100 nm). Analysis of nanofibre scaffolds have indicated that cells cultured on these fibre dimensions support a cell monolayer. However, some nanofibre scaffolds have been shown to inhibit cellular infiltration, limiting their use for 3D tissue engineering (Pham et al., 2006).

Scaffolds can be fabricated using conventional methods such as: emulsion and freeze-drying, casting and post freeze-drying, phase separation, and gas foaming, which are the easiest and common ways to produced scaffolds. However, architecture features such as pore size, interconnectivity and distribution cannot be controlled easily by these methods. Solid freedom fabrication (SFF) techniques could be used to fabricate scaffolds with precise control of pore size and structure. Some of the SFF techniques include but are not limited to: fusion deposition modelling (FDM), 3D printing, stereolithography and selective laser sintering. SFF uses complementary technology such as mCT and computer-aided design to pre-design the scaffolds. The use of SFF technologies to fabricate scaffolds allows the pre-design of. fibre size, shape and fibre distribution (Seol et al., 2012).

4.1.1.ii Electrospinning

Briefly, electrospinning consists in the use of polymeric solution that, by the application of an electrostatic field, produces a fibre. Electrospinning systems consist of a syringe pump, spinneret, high voltage source and a collector (Figure 4.1).

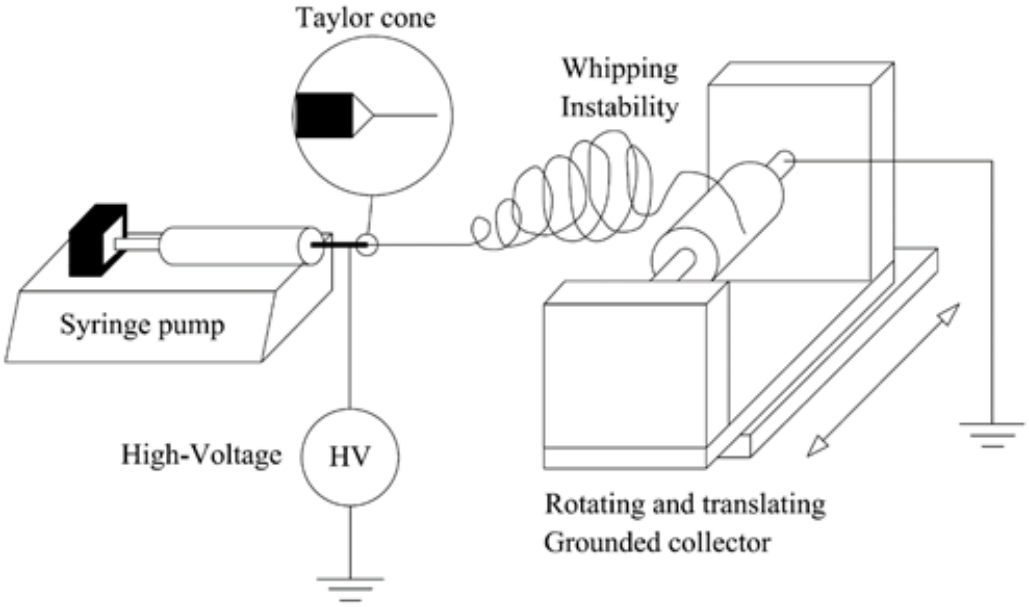


Figure 4.1 Schematic representation of the electrospinning setup. Extrusion of polymer solution through the needle and spinneret connected to a high voltage power supply. Polymer solution with charge, viscosity and superficial tension to form a Taylor cone jet. Polymeric jet is attracted by the collector where the mat is deposited. Extract from (Sill and von Recum, 2008).

Electrospinning allows the use of natural and synthetic polymers. Natural polymer-based dressings, including chitosan, alginate, and silk among others, have been shown to have a significant potential for biomedical applications because of their biodegradability, biocompatibility, and bioresorbability (Moura et al., 2013, Sell et al., 2010). Nevertheless, biological variation between batches and standardization issues may limit their application (Mano et al., 2007). Moreover, electrospinning is affected by three groups of variables: a) solution parameters such as polymer concentration, viscosity, molecular weight, conductivity, surface tension, solvent system, and b) processing parameter such as applied voltage, flow rate, collector, distance to the collector, and c) ambient parameters such as temperature and humidity. The combination and balance of this variable will affect directly the fibre formation (Rošic et al., 2012, Qin and Wu, 2011, Yousefzadeh and Ramakrishna, 2016).

Electrospinning is a known process used to develop 3D fibre based scaffolds (Braghirolli et al., 2014, Bhattarai et al., 2014, Erencia et al., 2014). Electrospun nanofibre scaffolds have shown potential for use in wound healing due to their capacity to support cell attachment, proliferation and phenotype cell differentiation (Kataria et al., 2014, Gupta et al., 2010). Moreover, they can be easily modified during the electrospinning process (*in situ*) and can also be modified post-processing (Schiffman et al., 2011). Recently, strategies in the field of skin wound healing have included the incorporation of different growth factors via coaxial electrospinning which can enable controlled

release (Liu et al., 2010). On the other hand, the major limitation of the use of electrospun nanofibres scaffolds is their poor cell infiltration *in vitro* and poor tissue ingrowth into the scaffolds *in vivo* (Rnjak-Kovacina and Weiss, 2011).

Synthetic polymer-based dressings used in wound healing applications include, poly (ethylene glycol) (PEG), polyesters (i.e. polycaprolactone (PCL), polyglycolic acid (PGA), polylactic acid (PLA)), poly (vinyl pyrrolidone) (PVP), poly (vinyl alcohol) (PVA) and polyurethanes (PU). The advantages of using synthetic polymers are that they can be tuned to enhance specific properties such as mechanical strength, shape and biodegradation rate (Armentano et al., 2010). Comparatively, synthetic polymers are often cheaper than natural polymers because they can be produced in large-scales and with minimal post-synthetic processing (Armentano et al., 2010). In spite of these advantages, synthetic polymers can present some biocompatibility problems due to a lack of specific cell-recognition motifs and sub-optimal cell-surface interfacial interactions (Cho et al., 2015).

Polycaprolactone (ε-PCL) is an aliphatic linear polyester that has drawn considerable attention for biomedical applications because it is a biocompatible, biodegradable and a low cost synthetic polymer. The US FDA first approved its use for clinical application as a drug delivery device in 1980 (Cipitria et al., 2011). Depending on the molecular weight and conditions, PCL can take between 2-4 years to completely degrade (Yang et al., 2015). Some disadvantages of PCL are its hydrophobicity and lack of functional groups for cell attachment and

proliferation. However, *in vivo* studies have revealed that PCL can undergo partial surface hydrolysis that leads to end carboxyl and hydroxyl group formation on the surface which can promote protein adhesion via integrin binding (Karahaliloğlu et al., 2014, Augustine et al., 2015). Integrin is a heterodimer trans-membrane receptor, which provides a physical and biochemical bridge between the substrate and cell (Balasundaram and Webster, 2006).

In addition, poly (ethylene glycol) (PEG) is a hydrophilic and non-toxic, FDA-approved polymer, which is soluble in water and in many other polar and some non-polar solvents. PEG possesses a terminal hydroxyl group and repeat oxyethane linkages that promote hydrogen-bonding with water and other polar or charged groups. It has been reported that hydrogen-bonding of PEG, or conjugation by chemical linkages to proteins can take place without denaturing the biopolymers or decreasing their bioactivities (Harris, 2013).

The formation of PEG-PCL co-polymers has been used as a strategy to modify the mechanical properties, wettability, biocompatibility, and solubility in water, as well as in reducing the immunogenicity of the PCL component. Additionally, PEG should be capable of delivering therapeutics at the right dosage and also function as a preserver for bioactivity of proteins (Lin and Anseth, 2009).

In addition, it reported that co-polymer formation with PEG has substantially improved the degradability of PCL scaffolds (Lu et al., 2006). PCL-PEG has been used as a delivery system for diverse biomedical applications such as :i) delivery of drugs (Gou et al., 2011), ii) genes(Jeong Soon et al., 2006), iii) protein antigens(Gou et

al., 2007), and v) growth factors, such as (EGF) for wound healing purposes (Choi et al., 2008).

4.2 Aims and objectives

Scaffolds need to provide structural stability for cellular proliferation and infiltration. Mechanical properties, degradation rate, porosity (Baker et al., 2009) and wettability properties need to meet cell and application requirements (Chang and Wang, 2011, Nyame et al., 2014).

In the frame of this research it was hypothesized that i) a PCL electrospun scaffolds with suitable geometrical, physicochemical, mechanical and biological properties provide a proper environment that allow fibroblasts to grow and infiltrate into the scaffolds. In addition, literature has indicated that the incorporation of PEG into electrospun scaffolds enhanced degradation, wettability and cell-compatibility (Jiang et al., 2011, Hoque et al., 2014). On the bases of this background it was hypothesized that ii) scaffolds composed of PCL-b-PEG fibres show enhanced degradation, wettability, cell-compatibility and cell-infiltration.

To address these hypothesises, a number of aims have been set as part of this study, as following:

- Synthesis of PCL-b-PEG copolymer
- Evaluate PCL and PCL-b-PEG solutions and electrospinning parameters using commercial PCL (80.000 g/mol) and in-house

synthesised PCL-b-PEG (~57.000 g/mol) to understand the variables involved in the resultant electrospun scaffolds.

- Fabricate PCL and PCL-b-PEG electrospun scaffolds in a micron scale range.
- Assess and compare geometrical, physicochemical, degradation rate and mechanical properties of the PCL and PCL-b-PEG electrospun scaffolds that may provide a suitable environment for cells to grow and infiltrate.
- Evaluate *in vitro* biocompatibility and infiltration behaviour of 3T3 GFP expressing mouse dermal fibroblasts as an exemplar mammalian cell type on PCL and PCL-b-PEG electrospun scaffolds.

This chapter will address the development of PCL and PCL-b-PEG electrospun scaffolds that possess suitable geometrical, mechanical, physicochemical properties that provide a structural support for fibroblast growth and infiltration. The electrospinning of Poly (ε-caprolactone) (PCL) will initially be evaluated and the solution and electrospinning parameters will be optimised. Follow this PCL-PEG electrospinning condition will be optimised and evaluations to elucidate fibroblast response will be conduce between PCL and PCL-b-PEG scaffolds.

4.3 Results and discussion

4.3.1 Characterization of PCL-b-PEG/PCL polymer (NMR and GPC)

A series of five different batches of PCL-PEG diblock copolymers were prepared through ring-opening copolymerization of ε -CL, using TBD as catalyst as described in chapter 2 section 2.4.2 (Figure 4.2). ^{1}H NMR and Gel permeation chromatography (GPC) were used to characterize the chemical structure of PCL-PEG copolymers (Figure 4.2). The results from ^{1}H NMR and GPC for the five batches are summarized in Table 4.1. Molecular weight and PCL-PEG block ratios estimated from ^{1}H NMR spectra were consistent with the theoretical values calculated. ^{1}H NMR and GPC results indicated that only batch 1, 4 and 5 of PCL-PEG were synthesized successfully. Finally, the polydispersity index (*Đ*), which refers to the degree of polymerization, was analyzed. For electrospinning purposes batches 1 and 4, with a molecular weight ~ of 57.000 g/mol, and a *Đ* of 1.77 and 1.44, respectively, were used

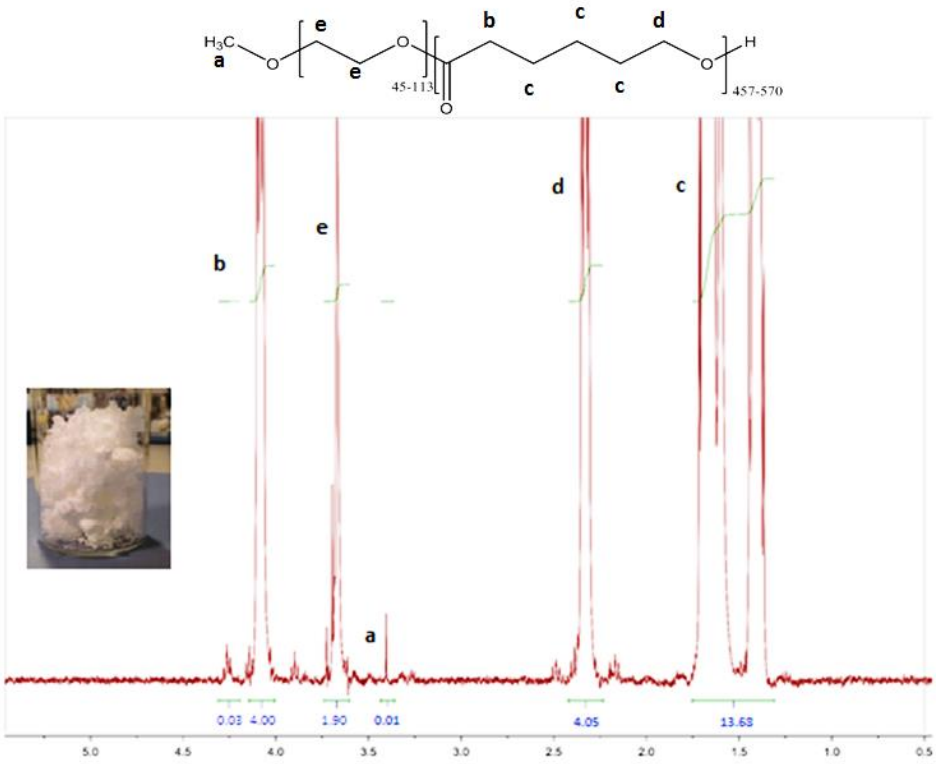


Figure 4.2 - Representative NMR of PCL-b- PEG polymer after its purification. Inset image shows the final polymer after drying.

Table 4.1 - A summary of the chemical characterization of different batches of PCL-PEG copolymer. Batches 1 and 4 denoted by red box were used in this study.

Batch number	Theoretical Molecular weight g/mol	NMR Molecular weight g/mol	GPC Molecular weight (Mw) g/mol	Đ
Batch 1	62070	54.000	57022	1.77
Batch 2	62070	23753	19400	1.79
Batch 3	62070	20903	17799	1.62
Batch 4	62070	56.000	57000	1.44
Batch 5	62070	59361	491400	2.05

4.3.2 Characterization of PCL solution prior electrospinning

Figure 4.3-A) shows the change in viscosity of different poly (ε-caprolactone) solutions as a function of the shear rate (rotational test). Different concentrations of PCL solution in a range of 4-14% (*w/w*) were tested, applying a shear rate from 0.9 to 110 (1/s). The viscosity increased as a function of polymer solution concentration: at a higher concentration, PCL solutions showed a greater decrease in viscosity. For example, the viscosity of PCL 14% (*w/w*) varied from 100 to 12 Pa s, PCL 12% (*w/w*) viscosity varied from ~90 to 9 Pa s, PCL 10% (*w/w*) from ~28 to 4 Pa s and PCL 8% (*w/w*) from ~11 to 2 Pa s. Moreover, the application of shear rates higher than 40 (1/s) did not affect the rheology of the individual solutions; the viscosity slopes reached a plateau value. PCL 6% and 4% (*w/w*) solutions showed reductions in viscosity from ~3 to 1 Pas and from 2 to ~1 Pas, respectively.

Figure 4.3-B shows shear stress versus shear rate curves as a function of PCL solution concentration. Concentrated solutions of PCL (14-8 % w/w) presented a dual behaviour; at the beginning a shear-thinning behaviour was observed, expected of non–Newtonian fluids, while beyond shear rates of ~ 40 1/s, the polymer exhibited linear and exponential curves dependent on polymer concentration, which is typical of Newtonian fluids.

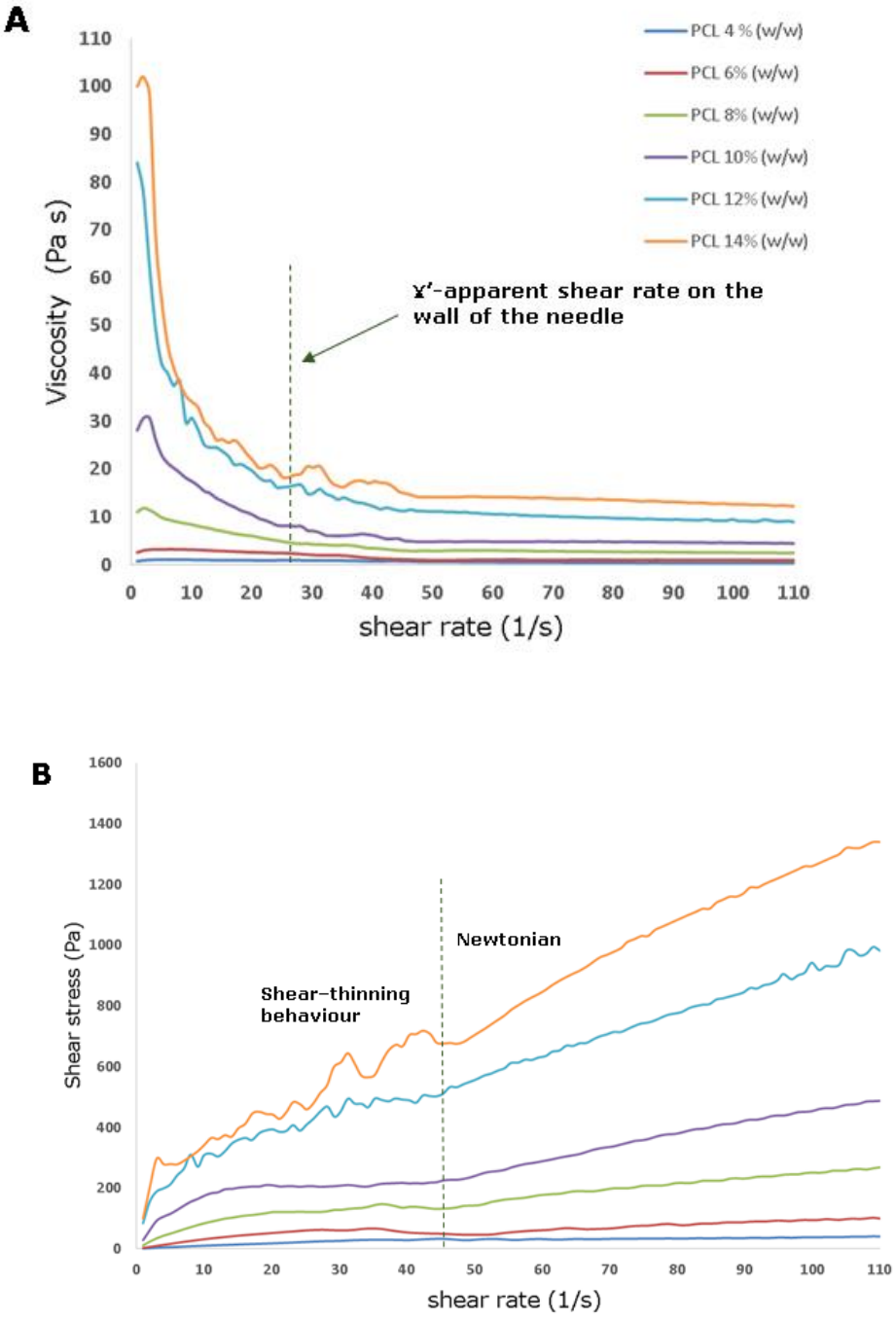


Figure 4.3- A) Representative viscosity curves showing the shear behaviour for different concentrations of Poly(caprolactone) (PCL) 4-14 % w/w. B) Shear stress versus share rate of PCL solutions dissolved in chloroform.

It has been reported that the major factor which influences the rheology of non-Newtonian fluids is polymer chain entanglement (Xu et al., 2011, Munir et al., 2009). The results presented here show a pronounced shear thinning effect of PCL as a function of the solution concentration. Shear thinning behaviour is characterized by the decrease in viscosity as shear rate progressively increases, which is typical of non-Newtonian fluids and commonly reported for polymeric solutions (Rošic et al., 2012, Suman et al., 2011, Al-Shammari et al., 2011). Hence, the highly shear thinning effect showed in the present study by high concentrations of PCL may be caused by the presence of a high number of polymer chain entanglements. Following the shear thinning region, the polymer reached a plateau (Figure 4.3). This effect may be explained by the fact that polymer molecules became aligned under the application of higher shear rate, which allow an easier flow of the molecules, decreasing viscosity values (Rošic et al., 2012). In addition, lower concentrations of PCL (6-4 %) did not exhibit the shear thinning phenomenon, suggesting that their behaviour was approaching that of a Newtonian fluid. (Gupta, 2000) pointed out that diluted polymer solutions behave as Newtonian fluids because the solvent reduces the chain entanglement per unit volume. Also (Shenoy et al., 2005) and (Chisca et al., 2012) reported that the effect of self-entanglement is reduced or absent in dilute solutions, allowing the fluid to flow without resistance. The curves presented here are in agreement with the curves showed by (Qin and Wu, 2012) who tested the rheological behaviour of PCL solution. The PCL used was 80.000 g/mol and the final concentration was 15% *w/w*.

Analyses of shear stress versus shear rate graph revealed linear and exponential curves beyond 40 1/s, which is the same tendency observed in the current study. In addition, studies conducted by (Kim et al., 2012) showed similar viscosity and shear rate curves for 5% *w/w* PCL solutions.

Polymer solution concentration and viscosity play an important role in electrospinning (Jamnongkan et al., 2014, Tiwari et al., 2014). To calculate the approximately apparent shear rate at the needle wall, considering polymer solutions as Newtonian fluids, the following equation was used (Jamnongkan et al., 2014):

$$\gamma' = \frac{4Q}{\pi R^3}$$

γ' is the apparent shear rate at the needle wall, Q is the flow rate and R is the radius of the needle (0.3 mm). The calculated apparent shear for a flow rate of 2 mL/h was ~26 (1/s), which in the thinning share rate region. Table 4.2 shows the average viscosity at the share rate of the electrospinning needle wall at different concentrations of PCL polymer solutions.

Table 4.2 - Viscosity of PCL polymers solutions at the same shear rate that the needle wall of the electrospinning

PCL concentration (% *w/w*)	Viscosity (Pa s) at shear rate at the needle wall (26 s^{-1})
4	0.9±0.1
6	2.3±0.3
8	3.6±0.6
10	7.1±0.6
12	16.6±1.9
14	20.0±1.6

The apparent shear rate at the needle wall was calculated and the viscosity was inferred for that point. The results showed that PCL solutions from 8-14% *w/w* presented a viscosity within the shear thinning region, indicate of chain entanglement. Experimental observation and previous literature have pointed out the importance of working with a solution which contain enough chain entanglement to avoid bead formations (Gadkari, 2014). In order to electrospin fibres successfully, a minimum level of chain entanglement is needed which can be reached by increasing molecular weight of the polymer or increasing the concentration (Kołbuk et al., 2013, Shenoy et al., 2005). Based on the results presented here and the literature review, it was decided to electrospin PCL solutions with concentrations ranging from 8-14% *w/w* to achieve scaffolds with uniform fibre formation, free of beads.

4.3.3 Characterization of PCL-b-PEG solutions and its blends with PCL (PCL-b-PEG/PCL) prior to electrospinning

Figure 4.4 shows the rheological evaluation of different ratios of PCL-b-PEG blended with PCL as function of the shear rate. Initially, blends of PCL-b-PEG polymer 10% *w/w* were electrospun, however, this procedure led to bead formation or non-uniform fibres (appendix). Hence, it was decided to blend PCL-b-PEG with PCL in order to increase the viscosity. Different ratios of PCL-b-PEG were blended with PCL as follows PCL-b-PEG/PCL 40:60, PCL-b-PEG/PCL50:50 and PCL-b-PEG/PCL 60:40, all prepared at a final polymer concentration of 15% (*w/w*). Additionally, PCL-b-PEG/PCL 40:60 at a final concentration of 20% (*w/w*) was also tested. It was noticed that viscosity increased as a function of solution composition; solutions with a lower percentage of PCL-b-PEG showed a greater decrease in viscosity with the increment of shear rate. For example, the viscosity of PCL-b-PEG/PCL 40:60, containing 40% of PCL-b-PEG and at final concentration of 15% (*w/w*), varied from ~14 to 6 Pa s while the viscosity of PCL-b-PEG/PCL 50:50 (15% *w/w*) varied from 11 to 3 Pa s. Solutions containing a higher concentration of PCL-b-PEG (60%) to achieve the blend of PCL-b-PEG/PCL 60:40 (15% *w/w*) varied from 5 to 3 Pa s. In terms of final polymer concentration, solutions of PCL-b-PEG/PCL 40:60, final concentration of 15% (*w/w*), were compared with those PCL-b-PEG/PCL 40:60, final concentration 20% (*w/w*). Here it can be seen that higher solution concentrations (PCL-b-PEG/PCL 40:60 20% (*w/w*) resulted in a greater decrease in viscosity, from 42 to 31 Pa s.

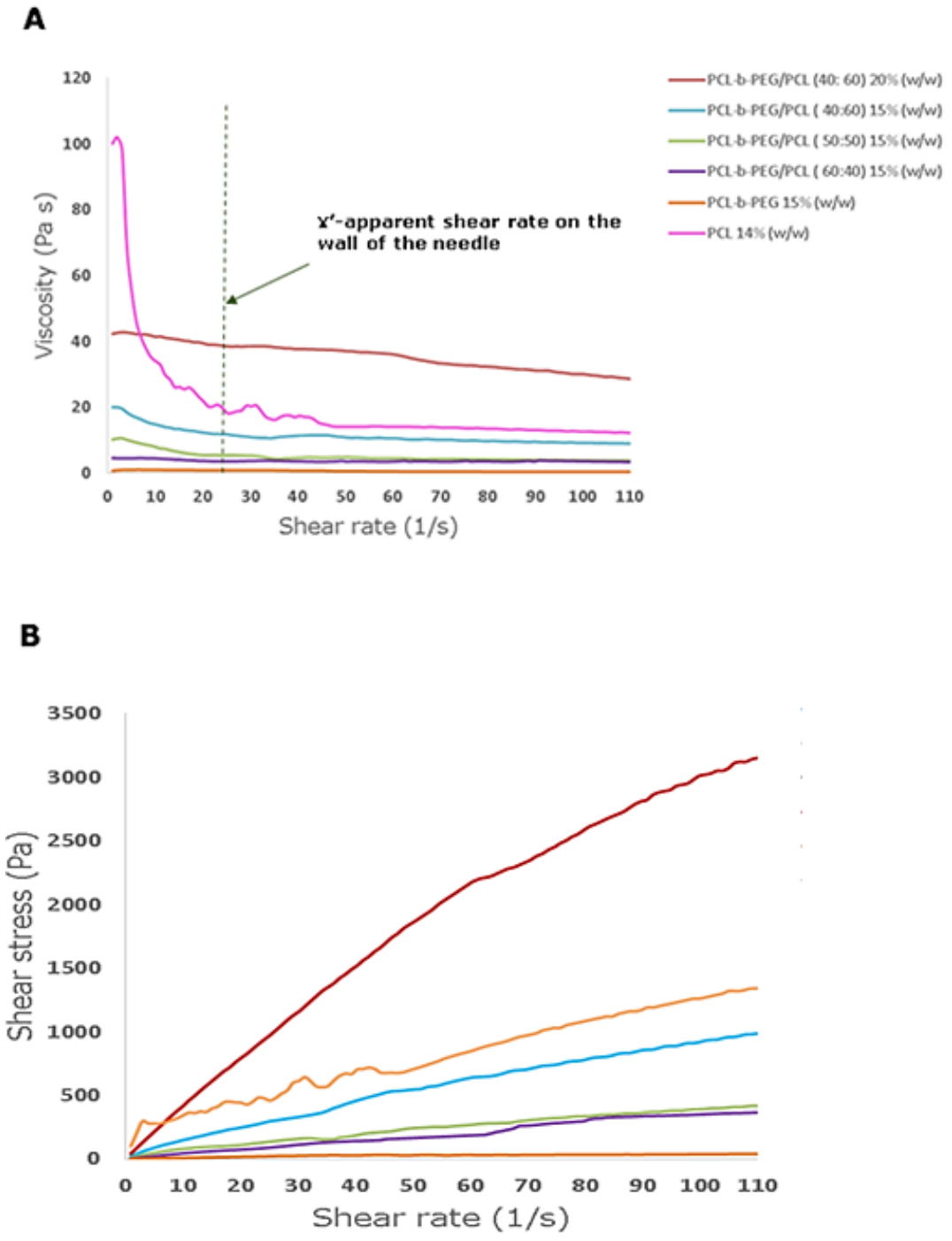


Figure 4.4 - A) Representative viscosity curves showing the shear behaviour for the different concentrations and ratios of the mixture PCL and PCL-b-PEG blends B) Shear stress versus shear rate of the mixture of PCL and PCL-b-PEG blends dissolved in chloroform.

Comparing the rheological properties of pure PCL solutions (14% *w/w*) and those containing PCL-b-PEG/PCL, it was noticed that similar concentrations of pure PCL solutions (14% *w/w*) exhibited a viscosity of 20.0±1.6 Pa s under a shear rate similar to that which will be experienced at the wall of the needle used for electrospinning 26 (1/s) (section 4.3.2 for calculation details). PCL-b-PEG/PCL polymer solutions of 15% (*w/w*) exhibited a range of viscosity values from 3.6±0.1 to 9.6±1.5 Pa s, which was lower than for PCL alone solutions. The viscosity of the PCL-b-PEG/PCL polymer solutions varied depending on the proportion of PCL-b-PEG polymer added to the blend; lower viscosities (3.6±0.1 Pa s) were revealed by solutions containing the highest proportion of PCL-b-PEG (60%) polymer. A possible explanation for this effect is the fact the home-synthesised polymer PCL-b-PEG (57,000 g/mol) has a molecular weight lower than commercial PCL (80,000 g/mol). Which is likely to influence, the extent of polymer chain entanglement and hence viscosity. Hence, by increasing the proportion of PCL-b-PEG in the mixture, the chain entanglement is also reduced and thus a lower resistance to flow was found. A similar effect was described by (Rošic et al., 2012), who worked with chitosan and PEO polymers. They found that by increasing the PEO concentration in blends of chitosan and PEO, the viscosity was reduced. They explained this reduction of viscosity by the increment of PEO was produced due to the increase in repulsive forces between polymer chains when the amount of PEO increased. In the current study, PCL and PCL-b-PEG blends may exhibit stronger repulsion in those samples with a higher content of PCL-b-PEG. These

repulsion forces impede chain entanglement, and again reduce the viscosity. In addition, the viscosity at the shear rate experienced at the needle wall during electrospinning was estimated (4.3.2) for the different concentration and ratios of the mixture PCL and PCL-b-PEG polymers (Table 4.3).

Table 4.3 - Viscosity of different concentration and ratios of the mixture PCL and PCL-b-PEG polymers determined at the same shear rate as that experienced at the needle wall during electrospinning.

PCL-b-PEG/PCL Concentration (% *w/w*)	Viscosity (Pa s) at shear rate at the needle wall (26 s^{-1})
PCL 14% (*w/w*)	20±1.6
PCL-b-PEG 15 % (*w/w*)	0.9±0.1
PCL-b-PEG (40:60) 20% (*w/w*)	28.9±4.4
PCL-b-PEG (40:60) 15% (*w/w*)	4.3±0.7
PCL-b-PEG (50:50) 15% (*w/w*)	9.6±1.5
PCL-b-PEG (60:40) 15% (*w/w*)	3.6±0.1

In general, the viscosities of PCL-b-PEG/PCL (40:60) 15% (*w/w*) and PCL-b-PEG/PCL (50:50) 15% (*w/w*) were within the shear thinning region (at shear rate of the needle wall), which is an indication of sufficient chain entanglement to achieve the required viscosity to produce homogenous fibres during electrospinning. PCL-b-PEG/PCL blends (40:60) at the higher concentration of 20% (*w/w*) resulted in blockage of the needle. In contrast, solutions of PCL-b-PEG/PCL (60:40) 15% (*w/w*) and PCL-b-PEG 15% (*w/w*) were not sufficiently viscous to create a bead-free scaffolds (viscosity 3.6±0.1 Pa·s).

4.3.4 Geometrical evaluation of PCL electrospun scaffolds.

4.3.4.i Fabrication and morphology analysis (SEM)

Figure 4.5 shows representative SEM images of PCL microfibre scaffolds. Overall, these scaffolds showed randomly distributed fibres, with interconnected pores, without beads or any another defect. In order to obtain these scaffolds, there were varying different electrospinning parameters used, such as applied voltage, flow rate of polymeric solution, solvent, polymeric concentration, collector distance and motion (rpm) of the drum collector. The conditions used to fabricate these scaffolds are described Table 4.4. Figure 4.5 shows uniform electrospun fibres with an average of fibre diameter of a) 2.6±0.5 b) 3.6±0.4; c) 5.9±0.5; d) 6.5±0.5; e) 6.9±0.6; f) 7.5±0.5; g) 12.3±1.0; h) 14.3±1.1 µm. Figure 4.5-a) shows an SEM image of a electrospun scaffold of PCL produced from dissolving PCL in a chloroform: methanol mixture at a ratio of 3:1. The rest of the scaffolds shown in Figure 4.5 were electrospun from a polymeric solution prepared with chloroform (flow rate 2 mL/h and a motion 50 rpm was maintained constant) (Table 4.4). Figure 4.5 -f) and g) show the scaffolds produced with the largest fibre diameters, which were obtained by using a PCL solution of 10% *(w/w*) concentration, applying a lower voltage (12 kV) and shortening the collector plate distance during the electrospinning process (flow rate 2 mL/h and motion 50 rpm of the mandrel). In general, applied voltage, polymer solution concentration, and solvent parameters were found to be the key parameters in modifying the fibre diameter in agreement with other reports (Diasa et al., 2013, Wise et al., 2014).

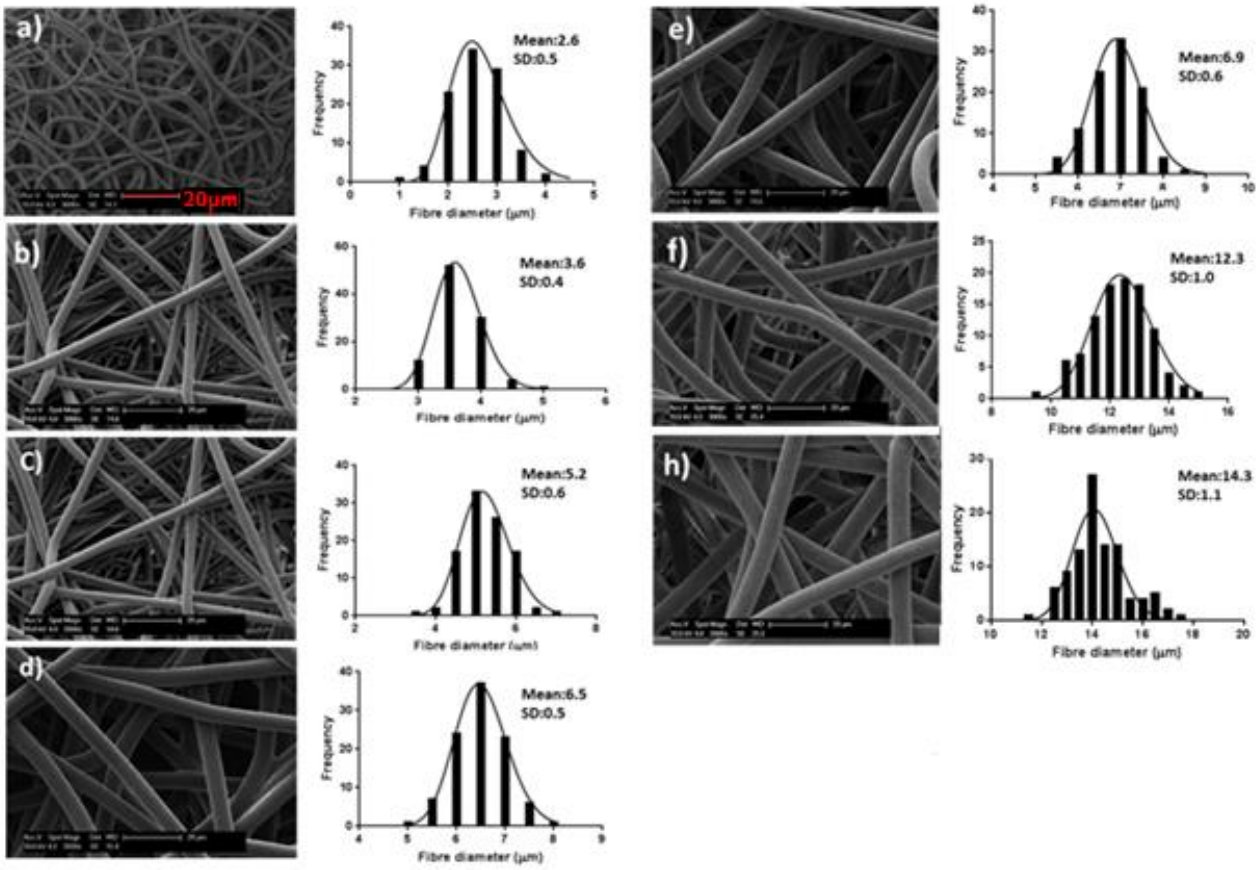


Figure 4.5 - Representative scanning electron micrographs of PCL electrospun microfibres (at x 3000 magnification) and Log-normal distribution histograms of the size and frequency of their respective fibre diameters. **Table 4.4** shows the corresponding electrospinning and solution parameters used here to obtain these set of electrospun scaffolds.

Table 4.4 - Electrospinning parameters for PCL scaffold production with a fibre diameter range: 3-14 µm

PCL Concentration (w/w %)	PCL Molar mass.	Solvent	Collector distance (cm)	Voltage (kV)	Flow Rate (mL/h)	Motion (rpm)	Needle Inner diameter mm	Collector	Sample	Fibre diameter (mean±SD) µm
10	80.000	Chl: MeOH	20.5	18	2	50	0.6	RTC	Fig. a	2.6±0.5
8	80.000	chloroform	17	25	2	50	0.6	RTC	Fig. b	3.6±0.4
8	80.000	chloroform	17	20	2	50	0.6	RTC	Fig. c	5.2±0.6
10	80.000	chloroform	17	18	2	2	0.6	RDC	Fig. d	6.5±0.5
10	80.000	chloroform	20.5	15	2	50	0.6	RTC	Fig. e	6.9±0.6
10	80.000	chloroform	17	12	2	50	0.6	RTC	Fig. f	12.3±1.0
10	80.000	chloroform	20.5	12	2	50	0.6	RTC	Fig. g	14.4±1.2

Figure 4.6 reveals the effect of changing flow rate, from 0.5-2 mL/h, on fibre diameter (14 kV, motion 50 rpm, polymer concentration 8% (w/w) dissolved in chloroform, collector distance: 20.5 cm (Table 4.5). Overall, increasing the flow rate from 0.5-2 mL/h caused a significant increase in fibre diameter ($P \leq 0.0001$). Results showed that a flow rate below 2 mL/h produced non-uniform fibre diameters. It was observed that fibre diameters increased when the flow rate also increased. A flow rate of 0.5 mL/h produced non-uniform fibres with an average of fibre diameter of 1.8±1.2 μm, while a significant increase in fibre diameter (4.0±1.6 μm) was observed at 1 mL/h, (although the fibres were still non-uniform). At 2 mL/h the fibres appeared uniform and with an average diameter of 6.0±0.6 μm. Flow rate is an important parameter that impacts the volume of polymer supplied to the Taylor cone, which affects jet velocity, and therefore influences the morphology and fibre diameter (Bhardwaj and Kundu, 2010, Cramariuc et al., 2013). (Milleret et al., 2011) reported that when poly (lactic-co-glycol acid) was coaxially electrospun with Degrapol® (biodegradable and biocompatible polyester-urethane), varying only the flow rate from 4 to 12 mL/h, it resulted in an increase in fibre diameter from 4 to 10 μm respectively. The present study has confirmed that the fibre diameter increased with increasing flow rate (whilst keeping other parameters the same i.e, applied voltage 14 kV, motion 50 rpm, polymer concentration 8% (*w/w*) dissolved in chloroform, and collector distance: 20.5 cm). Also, 2 mL/h feed rate was sufficient to allow the formation of uniform microfibers.

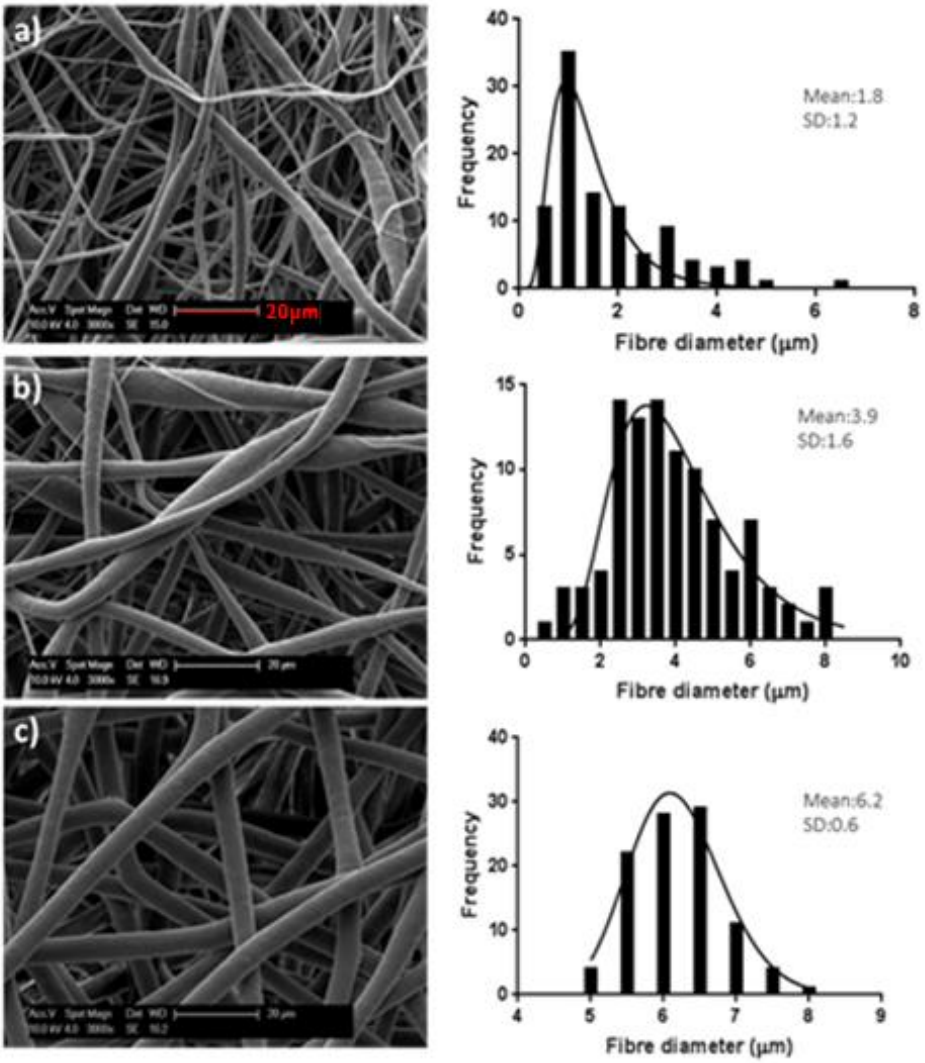


Figure 4.6 - Effect of flow rate on fibre morphology and diameter: scanning electron microscopy of PCL scaffolds from solutions of 8 % (w/w) of PCL in chloroform; flow rate: a) 0.5 mL/h, b) 1mL/h and c) 2mL/h and Log-normal distribution histogram of the size and frequency of their respective fibres. **Table 4.5** shows the corresponding electrospinning and solution parameters used here to obtain these set of electrospun scaffolds.

Table 4.5 – Electrospinning parameters used to evaluate the effect of flow rate on fibre diameter and morphology.

PCL Concentration (*w/w* %)	PCL Molar mass.	Solvent	Collector distance (cm)	Voltage (kV)	Flow Rate (mL/h)	Motion (rpm)	Needle Inner diameter mm	Collector	Sample	Fibre diameter (mean±SD) µm
8	80.000	chloroform	20.5	14	0.5	50	0.6	RTC	Fig a	1.8±1.2
8	80.000	chloroform	20.5	14	1	50	0.6	RTC	Fig b	3.9±1.6
8	80.000	chloroform	20.5	14	2	50	0.6	RTC	Fig c	6.2±0.6

RTC: Rotating target collector

Figure 4.7 reveals the effect of the applied voltage (15-25 kV) on fibre diameter (flow rate; 2 mL/h, motion 50 rpm, polymer concentration 10% (*w/w*) dissolved in chloroform, collector distance: 20.5 cm. (Table 4.6). Overall, a significant effect on fibre diameter was found when the applied voltage increased from 15 kV to 18 kV ($P \leq 0.0001$). However, an increment from 18 kV to 25 kV was found not to impact the fibre diameter (ns). Also, a significant reduction in fibre diameter was observed between the lower applied voltage (15 kV) and the higher applied voltage (25 kV) that produced fibres with an average diameter of 6.9±0.6 µm and 5.9±0.4 µm respectively.

Electrospinning voltage affects the electric force that stretches the polymer jet into fibres. High voltages may affect the jet in two ways. Firstly, high voltage may induce a larger initiating jet that yields a large fibre formation. On the other hand, a high voltage further stretches (by increasing the electric repulsive forces) the polymeric jet resulting in thinner fibres. These two processes happen simultaneously during the electrospinning process and may cancel each other out (Tong and Deng, 2013). Studies conducted by Zhang and colleagues reported that a slight increase in fibre diameter from 218±20 to 254±76 nm using poly (vinyl alcohol (PVA) solution was found when applied voltage increased from 5 to 13 kV (Zhang et al., 2005a). On the other hand, studies conducted by (Cramariuc et al., 2013) showed that a decrease in fibre diameter from 2193-973 nm occurred using PEI (polyetherimide) when the applied voltage increased from 15-35 kV. The findings presented here suggest that increasing applied voltage (15-18 kV) significantly favours smaller

fibre diameter formation due to increasing electric repulsive forces stretching the jet. Also, applied voltages above 18 kV seemed not to increase the electric repulsive forces on the polymer solution and thus no significant change in jet formation and fibre diameter was observed.

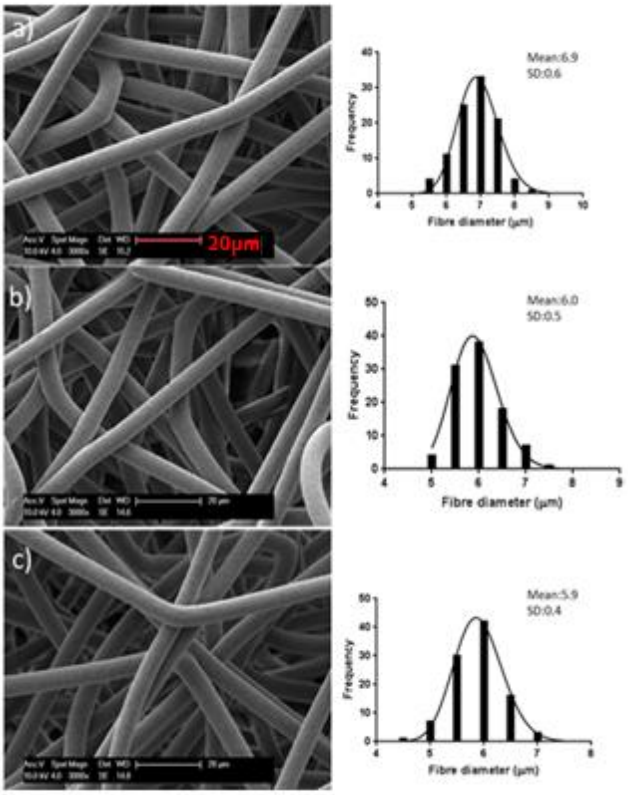


Figure 4.7 - Effect of voltage on fibre diameter. Scanning electron microscopy of PCL scaffolds from solutions of 10% (w/w) of PCL in chloroform. Applied voltage: a) 15 kV b) 18 kV and c) 25 kV and Log-normal distribution histogram of the size and frequency. Table 4.6 shows the corresponding electrospinning and solution parameters used here to obtain these set of electrospun scaffolds.

Table 4.6 - Electrospinning parameters used to evaluate the effect of applied voltage on fibre diameter

PCL Concentration (w/w %)	PCL Molar mass.	Solvent	Collector distance (cm)	Voltage (kV)	Flow Rate (mL/h)	Motion (rpm)	Needle Inner diameter mm	Collector	Sample	Fibre diameter (mean±SD) µm
10	80.000	chloroform	20.5	15	2	50	0.6	RTC	Fig a	6.9±0.6
10	80.000	chloroform	20.5	18	2	50	0.6	RTC	Fig b	6.0±0.5
10	80.000	chloroform	20.5	25	2	50	0.6	RTC	Fig c	5.9±0.4

RTC: Rotating target collector

Figure 4.8 compares the effect of PCL concentration and solvent type on the fibre diameter. It was found that concentrations of PCL below 8% (*w/w*) were not able to produce electrospun fibre scaffolds without defects and beads. In this study, PCL solution concentrations of 8 and 10 % (*w/w*) were tested; the applied voltage, flow rate and motion were maintained constant whereas the collector distance was modified to ensure the collection of the fibres on the drum collector (Table 4.7). The results showed a significant increase in fibre diameter from 5.1±0.7 to 6.9±0.6 μm when the PCL solution concentration was increased from 8-10% (*w/w*) (whilst keeping other parameters the same- applied voltage 15 kV, flow rate 2 mL/h motion 50 rpm, polymer dissolved in chloroform).

In addition, Figure 4.8 shows a representative example of the effect of solvent choice on fibre diameters. Chloroform: methanol mixtures has been widely used to electrospin PCL (Luo et al., 2012, Nisbet et al., 2008). The study here found that in the majority of the parameters tested, the Taylor cone was unstable leading to irregular fibre formation. Figure 4.8-c shows a scaffold with uniform fibre distribution and an average fibre diameter of 3.7±0.6 μm using chloroform: methanol (3:1) and the following electrospinning settings: 15 kV, 2 mL/h and 50 rpm collector drum speed and a collector distance of 20.5 cm. An applied voltage above or below 14-18 kV led to irregular fibre formation. In addition, the average fibre diameter when using the solvent mixture (chloroform: methanol 3:1) was significantly reduced to 3.7±0.6 μm ($P \leq 0.0001$) compared with the same conditions using chloroform alone as the solvent 6.9±0.6

μm (compare Figure 4.8-a) with Figure 4.8-c). It is clear that solvents influence the capability of the electrospinning process, and that it is associated with the dielectric constant of the solvents. The dielectric constant of chloroform is 4.8 (F/m) at 20°C while the mixture of chloroform: methanol (3:1) has a higher dielectric constant of 18.7 (F/m).

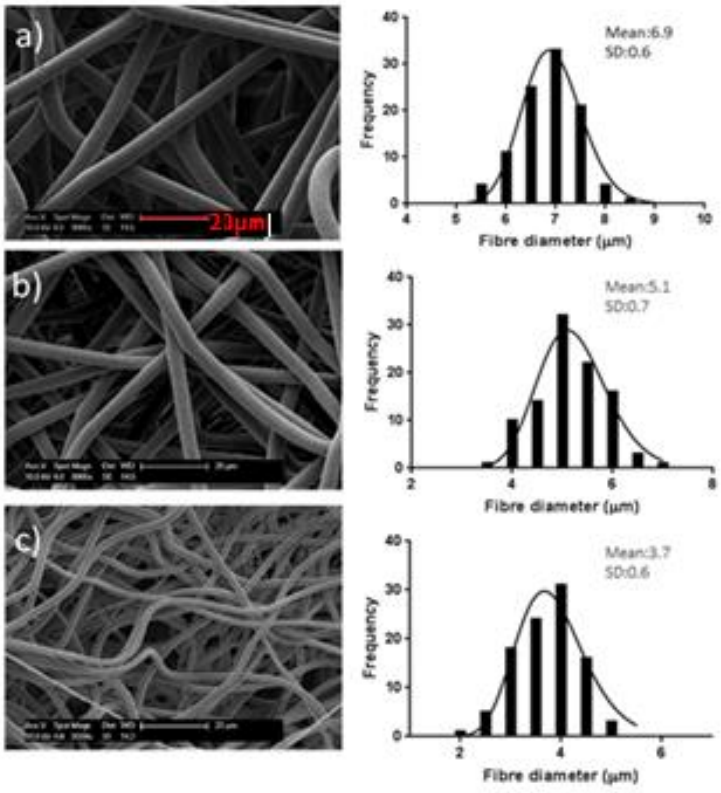


Figure 4.8 - Effect of PCL solution concentration and solvent on fibre diameter. Scanning electron microscopy of a) PCL scaffolds from solutions of 10% *w/w* of PCL in chloroform b) 8% (*w/w*) of PCL in chloroform c) 10% (w/w) of PCL in chloroform d) 10% (*w/w*) of PCL in chloroform: methanol (3:1) x 3000 and Log-normal distribution histogram of the size and frequency of the respective fibres. **Table 4.7**shows the corresponding electrospinning and solution parameters used here to obtain these set of electrospun scaffolds.

Table 4.7 - Electrospinning parameter used to evaluate the effect of PCL solution

PCL Concentration (*w/w* %)	PCL Molar mass.	Solvent	Collector distance (cm)	Voltage (kV)	Flow Rate (mL/h)	Motion (rpm)	Needle Inner diameter mm	Collector	Sample	Fibre diameter (mean±SD) μm
10	80.000	chloroform	20.5	15	2	50	0.6	RTC	Fig a	6.9±0.6
8	80.000	chloroform	17	15	2	50	0.6	RTC	Fig b	5.1±0.7
10	80.000	Chl: MeOH	20.5	15	2	50	0.6	RTC	Fig c	3.7±0.6

Chl:MeOH: chloroform; methanol mixture ratio 3:1
RTC: Rotating target collector

The current findings showed that a minimum concentration of 8% (*w/w*) of PCL (80.000 g/mol) was required to produce uniform fibres. This suggests that a minimum concentration to stabilize fibre formation exists. Furthermore the observed increase in fibre diameter by increasing the concentration of PCL has been related to viscosity which varies according to polymeric solution concentration and molecular weight (Ki et al., 2005). At lower viscosities, there are not enough viscoelastic forces in the polymeric jet to overcome the repulsive forces of charge, resulting in a fragmentation of the jet (Ki et al., 2005). Contrary, it was reported that increasing polymeric concentration influences the morphology of fibres progressing from beads, beaded fibres, fibres only and globular fibres (Chisca et al., 2012). In addition, at higher concentrations of polymeric solution, viscoelastic forces cause the polymeric jet to resist stretches, resulting in an increase in fibre diameter (Ki et al., 2005). Similar conclusions were obtained by (Zhang, 2011), who evaluated the effect of PLGA concentration on fibre morphology. They found that fibre diameter increased significantly from 327 to 856 nm when the concentration of PLGA increased from 17-20 wt%.

In addition, findings related to the influence of the solvent system on fibre formation presented here are in agreement with the findings shown by (Luo et al., 2012) who indicated that PCL dissolved in a solvent of partial to high solubility with a moderate dielectric constant and high rate of evaporation (such as chloroform) led to the formation of fibres with an average diameter in the order of 6 µm.

4.3.5 Biological evaluation of PCL scaffolds

4.3.5.i Cell metabolic activity

Figure 4.9 shows fluorescence readings at ex/em 560/590 nm produced by fibroblasts cultured on various PCL scaffolds on day 0 (6 h post seeding), 3, 6, 9 and day 12 post-seeding. Overall, significant differences in terms of metabolic activity were observed after 3 days post-seeding. Metabolic activity of cells cultured on scaffolds with an average fibre diameter of 3.6±0.8 μm and 6.9±0.8 μm increased significantly ($p \leq 0.05$) compared with 14.4±0.8 μm after 3 days post seeding. On day 6 and onward, a significant enhancement ($P \leq 0.0001$) in metabolic activity of fibroblasts cultured on scaffolds with an average fibre diameter of 3.6±0.5 μm was observed, compared with other PCL scaffolds. These results revealed that PCL scaffolds were not toxic to the cells and scaffolds composed of fibres with average diameters ~4 μm supported cell proliferation.

Some authors correlate the importance of fibre diameter with cell attachment, cell growth and cellular infiltration (Farrugia et al., 2013, Chen et al., 2007, Pham et al., 2006, Balguid et al., 2008, Zander et al., 2013, Maghdouri-White et al., 2014). Fibre diameter modifies pore size (Skotak et al., 2011) and porosity, mechanical properties (Maghdouri-White et al., 2014) and thus cell infiltration and cell growth.

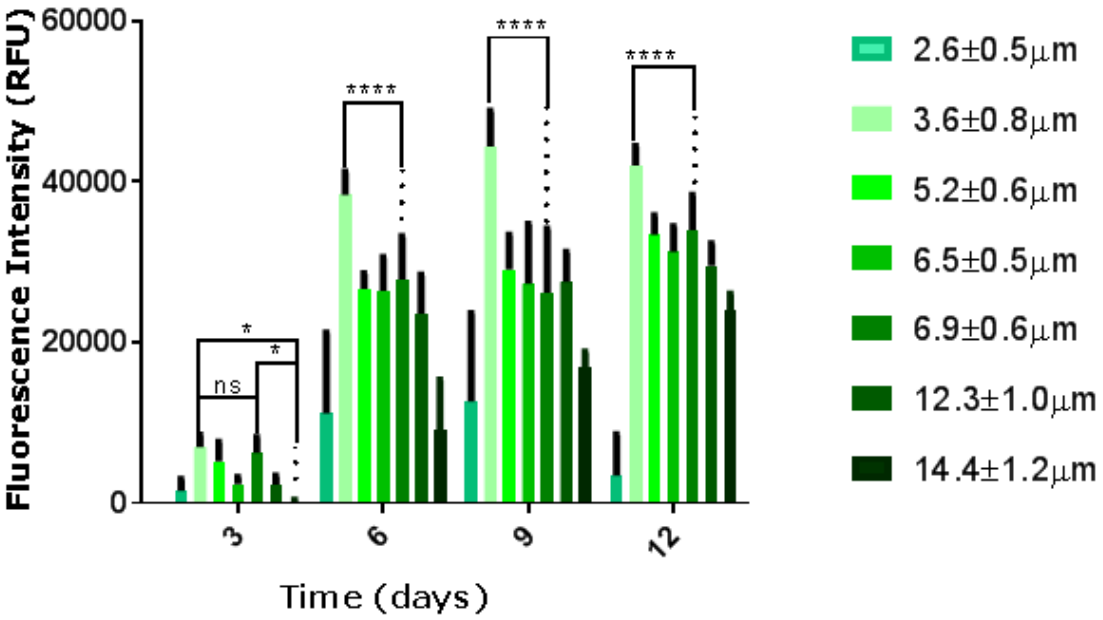


Figure 4.9 - Fluorescence readings of metabolic activity of 3T3 GFP fibroblasts cultured on PCL scaffolds with different fibre diameters, over 12 days. 3T3 metabolic activity was assessed using AlamarBlue®. Two way-ANOVA, Tukey's multiple comparison test. Three independent experiments carried out in triplicate (means±SD).

A scaffold that possesses a larger fibre diameter would correspond to greater pore size. This means that the balance between porosity and fibre diameter are crucial for achieving successful tissue regeneration (Zander et al., 2013). In this sense, pores need to be large enough to allow cell growth, infiltration and nutrient/waste transport, but not so large that cells are not retained within the scaffold (Balguid et al., 2008). They indicated that fibre diameter between ~4 and 10 μm should be optimal to support cell growth and infiltration. In addition (Wang et al., 2014b) correlated the importance of a scaffold with an average fibre diameter of ~5-6 μm to support tissue remodelling, indicating that thicker fibres induce the polarization of macrophages supporting a M2 phenotype, while scaffolds composed of thinner fibre (nano scale) caused macrophages to express an inflammatory phenotype (M1). Hence, scaffolds with a moderate fibre diameter and

pore size allow cellular infiltration and cell growth whilst not supporting prolonged inflammation (Zander et al., 2013). In another study, the authors (Pham et al., 2006) fabricated PCL scaffolds in a range from 2-10 μm and pore size ranging from 20-45 μm with a constant porosity between 84-89 %. They found that cells were homogenously distributed on scaffolds with average fibre diameters between 4-10 μm. Another author (Farrugia et al., 2013) more recently published that scaffolds with an average of 7.5±1.6 μm allowed dermal fibroblast infiltration into PCL scaffolds with 87% porosity. Moreover (Del Gaudio et al., 2009) electrospun fibres with 2 different fibre diameters and evaluated the cellular response. Human umbilical vein endothelial cells (HUVECs) were cultured on PCL scaffolds with average fibres diameters of 0.8±0.2 um and 3.6±0.8 μm. What they found is in completely agreement with the findings in the present study. It was found that fibre diameters around 4 μm supported a significantly higher viability of HUVEC cells compared with 0.8 ±0.2 μm after 7 days. This can be explained by the fact that cells growing on small fibres tend to proliferate in a monolayer on the scaffold surface, while cells penetrate through the scaffolds consisting of bigger fibres allowing growth within the scaffolds (Chen et al., 2007, Lowery et al., 2010).

4.3.5.iiCell morphology and cell-scaffold interactions

Figure 4.10 shows phase contrast and fluorescence merged images and SEM images of fibroblasts adhered to different PCL scaffolds after 5 days of culture. Fibroblasts adhered strongly to the scaffold fibres and there is evidence of spreading. From SEM micrographs, it can be clearly observed that cells created bridges between fibres forming a 3D network with the surrounding mesh. These properties are required for an adequate physiological function (Choi et al., 2015).

Figure 4.11 shows confocal imaging of fibroblasts on the different scaffolds. Fibroblasts grew on all the scaffolds and it observed that the morphology of fibroblasts on the scaffold with an average fibre diameter of 3.6±0.8, 5.2±0.6, 6.5±0.5, 6.9±0.6, 12±0.1 and 14±1.2 μm was elongated characteristic of fibroblasts. By contrast, fibroblasts on scaffold 2.6±0.5 μm were poorly spread. This may be due to the decreased fibre diameter and the fact that these scaffolds were very thin.

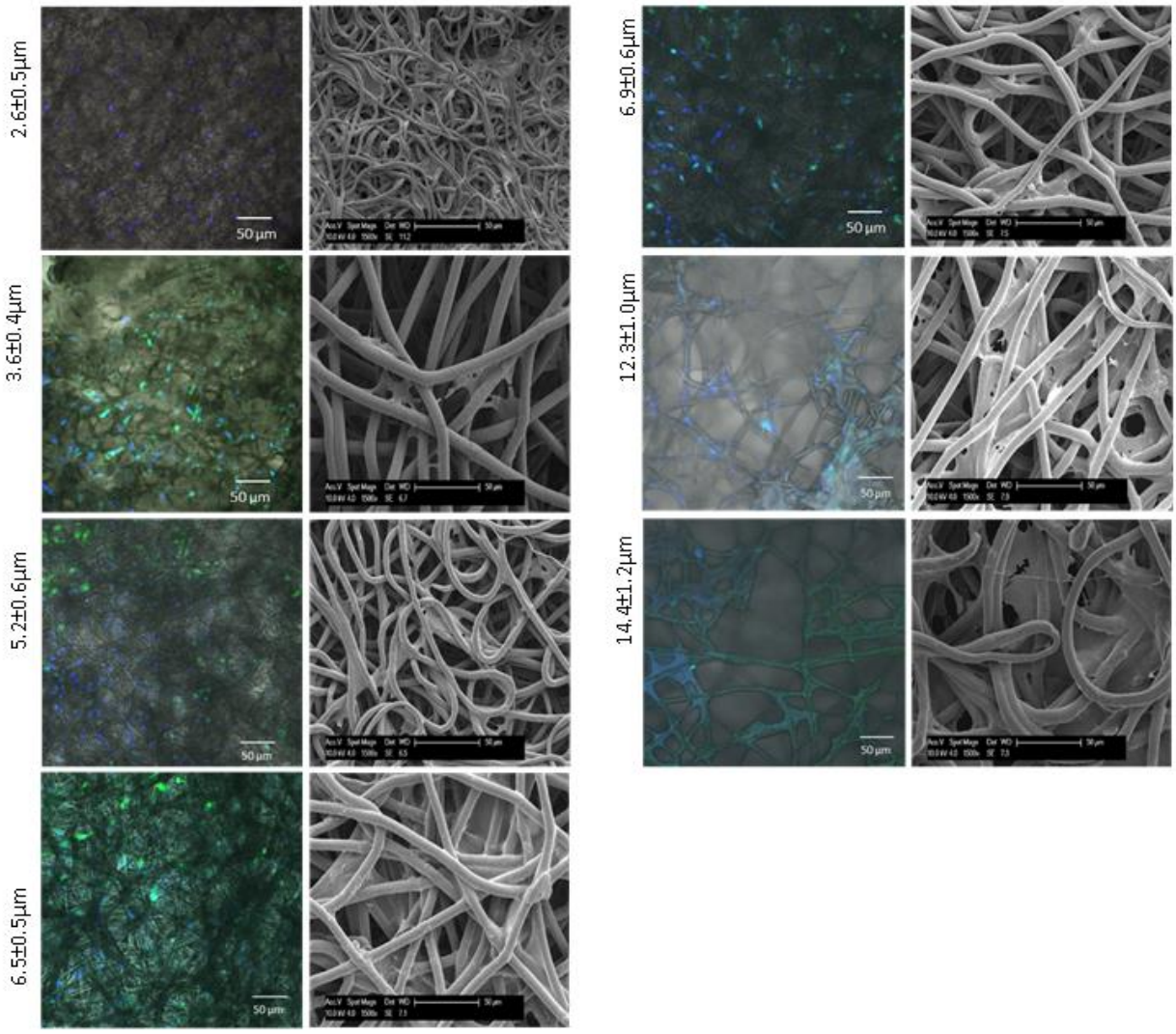


Figure 4.10 - On the left side phase contrast and fluorescence merged images of fibroblast 3T3 GFP attached to the different PCL scaffolds. Magnification x20, scale bar = 50 µm. On right side SEM images from 3T3 fibroblast on different PCL scaffolds showing normal attachment to the scaffold surfaces.

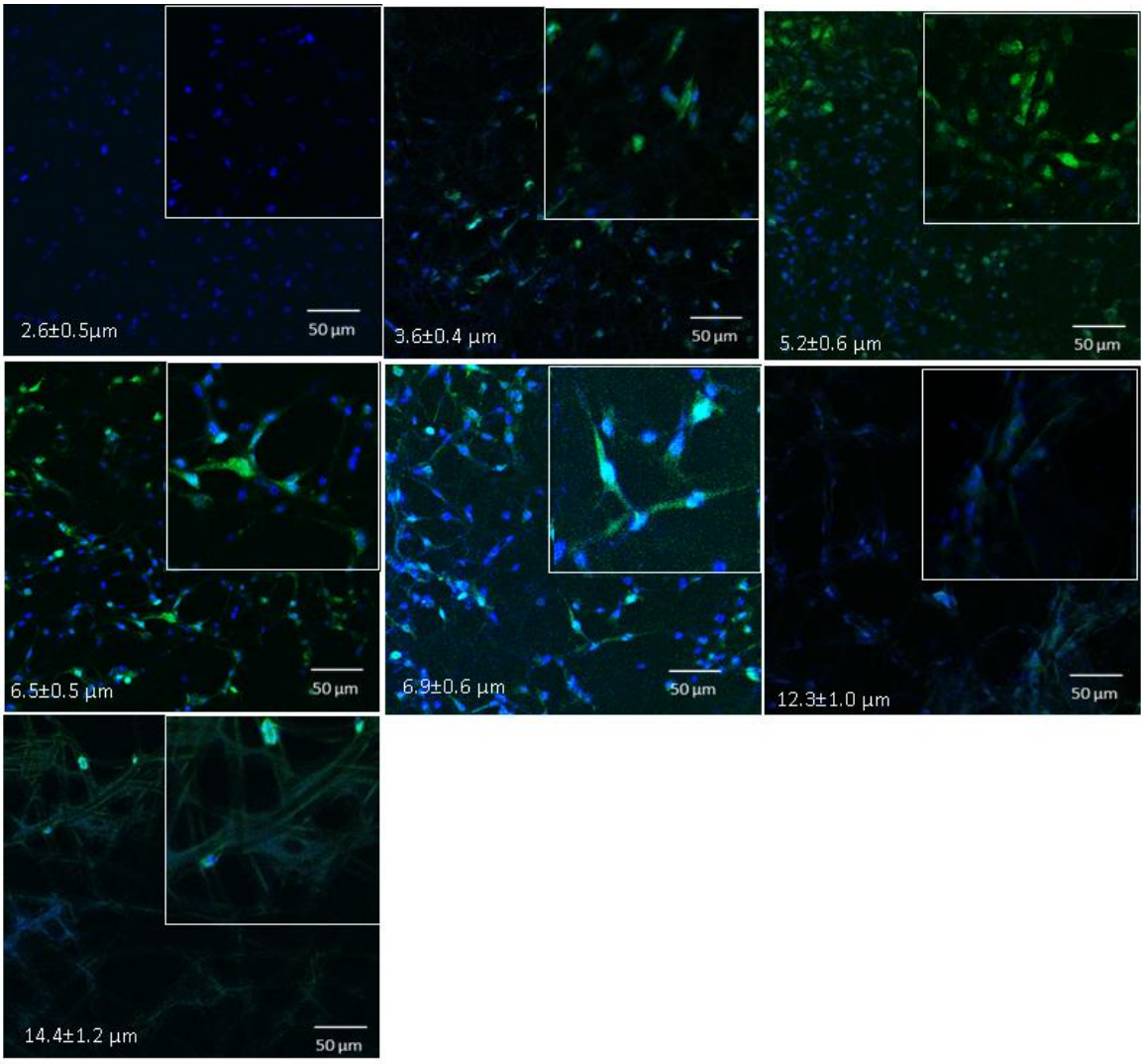


Figure 4.11 - Confocal images of GFP 3T3 fibroblasts cultured on PCL scaffolds. Images taken using 405 nm and 488 nm laser lines and sequential imaging of Hoechst and GFP was performed. Fibroblasts were genetically modified to express GFP (green) and stained with Hoechst. Magnification x20, scale bar = 50 µm. The inset images in the figures is a zoom of an area to visualise the cell morphology.

4.3.5.iii Cell infiltration

Figure 4.12 and Figure 4.13 show the maximum depth of cell infiltration from top to bottom for PCL scaffolds with different fibre diameters. In general, fibre diameter 3.6±0.8, 5.2±0.6 and 6.5±0.5 µm did not influence cell infiltration (maximum infiltration 40%) (ns p value >0.05). In scaffolds with an average fibre diameter of 6.9±0.6 µm cells were able to migrate further into the scaffold (52%) and found to be which is statistical significant ($p \leq 0.01$) compared with 3.6±0.8 µm ($p < 0.001$) and with material 5.2±0.6 and 6.5±0.5 µm. A lower level of cellular infiltration was observed for scaffolds of average fibre diameter of 12±0.1 and 14±1.2 µm. The necessity to develop a scaffold that allows cell infiltration rather than a simple substrate for cell adhesion has been recognised in the literature (Kurpinski et al., 2010, Zaiss et al., 2016). It has been reported that scaffolds need a minimum depth more than 100 µm to permit cell infiltration, large fibre diameter and hence open pores (Zaiss et al., 2016, Zander et al., 2013). However, the porosity should not be so high to allow cells to split (Zander et al., 2013). In the study presented here, the scaffolds supported an infiltration of ~40-50% 5 days post seeding. Only fibres with larger diameters (14±1.2 µm and 12±0.1) presented low infiltration of ~15%. Also, it seems that smaller fibres were not found to support cell infiltration according to the confocal images. The data presented here illustrates that scaffolds with average fibre diameters between ~4-7 µm and, with a porosity of around 80 % supported cell growth and infiltration. These findings are in agreement with the results presented by (Pham et al.,

2006), who reported that the inner-fibre distances increased from 20-45 μm. The latter, by increasing fibre diameter of PCL scaffolds from 4 to 10 μm, which it seems to fit with the size of a cell, and thus enabling cellular infiltration. While, scaffolds with fibre diameter from 0.1 to 1 μm have been reported to have a small inner-fibre distances and limit cellular infiltration. This was also confirmed by (Zander et al., 2013). Cellular infiltration is an important parameter to consider for a wound healing application (Chong et al., 2007a, Zhong et al., 2010).In addition, a minimum scaffold thickness (~60 microns) is required in order to allow handling; as for cell culture the findings of this study differ from the minimum thickness reported in the literature (100-200 μm) (Vaquette and Cooper-White, 2011).

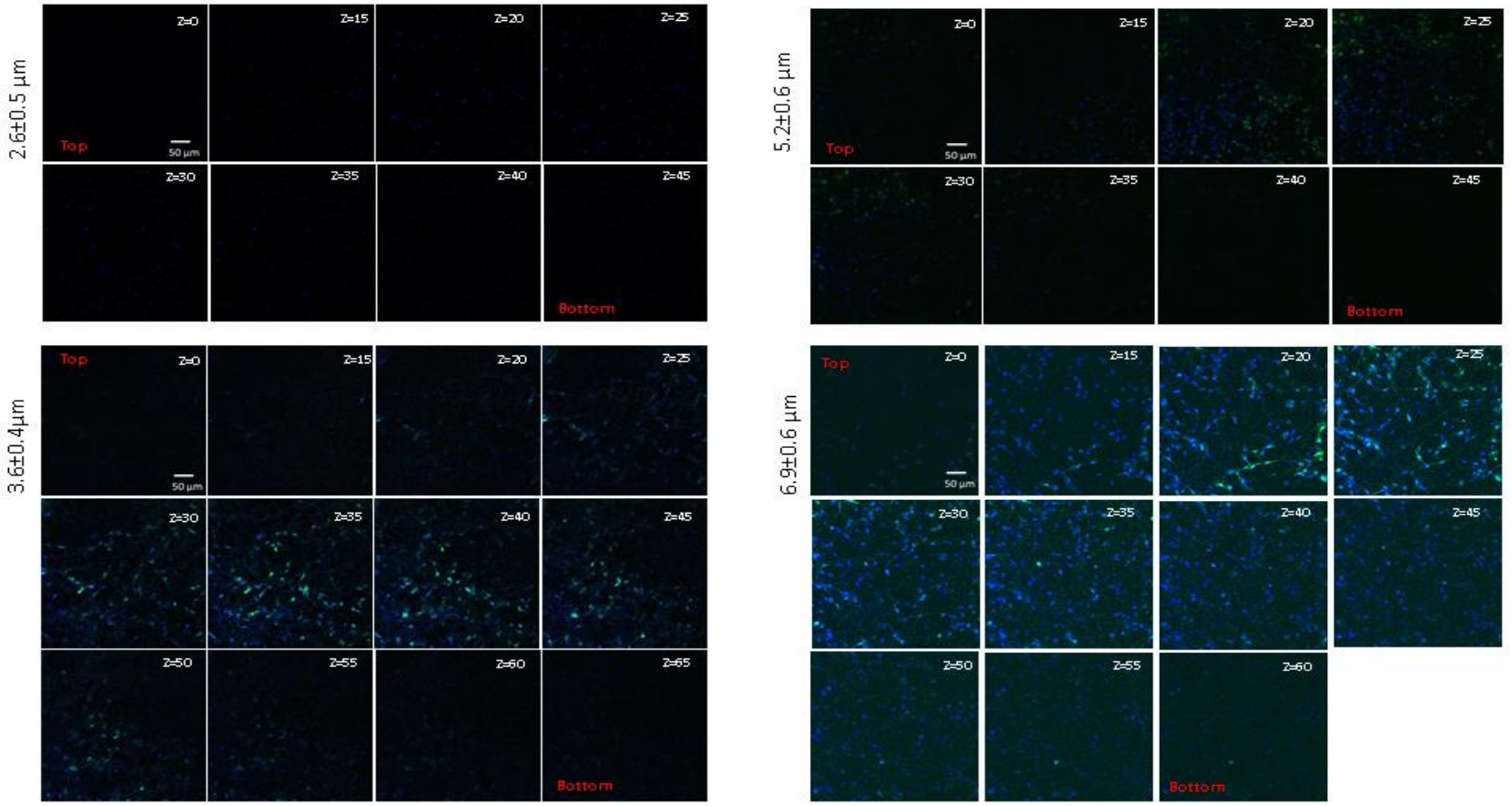


Figure 4.12 – Confocal microscope z-stack images of 3T3 GFP fibroblasts seeded onto the PCL microfibrous scaffolds after 5 days of growth. In each group z-stack images of different planes showing from surface to bottom are shown. Cells are pre-stained with GFP (green) and Hoechst for nucleus (blue). Magnification x20, scale bar = 50 µm.

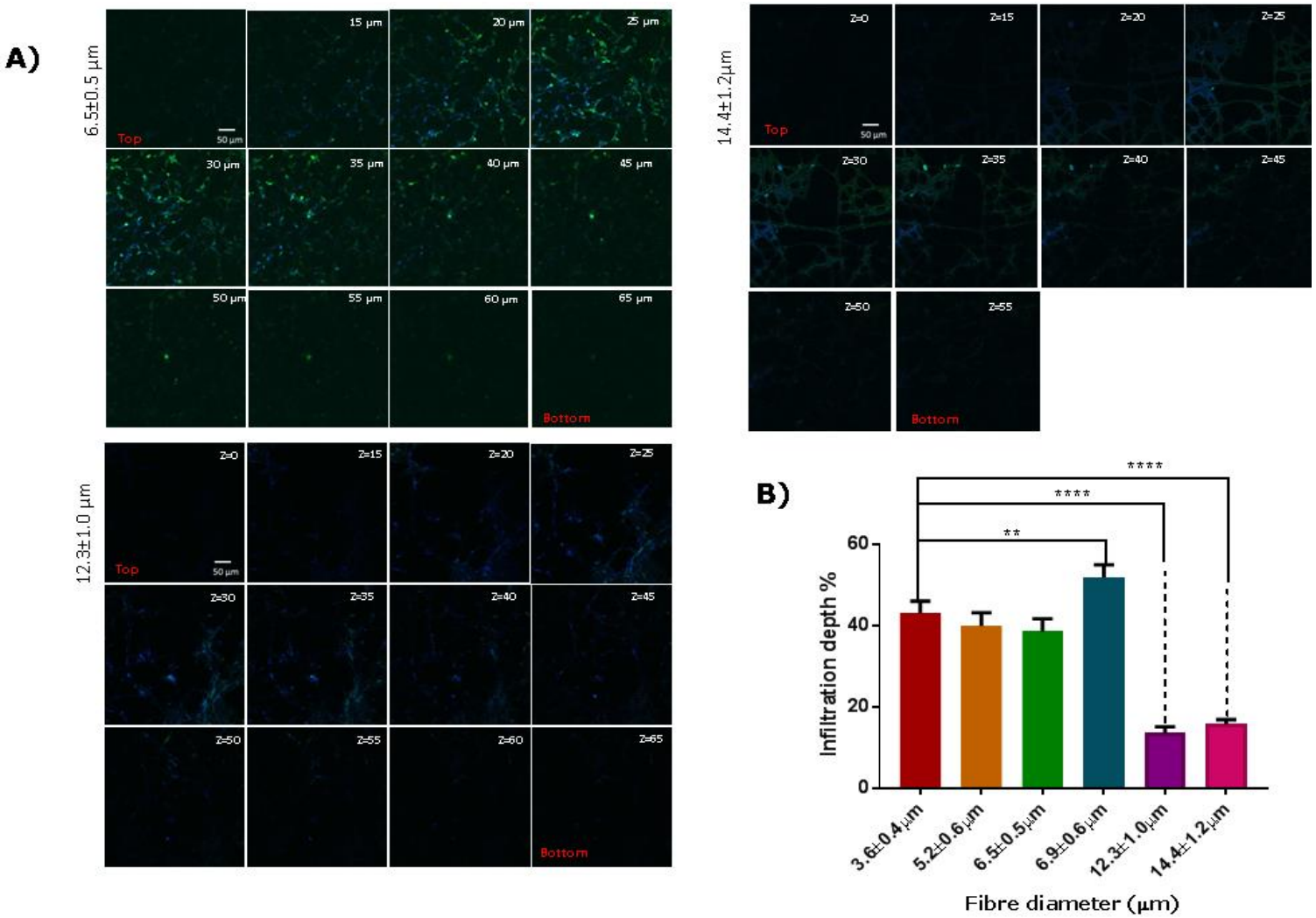


Figure 4.13 - A) Confocal microscope z-stack images of 3T3 GFP fibroblasts seeded onto the PCL microfibrous scaffolds after 5 days of growth. In each group z-stack images of different planes showing from surface to bottom with 5 µm plane thickness are shown. Cells are pre-stained with GFP (green) and Hoechst for nucleus (blue). Magnification x20, scale bar = 50 µm. Bottom right-figure show a graph relating fibre diameter and percentage of infiltration. **B)** Infiltration depth % of 3T3 GFP fibroblasts cultured on PCL scaffolds with different fibre diameters, over 5 days. Cellular infiltration was assessed using z-stack confocal analysis and SEM cross section analysis of thickness. Three independent experiments carried out in triplicate (means±SD).

4.3.6 Geometrical evaluation of PCL-b-PEG and its blends PCL-b-PEG/PCL scaffolds ratios 40:60; 50: 50 and 60:40.

4.3.6.i Fabrication and morphology analysis (SEM)

Figure 4.14 shows representative images of the main electrospun scaffolds produced, using the solutions and electrospinning parameter indicated in Table 4.8. Morphological and fibre distribution of the produced PCL-b-PEG and its blends PCL-b-PEG/PCL (ratios 40:60; 50: 50 and 60:40) scaffolds were examined.

A total of 4 scaffolds were produced for PCL-PEG solutions (without blending with PCL). One of these had an average fibre diameter of 0.1±0.1 μm (Figure 4.14-a). The rest of the scaffolds were seen to possess heterogeneous fibres, ribbons and beads likely to be due to the low viscosity of the blends as discussed above.

Initially, six electrospun scaffolds were produced by electrospinning PCL-b-PEG/PCL solutions, with ratios of 40:60 15% *w/w* (Figure 4.14-c)-e)). PCL-b-PEG/PCL solutions, with a ratio of 40:60, tended to clog the needle and only 3 scaffolds were produced. A total of 14 scaffolds were produced from the electrospinning of PCL-b-PEG/PCL solutions, with ratios of 50:50 and 60:40 (15% *w/w*). The average fibre diameter ranged from 0.1±0.1 and 3.1±0.7 μm for all. From SEM analysis (Figure 4.14) it was found that the distribution of fibres was homogenous. Figure 4.14-c), d) and f) correspond to the electrospinning of PCL-b-PEG/PCL solutions, with ratios 40:60 and 50:50 where the viscosity was amenable for electrospinning.

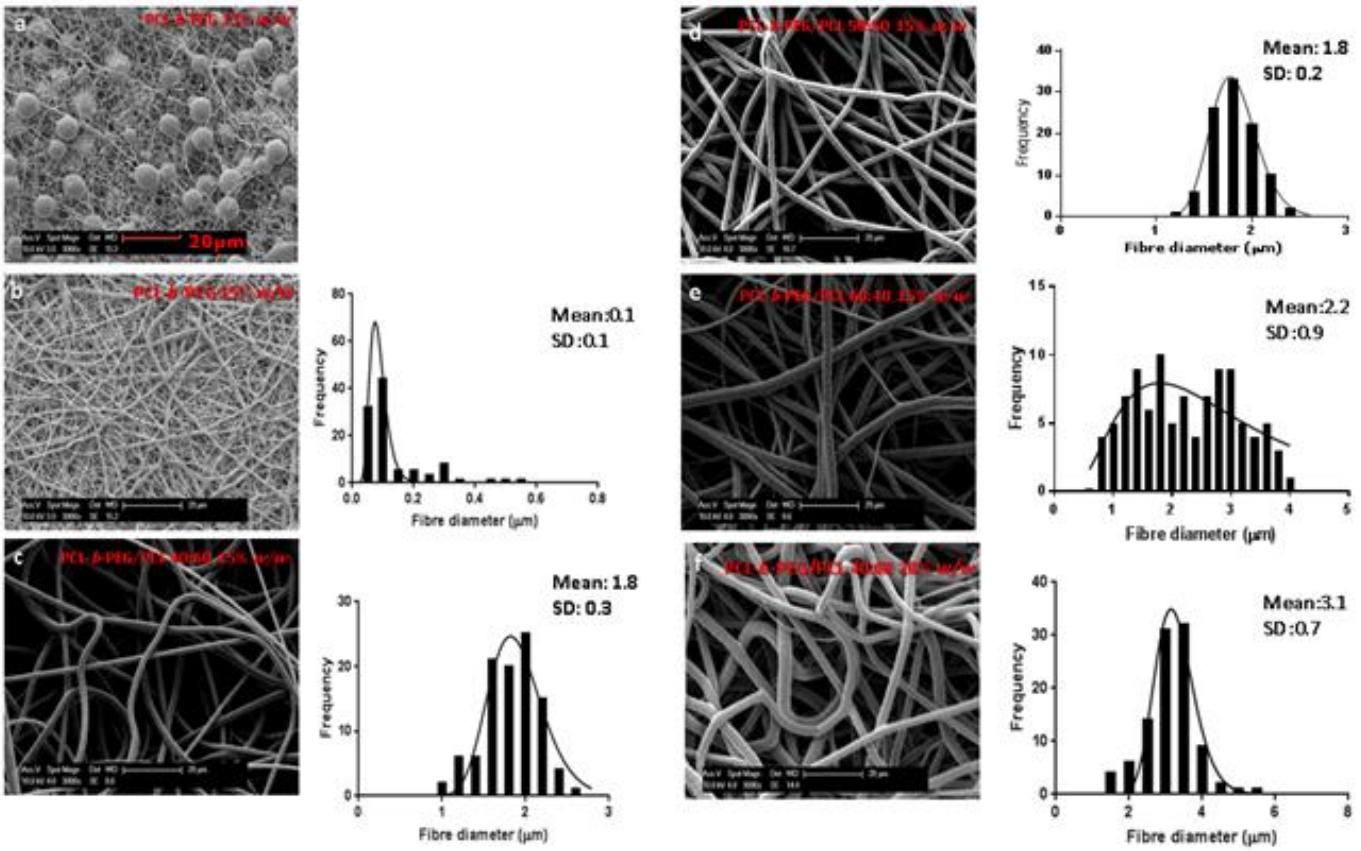


Figure 4.14 – Representative SEM micrographs (at x3000 mag, scale bar 20 μm) of PCL-PEG scaffolds (a and b) and blended PCL-b-PEG/PCL scaffolds (c-f) produced under different conditions summarised in **Table 4.8**. Graphs illustrate log normal distribution of the size and frequency of their respective fibres

Table 4.8 - Electrospinning parameters for PCL-b-PEG and PCL-b-PEG/PCL scaffold production

PCL-b-PEG/ PCL (*w/w* %)	Ratio PCL-*b*-PEG:PCL	Solvent	Collector Distance (cm)	Voltage (KV)	Flow rate (mL/h)	Motion (rpm)	Figure	Fibre diameter (μm)
15	PCL-b-PEG	CF	20-17	10-18	1.25-2	50	Fig. a	Only beads
15	PCL-b-PEG	CF	20.5	20	2	50	Fig. b	0.1±0.1
15	40:60	CF	20.5	18	2	50	Fig. c	1.8±0.3
15	50:50	CF	20.5	18	2	50	Fig. d	1.8±0.2
15	60:40	CF	20.5	18	2	50	Fig. e	2.2±0.9
20	40:60	CF	20.5	18	2	50	Fig. f	3.1±0.7

4.3.7 Fabrication of electrospun scaffolds based on PCL-b-PEG/ PCL blends at a ratio 40:60 (15 % *w/w*).

Figure 4.15 shows representative SEM images of these PCL-b-PEG/ PCL 40:60 (15% *w/w*) scaffolds. After a preliminary biological compatibility study of scaffolds containing various levels of PEG a PCL-b-PEG/PCL blend ratio 40:60 (15% *w/w*) was chosen (appendix) because present the highest metabolic activity of fibroblasts. Overall, the scaffolds were characterised by uniform and random fibres, with interconnected pores, without beads or any another defect. In order to obtain these scaffolds, electrospinning parameters were varied as shown in Table 4.9. Figure 4.15 shows uniform electrospun fibres with an increasing average fibre diameter of a) 1.0±0.4 b) 1.8±0.9; c) 2.0±0.4; d) 2.1±0.5; e) 2.2±0.3; f) 2.5±0.8; g) 3.1±0.7 and h) 3.5±0.4 µm. Figure 4.15-g) and h) show the scaffold produced with the largest fibre diameters, which were obtained by using a PCL-b-PEG/ PCL 40:60 solution of 15% (*w/w*) concentration, applying a lower voltage (10 kV), and shortening the collector plate distance during the electrospinning process (flow rate 2 mL/h and rotation speed 50 rpm).

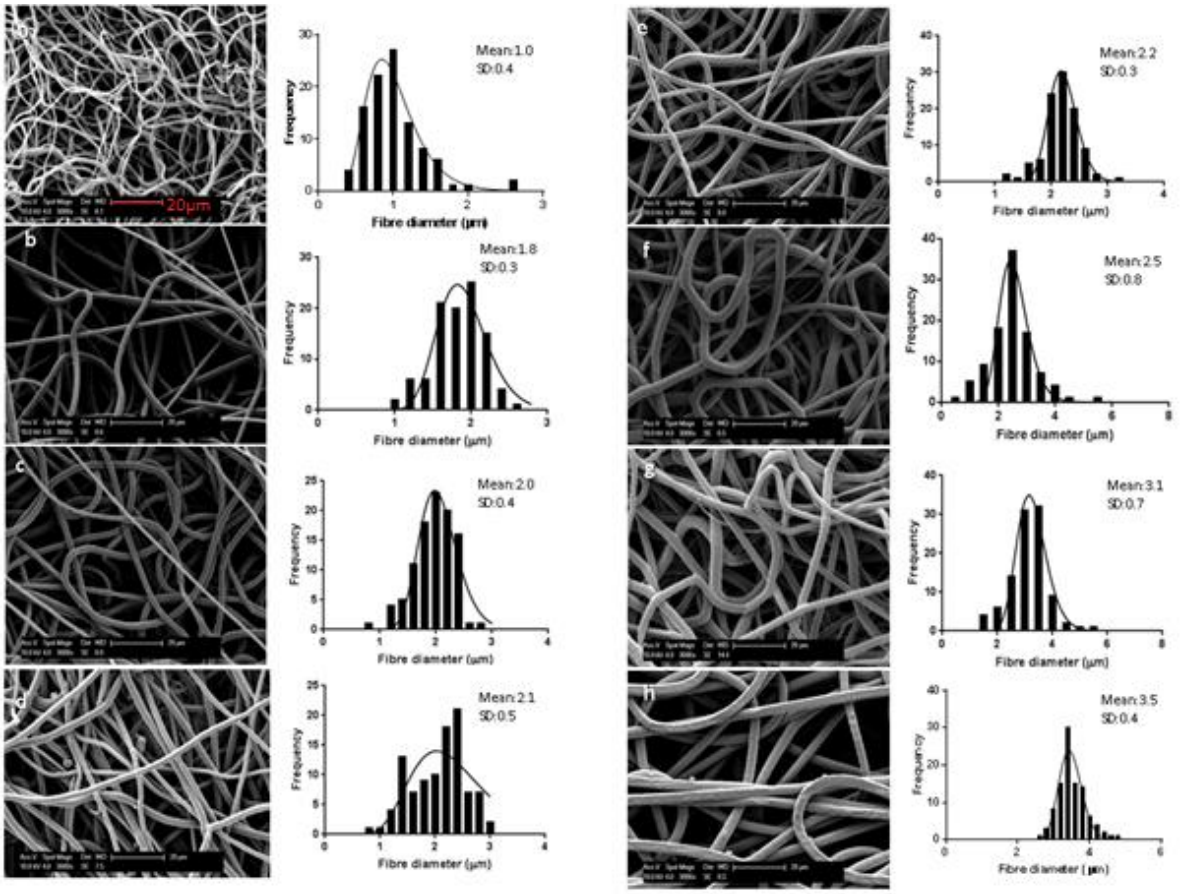


Figure 4.15 - SEM micrographs (at x3000) of PCL-PEG/PCL 40:60 scaffolds produced under different conditions summarised in **Table 4.9**. Scale bar 20 µm and log –normal distribution of the size and frequency of their respective fibres

Table 4.9 - Electrospinning parameters for PCL-b-PEG/PCL 40:60 scaffold production

PCL-b-PEG/ PCL (w/w %)	Ratio PCL-*b*-PEG:PCL	Solvent	Collector Distance (cm)	Voltage (KV)	Flow rate (mL/h)	Motion (rpm)	Figure	Fibre diameter (µm)
15	40:60	CF	16.5	10	2	50	Fig. h	3.5±0.4
15	40:60	CF	20.5	15	2	50	Fig. e	2.2±0.3
15	40:60	CF	20.5	18	2	50	Fig. c	2.0±0.4
15	40:60	CF	20.5	20	2	50	-	No scaffold
15	40:60	CF	16.5	18	2	50	Fig. f	2.5±0.3
15	40:60	CF	11.5	18	2	50	Fig. a	1.0±0.4
15	40:60	CF	20.5	18	1.25	50	Fig. b	1.8±0.3
15	40:60	CF	20.5	18	3	50	Fig. d	2.1±0.4
20	40:60	CF	20.5	18	2	50	Fig. g	3.1±0.7

4.3.8 Biological evaluation of fibrous scaffolds of different fibre diameter fabricated from PCL-b PEG/PCL 40:60 (15% *w/w*) blend

4.3.8.i Cellular metabolic activity

Figure 4.16 shows metabolic activity of GFP expressing 3T3 fibroblasts cultured on scaffolds fabricated from PCL-b-PEG/PCL 40:60 (15% *w/w*) with different fibre diameters. From these results, it can be seen that there is no significant difference in fibroblast metabolic activity observed 3 days post seeding. On day 6, a significant increase ($P<0.001$) in fibroblast metabolic activity was observed on scaffolds with an average fibre diameter of 3.5±0.5 μm compared with other scaffolds with a smaller fibre diameter. Day 9 and onwards, no significant statistical differences were observed in terms of fibroblast metabolic activity when cultured on scaffolds with average fibre diameters between 3.5±0.5 μm, 1.8±0.3 μm and 2.5±0.3 μm. A lower metabolic activity was observed for fibroblasts cultured on scaffolds comprised of the smallest fibre diameter 1.0±0.4 μm. Statistical differences were found in terms of fibroblast metabolic activity for fibroblasts on 3.5±0.5 μm ($p <0.001$) and fibroblasts cultured on 1.0±0.4 μm.

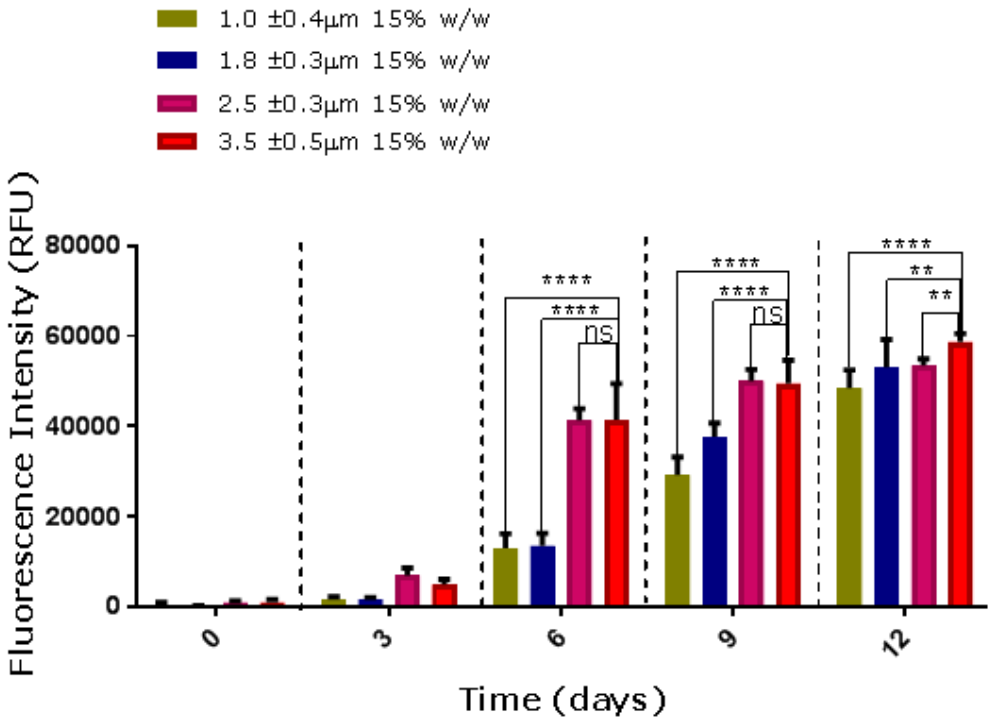


Figure 4.16 - 3T3 metabolic activity was assessed using Alamar Blue™. Fluorescence readings of metabolic activity of 3T3 GFP fibroblasts cultured on PCL-b-PEG/PCL 40:60 15% w/w scaffolds with different average fibre diameter over 12 days. Two way-ANOVA, Tukey's multiple comparison test. Three independent experiments carried out in triplicate (means±SD).

4.3.8.iiCell morphology and cell-scaffold interactions

Figure 4.17 shows phase contrast and fluorescence merged images and SEM images of fibroblasts adhered to different PCL-b-PEG/PCL 40:60 scaffolds after 5 and 12 days of culture. Figure 4.18 shows confocal imaging of fibroblasts on the same scaffolds. In general, it was observed that fibroblasts adhered to the scaffold fibres and there was evidence of spreading. Fibroblasts covered the whole surface of the scaffolds after 12 days of culture. In addition, from these images, it was clearly observed that fibroblasts attached well and spread over the whole of the scaffold with the highest average fibre diameter (3.5±0.5 μm) scaffold from an earlier stage (5 days). This cellular morphology is associated with the desired physiological function (Choi et al., 2015). On the other scaffolds, fibroblasts achieved the same pattern of coverage by day 12.

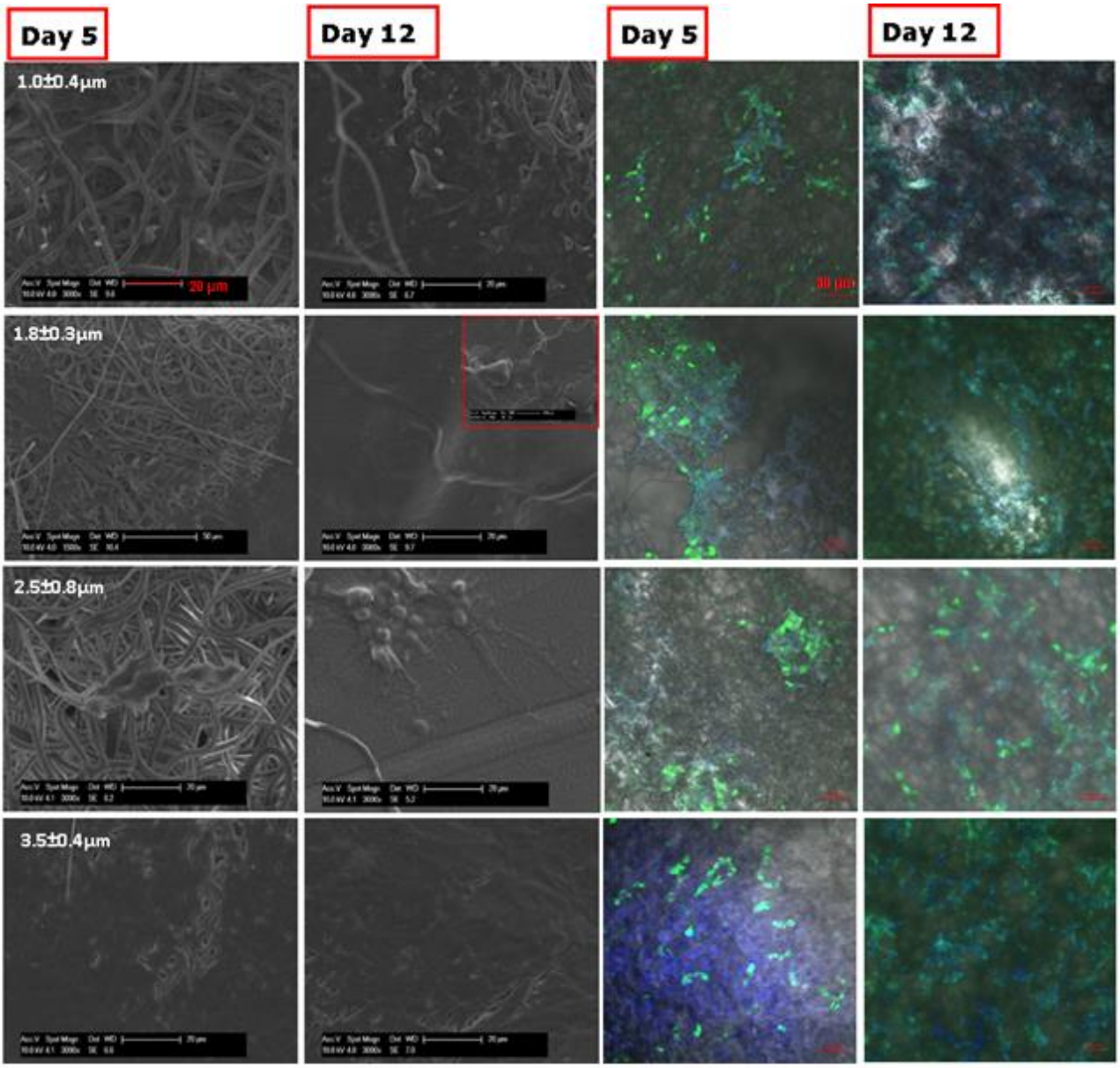


Figure 4.17 - On left side SEM images from 3T3 fibroblast on PCL-b-PEG/PCL scaffolds with different average of fibre diameter. On the right-side phase, contrast and fluorescence merged images of fibroblast 3T3 GFP attached to PCL-b-PEG/PCL with different average of fibre diameters. Magnification x20, scale bar = 50 µm. Samples were taken at day 5 and day 12 post fibroblast cultured on PCL-b-PEG/PCL scaffolds.

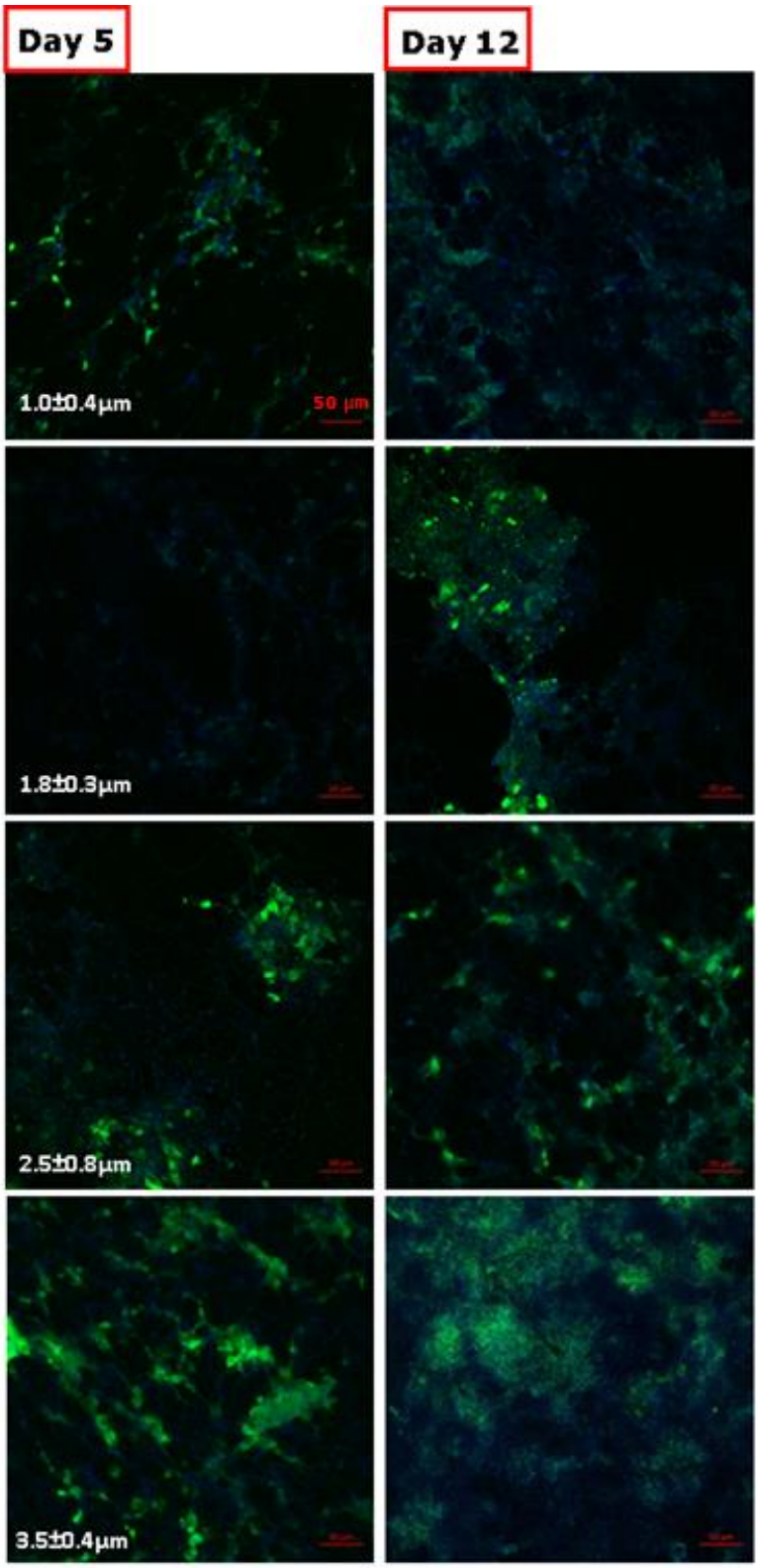


Figure 4.18 - Confocal images of PCL-b-PEG/PCL scaffolds with different average of fibre diameters. Fibroblasts were genetically modified to express GFP (green) and stained with Hoechst Images taken using 405 nm and 488 nm laser lines and sequential imaging of Hoechst and GFP was performed. Magnification x20, scale bar=50 µm

4.3.9 Porosity and thickness evaluation of electrospun scaffolds

4.3.9.i Evaluation of PCL electrospun scaffolds porosity

Figure 4.19-A shows porosity measurements (ε%) conducted by the gravimetric method, for PCL scaffolds with fibre diameter 3.6±0.8,5.2 ±0.6, 6.5±0.5, 6.9±0.6, 12±1.0 and 14±1.2 μm. No clear correlation was observed between fibre diameter and porosity. No statistical differences were found between scaffold porosity (ε%) with the porosity of scaffolds ranging from 84% to 92%. Figure 4.19-B shows images of PCL electrospun scaffolds through micro CT. No clear differences from reconstructed images were observed between materials. In addition, for gravimetric estimation of porosity, microCT analyses were performed for PCL scaffolds (Figure 4.19-C). Scaffolds with average fibre diameter of 3.6±0.8 μm showed lower porosity of 59 % compared with an average fibre diameter of 6.5±0.5 μm, which had 79 % porosity (p 0.034). Also porosity (%) was significantly higher (P 0.0030) with a fibre diameter of 12±0.1 μm (98%) and 14±1.2 (p 0.0168) (80%) compared with 3.6±0.8 μm. From these results, it was observed that porosity increased with the increasing fibre diameter. For instance, scaffolds with fibre diameter of 3.6±0.8 presented porosity of 59 %< 6.5±0.5, 79 % <6.9±0.6, 80 % < 12±0.1, 98 %. The porosity of scaffolds with a fibre diameter of 14±1.2 μm slightly dropped to 80% porosity. (Zander et al., 2013) reported that porosity and pore size of scaffolds increased as the fibre diameter of the scaffolds increased.

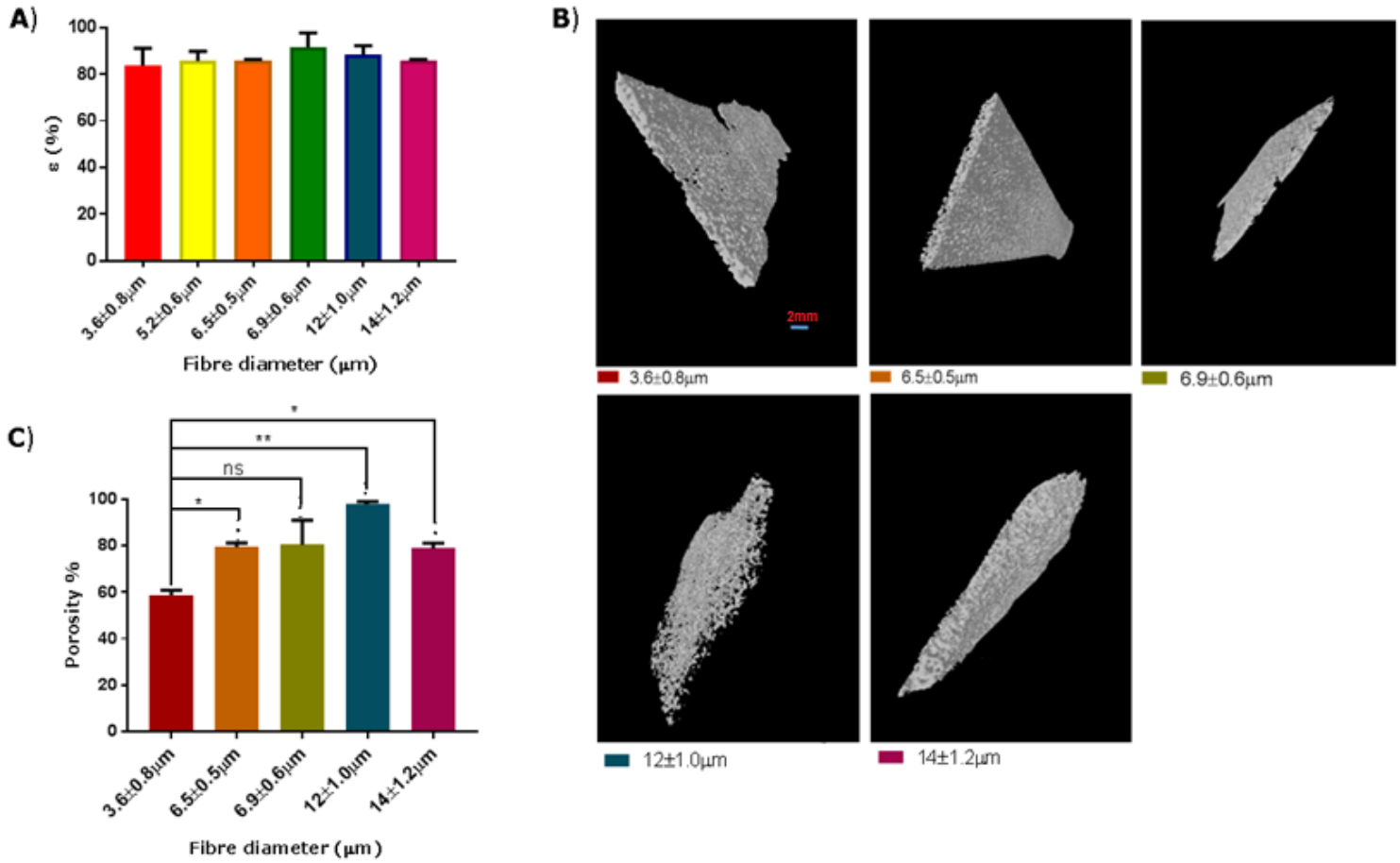


Figure 4.19 - A) porosity estimated by gravimetric method versus fibre diameter B) Visualization of electrospun scaffold through µ-CT method C) porosity versus fibre diameter estimated though microCT technique. Three independent experiments carried out in triplicate (means±SD).

In general, gravimetric analysis yielded higher porosity values compared with results obtained by microCT technique. (Lin-Gibson et al., 2007) discussed that microCT provided consistent porosity data and more reliable way to measure porosity on scaffolds.

Many authors have pointed out the importance of a high scaffold porosity to allow the diffusion of nutrients and waste and also allow the cell ingrowth (Balguid et al., 2008, Zander et al., 2013, Lowery et al., 2010). However, the optimal porosity is a controversial point. Some authors indicated that porosity should be as high as ~92% for skin regeneration (Zhu et al., 2008) while other authors (Loh and Choong, 2013) have suggested that the porosity does not need to be so high. The crucial point is to maintain the balance between mechanical properties and porosity to avoid compromising the structure integrity. The evaluation of the effect of scaffold porosity on human dermal fibroblast (HDF) penetration during 7 days concluded that the optimal porosity to allow infiltration should be within the range of 60-90% (Rnjak-Kovacina et al., 2011), which is in agreement with the study presented here, where porosity ranged from 60-92%.

4.3.9.iiEvaluation of PCL electrospun scaffolds thickness

Figure 4.20 shows representative scanning electron micrographs of PCL electrospun cross-section of different PCL scaffolds. The thickness of the scaffolds varied from 59 to 285 microns.

On the other hand, electrospun scaffolds with a low thickness were difficult to handle (i.e scaffold 2.6±0.5 μm), which agreed with the results from (Cipitria et al., 2011). In this sense, scaffolds with a thickness of ≤100 μm are considered to be thin (Huang et al., 2011). Further investigation on ticker scaffolds e.g. over 100 μm and particularly for cell infiltration scaffold with fibre diameter of 3.6±0.8, 6.5±0.5, 12±0.1 and 14±1.2, which had thicker scaffolds (over 100 μm) should reveal more cell infiltration than the thinner scaffolds.

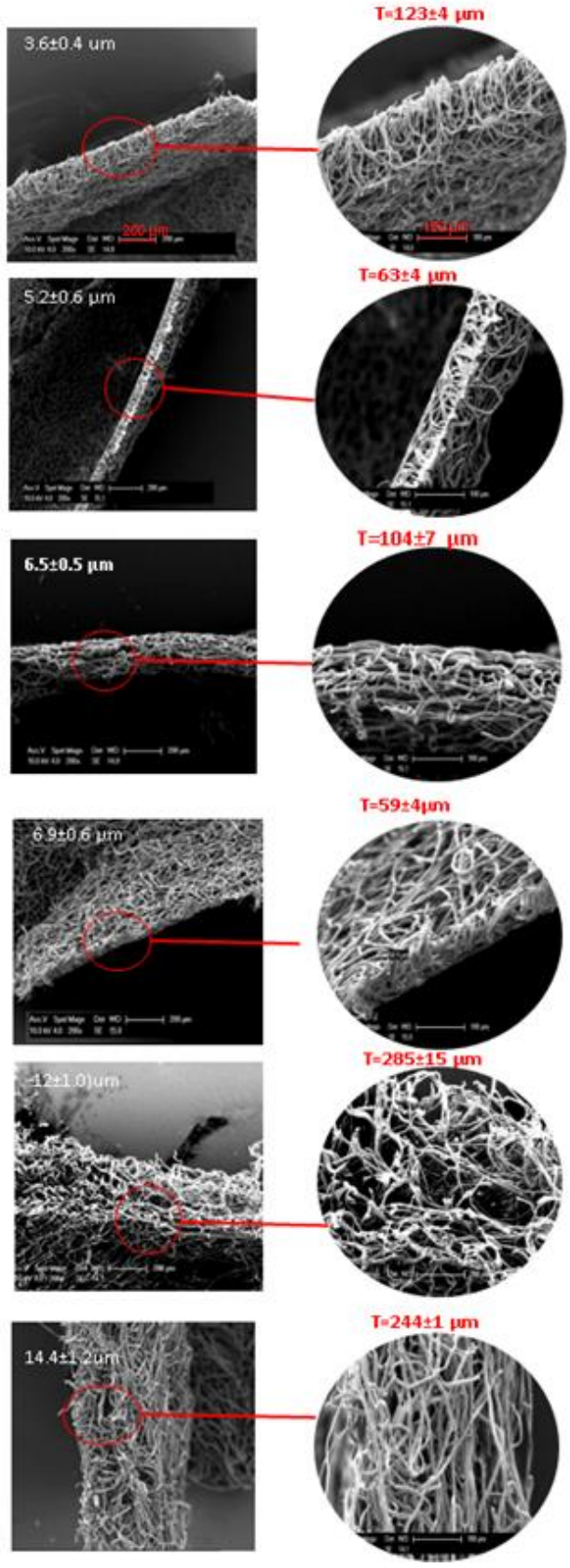


Figure 4.20 - PCL scaffold thickness. Representative scanning electron micrographs of cross-sections of PCL electrospun scaffolds (at x 200 and x100 magnification).

4.3.9.iii Porosity, pore size and thickness evaluation of the two selected types of scaffolds produced (PCL alone and PCL-b-PEG/PCL 40:60 (15% *w/w*))

Comparison of scaffolds PCL and PCL-b-PEG/PCL 40:60 (15% *w/w*) in term of porosity and their thicknesses were conducted. Porosity of the scaffolds was evaluated both by a gravimetric method (Figure 4.21-A) and through mCT (Figure 4.21-B). Both methodologies revealed that PCL-b-PEG/PCL 40:60 (15% *w/w*) scaffolds with an average fibre diameter of 3.5±0.4 µm presented similar porosity compared with PCL scaffolds with an average fibre diameter of 3.6±0.8 µm. Although the porosity was similar, estimations by the gravimetric method revealed higher values then when measured by mCT.

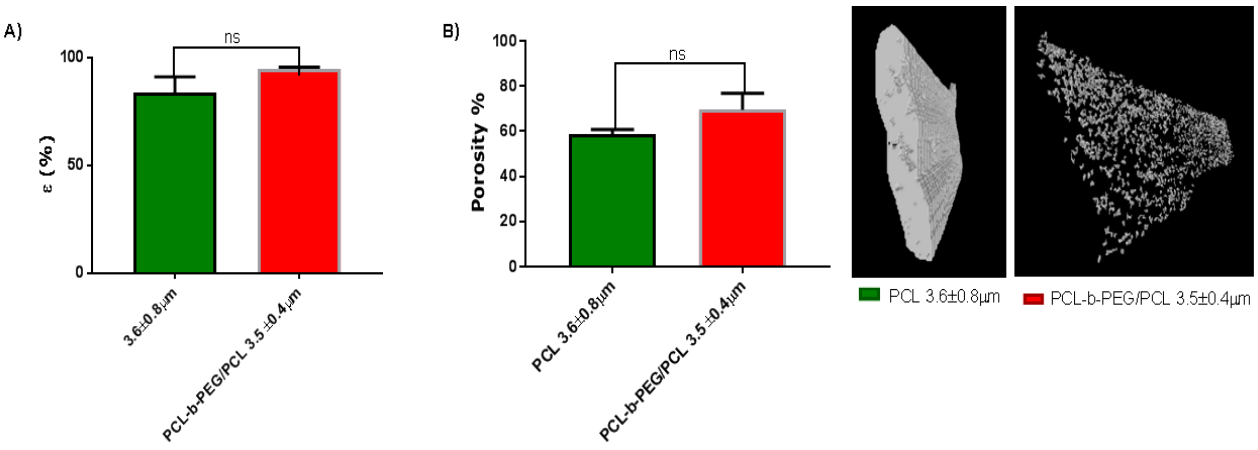


Figure 4.21 - A) shows a graph of ε % (porosity estimated by gravimetric method) of PCL and PCL-b-PEG/PCL scaffolds with an average fibre diameter ~4 µm, B) porosity of PCL and PCL-b-PEG/PCL scaffolds estimated though mCT technique and visualization of electrospun scaffold through mCT methodology. Three independent experiments carried out in triplicate (means±SD).

PCL and PCL-b-PEG/PCL scaffolds showed a porosity of the order of 80-95% using the gravimetric method while the same PCL and PCL-b-PEG scaffolds showed a lower porosity (60-70%) using mCT. Literature has reported that porosity is influenced by fibre diameter (Zander et al., 2013). Nevertheless, in the current study no significant differences were found between PCL and PCL-b-PEG/PCL due to both present similar fibre diameter ~4 μm. In addition, estimation of pore size was made though mCT for the three scaffolds, and results showed that PCL and PCL-b-PEG/PCL scaffolds exhibited an average pore size of ~40 microns. Furthermore, the optimal porosity to allow fibroblast infiltration should be within the range of 60-90%, according to (Chong et al., 2007b). In addition, pore size should be between 20 and 45 μm (Skotak et al., 2011). Here, the PCL and PCL-b-PEG/PCL scaffolds exhibited a porosity ranging from 80-90% (from gravimetric data) and 60-70% (mCT), which is in the range of the porosity that should allow cell infiltration and proliferation. In addition, it has been reported that porosity and pore size of scaffolds may influence scaffold degradation rate (Zhang et al., 2013). This point will be discussed in detail in section 5.3.7.vi-degradation rate studies.

The thickness of the scaffolds was measured by performing cross sections of the scaffolds and subsequent SEM analysis (Figure 4.22). PCL scaffolds were produce with a thickness of 121±4 μm, and PCL-b-PEG/PCL 115±3 μm. As previously pointed out in section 4.3.9 i and 4.3.9.ii, porosity and thickness of scaffolds play an important role as the structural support for cellular proliferation and infiltration

(Chang and Wang, 2011, Ghasemi-Mobarakeh et al., 2009, Farrugia et al., 2013). As it was already showed in section 4.3.5, scaffolds fabricated in the current study, with a thickness ~60 µm support good cellular infiltration and proliferation.

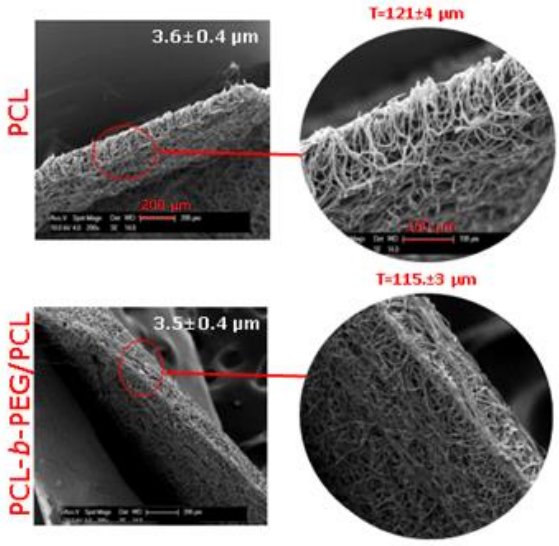


Figure 4.22 – PCL and PCL-PEG/PCL scaffold thickness. Representative scanning electron micrographs of cross-sections of PCL and PCL-PEG/PCL electrospun scaffolds (at x 200 and x100 magnification).

4.3.10 Physicochemical evacuation of PCL electrospun scaffolds

4.3.10.i Contact angle measurements of PCL electrsopun scaffolds

Figure 4.23 and Table 4.10 show advancing /receding water contact angle including calculation of the hysteresis (H=(θa)- (θr)).and sessile drop tests for PCL scaffolds with different fibre diameters. In general, electrospun scaffolds from ~3-14 µm fibre diameter showed a static angle between 101 to 111°.

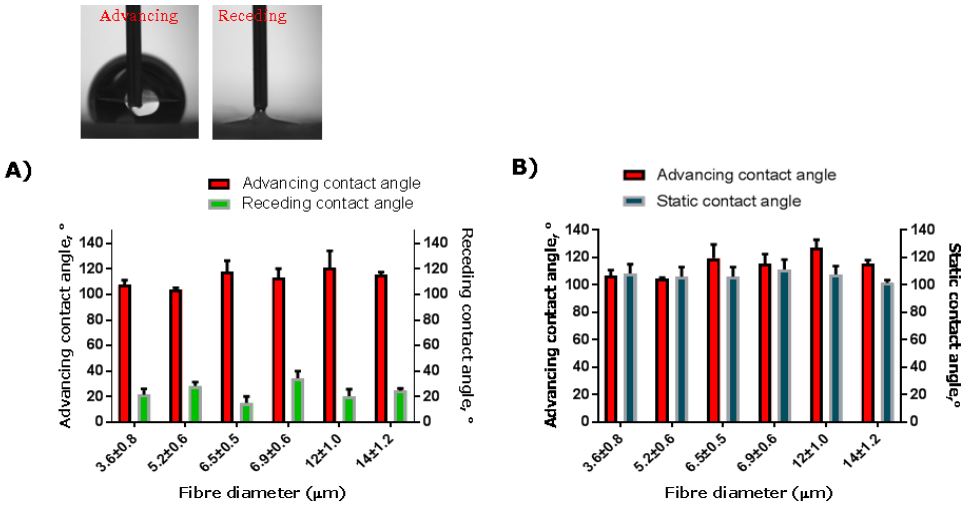


Figure 4.23 - A) graphs comparing different fibre dimeter scaffolds and their respective advancing/receding water contact angles. Advancing and receding water contact angles images are shown as example and **B)** Graph compared advancing contact angle and static. Three independent experiments carried out in triplicate (means±SD).

Table 4.10 - Table summarizing advancing/ receding contact angle, hysteresis and static contact angle.

Fibre diameter (µm)	Static contact angle,°	Advancing contact angle,°(θa)	Receding contact angle,°(θr)	Hysteresis (H=(θa)- (θr))
3.6±0.8	108±5	108±3	22±4	86±6
5.2±0.6	106±6	104±1	28±3	76±2
6.5±0.5	106±6	118±8	15±4	103±10
6.9±0.6	111±6	113±6	34±5	79±4
12±1.0	108±5	121±12	20±5	101±16
14±1.2	101±2	116±2	25±1	91±3

Scaffolds averaging fibre diameters of 3.6, 5.2, 6.5, 6.9 and 14 μm yield static and advancing contact angle measurements that are well correlated, which presumably exhibit smooth surfaces (Yuan and Lee, 2013). Some exceptions from this correlation were found in scaffolds with a fibre diameter of 12 μm, which showed higher values (p 0.0144) of advancing contact angle (121°) compared with static contact angle (108°). The possible explanation for this particular scaffold (e.g 12 μm diameter), is that it may have presented rough surface which may impede the motion of the drop (Yuan and Lee, 2013). Further investigation of scaffold surface (i.e white light interferometry (Francis et al., 2010)) may be necessary to correlate the contact angle values and topography of scaffolds. The literature reported that contact angle is directly related with the porosity, fibre density, roughness of the material and chemical composition (Shalumon et al., 2012). In addition, materials that show a contact angle less than 90° are considered hydrophilic because they present high wettability. Scaffolds fabricated and characterised in the current study, based on PCL alone corresponded to a hydrophobic material (contact angles > 90°) with low wettability, which is in good agreement with the work of (Jiang et al., 2017). They showed a contact angle of 101-91 ° for PCL scaffolds (fibrous scaffolds with an average fibre diameter of 0.8 ± 0.5 μm).

In this study, receding contact angle of scaffolds were similar (ns differences) with an average of 24°, with exception of those scaffolds with an average fibre diameter of 6.5 and 6.9 μm. In fact, scaffolds with an average fibre diameter of 6.9 μm showed a significantly (P

0.0030) higher receding contact angle (34°) compared with scaffolds with a fibre diameter of 6.5 μm (15°) (Table 4.10). In general, it can be suggested that hydrophobic surfaces may hold back the water drop when water recedes causing a decrease in the receding contact angle (Mateo et al., 2010, Yuan and Lee, 2013). This can be seen by the differences found in samples with an average fibre diameter of 6.5 and 6.9 (in term of receding contact angle) which may be attributed to roughness, porosity and fibre density of the scaffolds (Shalumon et al., 2012). In addition, PCL scaffolds fabricated in this study, presented a hysteresis between 76 and 103°, which was found to be higher when compared with the values reported by (Domingos et al., 2013) for similar PCL scaffolds, which exhibited a hysteresis of 26.7±3.2°. These differences in term of hysteresis may be related to porosity and surface roughness (Eral and Oh, 2013, Mateo et al., 2010).

4.3.10.ii Water Contact Angle (WCA) measurements of the two selected types of scaffolds produced (PCL alone and PCL-b-PEG/PCL 40:60 (15% *w/w*))

Table 4.11 shows a summary with static contact angle, advancing and receding water contact angle, and hysteresis for scaffolds PCL and PCL-b-PEG/PCL. Static and advancing angles on PCL and PCL–b-PEG/PCL scaffolds were the same (ns) (100-108°) (Figure 4.24-A) and B)). Both scaffolds possessed contact angles higher than 90°, thus could be regards as hydrophobic scaffolds overall (Marmur, 2012).

In term of hysteresis, higher values were exhibited by PCL scaffolds with 83±4° compared with PCL-b-PEG/PCL scaffold with 72±29. Lower hysteresis is an indication of lack of resistance to capillary mobility. Water drops spread out almost across the whole polymer surface without capillary flow (Eral and Oh, 2013).

It was hypothesised that an improvement on hydrophilicity by the incorporation of Peg to the scaffolds may help in cell biocompatibility and degradation rate of the material. In the present study, no significant differences were found in terms of wettability between both materials (PCL and PCL-b-PEG/PCL scaffolds) using water contact angle technique. This phenomenon may be caused by the roughness of the electrospun scaffolds. Therefore, further investigation using the polymers as a film need to be carried out to test differences in hydrophilicity without the roughness matter.

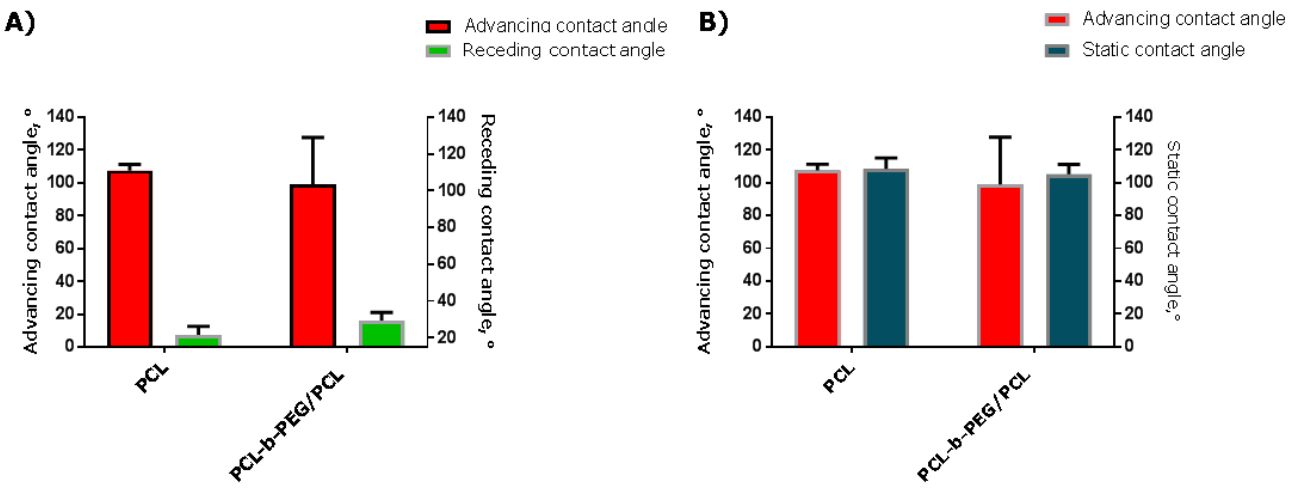


Figure 4.24 - A) Graphs comparing PCL and PCL-b-PEG/with their respective advancing/receding contact angles and **B)** comparing PCL and PCL-b-PEG/with their respective advancing and static contact angles. Three independent experiments carried out in triplicate (means±SD).

Table 4.11 - Table summarizing advancing/ receding contact angle, hysteresis and static contact angle of PCL and PCL-b-PEG/PCL scaffolds

Fibre diameter (µm)	Static contact angle,°	Advancing contact angle,°(θa)	*Receding contact angle,°(θr)	Hysteresis (H=(θa)- (θr))
3.6±0.8	108±5	108±3	22±4	86±6
3.5±0.4	101±3	99±29	30±5	71±29

*Fibres probably were rough and water adsorbed into the matrix

4.3.11 Mechanical properties evaluation of PCL scaffolds

Figure 4.25 shows stress-strain curves of different selected PCL electrospun scaffolds with an average fibre diameter of 3.6; 6.9; 12 and 14 μm, using uniaxial tensile tests. Evaluation of the selected PCL electrospun scaffolds showed a linear region in the stress-strain plot followed by a nonlinear region. The scaffold behaviour was characterized by a considerable elongation without a considerable variation in the stress. This behaviour corresponded with the random orientation of the fibres on the mat which is expected to change during the elongation process as previously reported by (Jin et al., 2013). The fibres tend to align in the same direction of the applied force, which occurs before the breaking point. Young's modulus, yield point, and elongation at break are summarized in Table 4.12.

As for the results presented in this study, there was no clear correspondence between fibre diameter and Young's modulus. Scaffolds with an average fibre diameter of 3.6 μm had a Young's modulus of 6.5±0.8 MPa similar (ns) to scaffolds with fibre diameter that were double or three times greater (5.2±0.1 and 5.1±0.2 MPa respectively).

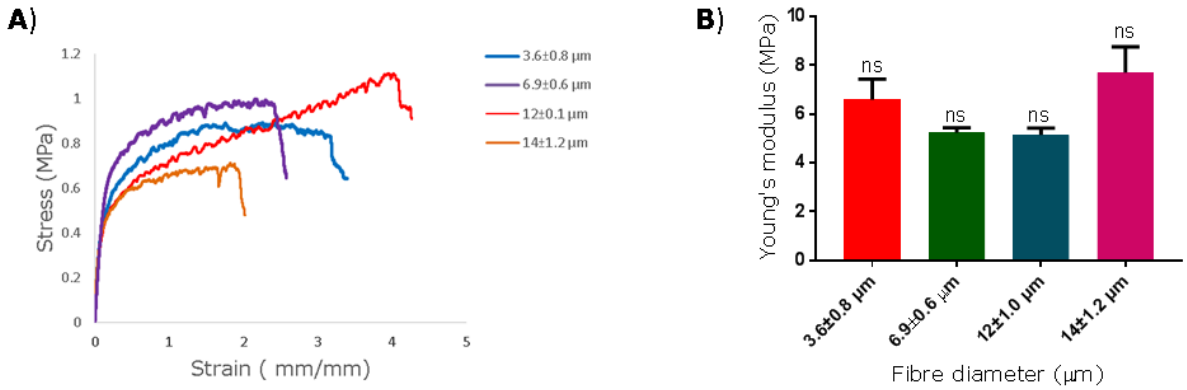


Figure 4.25 - A) Representative stress-strain curves of PCL scaffolds with different fibre diameter s. B) graph showing Young's modulus of PCL scaffolds with different fibre diameters. Three independent experiments carried out in triplicate (means±SD).

Table 4.12 - Summary of the mechanical properties of PCL scaffolds with different fibre diameters.

Fibre diameter µm	Yield point MPa	Young's modulus (MPa)	Elongation at break (mm/mm)	Ultimate tensile strength (MPa)
3.6±0.8	0.6±0.1	6.5±0.8	3.4±0.2	0.9±0.4
6.9±0.6	0.5±0.1	5.3±0.1	2.0±0.4	0.9±0.1
12.0±1.0	0.5±0.1	5.1±0.2	4.4±0.3	1.1±0.1
14.0±1.2	0.4±0.1	8.8±1.0	1.8±0.1	0.7±0.1

In addition, no clear correlation was apparent between the scaffolds' fibre diameter and the elongation at break and ultimate tensile strength measurements. The highest elongation and tensile strength measurements were observed in scaffolds with a fibre diameter of 12 μm compared with scaffolds with lower fibre diameter (3.6 and 6.9 μm) as well when comparing with higher fibre diameter (14 μm). The scaffold with fibre diameters of 12 μm reached values of elongation at break of 4.4 mm/mm and ultimate tensile strength of 1.1 MPa. These results were not expected because from the literature the modulus was reported to increase as the fibre diameter decreased (Baji et al., 2010, Wong et al., 2008). However, (Wong et al., 2008) pointed out that this correlation between mechanical properties and fibre dimeter is more predominant among scaffolds with fibres of average diameters under 700 nm. In the present study, no significant differences or correlation were found maybe due to the larger range of fibre diameters being tested (over 2.5 μm). The results presented here are in agreement (Del Gaudio et al., 2009) reported a PCL scaffold with an average fibre diameter of 3.6 μm with a Young's modulus of 6.4±0.2 MPa, yield stress of 0.43±0.43 (MPa) and ultimate tensile stress 0.8±0.1 (MPa), which is very similar to the results of scaffold with similar fibre diameter presented here in this study.

4.3.11.i Mechanical properties of the two selected types of scaffolds produced (PCL alone and PCL-b-PEG/PCL 40:60 (15% *w/w*))

From Figure 4.26-A) and Figure 4.26-B) it can be seen that PCL-b-PEG/PCL scaffold exhibited the best mechanical properties. Table 4.13 summaries the main mechanical parameters. In general, PCL and PCL-b- PEG/ PCL scaffolds presented a similar stress-strain behaviour. A linear relationship was observed at the beginning, followed by a non-linear curve, characterized by a great elongation without a considerable increase in the stress, which is an indication of a flexible and deformable material. The elongation at the break point was 5.1±0.9 mm/mm for PCL-b-PEG/PCL and 3.4±0.2 mm/mm for PCL scaffolds. Moreover, in terms of Young's modulus, the blend of PCL-b-PEG/PCL 40:60 showed an improvement, reaching values of 8.8±0.8 MPa, compared with PCL electrospun scaffolds, with average values of 6.0±0.8 MPa. Statistically, Young's modulus of the PCL-b-PEG/PCL was significantly higher than the PCL (p 0.0190). In addition, the ultimate strength of PCL-b-PEG/PCL and PCL were similar reaching value of ~0.9 MPa. Blends of both polymers (PCL-b-PEG/PCL 40: 60) exerted the highest viscosity (9.6±1.5 Pa s) compared with PCL viscosity (3.6±0.6 Pa s) at a shear of 26 s^{-1}. It seems that viscosity correlates with the improvement of the Young's modulus of PCL-PEG/PCL.

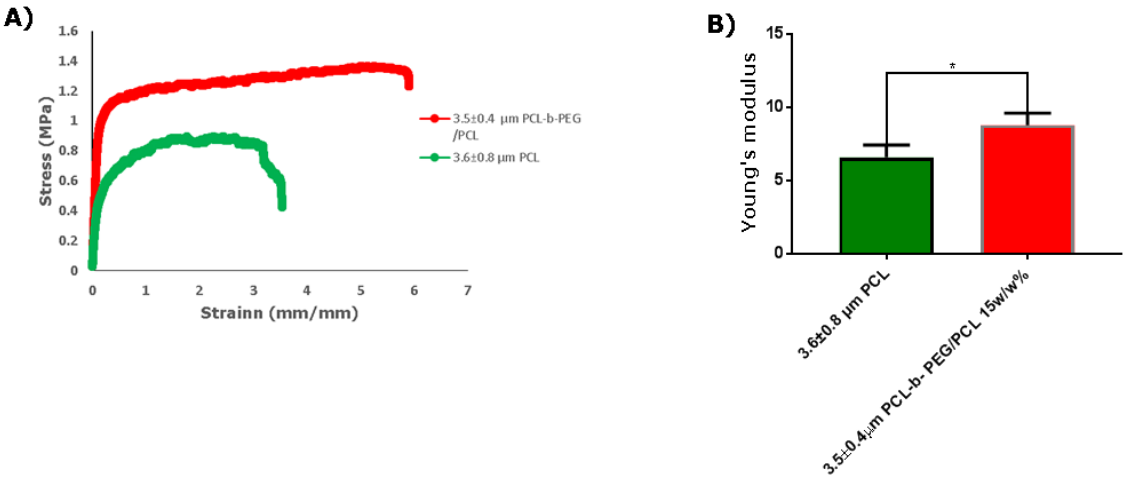


Figure 4.26 - A) Representative stress-strain curves of PCL and PCL-PEG/PCL scaffolds with average fibre diameter ~4 µm. **B)** Graph showing Young's modules of PCL and PCL-b-PEG/PCL scaffolds with an average fibre diameter ~4 µm. Three independent experiments carried out in triplicate (means±SD).

Table 4.13 - Summary of the mechanical properties of PCL and PCL-b-PEG/PCL scaffolds with an average fibre diameter ~4 µm.

Fibre diameter µm	Yield point MPa	Young's modulus	Elongation at break (mm/mm)	Ultimate tensile strength (MPa)
3.6±0.8	0.6±0.1	6.0±0.8	3.4±0.2	0.9±0.4
3.5±0.4	1.0±0.1	8.8±0.8	5.1±0.9	0.9±0.5

The literature points out that solutions with a high viscosity possess a high chain entanglement and limit solvent evaporation and, as a consequence, results in thicker fibres and high crystallinity following electrospinning. As a result, an improvement in Young's modulus and strength is observed. In contrast, low viscosity solutions exhibit fast evaporation of the solvent, decreased fibre diameter, low crystallinity following electrospinning, and a lack of fibre-fibre bonding, resulting in brittleness, as characterized by a reduction of tensile strength and strain at break, and reduction of Young's modulus (Baji et al., 2010, Papkov et al., 2013, Kuzelova Kostakova et al., 2017, Badrossamay et al., 2010, Veleirinho et al., 2008). Scaffolds for wound healing should provide the strength, strain to allow cell migration, change of cell shape and differentiation. The force exert for cell during migration is around 0.1nN per cell. Reports of Young's modulus of skin has not been very reliable varying from 0.008 to 20 MPa (Leung et al., 2011). From this, it is clear that PCL and the blend PCL-b-PEG/PCL scaffolds match the mechanical properties of the human skin, which is an important parameter to consider at the moment of choosing a material.

4.3.11.ii *In vitro* degradation studies of the two selected types of scaffolds produced (PCL alone and PCL-b-PEG/PCL 40:60 (15% *w/w*))

Figure 4.27 shows SEM micrographs of PCL and PCL-b-PEG/PCL scaffolds over 12 months of degradation studies at time point of 0, 2 months, 5 months and 12 months. Fibre morphology was not altered in any of the different types of materials after 12 months. Weight loss of the samples reflected the degradation of scaffolds into oligomers. PCL lost 5% of its weight in the first month. After that, the weight was constant for 7 months. Then PCL scaffolds presented a slight variation in weight loss of around 3% and again the weight was maintained. These results were in agreement with GPC analysis of molecular weight and polydispersity (Table 4.14). PCL slightly decreased in molecular weight from $2.9x10^5$ to $2.5x10^5$ and increased in terms of polydispersity from 1.2 to 1.4 over 5 months. In addition, PCL-b-PEG/PCL scaffolds showed an increment in terms of weight loss (around 10%) within the first month. After that, the electrospun scaffolds lost around 20% of weight in a period of 9 months. Complementary GPC analysis of molecular weight showed the variation on Mw of PCL-b-PEG/PCL scaffold from $2.5x10^5$ to $1.6x10^5$ with an increase in polydispersity Mw/Mn from 1.3 to 2.4 over a period of 5 months.

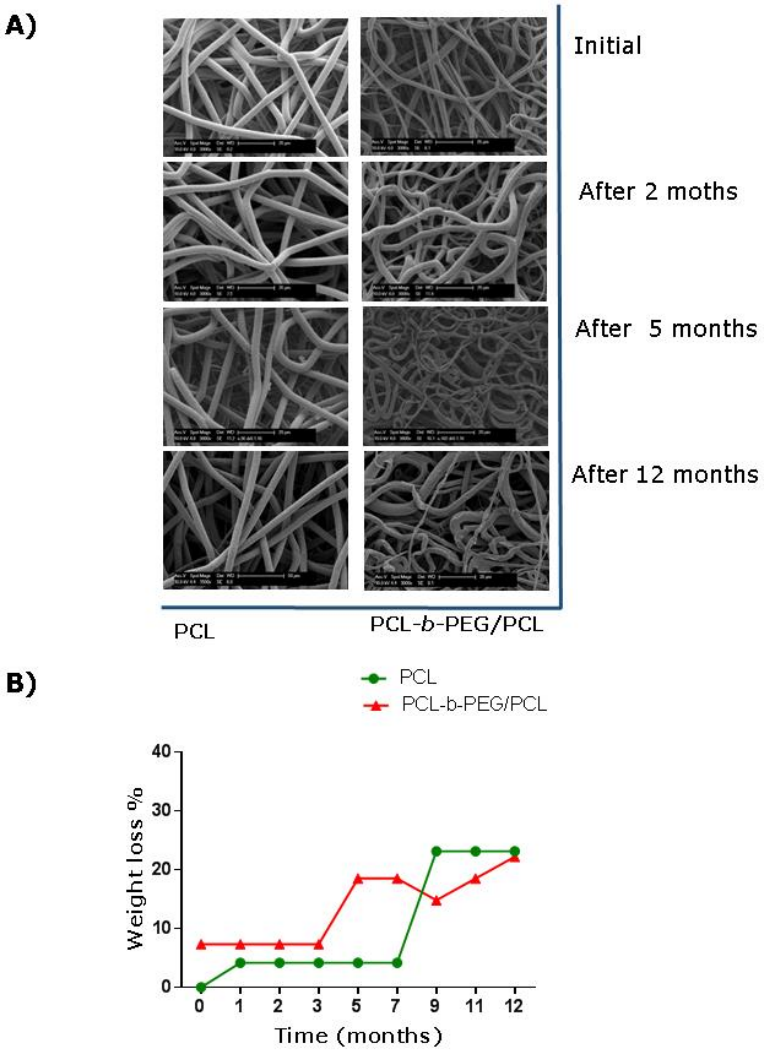


Figure 4.27 - Degradation rate study. **A**) SEM micrographs of PCL and PCL-b-PEG/PCL scaffolds at four-time points (0,2,5 and 12 months) **B)** graph of weight loss of PCL and PCL-b-PEG/PCL scaffolds over a period of 12 months (no error bars). One independent experiments carried out in triplicate (means±SD)

Table 4.14 - GPC analysis. Molecular weight and polydispersity evaluation of PCL, and PCL-b-PEG/PCL scaffolds.

Time	Scaffold	Mw	Polydispersity Mw/Mn	Polydispersity Mz/Mn
Initial	PCL	$2.9x10^5$	1.2	1.4
	PCL-b-PEG	$6.5x\ 10^4$	2.2	3.6
	PCL-b-PEG/PCL (40:60)	$2.5x10^5$	1.3	1.6
5moths	PCL	$2.5x10^5$	1.4	1.9
	PCL-b-PEG	$6.5x\ 10^4$	1.4	1.9
	PCL-b-PEG/PCL (40:60)	$1.6x10^5$	2.4	4.0

The findings presented showed that both scaffolds experienced degradation. The findings presented here are in agreement with studies conducted by (Huang et al., 2004), who compared the degradation of three different types of scaffolds (macrostructures): PCL, PCL-b-PEG and PCL-PEG-PCL. They pointed out that all the polymers maintained their geometry during degradation studies. No significant weight loss was reported for PCL scaffolds and a weight loss of 3.5% for PCL-PEG scaffold after 60 weeks. PCL-PEG scaffolds release soluble oligomers that contain PEG reaches species (NMR evaluation). They explained that PCL-b-PEG scaffolds degraded faster than PCL due to PEG-rich species, which are water-soluble products that diffuse into the media. In contrast, PCL scaffolds exhibited very low levels of weight loss, which is in agreement with the literature, which points out that PCL scaffolds degrade over a long period of time, from 2-4 years depending the polymer molecular weight (Lam et al., 2007).

A comparison between PCL and PCL-b PEG/PCL scaffolds revealed that PCL and PCL-b-PEG/PCL scaffolds had similar fibre diameters around ~4 μm and pore size (respectively). Porosity of PCL-PEG/PCL was 70%, which was slightly higher than PCL scaffolds (59%). Both polymers had a different chemical composition: PCL-b-PEG/PCL contained PEG-rich species which are soluble in PBS. The combination of all these factors contributed to a faster degradation of PCL-b-PEG/PCL scaffolds.

4.3.11.iii Cell proliferation 3T3 and BJ6 comparison between PCL and PCL-b-PEG/PCL scaffolds

Figure 4.28- A) shows the metabolic activity of murine 3T3 fibroblast on PCL and PCL-b-PEG/PCL over 12 days of culture. The fibroblasts cultured on PCL-b-PEG/PCL scaffolds with an average fibre diameter of 3.5±0.5 μm showed a significantly higher fibroblast metabolic activity ($p < 0.0001$) than PCL scaffolds with an average fibre dimeter of 3.6±0.8 μm on day 12. No statistically significant differences were found in terms of metabolic activity between fibroblast metabolic activity on PCL-b-PEG/PCL scaffolds with an average fibre diameter of 3.5±0.5 μm and PCL scaffolds with an average fibre diameter 3.6±0.8 μm during the first 9 days of culture. Figure 4.28- B) shows SEM micrographs of murine fibroblasts, which spread well across PCL-b-PEG/PCL scaffolds over 12 days.

Figure 4.28-C) shows the metabolic activity of human BJ6 fibroblasts on PCL and PCL-b-PEG/PCL over 15 days of culture. The fluorescence intensity that reflects the metabolic activity of the BJ6 fibroblasts decreased dramatically compared to the fluorescence intensity of murine 3T3 fibroblasts; this tendency was maintained over the time of culture. For example, murine fibroblasts proliferating on PCL-b-PEG/PCL reached values of 60000 fluorescence intensity RFU after 12 days while Bj6 fibroblasts on the same scaffold did not reach values over 3000 fluorescence intensity RFU after 15 days. Moreover, it is also important to notice that BJ6 fibroblasts on PCL did not increase metabolic activity over 15 days of culture. It seems that the cells had detached from the scaffolds. From this result it is clear that PEG

content on PCL-b-PEG/PCL 40:60 (15% *w/w*) improved BJ6 metabolic activity when results are compared with fibroblasts on PCL.

Major differences in terms of biocompatibility of PCL and PCL-b-PEG/PCL scaffolds were found on human fibroblast metabolism compared with murine fibroblasts. It was expected to find the same tendency using both cell types, possibly due to BJ6 requiring more time to determine a significant difference. Also, it will be important to take into consideration that human fibroblasts are more sensitive cells compared with murine fibroblasts. In the case of cytotoxicity tests of drug a phenotype dependent sensibility to drugs is frequently found (Ölschläger et al., 2009, Tomizawa et al., 2013).

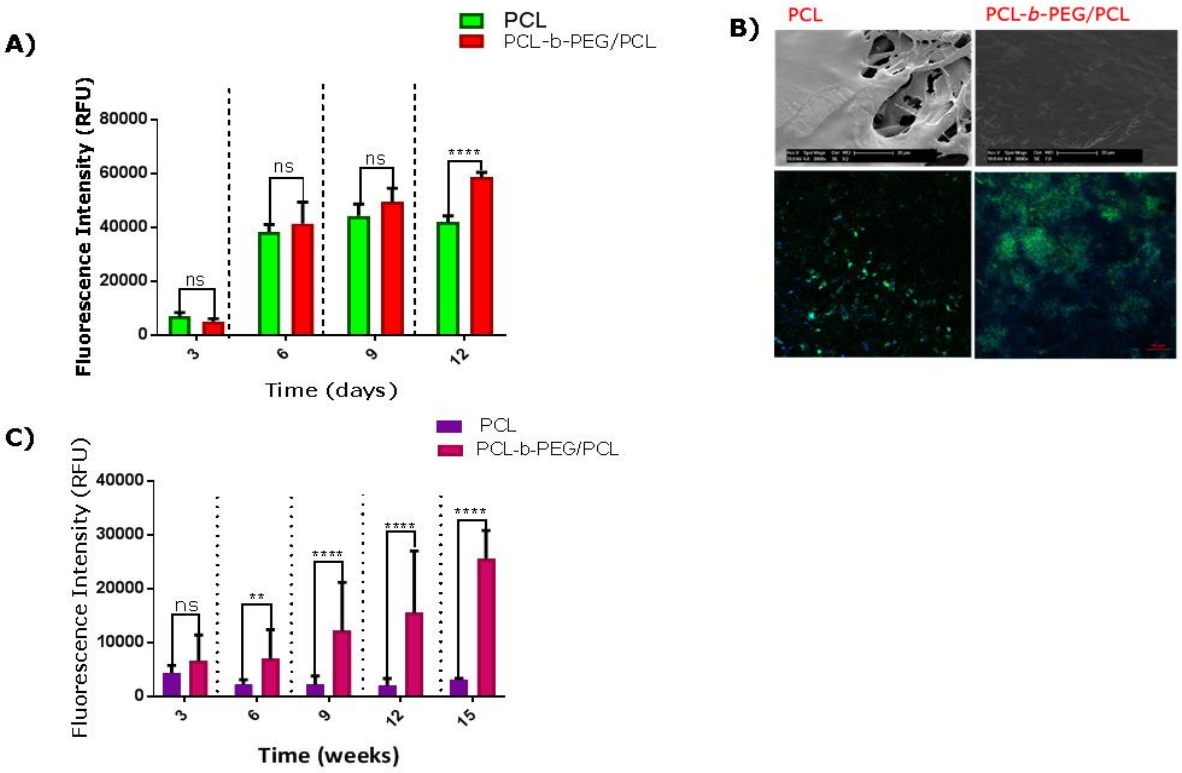


Figure 4.28 - 3T3 metabolic activity was assessed using Alamar Blue™**A)** Fluorescence readings of metabolic activity of 3T3 GFP fibroblasts cultured on PCL and PCL-b-PEG/PCL scaffolds, over 12 days. . B) SEM micrograph of fibroblasts 3T3 cultured on PCL, and PCL-b-PEG/PCL scaffolds over 12 days and C) Fluorescence readings of metabolic activity of dermal human fibroblasts BJ6 cultured on PCL and PCL-b-PEG/PCL over 15 days of culture. Two way-ANOVA, Tukey's multiple comparison test. Three independent experiments carried out in triplicate (means±SD).

4.3.11.iv Cell infiltration

Figure 4.29-A shows the maximum depth of fibroblast infiltration of on from top to bottom for PCL and PCL-b-PEG/PCL scaffolds. Figure 4.29-B shows the infiltration z-stack for the PCL and PLC-b-PEG/PCL, which compares the percentage of fibroblast infiltration, referring to the total thickness of the scaffolds. From the results, it is clear that scaffolds made of PCL-b-PEG/PCL exhibited a significantly higher infiltration of fibroblasts ($p \leq 0.0001$) compared with PCL scaffolds. Fibroblast infiltration on PCL-b-PEG/PCL reached values of 60% compare with 40% of fibroblast infiltration on PCL. PCL-b-PEG/PCL scaffolds exhibited the highest fibroblast infiltration, and the highest fibroblast metabolic activity. PCL-b-PEG/PCL had the same fibre diameter (~4 μm) and same pore size as PCL (~40 μm), which was in the order of fibroblast size (Zander et al., 2013). It is therefore likely that differences in chemical composition and/or mechanical properties may explain the improvement of cellular infiltration and biocompatibility on PCL-b-PEG/PCL scaffolds. PCL-b-PEG/PCL has a content of PEG that may have a beneficial effect on cell proliferation and cellular infiltration (Suk Choi and Sang Yoo, 2007). In addition, Young's modulus was significantly higher in PCL-b-PEG/PCL scaffolds compared with PCL scaffolds with the same fibre diameter and pore size.

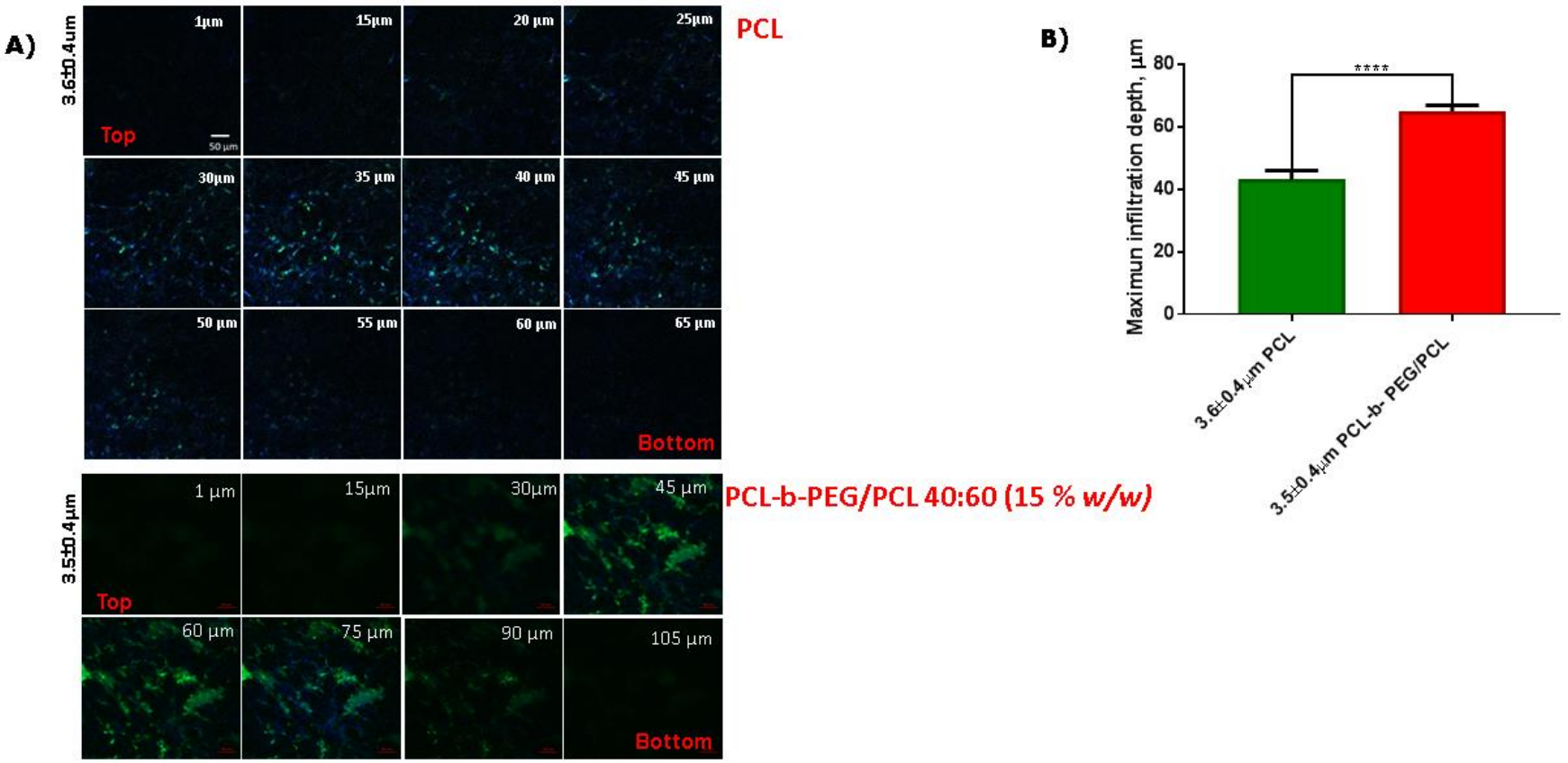


Figure 4.29 - A) Confocal microscope z-stack images of 3T3 GFP fibroblasts seeded on PCL and PCL-b-PEG/PCL micro fibrous scaffolds after 5 days of growth. In each group z-stack images of different planes showing from surface to bottom are shown. Fibroblasts were genetically modified to express GFP (green) and stained with Hoechst (blue). Magnification x20, scale bar = 50 µm. **B)** Infiltration depth % in term of total thickness of the scaffolds PCL and PCL-b-PEG/PCL. Two way-ANOVA, Tukey's multiple comparison test. Three independent experiments carried out in triplicate (means±SD).

Summary table with results

Table 4.15 - Comparison of scaffolds PCL and PCL-b-PEG/PCL in terms of geometrical, mechanical, physicochemical and biological properties

Material	Fibre diameter (μm)	Porosity %	Pore-size (μm)	Young's modulus MPa	Thickness (μm)	Metabolic activity	cellular infiltration %
Literature reported as optimal	~4-10	60-90[a]	20-45	~10	100-200		
PCL	~4	~84[a]/~59[b]	~40	~6	~121	**	~40
PCL-b-PEG/PCL 40:60 (15%*w/w*)	~4	~95[a]/~70[b]	~40	~9	~115	****	~60

[a]: values estimated by gravimetric method

[b] : values from mCT analysis

*: Poor metabolic activity

**: Good metabolic activity and cell morphology

Even though many groups have reported the development of electrospun scaffolds made of PCL, the major focus in the fabrication of these electrospun scaffolds has been with respect materials with fibre diameters in the nanoscale range(Chong et al., 2007b, Diasa et al., 2013, Gautam et al., 2013)). There are a couple of *in vitro* and *in vivo* studies performed on PCL electrospun scaffolds which compare different fibre diameter (nano and microscale) and its correlation with cell proliferation and infiltration (Li 2014).

On the other hand, PCL-b-PEG scaffolds has been used to fabricated materials in the nano (electrospun scaffolds) and macro scale (3D printing scaffold fabrication) for tissue engineering purposes. Comparison in terms of degradation rate, mechanical properties and biological properties of PCL and PCL-b-PEG polymers as well has been reported for nano and macro scale scaffolds. However, the novelty of the work presented here is the development of a PCL-b-PEG electrospun scaffold with a fibre diameter of 4 microns (microscale) with improved biological properties such as fibroblast proliferation and cell infiltration compared with electrospun PCL scaffolds. In addition, this research gathers the requirements of fibre diameter, porosity, mechanical properties previously reported for other materials (collagen, gelatine, PLGA) to generate an optimal prototype scaffolds for wound healing.

4.4 Conclusions

The ultimate aim of this study was to fabricate a biocompatible 3D electrospun scaffold with a fibre diameter within microscale range (4-10 μm) (Lowery et al., 2010, Farrugia et al., 2013, Powell and Boyce, 2009, Kempf et al., 2011), average pore size between 20-45 μm (Skotak et al., 2011), porosity between 60-90% (Chong et al., 2007a), and Young's modulus ~10 MPa (Leung et al., 2011), that allow fibroblasts to grow and infiltrate and therefore may enhance granular tissue formation in non-healing skin wounds.

Poly (ε-caprolactone) (PCL) is a commercially available polymer that has been previously used for wound healing applications (Gazzarri et al., 2013) (Zhong et al., 2010, Augustine et al., 2015, Gautam et al., 2013). After electrospinning, the PCL scaffolds with different fibre diameters, were mechanically, chemically and biologically evaluated. Optimization and characterization of PCL scaffolds revealed that a fibre diameter ~4 μm with a porosity between 60-80%, thickness ~60-144 μm, Young's modulus of ~6 MPa resulted in a scaffold suitable for fibroblasts growth and infiltration and thus with potential to be used in medical application on wound healing. It was decided to incorporate PEG into the scaffolds in order to improve hydrophilicity, biocompatibility, and as means to modulate degradation and release of drugs (Dash and Konkimalla, 2012, Choi et al., 2008, Suk Choi and Sang Yoo, 2007).

It was hypothesized that the incorporation of PEG into the scaffolds may enhance biocompatibility, mechanical properties and degradation rate compared with PCL scaffolds. The synthesis of PCL-

b-PEG polymer was successfully carried out though ring opening polymerization. Rheological properties of PCL-b-PEG solution showed low viscosity, which made the electrospinning of this solution difficult. This resulted in beads, since PCL-b-PEG polymer was blended with PCL. Blend of polymers PCL-b-PEG/PCL 40:60 (15% *w/w*) enabled the fabrication of scaffolds. It was found that PCL-b-PEG/PCL scaffolds have similar hydrophilicity compared with plain PCL. However, this modification significantly enhanced biocompatibility and also improved degradation. A proper balance of PEG content within the material enhanced fibroblasts metabolic activity and infiltration. In this study, the balance of PEG content in PCL-b-PEG/PCL scaffold was found to be (40:60 15% *w/w*). The scaffolds prepared from PCL-b-PEG/PCL (40:60 15% *w/w*) solution exhibited the greatest cellular infiltration of fibroblasts (60%) compared with PCL (40%) and the greatest biocompatibility of murine fibroblasts and human fibroblasts. Pore size (~40 microns) and porosity of PCL-b-PEG /PCL (70%) scaffold suited the requirements for fibroblast to proliferate and infiltrate. Also, the strength of PCL-b-PEG /PCL was similar to those of ECM components. In addition, the degradation rate of PCL-b-PEG /PCL was faster than PCL and PCL-b-PEG. The balance of chemical, geometrical, and mechanical properties produced a scaffold that suited with fibroblast requirements and that might possess a good potential for skin wound regeneration. In the light of the results present in this chapter, further investigations will be considered to test PCL and PCL-b-PEG /PCL as a platform for therapeutic biomolecules aimed to enhance wound healing.

CHAPTER 5 Loading and release of model and therapeutic proteins on PCL and PCL-b-PEG/PCL scaffolds

5.1 Active wound dressing

An active wound dressing refers to a dressing that can interact with cells and allow their growth and infiltration whilst managing the healing events though the release of therapeutic molecules. On the market, such active dressing containing growth factors (Biovance, Covadernm), and antimicrobials (Verbelen et al., 2014) are available and is a current area of research.

5.1.1 Requirements of the active dressing

Active dressings should release therapeutic molecules in an appropriate manner in response to the requirements of wound. For example, open-wounds, or exudative wounds, which need a frequent replacement of the dressing (every couple of days) may need a burst or fast release of antibiotics, growth factors, or cell signalling agents. On the other hand, surgical wounds or wounds where interruptions are not desirable, require a more sustainable release of therapeutic molecules. In addition, re-epithelialized wounds may require a stable release of remodelling agents to support completion of the wound healing process (Leung et al., 2011).

5.2 Scaffolds as a platform for protein release

Electrospinning is a versatile technique that allows the development of fibrous scaffolds that support cell growth and infiltration as well as serving as a platform for drug release (Leung et al., 2011, Gelain et al., 2010, Buschle-Diller et al., 2007). For more details about electrospinning technique and experimental parameters that influence the resultant scaffolds morphology, refer to Chapter 4. This section will focus on the use of electrospun scaffolds as platforms for drug release. Electrospun scaffolds used as a platform for drug delivery, should provide a stable environment to preserve the bioactivity (Buschle-Diller et al., 2007) and integrity of the therapeutic molecules. Electrospun scaffolds have been used in other areas such as cancer treatment to release of doxorubicin (Zhang et al., 2009), and heart disorders to release of basic fibroblast growth factor (bFGF) (Somers et al., 2008). In wound healing, the loaded drugs are antibiotics (Buschle-Diller et al., 2007), and proteins (i.e cytokines and growth factors) (Gelain et al., 2010).

5.2.1 The method used for drug-loading onto electrospun scaffolds

Drug loading can be achieved by using different electrospinning methods (Zamani et al., 2013): a) Post electrospinning modification: it is a technique where the drug absorbed to the surface of the fibres. (Mohammadian and Eatemadi, 2016). b) Electrospinning of a Polymer/drug blend: this method consists of electrospinning an

emulsion or suspension of a mixture of the polymer and drug (Ji et al., 2010, Szentivanyi et al., 2011). c) Coaxial electrospinning: this method consists of co-electrospinning two different polymeric solutions through two concentric nozzles, which results in a core-sheath fibre (Ji et al., 2010, Szentivanyi et al., 2011).

5.2.2 Mechanism of protein release

The predominant mechanism of release from electrospun fibres is diffusion. In the diffusion mechanism from a matrix, the concentration gradient of a solute inside of the matrix is the driving force for diffusion. This explains the first release phase that is characterised by a fast release of the drug, and it is known as the 'burst release' (first order kinetics) (Szentivanyi et al., 2011). This type of release is dependent on the features of the drug, such as diffusivity on the scaffolds, loading level, and physical size (Prabaharan et al., 2007).

5.2.3 Factors affecting loading and release of drugs:

In general, protein absorption and release from a polymer is controlled by physicochemical interaction between polymer, protein, and solvent. It involves nonspecific electrostatic forces and ionic interactions between the polymer and the protein in addition to local noncovalent interactions, such as hydrogen bonds and salt bridges. Non polar interactions such as those arising as a result of Van der

Walls forces and hydrophobic attraction or hydration repulsion forces will also influence drug-polymer interactions (Wei et al., 2014).

5.3 *Lucilia sericata* maggot excretion/secretion as therapeutic molecule for wound healing

Three types of proteolytic enzymes in *Lucilia sericata* maggot excretion/secretion (*L. sericata* maggot E/S) has been reported, where the majority are serine proteinases (pH optimal 8-9), aspartyl proteinases and metalloproteinases (pH 9)(Chambers et al., 2003). Proteinases possess a molecular weight ranging from 20 to 50 KDa (Schmidtchen et al., 2003).

Larval therapy has been reported to exert beneficial actions upon chronic wound healing. The alimentary fluid from *Lucilia sericata* maggot contains serine proteinase, which degrades necrotic tissue (Telford et al., 2010), disinfects the wound site (Harris et al., 2009) and promotes granulation tissue formation on the wound (Horobin et al., 2005). The beneficial effect of larval excretion/secretion on wound healing is strongly supported by 8 clinical trials (Sherman, 2014), (Dumville et al., 2009), (Mumcuoglu, 2012), and supporting *in vitro* studies (Bexfield et al., 2010).

The FDA (Food and Drug Administration, USA) approved *Lucilia sericata* maggot therapy as a medical device in January 2004 (Davydov, 2011). In the same year, the National Health Service in the UK approved the prescription of sterile *Lucilia sericata* maggots (Mumcuoglu, 2012). However, some of the limitations of the use of sterile *Lucilia sericata* maggots (located within a bag) for wound

healing are: i) maggots require a moist environment to survive, for this reason the use of *Lucilia sericata* maggot is accepted exclusively for treatment of exudative wounds and contraindicated on dry wounds ii) maggots produce malodour and, discomfort to the patient and iii) there is poor acceptance by the patient and medical staff (Chan et al., 2007). For this reason, research groups have tried to incorporate the active molecules from *L. sericata* maggot E/S in pharmaceutical formulations such as hydrogels. Prototype hydrogels containing recombinant *Lucilia sericata* chymotrypsin has been developed, and were shown to accelerate wound closure *ex vivo* (Britland et al., 2011). In addition, *L. sericata* maggot E/S has been incorporated and released in a PVA hydrogel. Findings showed a significant enhancement on the rate of closure (*in vitro* scratch assay) on wounds exposed to *L. sericata* maggot E/S released from hydrogel compared with control (Smith et al., 2006).

5.3.1 Mechanism of actions of *Lucilia sericata* maggot excretion/secretion.

The bio-activities of larval excretion/secretion include antibacterial, stimulating angiogenesis and tissue remodelling, among others (Cazander et al., 2013). Allantoin content from *L. sericata* maggot E/S has a beneficial effect on stimulating granulation tissue formation (Prete, 1997). In addition, amino acid-like compounds of *L. sericata* maggot E/S such as histidine, valinol and 3-guanidinopropionic *acid* were identified to enhance proliferation of endothelial cells, stimulating angiogenesis (Bexfield et al., 2010). *L. sericata* maggot

E/S products contain also Deoxyribonuclease (DNAse) (45 kDa) which has been associated with DNA digestion of slough/eschar of wounds and bacterial biofilms (Brown et al., 2012). Serine proteases from *L. sericata* maggot E/S have a positive impact on wound healing through their antimicrobial actions and by promoting fibroblast motogenesis (Smith et al., 2006). Cells are tightly bound integrin, which may reduce the ability of the fibroblasts to migrate. In the presence of *L. sericata* maggot E/S, this binding is reduced, allowing cell migration. It was found that *L. sericata* maggot E/S was rich in proteases such as chymotrypsin, serine proteases and peptidases that have the capability to degrade fibronectin to reduce the cell contact points with the substrate promoting their migration (Horobin et al., 2003, Chambers et al., 2003). Chymotrypsin from *Lucilla sericata* is functional and stable in metalloproteinase rich environments. The action of chymotrypsin is complemented with trypsin and probably with other enzymes (Chambers et al., 2003). Alpha-2 macroglobulin is abundant in plasma and inhibits the action of chymotrypsin I (Pritchard and Brown, 2015). For that reason, larval enzymes exhibit a selective activity, specifically debriding necrotic tissue. Also, when tissues become well perfused with blood, chymotrypsin I may become inhibited (Maeda et al., 2014).

5.4 Aims and objectives:

Electrospun scaffolds have been used as platforms for drug release with applications in tissue regeneration. The incorporation of bioactive molecules such as growth factors for wound healing on electrospun scaffolds has also been evaluated (Sahoo et al., 2010). However, the sensitivity and the inability to control off-target effects are the main issues to resolve for drug-eluting scaffolds in tissue regeneration (Chen et al., 2010).

On the basis of these observations, and the background presented here regarding the use of electrospun scaffolds as a controlled release device for protein therapies, it was hypothesized that *L. sericata* maggot E/S may be incorporated into electrospun scaffolds made of PCL and PCL-b-PEG/PCL fibrous scaffolds (developed in chapter 4) (Figure 5.1) and may have a beneficial effect on wound healing, assuming bioactivity could be retained, by disinfect the wound bed and enhance fibroblast migration.

For this hypothesis, a number of aims have been set as part of this study, as following:

- To incorporate two different hydrophilic proteins (lysozyme and avidin) into electrospun fibres by post modification and evaluate loading and release profiles of the proteins from PCL and PCL-b-PEG/PCL platforms.
- To incorporate *L. sericata* maggot E/S, a complex mixture of proteins with different size and charge into electrospun fibres of PCL and PCL-b-PEG/PCL by post modification.

- To evaluate *in vitro* protein release profile of lysozyme, avidin and *L. sericata* maggot E/S. Sustainable release profile of *L. sericata* maggot E/S biomolecules within a given time that allows granulation tissue formation will be preferred.
- To confirm the bioactivity of the enzymes by examining protease (*L. sericata* maggot E/S) and lysozyme activity after release.

This investigation aims to create an innovative alternative for wound healing though the development of a novel bioactive prototype dressing. The beneficial effect of electrospun scaffolds to support fibroblast ingrowth into the scaffold (Chapter 4) and the incorporation of bioactive molecules from *L. sericata* maggot E/S proven to support wound healing. It will be the first electrospun scaffolds which incorporated *L. sericata* maggot E/S.

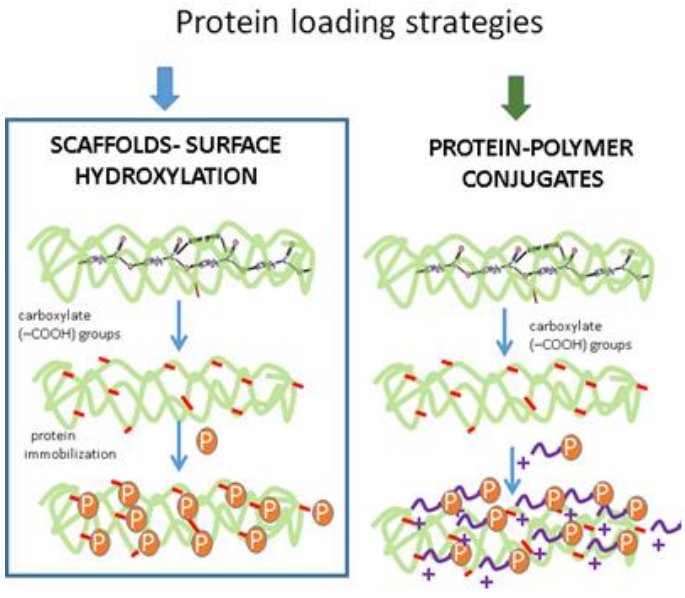


Figure 5.1 - Schematic approach of protein loading on electrospun scaffolds. Chapter 5 will focus on the first approach, framed on light blue (and light blue arrow). Second approach will be developed in chapter 6 (green arrow)

5.5 Results and discussion

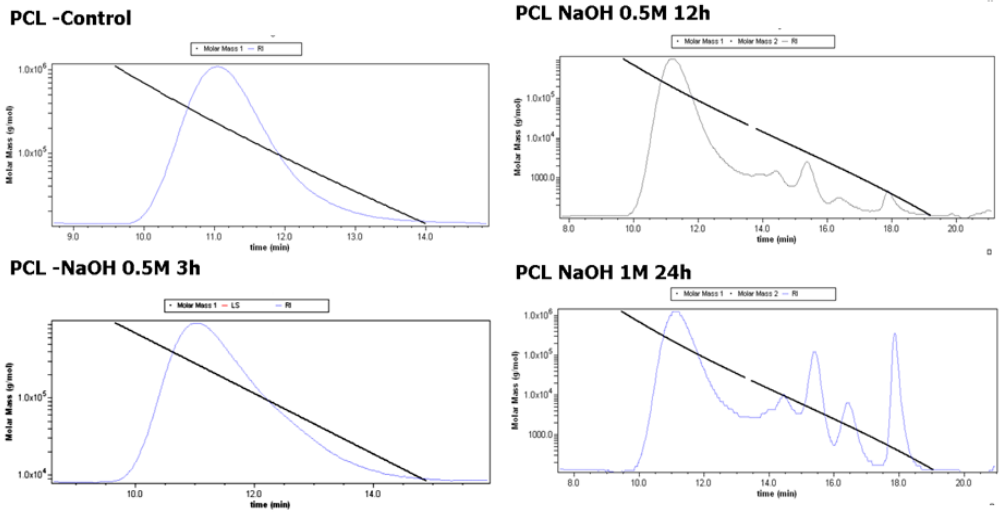
5.5.1 Wet chemical surface modification prior protein absorption

From Figure 5.2-A) it is observed that alkaline treatment on PCL scaffolds, using NaOH concentration 0.5 M for 3-12 h, did not cause any gross morphological changes when compared with the control. From Figure 5.2-B) a decrease in molecular weight (Mn) of PCL scaffolds treated with NaOH 0.5 M for 3 h from $1.4x10^5$ to $1.1x10^5$ can be seen. Longer incubation times (12 h) and the same NaOH concentration (0.5 M) generated two polymer populations with different molecular weights (GPC analysis); the molecular weight of one species was $\sim 1.9x\ 10^5$ while other was $\sim 9x\ 10^3$ grams/mole. Longer incubation periods of 24 h, at higher concentrations of NaOH of 1 M, did results in morphological variation (as seen in SEM images Figure 5.2-A)) of the electrospun fibres and GPC analysis of treated PCL scaffolds, showed two polymer fractions of $\sim 1.0x10^5$ and $\sim 1.4x10^3$ grams/mole.

A)



B)



Sample	M_n g/mol	M_w g/mol	Đ Mw/MN
PCL control	$1.368x10^5$	$2.163x10^5$	1.582
PCL-NaOH 0.5 M 3 h	$1.110x10^5$	$2.226x10^5$	2.005
PCL-NaOH 0.5 M 12 h	$9.190x10^4$ and $1.854x10^3$	$1.684x10^5$ and $6.141x10^3$	1.832 and 3.313
PCL-NaOH 1 M 24 h	$1.031x10^4$ and $1.367x10^3$	$1.807x10^5$ and $5.795x10^3$	1.752 and 4.239

Figure 5.2 - A) Representative micrographs of NaOH modified PCL fibre scaffolds, **B)** GPC analysis of PCL scaffolds following incubation with different concentrations of NaOH for different lengths of time **.**

The partial hydrolysis of PCL scaffolds was carried out by immersing scaffolds in NaOH 0.5M or alternatively in NAOH 1M and incubating for different amount of time, 3 h, 12 h and 24 h. The results presented here are in agreement with (Lam et al., 2007) who pointed out that PCL scaffolds have a surface erosion hydrolysis under alkaline conditions. Whereas amorphous regions (random coils) are more affected compared with crystalline regions (highly order). This surface erosion mechanism is explained by the diffusion-reaction phenomena. (Lam et al., 2007) explained that the degradation that takes place on the surface of PCL scaffolds resulted in the cleavage of small oligomers with small molecular weight. Also, they reported that scaffold morphology seems unaffected. In the present study, only PCL scaffolds treated with higher concentrations of NaOH (1M) for 24 h of incubation revealed a degradative process of its fibres after SEM micrograph analysis.

It was decided to incubate the scaffolds for periods not longer than 3 h using lower concentrations of NaOH of 0.5M, in order to not compromise the structure of the scaffolds. For the next sections nomenclature H-PCL scaffolds will refer to scaffolds treated with 0.5M of NaOH for 3 h.

It was hypothesized that the incorporation of PEG to scaffolds (PCL-b-PEG/PCL) and the hydroxylation of PCL scaffolds (H-PCL) may enhance protein loading.

5.5.2 Avidin–fluorescein (AVI-FITC) conjugate loading on PCL and H-PCL and PCL-b-PEG/PCL scaffolds

Figure 5.3-A shows fluorescence images AVI-FITC absorbed on three types of scaffolds PCL, H-PCL, PCL-b-PEG/PCL. From Figure 6.3- A) and B) it can clearly be seen that the green-fluoresce intensity emitted by AVI-FITC adsorbed to the hydrolysed scaffolds (H-PCL) was higher compared with PCL and PCL-b-PEG/PCL scaffolds over 24 h of incubation. Figure 5.3-B) shows the percentage of AVI-FITC loaded on PCL, H-PCL and PCL-b-PEG/PCL scaffolds. Higher percentages of AVI-FITC were successfully loaded onto, H-PCL scaffolds compared with PCL scaffolds. After 3 h, H-PCL were loaded with 50% of AVI-FITC, which is more significant (P 0.0003) than the percentage of AVI-FITC loaded on PCL scaffolds (6%). After 6 h of incubation, 67% of AVI-FITC was loaded on H-PCL, which was higher (P 0.0006) than the percentage of AVI-FITC loaded on PCL scaffolds (28%). After 24 h 64% of AVI-FITC was loaded on H-PCL while AVI-FITC loaded on PCL scaffolds reached 40% (P 0.0076). Comparing PCL-b-PEG/PCL with PCL scaffolds, it was also noticed that in the first 3 h of incubation, a greater percentage (p 0.0001) of AVI-FITC (40%) was loaded onto the PCL-b-PEG/PCL scaffolds compared with the PCL scaffold (6%). By 6 hours, PCL scaffolds showed a percentage of AVI-FITC loading of 28% which still lower ($P<0.0001$) compared with the percentage of AVI-FITC loaded on PCL-b-PEG/PCL (37%). In addition, 43% of AVI-FITC was loaded on PCL-b-PEG/PCL, significantly higher (P 0.0022) to the percentage of AVI-FITC loaded on PCL scaffold (40%) after 24 h of incubation.

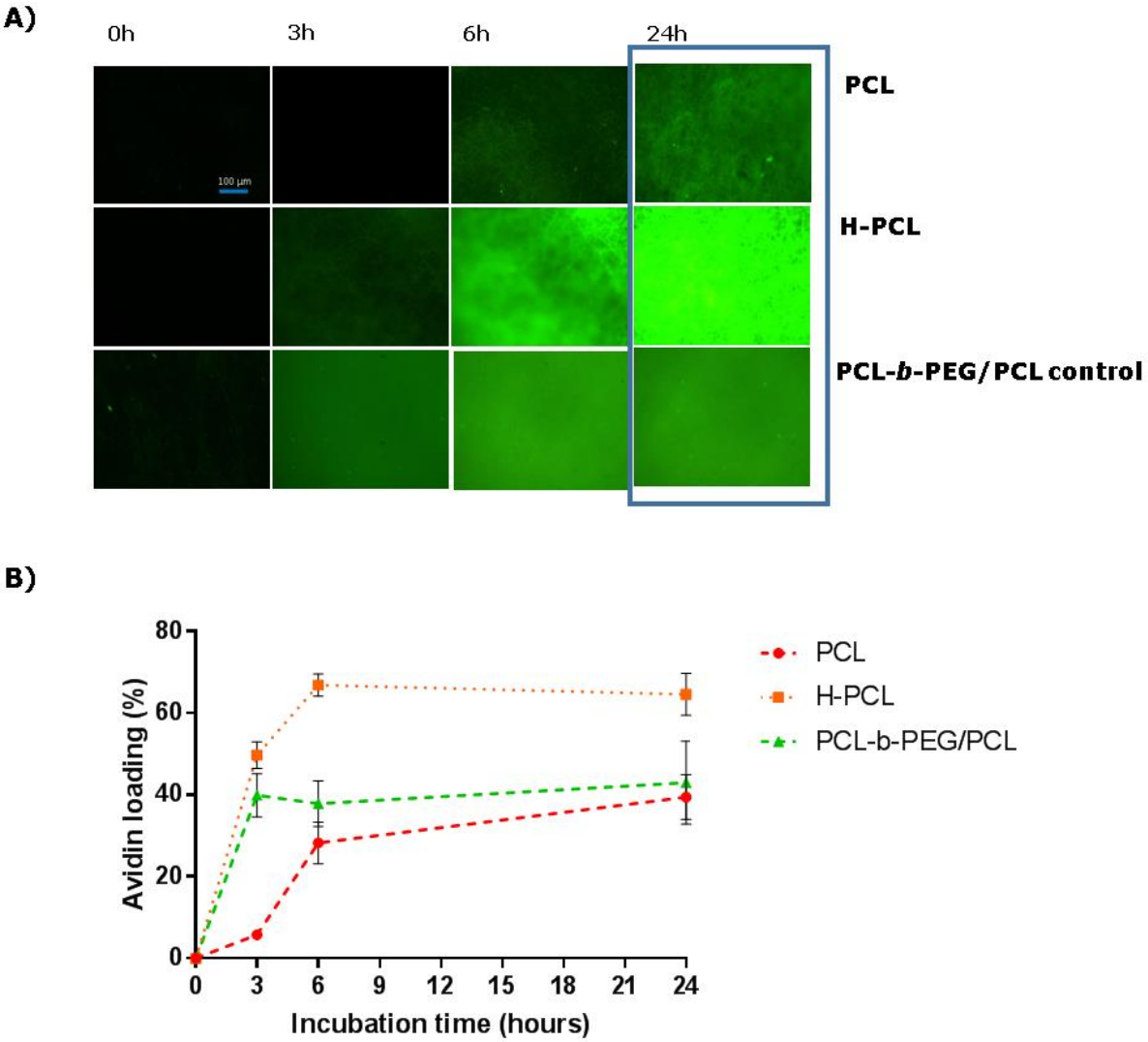


Figure 5.3 - A) Representative fluorescence microscopy images of avidin-fluorescein conjugate protein (AVI-FITC) adsorbed onto PCL, H-PCL and PCL-b-PEG/PCL fibre scaffolds. Magnification 10x, scale bar 100 µm. B) AVI-FITC loading percentage on PCL, H-PCL and PCL-b-PEG/PCL scaffolds. Two way-ANOVA, Tukey's multiple comparison test. Three independent experiments carried out in triplicate (means±SD).

In order to determine the loading capacity of PCL, H-PCL and PCL-b-PEG/PCL scaffolds, AVI-FITC protein was absorbed as a model protein. Avidin is a homo tetrameric protein with a PI of 10-10.5 and has an estimated cationic charge density of 16 (Liao et al., 2005). The higher loading percentage of AVI-FIT on H-PCL surface compared with PCL may be explained by the fact that H-PCL possesses negatively charged functional groups, such as carboxyl and hydrogen bond donor and acceptors such as hydroxyl, which interact with the positive and polar amino acid residues of avidin at pH 7.4. This is in agreement with previous research by (Arima and Iwata, 2007), who found that proteins adsorbed significantly higher to surfaces that were rich in functional groups such as hydroxyl (OH) and carboxyl acid (COOH) groups.

It is widely known that PEGylated surfaces are used to reduce unspecific protein absorption, acting as a barrier by steric hindrance (Dhar et al., 2008, Sanders and Hendren, 1997). Protein repellent ability depended partially on PEG chain length and PEG architecture (Jeong et al., 2000). PEG has been incorporated in a variety hydrogels and scaffolds for tissue regeneration and drug delivery with the purpose of: a) to preserve the bioactivity of the therapeutics (Lin and Anseth, 2009), b) to provide an extended controlled and sustained release of the biomolecules (Lin and Anseth, 2009, Rahman et al., 2014) and c) to improve mechanical properties of scaffolds.

In the current study, for the PCL-b-PEG/PCL scaffolds it is probable that the content of PEG was not sufficient to cause a hydrated repulsion between the PEG chain and proteins, which allowed a higher

adsorption of avidin to the surface compared with PCL, but a lower loading than H-PCL which was influenced by a combination of electrostatic forces and hydrophobic interactions.

5.5.3 Avidin–fluorescein (AVI-FITC) conjugate release from PCL and H-PCL and PCL-b-PEG/PCL scaffolds

From Figure 5.4-B it can be seen that AVI-FITC release profiles from PCL, H-PCL and PCL-b-PEG/PCL scaffolds showed three phases of release. The first phase is characterized by first order kinetics, where the protein released increased as function of the time, i.e via a 'burst release'. Then, a reduction in the amount of protein released was observed, followed by a more sustained release profile, and zero order release, characterised by maintaining the dose over time. AVI-FITC release from PCL and H-PCL scaffolds shows a similar release profile. Burst release is low and occurs during the first 2 h. Between 2 and 6 hours of incubation, the release of avidin became slower and after 6 h the cumulative release of avidin reached values around 16%. This pattern of release continued till day 21. Statistic evaluation for PCL, H-PCL and PCL-b-PEG/PCL scaffolds reveals that during the first 5 h, avidin cumulative release was not statistically significantly (ns). In addition, AVI-FITC release from PCL-b-PEG/PCL scaffolds showed greater burst release after 6 h compared with AVI-FITC released from PCL and H-PCL scaffolds. After 6 hours avidin released from the PCL-b-PEG/PCL scaffolds was 25%, significantly higher than avidin released from the PCL and H-PCL scaffolds (16%) (P 0.0053 and 0.0066 respectively).

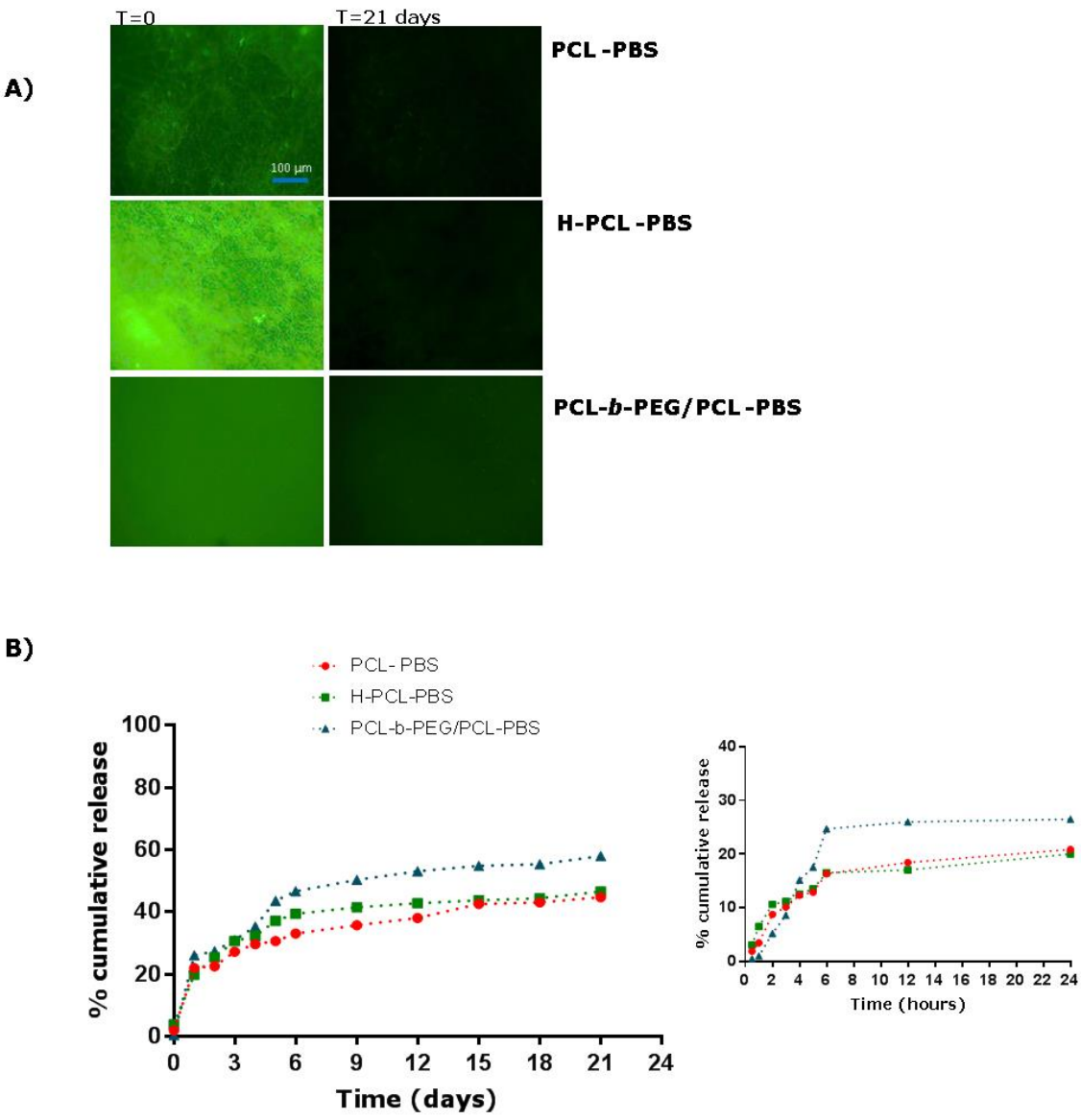


Figure 5.4 - A) Fluorescence microscopy images of avidin-fluorescein conjugate protein (AVI-FITC) adsorbed onto PCL and H-PCL fibres scaffolds. Magnification 10x, scale bar 100 microns. B).AVI-FITC release profiles from PCL, H-PCL and PCL-b-PEG/PCL scaffolds in PBS pH 7.4 at 37°C.

Over the following days until the end of the assay (21 days), no significant differences between avidin release (cumulative) were observed, with the exception of PCL and PCL-b-PEG/PCL scaffolds where after 9 and 12 days, avidin release from the PCL-b-PEG/PCL scaffolds was higher (~50%) compared with PCL scaffolds (~40%) (P 0.0318 and 0.00263 respectively).

In section 5.5.2 it was observed that a higher concentration of avidin was loaded on H-PCL scaffolds than on PCL scaffolds. Hence, it was expected that the release of avidin from the H-PCL scaffolds would be greater. However, the release of avidin from H-PCL scaffolds may not be as high as expected due to the electrostatic force that maintains polymer-protein interactions. In addition, PCL-b-PEG/PCL scaffolds were loaded with lower quantities of avidin compared with H-PCL scaffolds, but higher than PCL scaffolds, and the release of avidin was faster and greater from the PCL-b-PEG/PCL scaffolds. This effect may be due to the fact that PEG may not have a strong interaction with the protein, caused by steric interaction and hydration. Instead the hydrophilic PEG chain may help the aqueous media to penetrate and allow the release of avidin molecules from the surface. This is in agreement with other authors that pointed out that the release of protein is accelerated by the addition of PEG on the scaffolds (Ji et al., 2010), due to the enhancement of water's diffusion (Briggs and Arinzeh, 2014).

5.5.4 Lysozyme–rhodamine B (LYZ-RB) conjugate loading on PCL and H-PCL and PCL-b-PEG/PCL scaffolds

Figure 5.5-A) shows representative fluorescence images of lysozyme-rhodamine conjugates (LYZ-RB) adsorbed/loaded onto three types of fibrous scaffolds PCL, H-PCL, PCL-b-PEG/PCL. From Figure 5.5-A) and B) it can clearly be seen that the fluorescence of LYZ-RB adsorbed to the hydrolysed scaffolds (H-PCL) was higher compared with that adsorbed onto the PCL and PCL-b-PEG/PCL scaffolds over 24 h of incubation. Figure 5.5-B shows the percentage of LYZ-RB loaded on the PCL, H-PCL and PCL-b-PEG/PCL scaffolds. In terms of LYZ-RB loading percentage, there was significantly higher percentages of LYZ-RB adsorbed onto H-PCL scaffolds compared with PCL and PCL-b-PEG/PCL scaffolds. After 3 h H-PCL 42% of the initial amount of LYZ-RB was adsorbed, which is significantly higher than the percentage of LYZ-RB adsorbed onto PCL scaffolds (35%) ($P<0.001$) and PCL-b-PEG/PCL (35%) (P 0.0005). After 6 h of incubation, 57% of the initial amount of AVI-FITC was loaded onto the H-PCL scaffolds, which was similar to the percentage of AVI-FITC loaded onto the PCL scaffolds (55%) (ns), and higher than the amount of LYZ-RB loaded onto the PCL-b-PEG/PCL scaffolds (50%) ($P<0.0001$). After 24 h, 64% of the initial amount of LYZ-RB was loaded on H-PCL scaffolds while LYZ-RB loaded on PCL scaffolds reached 57% (P 0.0007) and PCL-b-PEG/PCL scaffolds 56% ($P<0.0001$).

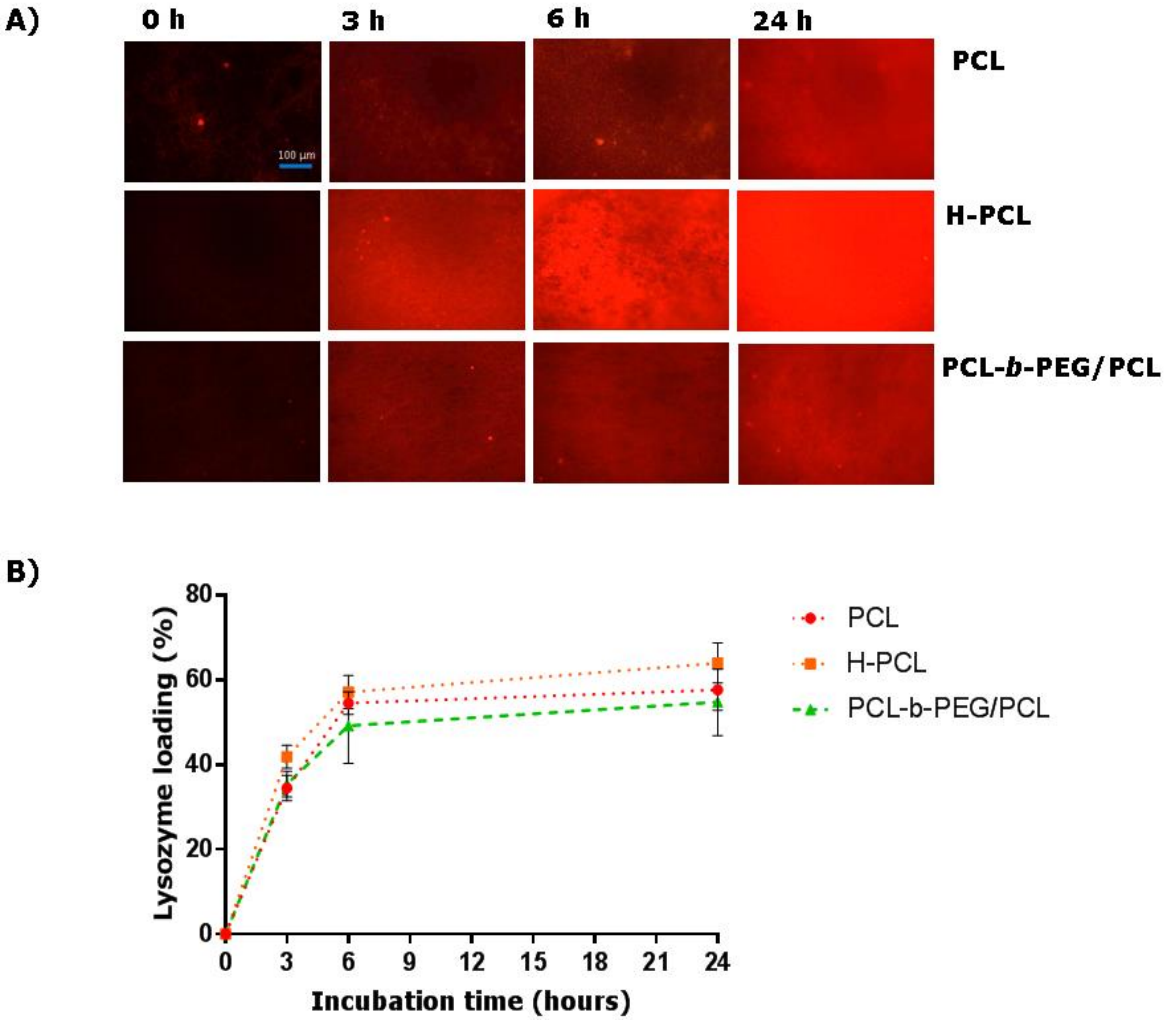


Figure 5.5 - A) Representative fluorescence microscopy images of lysozyme-rhodamine B conjugate protein (LYZ-RB) adsorption on PCL and H-PCL fibre scaffolds. Magnification 10x, scale bar 100 µm. B) LYZ-RB loading percentage on PCL, H-PCL and PCL-b-PEG/PCL fibrous scaffolds. Two way-ANOVA, Tukey's multiple comparison test. Three independent experiments carried out in triplicate (means±SD).

Comparing PCL-b-PEG/PCL with PCL scaffolds, no statistical significant differences were found in term of loading percentage of LYZ-RB.

Higher percentages of LYZ-RB were adsorbed onto H-PCL scaffolds compared with plain PCL and PCL-b-PEG/PCL scaffolds over 24 hours of incubation. These findings may be explained by the fact of H-PCL scaffolds possesses negative functional groups, which interact with positive amino acid residues of lysozyme at pH 7.4. This is in agreement with the avidin results (section 5.5.2), where increased numbers of functional groups on the surface of H-PCL scaffolds, as a result of NaOH hydrolysis, improved the loading efficiency of avidin.

Avidin and lysozyme were loaded as a model for *L. sericata* maggot E/S delivery for wound healing. Enzyme selection was based on molecular weight (range from 14-66 kDa).

Lysozyme is a proteinase, used as antibacterial agent because it has the capacity to destroy bacterial cell walls. Hen egg white lysozyme possesses a molecular weight of 14.3 kDa. The protein has a single polypeptide chain of 129 amino acids. It also has a positive net of +9 at pH 7.0 (PI:11), with 8 negative charge (2 glutamic acid and 6 asparagine acid) and 17 positively charged amino acids (6 lysine and 11 arginine) (Wang et al., 2009a).

A comparison of avidin and lysozyme (Figure 5.6) loading reveals that in general, higher amounts of protein were adsorbed onto the surface of H-PCL scaffolds than PCL and PCL-b-PEG/PCL scaffolds. It was also noted that the percentage of LYZ-RB loaded on the scaffolds is higher than the percentage of AVI-FITC loaded in the same type of scaffolds over the 24 h incubation period. After 24 h the loading % of avidin on the PCL scaffolds was lower (40%) compared with lysozyme in the same scaffold (57%). Loading % of avidin on PCL-b-PEG/PCL scaffolds was lower (40%) compared with lysozyme in the same scaffold (56%). H-PCL scaffolds adsorbed similar quantities of avidin and lysozyme ~65% of the initial concentration.

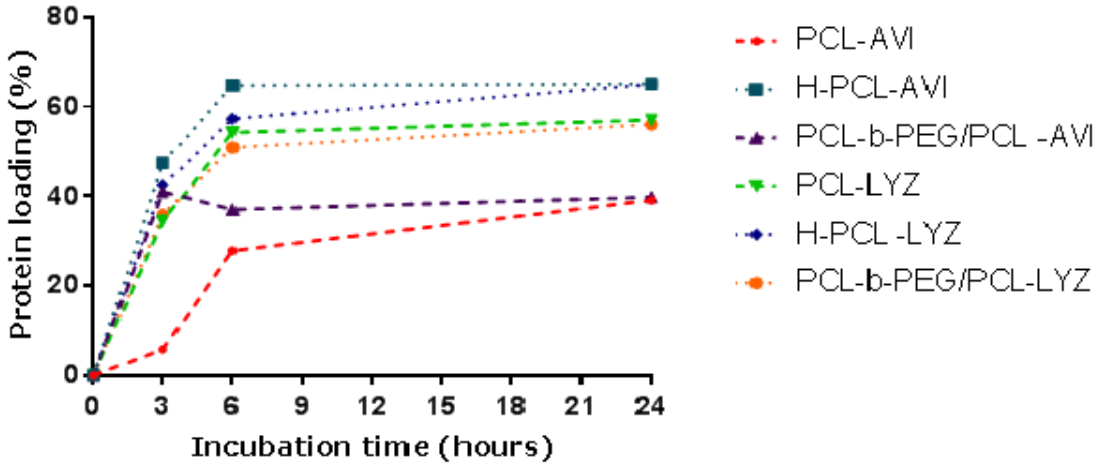


Figure 5.6 - Comparison between AVI-FITC and LYZ-RB loading percentages on PCL, H-PCL and PCL-b-PEG/PCL fibrous scaffolds.

The probable explanation for these differences between proteins loading behaviour is the size and shape of the proteins and different interactions that they may have with polymeric substrates. Avidin and lysozyme both possess an overall net positive charge. However, avidin has a more complicated tetrameric and glycosylate structure with 128 amino acid chains each. In contrast, lysozyme presents a simpler structure of a peptide chain of 129 amino acids. Hydrophobic and hydrophilic interaction phenomena between protein-protein and protein-substrate are still poorly understood and it is quite difficult reach an ultimate conclusion (Sarkar and Kellogg, 2010). However a possible explanation is that there may be an interaction between hydrophobic domains of the PCL scaffold surface with the hydrophobic domain of the protein (Lee et al., 2007). PCL-b-PEG/PCL scaffolds may balance the attractive and the repulsive hydrophilic-hydrophilic forces between the protein and the PEG-PCL surface, and between the protein and the media (Sanders and Hendren, 1997). In addition, H-PCL interacts with proteins through electrostatic interactions. Lysozyme and avidin are positively charged at physiological pH (7.4). However, lysozyme has a lower density charge (net charge+9) compared with avidin (net charge+16), that should allow more loading of avidin on the scaffolds compared with lysozyme. However the bigger size of avidin (66 kDa) and its complex structure (glycosylation) compared with lysosome (14 kDa) may cause a steric hindrance effect that makes it hard to attach to the surface or allow other avidin molecules to attach on the same surface (Zhao et al., 2010).

5.5.5 Lysozyme-rhodamine B (LYZ-RB) conjugate release from PCL and H-PCL and PCL-b-PEG/PCL scaffolds

Figure 5.7-A) shows representative fluorescent images of LYZ-RB absorbed onto PCL, H-PCL and PCL-b-PEG/PCL scaffolds. It is observed that after 21days fluorescence of LYZ-RB decreased and almost disappeared from the scaffolds. Figure 5.7-B) shows the release profile of lysozyme-rhodamine B conjugate protein (LYZ-RB) from these PCL, H-PCL and PCL-b-PEG/PCL scaffolds. From the results, it can be seen that the LYZ-RB release profiles showed 3 phases of LYZ-RB release. There was a delay during first 12 hours in the burst release where concentration of LYZ-RB remained constant over time (zero order kinetics). After that period (from 12 h-24 h), the burst release phase was observed. Then, LYZ-RB release was maintained over the period of 21 days. Sometimes, the LYZ-RB release profile from the PCL scaffolds showed a second burst release at day 15, which was extended until day 18. From Figure 5.7-B) it can be seen that the lysozyme cumulative release from the PCL-b-PEG/PCL scaffolds was similar (44%) to the lysozyme cumulative release from H-PCL scaffolds (40%) (ns) and statistically higher than LYZ-RB release from PCL (34%) (P 0.0165) at 30 min after incubation. In addition, from 12 h to 24 h an increment in the LYZ-RB cumulative release was observed, reaching values of 74% of the initial amount adsorbed from H-CPL scaffolds, 60% from PCL scaffolds, and 56% from PLC-b-PEG/PCL scaffolds (after 24 h). LYZ-RB release from the H-CPL scaffolds was significantly higher than LYZ-RB release from PCL and PCL-b-PEG/PCL scaffolds ($p<0.0001$).

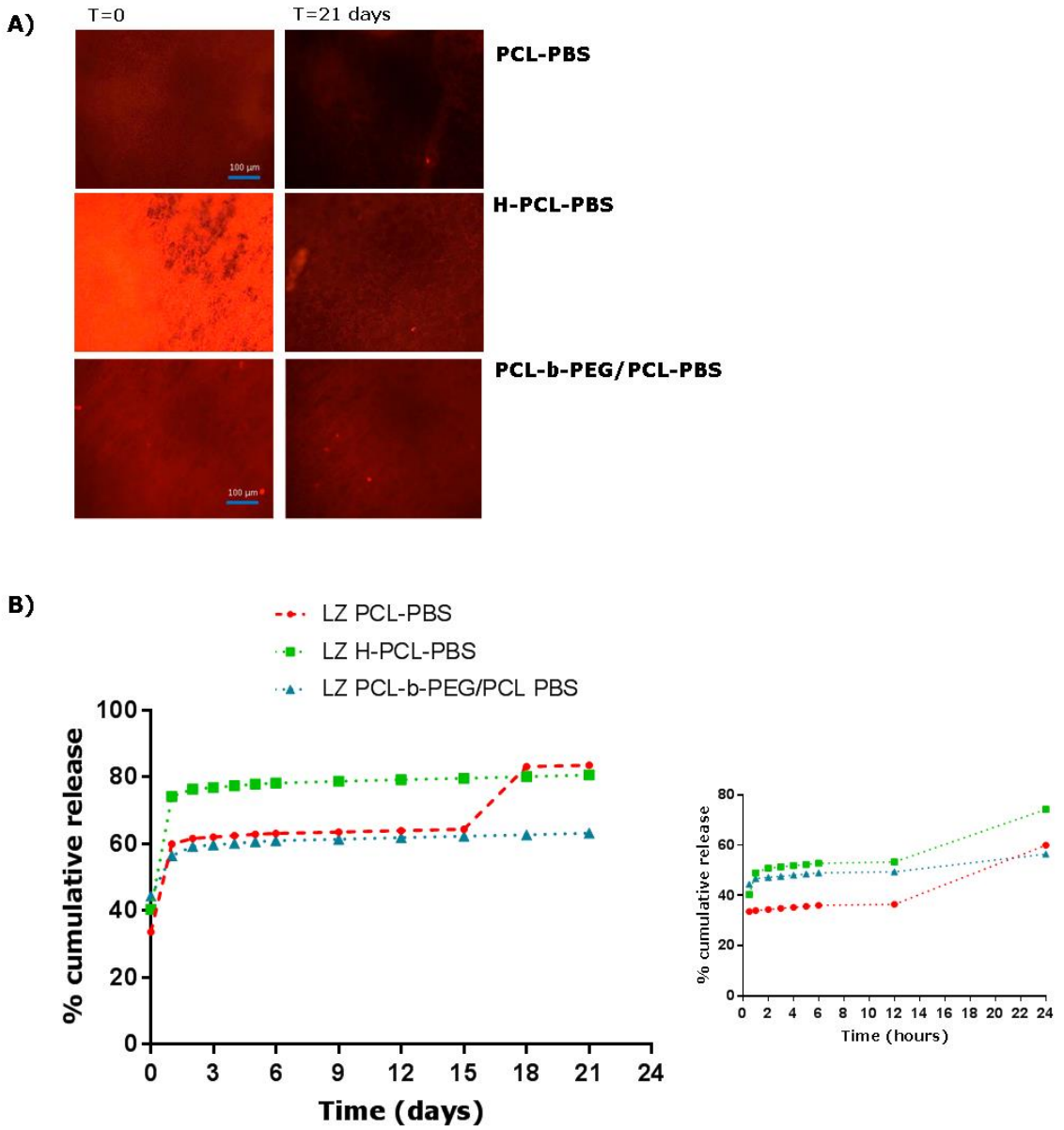


Figure 5.7 - A) Representative Fluorescent microscopy images of lysozyme-rhodamine B conjugate protein (LYZ-RB) adsorbed onto PCL, H-PCL, PCL-b-PEG/PCL fibres scaffolds. Magnification 10x, scale bar 100 microns. B). LYZ-RB release profiles from PCL, H-PCL and PCL-b-PEG/PCL scaffolds in PBS pH 7.4 at 37°C.

From 24 h to 21 days, LYZ-RB was released gradually and was sustained with LYZ-RB cumulative release. The differences in terms of LYZ-RB cumulative release were not significant between the H-PCL and PCL scaffolds (both ~80%). However, the LYZ-RB released from the H-PCL scaffolds was significantly higher (~80%) (p 0.0030) compared with that released from PCL-b-PEG/PCL scaffolds (63%). From day 3 to 15 days, the LYZ-RB cumulative release profile from PCL and PCL-b-PEG/PCL scaffolds were similar and no statistical differences were found. However, after day 15, release of LYZ-RB from PCL experienced a second burst release increasing the total amount of LYZ-RB released, reaching similar values of LYZ-RB cumulative release from H-PCL scaffolds (ns).

To H-PCL scaffolds, 64% of the initial amount of protein was adsorbed, a significantly higher quantity of lysozyme compared with the PCL-b-PEG/PCL (56%) and PCL (57%) scaffolds. And more lysozyme was released from the H-PCL scaffolds with a higher burst release compared with the PCL-b-PEG/PCL and PCL scaffolds, which is in agreement with (Wang et al., 2009a), who pointed out that the release of lysozyme is dependent on the quantity of protein loaded. They reported that higher % of lysozyme loaded on the scaffolds is characterized then by a faster release (80% within first days).

According to (Kim et al., 2007), the absorption of lysozyme in a blend of PEO/PCL fibres, which will be within hydrophilic PEG domain and the release of lysozyme from the PEO/PCL fibres will occur faster by increasing the concentration of PEG. In the current study, PCL-b-PEG/PCL scaffolds presented similar release profiles of lysozyme

release from PCL scaffolds. (Puhl et al., 2014) developed electrospun scaffolds made of PEG/PCL and PCL for protein control delivery. They reported that the initial release of lysozyme from PCL scaffolds was 40% and then a zero-order kinetic release was observed for 14 days. The release of lysozyme from PCL was lower, with a lower burst release compared with lysozyme release from PCL/PEG (containing 20% of PEG). Moreover, the same author specified that the faster release behaviour of lysozyme from PCL/PEG scaffolds is dependent on the concentration of PEG. For instance, PEG content less than 10% did not reveal any significant differences compared with PCL scaffolds. The results presented here showed PCL-b-PEG scaffolds released higher quantities of lysozyme compared with PCL in the first 12 hours and then the release of lysozyme was very similar for both scaffolds for the next 15 days. As a result, it seems that the quantity of PEG in the scaffolds developed here was insufficient to cause a significant impact on lysozyme release as (Puhl et al., 2014) reported.

Comparing the release profiles of AVI-FIT with LYZ-RB from PCL, H-PCL and PCL-b-PEG/PCL scaffolds (Figure 5.8), it was noticed that the percentage of lysozyme released into the media was higher compared with AVI-FITC. At the end of the 21 days, the maximum release of LYZ-RB was significantly higher (84%) ($P < 0.0001$) than AVI-FITC (58%). The most likely explanation for this phenomenon is that avidin limits the diffusion of molecules of water through steric hindrance (Marttila et al., 1998). In contrast, the mechanism of lysozyme release is diffusion without steric hindrance (Szentivanyi et al., 2011)

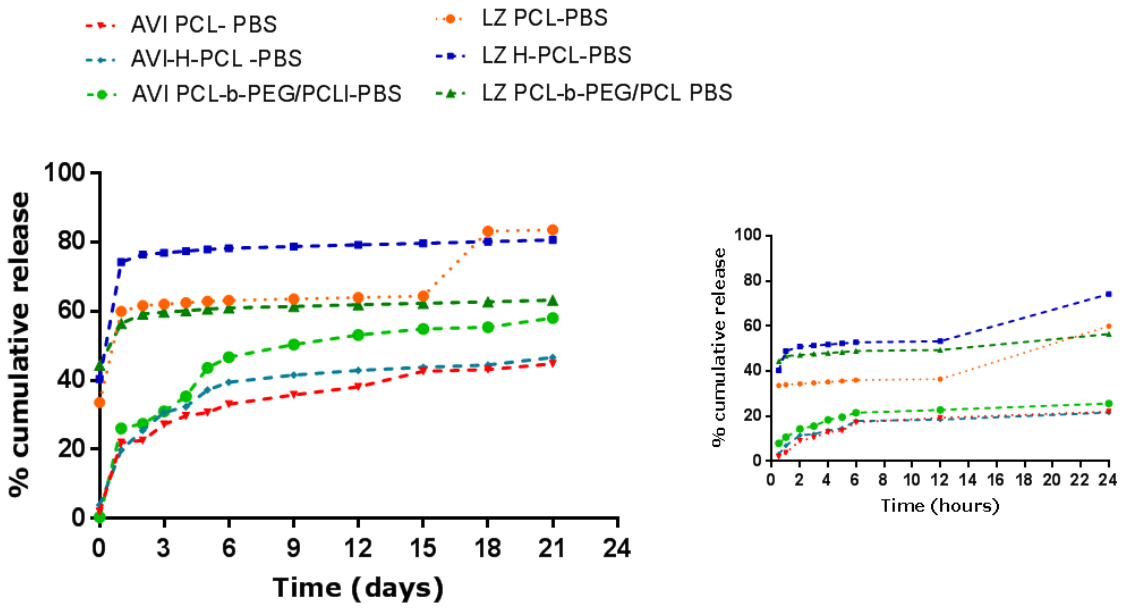


Figure 5.8 - Comparison between AVI-FITC and LYZ-RB release profiles from PCL, H-PCL and PCL-b-PEG/PCL scaffolds.

5.5.6 The bioactivity of lysozyme after release

Figure 5.9 shows the bioactivity of lysozyme at the end of the release studies and after all lysozyme fractions were pooled and concentrated to the same volume (1mL). It was found that the bioactivity of lysozyme remained active was significantly higher when the release of lysozyme was from the H-PCL scaffolds (P 0.0445) and from the PCL-b-PEG/PCL (P 0.0148) scaffolds compared with lysozyme released from the PCL scaffolds. Lysozyme release from H-PCL and PCL-b-PEG/PCL scaffolds in PBS, remained active (83%) after all loading, washing, drying and release, centrifugation, and storing procedures. The activity of lysozyme released from PCL scaffolds was reduced to 80%.

One of the important factors to consider during release studies is the stability of the protein (Wang et al., 2009a). The results presented here are in agreement with the results presented by (Wang et al., 2009a), who reported that after 11 days of lysozyme release from PCL scaffolds, the activity of lysozyme was reduced to 75-80%. This author pointed out that PCL possesses a poor compatibility with protein due to its hydrophobic nature, which may result in protein deformation, denaturation and aggregation. Also, a contributor of the loss of activity is the time period over which that enzymes were released (Wang et al., 2009a). (Bezemer et al., 2000) pointed out that lysozyme is more stable at pH 3.5-5 and as a result, a certain loss of activity is expected when this protein was absorbed to scaffolds stored at physiological pH.

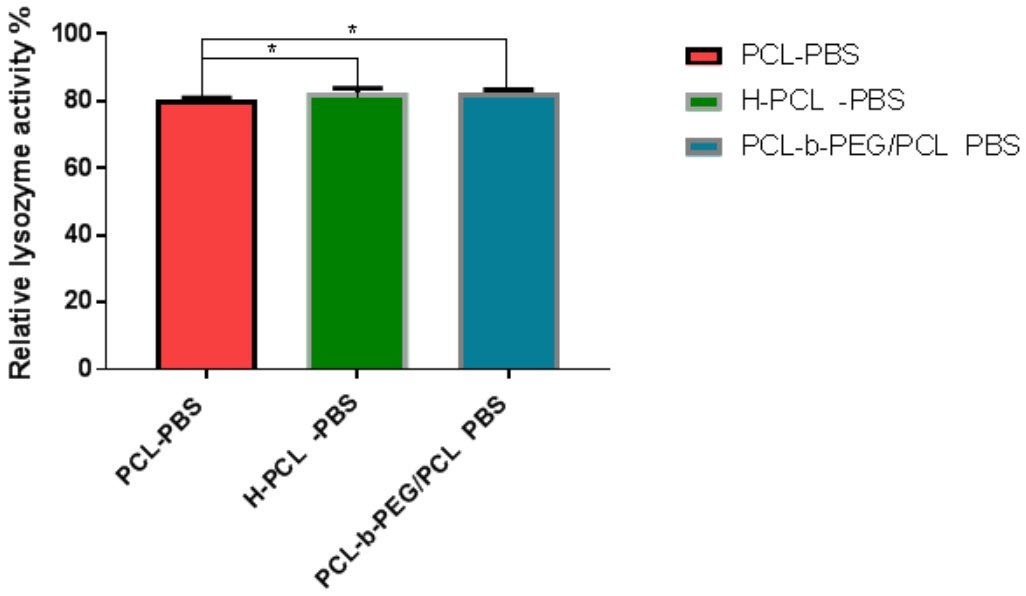


Figure 5.9 - Lysozyme bioactivity following release from the scaffold. Percentage of lysozyme activity is relative to the initial activity of lysozyme, before loading studies. Lysozyme released from the scaffolds (PCL, H PCL, PCL-b-PEG/PCL) was pooled and activity analysed using an EnzChek® lysozyme assay. Three independent experiments carried out in triplicate (means±SD).

5.5.7 *Lucilia sericata* maggot excretion/secretion loading on PCL and H-PCL and PCL-b-PEG/PCL scaffolds

Preliminary experiments were carried out using PCL and H-PCL scaffolds at 3 h, 6 h, 24 h, 48 h and 72 h. An initial concentration of *L. sericata* maggot E/S concentration 40 µg/mL (determined through a Bradford). From these results it was decided that all studies would adopt incubation of *L. sericata* maggot E/S for 24 h due the fact that no significant differences were found in terms of loading after that period of time. Figure 5.10–A) shows fluorescence images of *L. sericata* maggot E/S-labelled with NHS rhodamine adsorbed onto PCL, H-PCL and PCL-b-PEG/PCL scaffolds. Figure 5.10-B) shows a quantitative analysis of *L. sericata* maggot E/S loaded on PCL, H-PCL and PCL-b-PEG/PCL scaffolds. No significant differences were found in terms of percentage of *L. sericata* maggot E/S loaded on PCL-b-PEG/PCL scaffolds compared with PCL and H-PCL scaffolds.

Figure 5.11 depicts a comparison of three different proteins, avidin, lysozyme, and *L. sericata* maggot E/S loaded on the three types of scaffolds PCL, H-PCL and PCL-b-PEG/PCL. In general, it can be seen that avidin and lysozyme load higher quantity on H-PCL scaffolds, while avidin and lysozyme's loading % were similar on PCL and PCL-b-PEG/PCL scaffolds. For *L. sericata* maggot E/S no significant enhancements were observed when H-PCL scaffold was used as platform to load the mix of protein. *L. sericata* maggot E/S loaded the same quantity (~53%) in all the scaffolds. A possible explanation of these results is the complexity of *L. sericata* maggot E/S which contains a mix of proteins with different charge and molecular weights (Horobin et al., 2005).

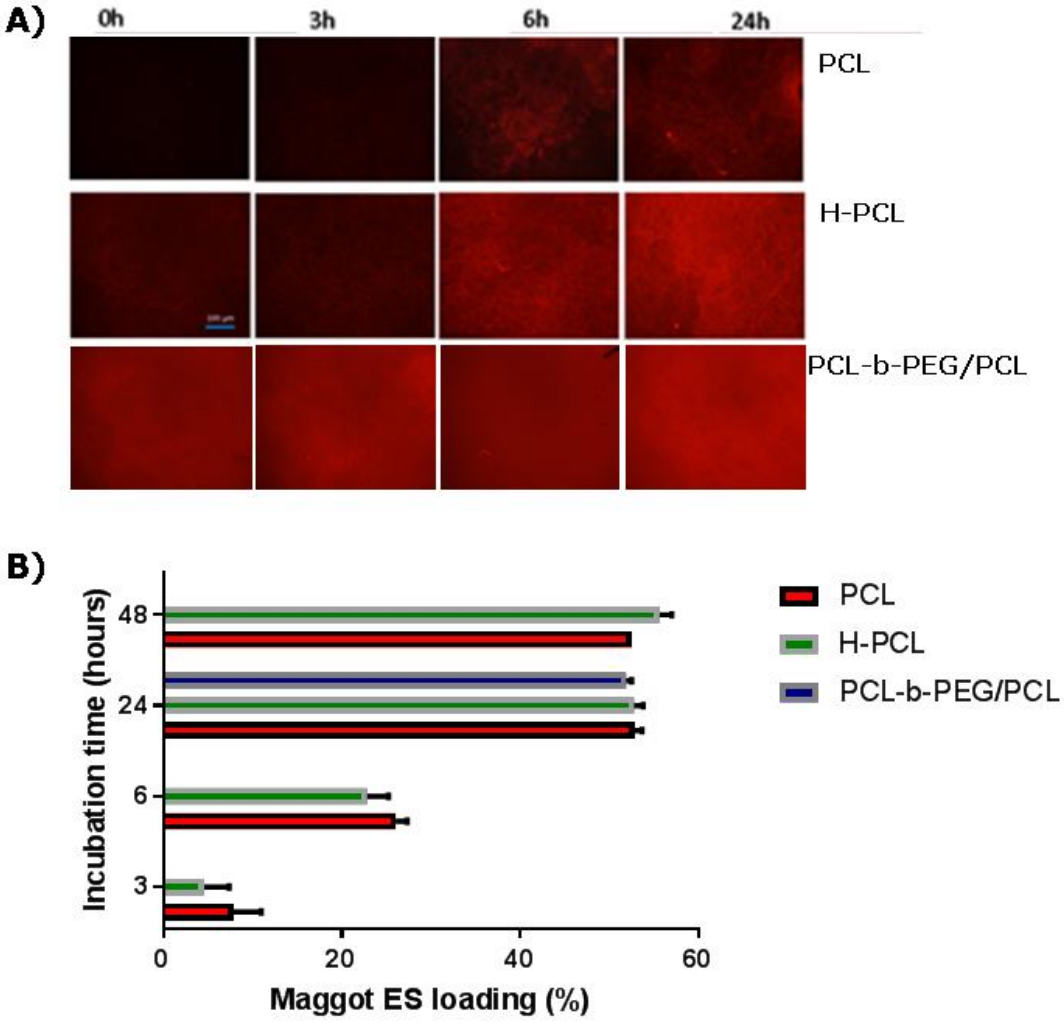


Figure 5.10 - A) Representative fluorescence microscopy images of *L. sericata* maggot-NHS rhodamine conjugate protein absorbed onto PCL, H-PCL and PCL-b-PEG/PCL scaffolds. Magnification 10x, scale bar 100 microns. B) *L. sericata* maggot E/S loading percentages on PCL, H-PCL and PCL-b-PEG/PCL scaffolds. Determination of protein concentration were done by Bradford assay. Two way-ANOVA, Tukey's multiple comparison test. Two independent experiments carried out in duplicate (means±SD).

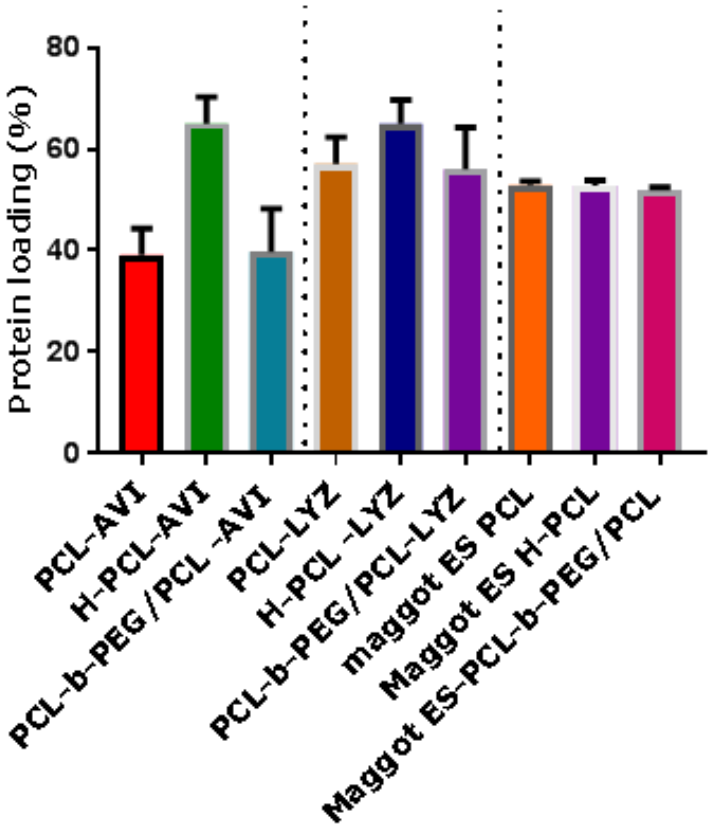


Figure 5.11 - Comparative analysis of *L. sericata* maggot E/S, avidin and lysozyme loading onto PCL, H-PCL and PCL-b-PEG/PCL fibrous scaffolds. Two way-ANOVA, Tukey's multiple comparison test. Three independent experiments carried out in triplicate (means±SD).

5.5.8 *Lucilia sericata* maggot excretion/secretion release from PCL and H-PCL and PCL-b-PEG/PCL scaffolds

From these results (Figure 5.12) it can be seen that *L. sericata* maggot E/S release profiles displayed 3 phases. The first 6 h displayed a burst release where concentrations of *L. sericata* maggot E/S increased over time. After that period (from 6 h-24 h), a slow-down release phase was observed, where *L. sericata* maggot E/S concentrations increased slowly and gradually over time. Then, *L. sericata* maggot E/S concentrations were released progressively and slowly over 21 days. The release profile of *L. sericata* maggot E/S from PCL and H-PCL scaffolds were similar, no statistical significance was found at any time. The release of *L. sericata* maggot E/S began immediately after the immersion of the scaffold in the media (PBS), reaching values of cumulative release of 3.5%. After 6 h, *L. sericata* maggot E/S reached values of accumulative release of 25% from PCL-b-PEG/PCL scaffolds, which was significantly higher compared with 22% from PCL (P 0.0027) and H-PCL (P 0.0007). By 24 h, the release of *L. sericata* maggot E/S from PCL and H-PCL was 28% and from PCL-b-PEG/PCL 32%. Again, statistics showed that PCL-b-PEG/PCL released significantly higher percentages of *L. sericata* maggot E/S after 24 hours compared with *L. sericata* maggot E/S released from PCL (P <0.0001) and H-PCL (P <0.0001). *L. sericata* maggot E/S cumulative release values increased progressively for 21 days, reaching values of cumulative release of 61% (H-PCL), 58% from (PCL) and 67% from PCL-b-PEG/PCL scaffolds. PCL-b-PEG/PCL released at a statistically significantly higher percentage of *L. sericata*

maggot E/S after 21 days compared with *L. sericata* maggot E/S released from PCL (P <0.0001) and H-PCL (P 0.0015).

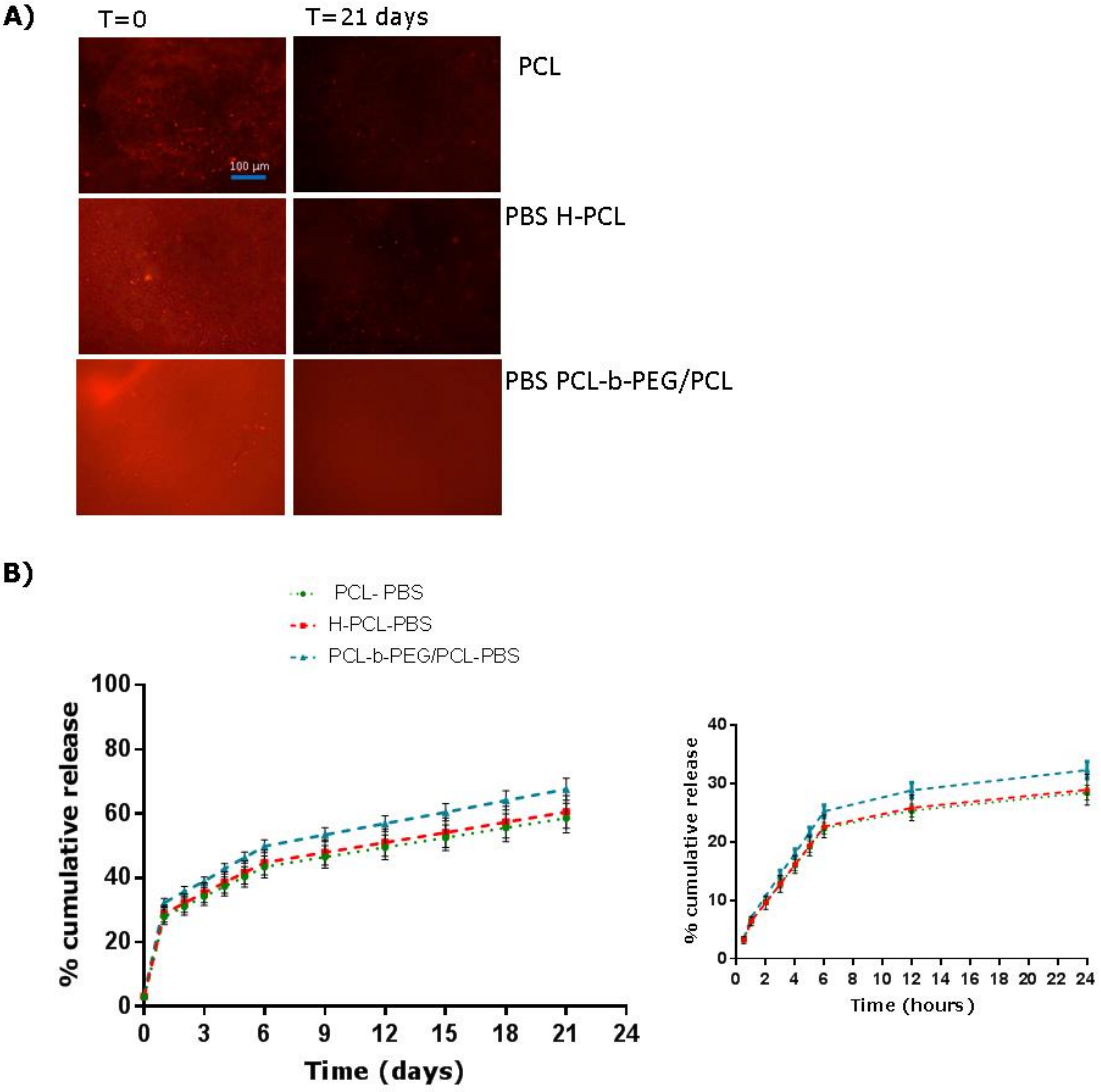


Figure 5.12 - Fluorescent microscopy images of *L. sericata* Maggot E/S-rhodamine B conjugate protein absorbed on PCL, H-PCL and PCL-b-PEG/PCL scaffolds. Magnification 10x, scale bar 100 microns. B). *L. sericata* maggot E/S release profiles from PCL, H-PCL and PCL-b-PEG/PCL scaffolds in PBS pH 7.4 at 37°C. Two independent experiments carried out in triplicate (means±SD).

In terms of cumulative amount of protein released, ~12 µg of *L. sericata* maggot E/S were measured from electrospun scaffolds after 24 h. After 21 days of release, 12.3 µg of protein was cumulative released from PCL and H-PCL scaffolds and 14.2 µg from PCL-b-PEG/PCL scaffolds. The cumulative released doses of *L. sericata* maggot E/S over 21 days were 0.015 µg of protein/µg of polymer (scaffold) from PCL and H-PCL scaffolds, and 0.018 µg of protein/µg of polymer (µg of scaffold) from PCL-b-PEG/PCL scaffolds. According with (Horobin et al., 2006) a dose of 1 µg/mL of fresh *L. sericata* maggot E/S enhanced fibroblast migration. A minimum dose of 0.1 µg/mL of fresh *L. sericata* maggot E/S also showed enhanced fibroblast migration (Horobin et al., 2005). In addition, (Smith et al., 2006) developed a prototype hydrogel which released 50 µg/mL of *L. sericata* maggot E/S and enhanced fibroblast migration. Preliminary *in vitro* scratch assays were conducted in the current study using a released *L. sericata* maggot E/S aliquots with concentrations between 12 and 14 µg/mL. However, released *L. sericata* maggot E/S did not show enhance fibroblast migration (further discussion in section 5.5.10).

In general, fluorescence images of avidin, lysozyme and *L. sericata* maggot E/S after 21 days of release, showed that proteins still absorbed to the scaffold surface, emitting florescence signal. (Srikar et al., 2008) pointed out that the release may not reach the 100% due to the tortuosity and pore interconnectivity of the scaffolds that may decreased the effective diffusion.

Figure 5.13 shows the cumulative release profiles of *L. sericata* maggot E/S, avidin and lysozyme. It was found that in the first 24 h, the release of *L. sericata* maggot E/S was similar to avidin release, characterized by a slow burst release, within ~ 6 hours. The values of cumulative release of avidin and maggot E/S were around 25% after 6 h, while lysozyme released faster and in higher quantities within 30 min. Values of cumulative release were 30-60% after just 1 hour. After 21 days of release maggot E/S, avidin and lysozyme from PCL-PEG/PCL were similar (ns). While for H-PCL *L. sericata* maggot E/S values of cumulative release were significantly lower compared with lysozyme 58% ($P < 0.0001$).and no significantly compared with avidin.

L. sericata maggot E/S loading and release was similar to that of avidin, while Lysozyme released in a different pattern and in a greater quantity.

It is hypothesized that large and complex proteins such as avidin show delayed release due to the hindrance effect that limits the water penetration deferring the release of molecules to the media. This hindrance effect may happen on a greater scale with *L. sericata* maggot E/S due to the complexity and variety of its proteins and other constituents. However, the release of *L. sericata* maggot E/S is higher than avidin which may be explained by the fact that avidin has a net positive charge at pH 7.4 while *L. sericata* maggot E/S contains a high number of proteins with different molecular weight and different net charges. Consequently, *L. sericata* maggot E/S may generate attractive interaction with the scaffolds as well as repulsive forces

between protein-protein, protein-scaffold and protein-media (Sanders and Hendren, 1997).

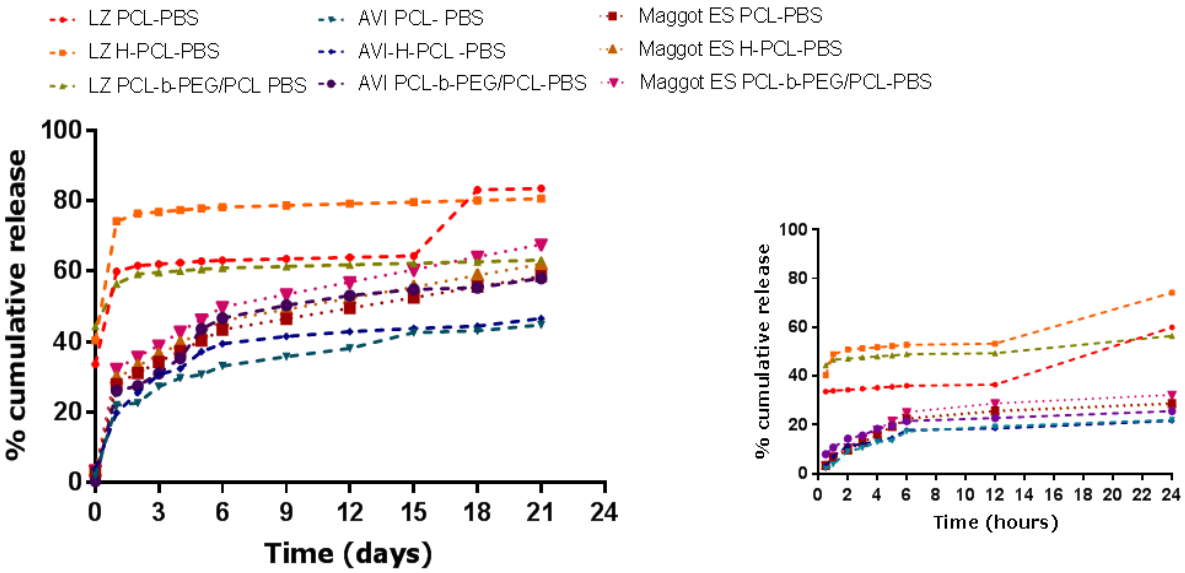


Figure 5.13 – Comparative release profile of avidin, lysozyme and L. sericata maggot E/S from PCL, H-PCL and PCL-b-PEG/PCL scaffolds.

5.5.9 Bioactivity of *Lucilia sericata* maggot excretion/secretion, after release

Figure 5.14 shows the bioactivity of *L. sericata* maggot E/S after being released from PLC, H-PCL and PCL-b-PEG/PCL scaffolds.

There were no significant differences in terms of bioactivity among all the analysed samples. However, a trend towards significance was observed. *L. sericata* maggot E/S released from PCL-b-PEG/PCL scaffolds showed 79% of activity remaining after the release process, while *L. sericata* maggot E/S activity of release fractions from H-PCL 71% and PCL scaffolds 59%. To confirm this trend a greater number of samples need to be tested.

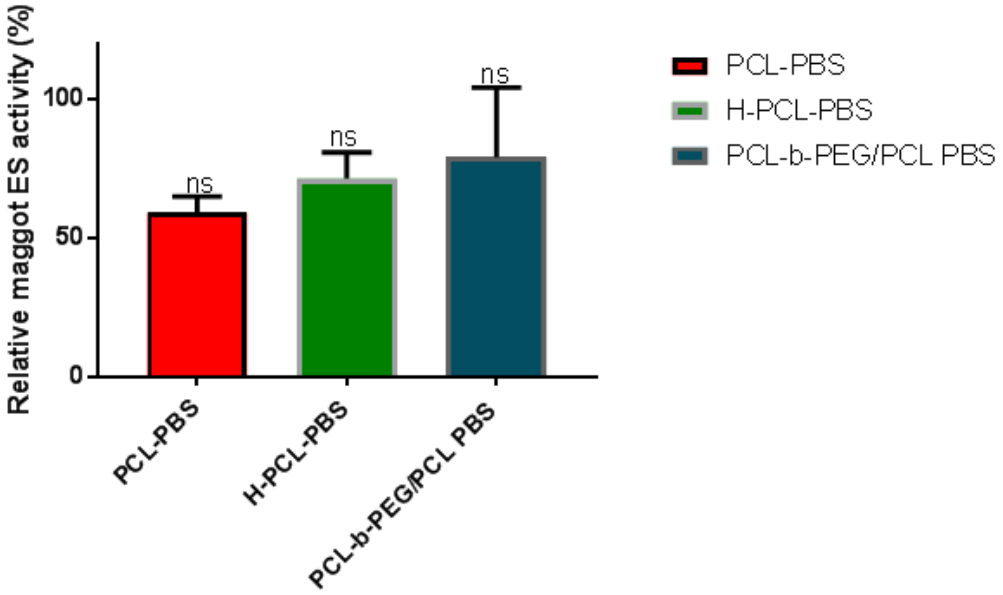


Figure 5.14 - Relative *L. sericata* maggot E/S activity. Maggot E/S release pooled fraction from PCL, H-PCL and PCL-b-Peg/PCL scaffolds were analysed through protease assay. The data was expressed relative to *L. sericata* maggot E/S activity (%), with respect to the initial maggot activity (just before loading efficiency tests). Two independent experiments carried out in triplicate (means±SD).

5.5.10 Activity of *Lucilia sericata* maggot excretion/secretion from controlled release scaffolds on fibroblast motility-*in vitro* scratch assay.

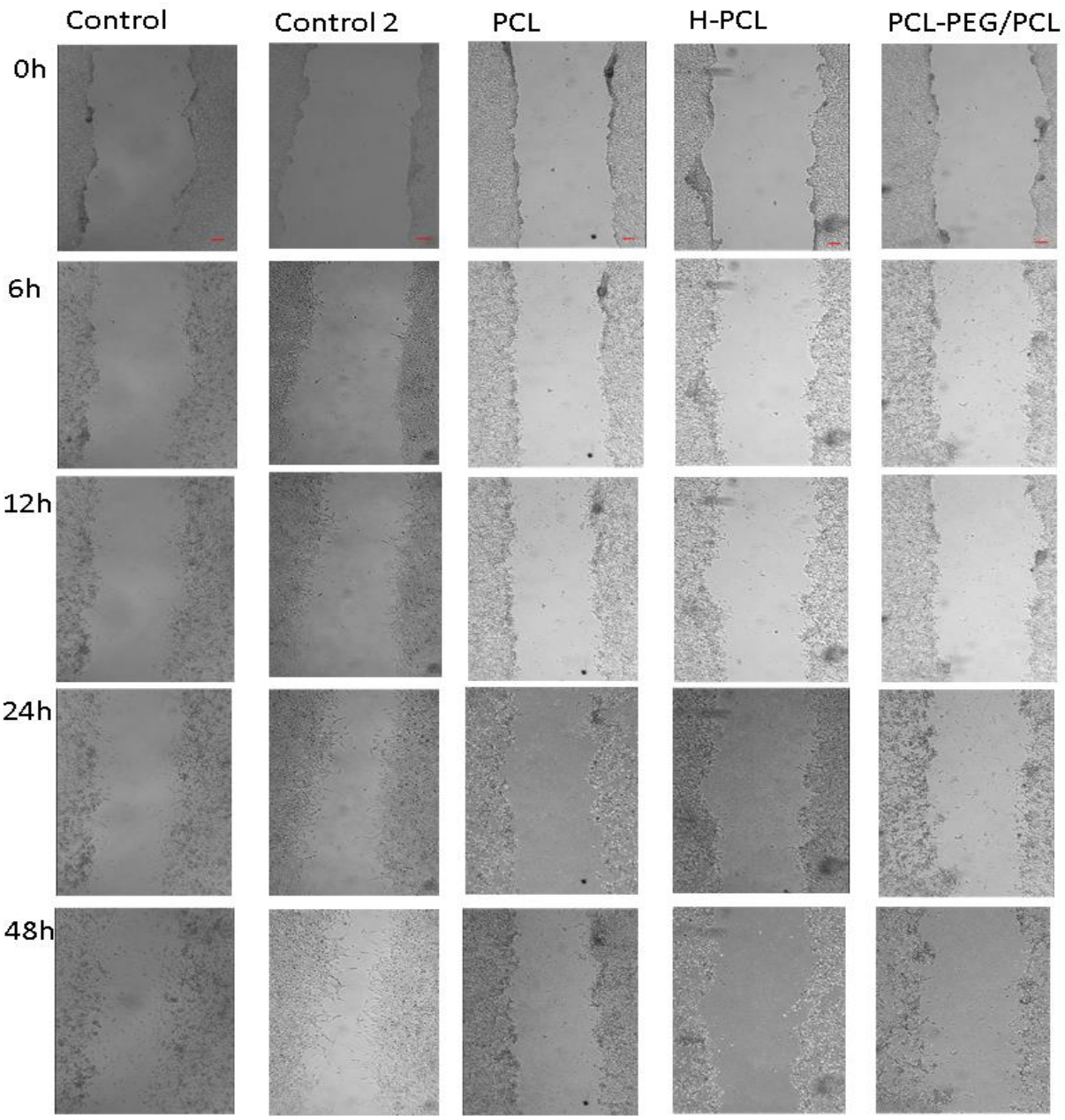
Fractions of the released *L. sericata* maggot E/S were taken to assess the motogenic-therapeutic effect on murine fibroblasts in serum free media. From Figure 5.15 it can be observed that no significant differences were detected between the different samples containing *L. sericata* maggot E/S in terms of percentage of cells covering the scratch wound. In fact, the fibroblasts exposed to only DMEM media (control) showed significantly higher percentages of wound closure compared with the aliquots containing *L. sericata* maggot E/S. The fibroblasts exposed to DMEM media migrated and covered 40% of the scratch in a period of 24 h, which is a significantly higher percentage compared with released- *L. sericata* maggot E/S from PCL, which showed 7% ($p<0.0001$), significantly higher than the released-maggot from H-PCL with 24% covering scratch ($p<0.0001$) and higher than released- *L. sericata* maggot E/S from PCL-b-PEG/PCL scaffolds with 13% of the scratch covered ($p<0.0001$).

As it was indicated in the literature review, *L. sericata* maggot E/S contains a mix of proteins and other components such as allantoin (Smith et al., 2006). Serine proteinase and other components such as defensine, amino acids-like compounds and DNase found in *L. sericata* maggot E/S have all been reported to have a beneficial impact on wound healing. Furthermore, it is important to consider that other compounds (i.e. not the serine proteinases) of *L. sericata* maggot E/S may be inactivated and this was not quantified. In

addition, the *L. sericata* maggot E/S fraction used here was not sterile which may have led to protein degradation.

Previous studies (Horobin et al., 2003, Horobin et al., 2005) have shown the powerful effect of *L. sericata* maggot E/S on the motogenesis of fibroblasts. Although this was not seen here, further investigations are required.

In addition, research has pointed out that scaffolds surface may play an important role loading, releasing and maintaining protein structure and thus their stability (Buschle-Diller et al., 2007). Since in order to improve loading, release and activity of enzymes next chapter (chapter 6) will focus on the modification of PCL, H-PCL and PCL-b-PEG/PCL scaffolds using cationic polymers.



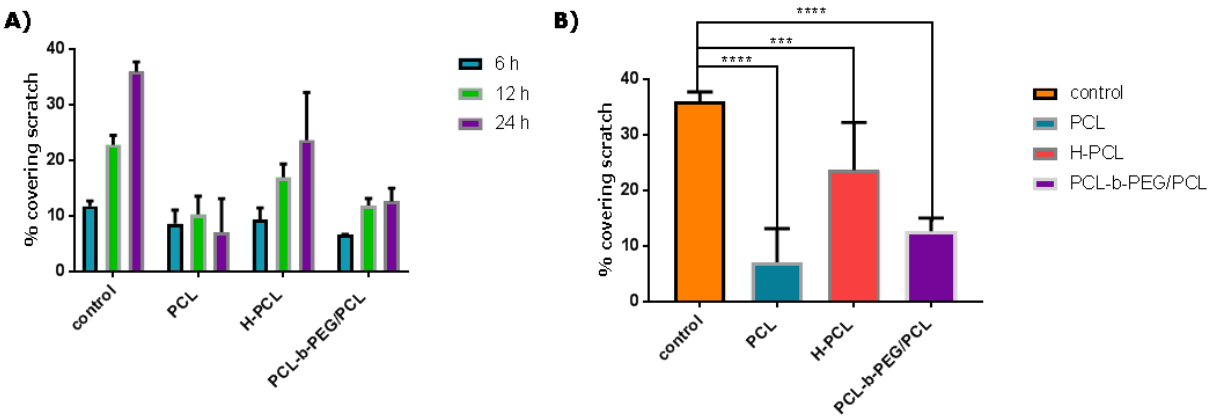


Figure 5.15 - *In vitro* scratch assay to evaluate different fraction of *L. sericata* maggot E/S released from PCL, H-PCL and PCL-b-PEG/PCL scaffolds. Magnification 5X scale bar 100 microns. One independent experiments carried out in triplicate (means±SD).

5.6 Conclusions

It was hypothesized that the *L. sericata* maggot E/S may be incorporated in electrospun scaffolds made of PCL, H-PCL and PCL-b-PEG/PCL and used for the controlled release of bioactive molecules. This chapter focused on the post electrospinning modification of PCL, H-PCL and PCL-b-PEG/PCL scaffolds as strategy to incorporate *L. sericata* maggot E/S enzymes, and the release of these proteins to the media, maintaining their bioactivity. To assess the surface modification strategies chosen (inclusion of PEG or surface hydrolysis with NaOH), avidin and lysozyme, used as model proteins, adsorption and release from the scaffolds was investigated.

Lysozyme, a small and simple protein with a positive net charge exhibited a faster and greater release than avidin and *L. sericata* maggot E/S from PCL and PCL-b-PEG/PCL scaffolds over 21 days.

Release of proteins adsorbed to the surface of the PCL-b-PEG/PCL scaffolds resulted in a reduction in the burst release and allowing a sustained release profile of avidin and *L. sericata* maggot E/S.

Maggot E/S released from PCL-b-PEG/PCL scaffolds presented a burst release in the first 24 hours, 32% of the initial protein adsorbed was released and then the release plateaued, reaching cumulative release values of 67% after 21 days. Cumulative amount of protein released from PCL-b-PEG/PCL scaffolds was ~12.8 µg over 24 h and 14.2 µg after 21 days. *L. sericata* maggot E/S aliquots were polled and volume adjusted to 1 mL, resulting in a final concentration of 12.8 µg /mL and 14.2 µg/mL respectively. Cumulative amount of *L. sericata* maggot E/S released per amount of scaffold (µg) was 0.018 over 21

days (PCL-b-PEG/PCL). The cumulative amount of *L. sericata* maggot E/S detected over 21 days (14 µg/mL) can be further compared with values presented by (Horobin et al., 2006). The amount of 1 µg/mL of fresh *L. sericata* maggot E/S showed a significant enhancement on fibroblast migration over 48 h. Whereas the total amount measured in the current study was 10x higher.

Moreover, according to (Leung et al., 2011) an open-wound, or exudative wound that needs frequent dressing replacement (every couple of days) may need a burst release or fast release of antibiotics, growth factors or cell signalling agents. While surgical wounds or wounds where interruptions are undesirable requires a more sustained release of therapeutic molecules. In addition, re-epithelised wounds may require a stable release of remodelling agents. In the current study, a controlled release profile of *L. sericata* maggot E/S from PCL-b-PEG/PCL scaffolds was obtained over 21 days. This may help tackle wounds whose healing process should not be interrupted. A sustained release of serine proteinase may provide the stimuli for fibroblast migration from the edges of the wound bed into the scaffold.

This investigation created an innovative alternative for wound healing through the development of a novel bioactive prototype dressing with *L. sericata* maggot E/S. This was the first time that controlled release of *L. sericata* maggot E/S has been achieved from fibrous scaffolds.

L. sericata maggot E/S was absorbed and released from the PCL-b-PEG/PCL electrospun scaffolds and the bioactivity successfully maintained and therefore has potential to be used for wound healing.

CHAPTER 6 Surface modification of PCL and PCL-b-PEG/PCL with cationic polymers

6.1 Cationic polymers

Cationic polymers have found numerous applications in pharmaceutical and biomedical science owing to their ability to associate with negatively charged molecules, genes and cells. The synthesis of acrylic polycationic polymers is frequently carried out by using free radical polymerization reaction (Jaeger et al., 2010). However, a major drawback of these structures is their potential cytotoxicity due to the large number of positive charges closely located in the polymer chain. It is well known that positively charged polymers with high charge density can induce cell toxicity (Agarwal et al., 2012, Paneva et al., 2006) due to destabilisation of the negatively charged cell membranes which can result in membrane disruption and death. Therefore, charge density is a crucial point not only to control toxicity but also to mediate the extent of electrostatic interactions. The copolymerization of cationic monomers with other non-ionic monomers has been raised as a suitable method to control charge density and avoid cell toxicity (Paneva et al., 2006).

6.1.1 Applications of cationic polymers

Polymers with quaternary ammonium groups on their chemical structure have been widely used in cosmetics and contact lens

products (Carmona-Ribeiro and de Melo Carrasco, 2013). Positively charged polymers, like poly (trimethylamino ethyl methacrylate chloride) (PTMAEMA), can interact with negative DNA by electronic forces and permit the transfer of DNA through the cell membrane (Bautista et al., 2011, Durmaz et al., 2013, Han et al., 2014). In addition, cationic polymers have also been used as antimicrobials (Carmona-Ribeiro and de Melo Carrasco, 2013).

Furthermore, cationic hydrophilic polymers have been used to promote protein/polymer association in drug transport and release (Bautista et al., 2011, Durmaz et al., 2013).

6.1.2 Interaction between cationic polymers and the surface of scaffolds, and between cationic polymers and proteins

The formation of protein/polymer complexes is often based on non-covalent bonds in order to avoid chemical modification of the protein. Based on the chemical composition of the polymer used, van der Waals forces, Coulombic binding, polymer bridging, depletion forces, hydrophobic forces, or specific lock-and-key type interactions can be involved (Salmaso and Caliceti, 2013, da Silva et al., 2006, Ganguli et al., 2009).

6.1.3 Incorporation of cationic polymers at scaffolds surfaces

Poly((N,N'-dimethylamino)ethylmethacrylate (p(DMAEMA)) chains have been used to complex gelatine through electrostatic interactions resulting in PCL-g-P (DMAEMA)/gelatine surfaces with enhanced cell adhesion and gene transfection (Li et al., 2011). Nanofibers of PCL-PDMAEMA produced by blended electrospinning enabled the incorporation of silver nanoparticles at the surface through electrostatic interactions. In this case, silver nanoparticles were prepared with citrate to stabilise their surfaces, providing electrostatic interactions between protonated amino groups (NH_3^+) of PDMAEMA and the carboxylate groups from citrate. This was found to be the driving force to load nanoparticles to the nanofiber scaffold (Santos et al., 2017).

6.2 Aim and objectives

On the basis of the background presented above, it was hypothesized that modification of PCL, H-PCL (hydrolysed PCL) and PCL-b-PEG/PCL scaffolds through the addition of polycationic polymers may have a beneficial effect on the loading and release of bioactive molecules with therapeutic action for wound healing.

For this hypothesis, a number of aims have been set as part of this study, as following:

- To synthesize and characterise the cationic polymer poly (trimethylamino) ethyl methacrylate hydrochloride-*block*-Poly(N-(2-hydroxypropyl) methacrylamide) (PTMAEMA-b-PHPMA).
- To assess the cytocompatibility of the cationic polymer with fibroblasts.
- To evaluate the incorporation of the model proteins lysozyme and avidin onto the cationically modified electrospun scaffolds.
- To evaluate the release profiles of avidin and lysozyme proteins from PCL, H-PCL and PCL-b-PEG/PCL platforms.
- To evaluate loading of *Lucilia sericata* maggot excretion/secretion (*L. sericata* maggot E/S), a complex mixture of proteins with a range of size and charge into electrospun fibres of PCL, H-PCL and PCL-b-PEG/PCL.
- To evaluate the *in vitro* protein release profile of *L. sericata* maggot E/S.

- To confirm the bioactivity of the enzymes by examining protease (*L sericata* maggots ES) and lysozyme activity after release.

The results will be then compared with those obtained on scaffolds without cationic polymer modification (refer to chapter 5). The goal was to improve the loading and release of *L. sericata* maggot E/S using cationically modified scaffolds as a platform for protein release with therapeutic action in wound healing (Figure 6.1).

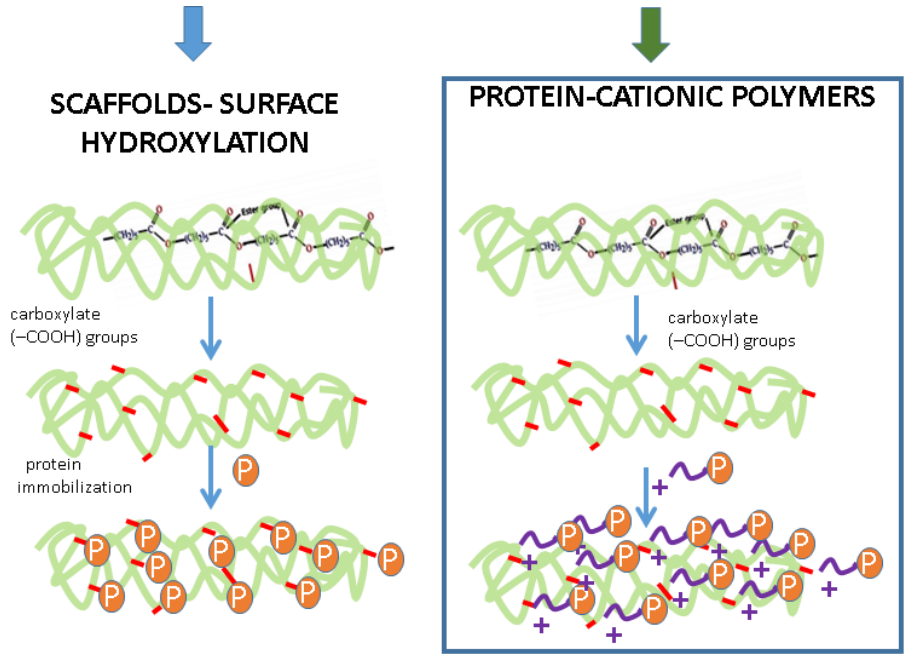


Figure 6.1 - Schemetic approach of protein loading through 2 different methodologies. This chapter will foccus on protein-cationic polymer association (blue box).

6.3 Results and Discussion

6.3.1 Synthesis of $PTMAEMA_{33}$-b-$PHPMA_{180}$ polymers

Reversible addition–fragmentation chain transfer (RAFT) polymerization reaction allowed the synthesis of $PTMAEMA_{33}$-b-$PHPMA_{180}$ polymers. RAFT polymerization is one of the most versatile techniques for controlled synthesis of polymers as it allows working with a vast number of monomers and can easily generate different architectures such as block co-polymers, graft co-polymers and dendritic structures (York et al., 2008). A disadvantage of RAFT is the potential toxicity of thiocarbonylthio groups, but this group can be easily eliminated after polymerization. Also toxicity will be dependent on polymer concentration, type of polymer and type of cells (Fairbanks et al., 2015).

PTMAEMA is a polycation widely used in gene delivery with good cytocompatibility when of molecular weight lower than 60.000 g/mol and because of its water soluble- properties (Agarwal et al., 2012). Additionally, PHPMA is a non-toxic, biocompatible and neutral polymer (Qi and Chilkoti, 2015).

6.3.1.i Characterizations of $PTMAEMA_{33}$-b-$PHPMA_{180}$ polymers

$PTMAEMA_{33}$ polymer was synthesized with a molecular weight of 6230 g/mol, estimated by NMR (Figure 6.2) while GPC showed a M_n of 4900 g/mol and M_w 5600 with a Đ (polydispersity) of 1.16 (Table 6.1). $PTMAEMA_{33}$-b-$PHPMA_{180}$ polymer was obtained with a molecular weight of 32000 g/mol, estimated by NMR and Mn 5917 (Figure 6.3) and Mw 7002 with a Đ (polydispersity) of 1.18 estimated by GPC (Table 6.1).

Table 6.1 - A summary of the chemical characterization of cationic polymers

Polymer	NMR molecular weight (g/mol)	GPC molecular weight (Mw) Da	Đ
$PTMAEMA_{33}$-	6230	5600	1.16
$PTMAEMA_{33}$-b-$PHPMA_{180}$	32000	7002	1.18

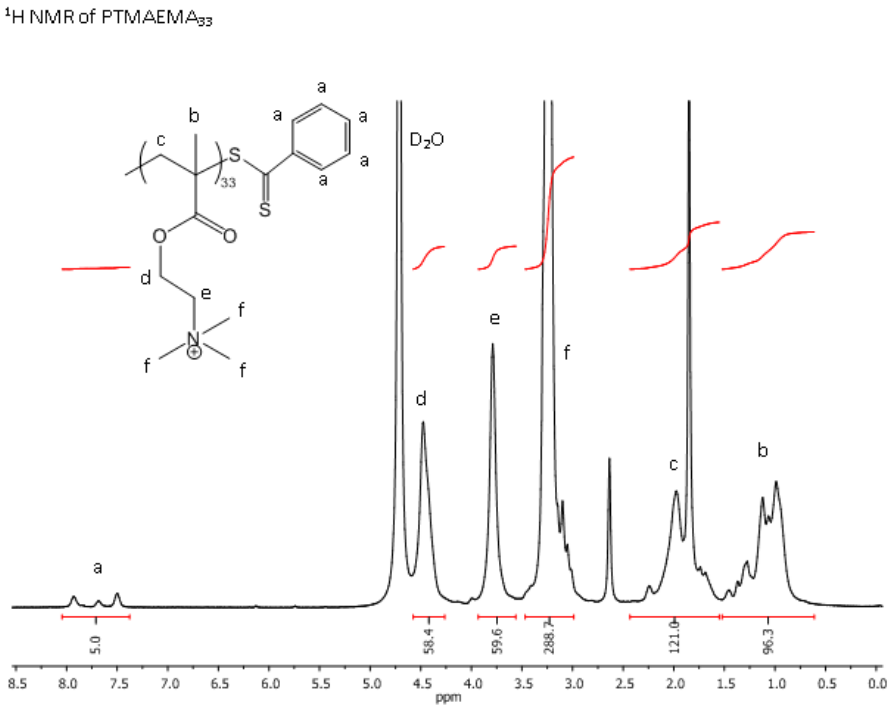


Figure 6.3 - Representative NMR of **PTMAEMA$_{33}$** polymer. ^{1}H NMR (400 MHz, D_2O): δ 7.4-7.5 (5H, C_6H_5), 4.5 (2H, OCH_2), 3.8 (2H, NCH_2), 3.2 (9H, $N(CH_3)_3$), 2.2-1.5 (2H, CCH_2), 1.5-

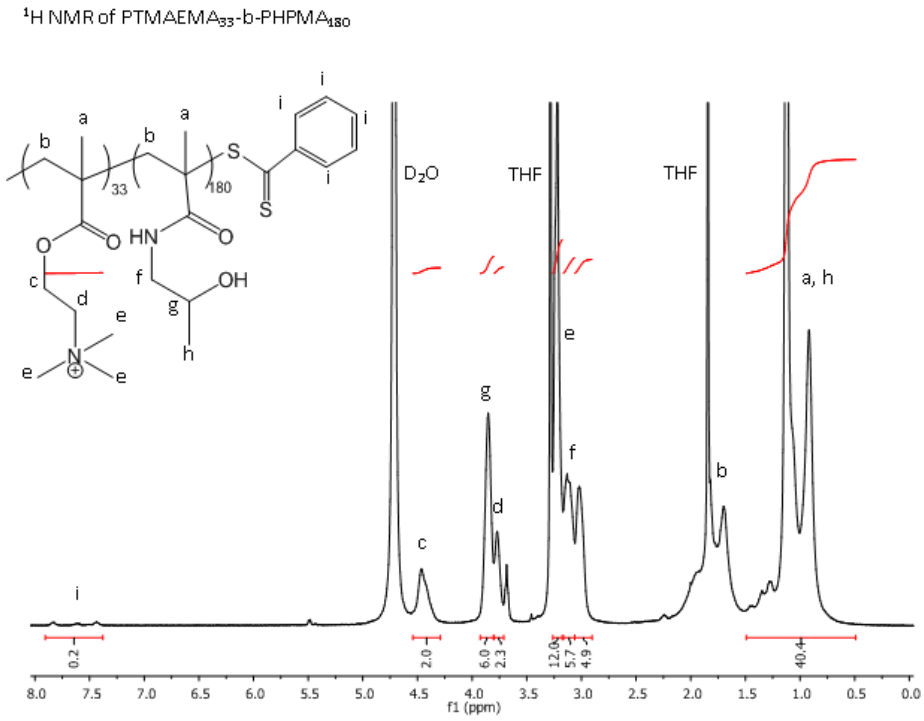


Figure 6.2 - Representative NMR of **PTMAEMA$_{33}$ –b-PHPMA$_{180}$.** polymer after its purification. PTMAEMA$_{33}$ –b-PHPMA$_{180}$. ^{1}H NMR (400 MHz, D2O): δ 7.4-7.5 (5H, C_6H_5), 4.5 (2H, OCH_2), 3.85 (1H, CHOH), 3.8 (2H, NCH_2), 3.2 (9H, $N(CH_3)3$), 3.0-3.1 (2H, $NHCH_2$) 2.2-1.5 (4H, 2 x CCH_2), 1.5-0.75 (9H, 2 x CCH_3 + 1 x $CHCH_3$)

6.3.1.ii Absorbance, emission and excitation spectra of FITC conjugated- $PTMAEMA_{33}$-b-$PHPMA_{180}$ polymer

Figure 6.4-A) shows FITC conjugated-$PTMAEMA_{33}$-b-$PHPMA_{180}$ polymer absorbance spectrum between 400-540 nm. Polymer showed a maximum of absorbance at 500 nm. Then, fluorescence emission scan was carried out between 470-750 nm by setting excitation wavelength at 450 nm (Figure 6.4-B)). FITC conjugated-$PTMAEMA_{33}$-b-$PHPMA_{180}$ polymer presented maximum emission at 520 nm. Finally, an excitation fluorescence scan was carried out between 400-540 nm, where the emission wavelength was set at 570 nm. Maximum excitation at 500 nm was observed. A λ_{ex} of 450 nm and λ_{em} of 518 nm were finally selected to quantify the loading of $PTMAEMA_{33}$-b-$PHPMA_{180}$ polymers on the following experiments.

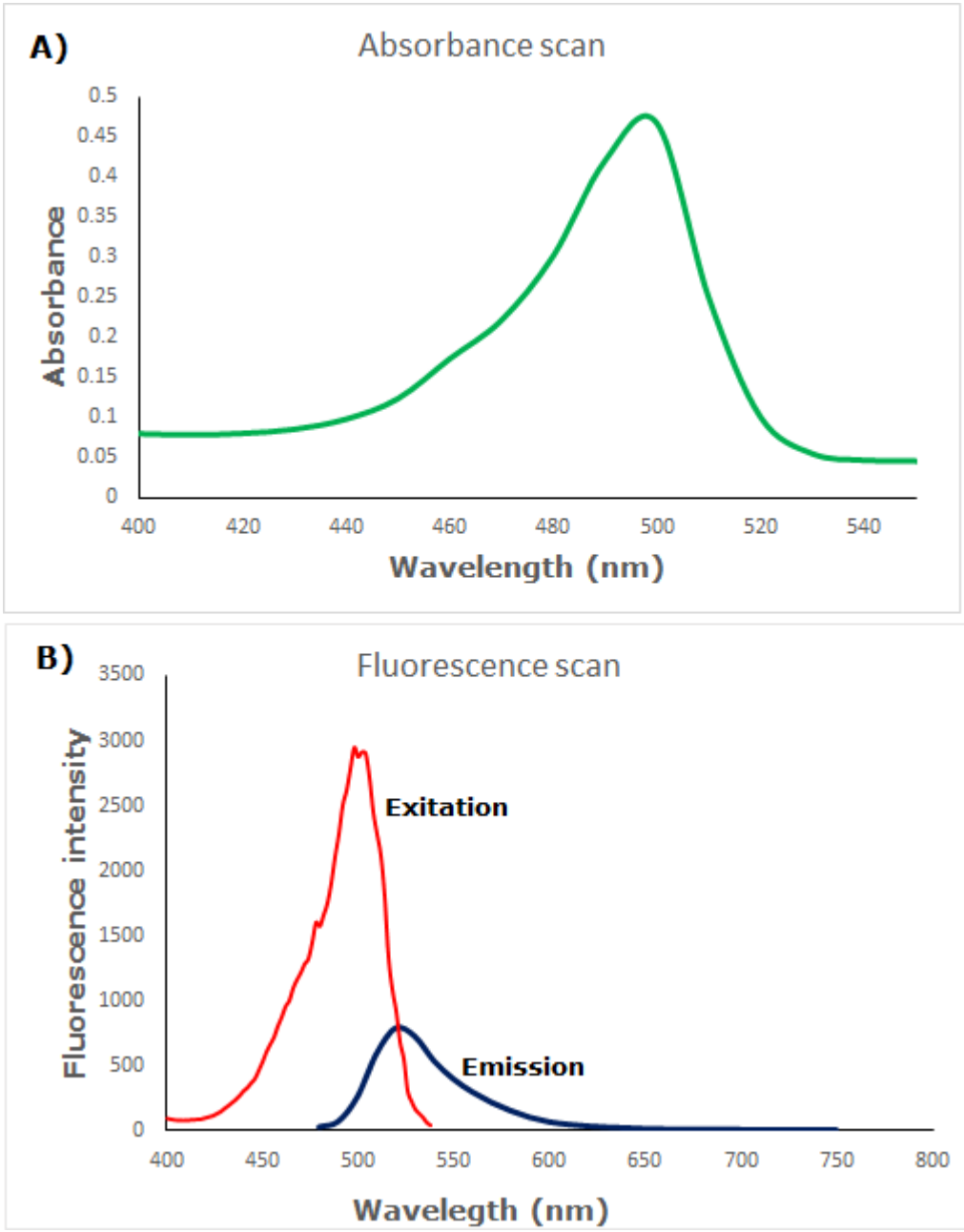


Figure 6.4 – A) absorbance spectrum of FITC conjugated $PTMAEMA_{33}$-b-$PHPMA_{180}$ polymer **B)** Fluorescence emission and excitation spectrum of $PTMAEMA_{33}$-b-$PHPMA_{180}$ polymer.

6.3.2 Cytotoxicity of $PTMAEMA_{33}$ and $PTMAEMA_{33}$-b-$PHPMA_{180}$ cationic polymers on murine fibroblasts.

Figure 6.5 shows *in vitro* metabolic activity analysis (AlamarBlue®) of $PTMEMA_{33}$ and $PTMAEMA_{33}$-b-$PHPMA_{180}$ polymers on fibroblasts. It was found that $PTMAEMA_{33}$ polymer had a concentration-dependent effect on fibroblast activity after 24 h of exposition, when the polymer was diluted in DMEM media containing 2% *w/w* of foetal calf serum (FCS) (Figure 6.5-A)). $PTMAEMA_{33}$ concentration of 200 and 500 µg/mL presented the lowest cell metabolic activity compared to their control (DMEM 2% *w/w* FCS), reaching relative fluorescence (RFU) values of of13898 (p 0.0449) and 10596 (P 0.0002) compared to the control 16141 fluorescence (RFU). Interestingly, concentration-dependent effect of $PTMAEMA_{33}$ upon fibroblasts was not significant when the serial dilutions of $PTMAEMA_{33}$ were carried out using DMEM 10% *w/w* FCS (Figure 6.5-B)). In addition, $PTMAEMA_{33}$-b-$PHPMA_{180}$ polymer did not reveal any significant toxic effect upon fibroblast metabolic activity compared with the control, nor when the dilution used was performed with DMEM 2% *w/w* (Figure 7.5-C)) and 10% *w/w* of FCS (Figure 6.5-D)) In fact, fibroblast metabolic activity was greater in samples with concentration of 5 µg/mL of $PTMAEMA_{33}$-b-$PHPMA_{180}$ (29600 RFU) (p 0.0015) compared with control (25681 RFU) in DMEM 2% *w/w* FCS. In addition, fibroblast metabolic activity was significantly higher (p 0.0001) in all the samples exposed to $PTMAEMA_{33}$-b-$PHPMA_{180}$ with DMEM 10% *w/w* FCS compared with their control (Figure 6.5-D)). Metabolic activity of fibroblasts exposed to 500 µg/mL of $PTMAEMA_{33}$-b-$PHPMA_{180}$ was reduced (p 0.0099)

compared with the control. A lower metabolic activity of fibroblast was observed using $TMAEMA_{33}$ homopolymer than $PTMAEMA_{33}$-b-$PHPMA_{180}$ copolymer with FCS 2% *w/w* in the cultured media.

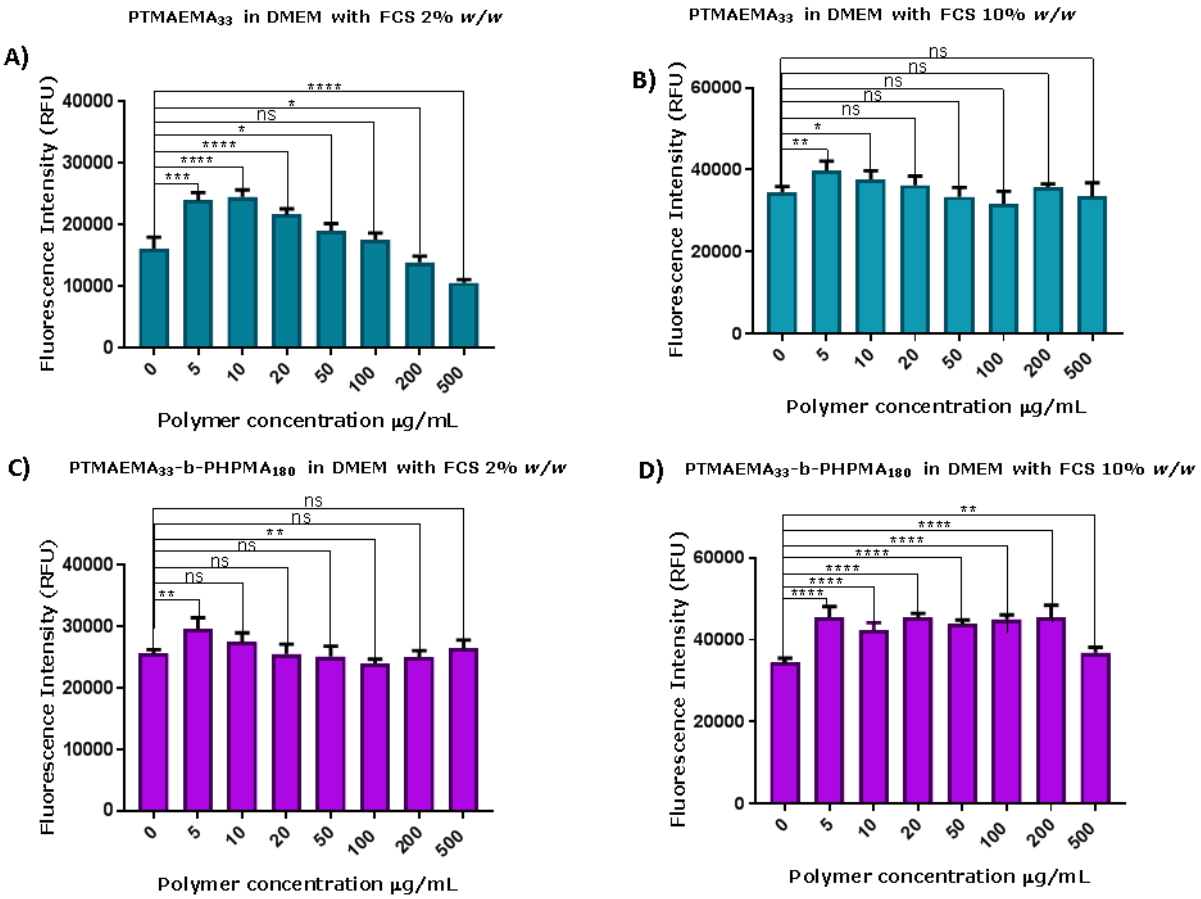


Figure 6.5 - A) and B) Cytotoxicity of $PTMAEMA_{33}$ on fibroblast after 24 h of incubation using DMEM 2% *w/w* FCS (left side) and DMEM 10 *w/w* % FCS (right side). **C)** and **D)** cytotoxicity of $PTMAEMA_{33}$-b-$PHPMA_{180}$ on fibroblast after 24h of incubation using DMEM 2% *w/w* FCS (left side) and DMEM 10 *w/w* % FCS (right side). Three independent experiments carried out in triplicate (means±SD).

Quaternary polycationic polymers such as PTMAEMA come with a positive charge that has a density that may increase the cytotoxic effect. By the formation of a copolymer, this charge density can be controlled and the cytotoxicity effect reduced (Paneva et al., 2006). This is in agreement with the results presented here; $PTMAEMA_{33}$ polymer showed higher cytotoxicity effect compared with the copolymer $PTMAEMA_{33}$-b-$PHPMA_{180}$.

The cytotoxicity of a dense positive charge of a cationic polymer might be caused by the strong interaction of the positive charge of the polymer with negative proteins located at the intra and extracellular spaces, disrupting protein pathway, resulting in apoptosis of the cells (Cai et al., 2011). The same author pointed out that cytotoxic effect was dependent on the length of the cationic chain; lower cytotoxicity was observed for the shortest chains of cationic polymers (Cai et al., 2011). Also, the results presented in this chapter are in agreement with the findings presented in chapter 3, where it was concluded that foetal calf serum may play a protective role on fibroblast viability at higher concentration of propolis.

6.3.3 Modification of PCL, H-PCL and PCL-b-PEG/PCL surface scaffolds using cationic polymer $PTMAEMA_{33}$-b-$PHPMA_{180}$.

As indicated in Figure 6.6-A), fluorescence images showed a homogenous distribution of the cationic polymer on the surface of the different scaffolds. In general, it can be seen from Figure 6.6-B) that there are no significant differences during the first 6 h of incubation in terms of loading % of cationic polymer on any of the three different scaffolds (PCL, H-PCL and PCL-b-PEG/PCL). Only cationic polymer loaded on PCL-b-PEG/PCL scaffolds showed significant increment in terms of the percentage loaded of 18% compared to PCL scaffolds at 14% (p 0.0187) after 24 h of incubation. No significant differences were observed between cationic polymer loaded on H-PCL and PCL-b-PEG/PCL scaffolds after 24 h of incubation.

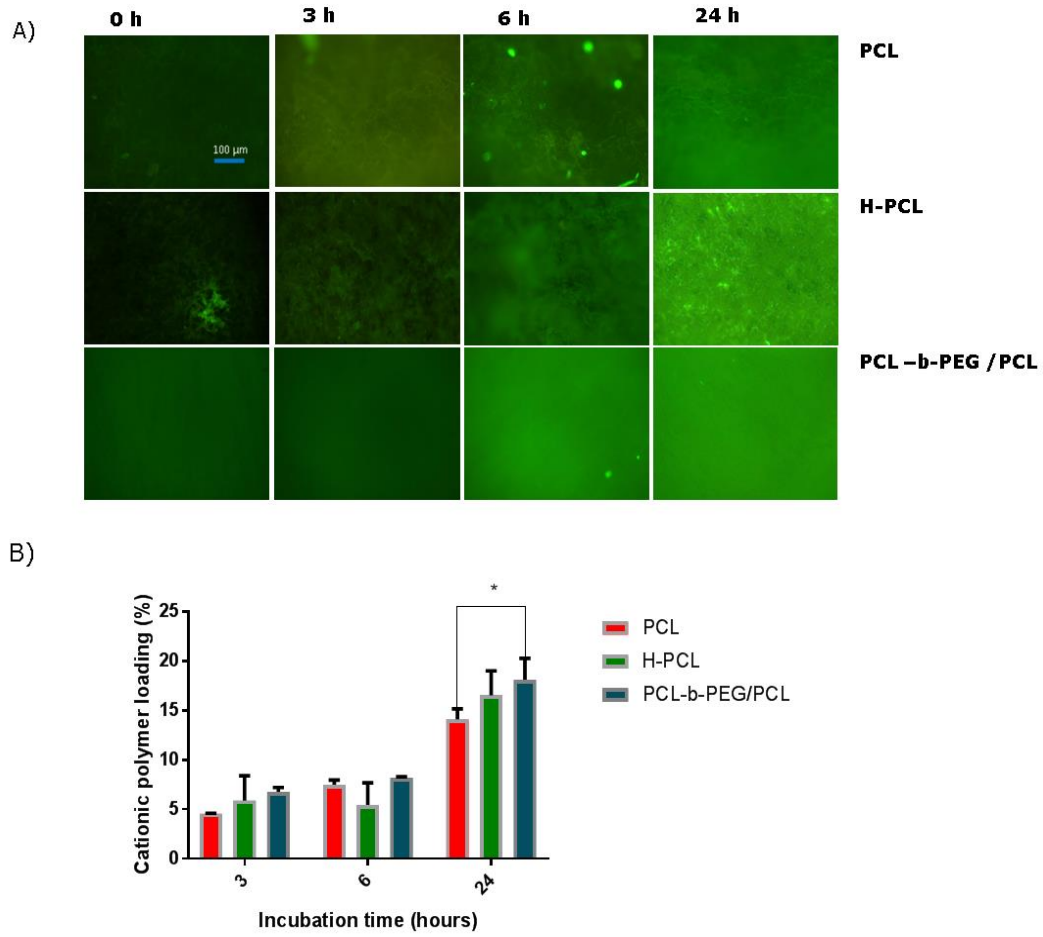


Figure 6.6 - A) Representative fluorescence microscopy images of cationic polymer-fluorescent conjugate protein (PTMAEMA-FITC) absorbed into PCL, H-PCL and PCL-b-PEG/PCL scaffolds. Magnification 10x, scale bar 100 microns. **B)** Cationic polymer--FITC loafing percentage on PCL, H-PCL and PCL-b-PEG/PCL scaffolds. Two way-ANOVA, Tukey's multiple comparison test. Three independent experiments carried out in triplicate (means±SD).

These findings could be explained by the fact that H-PCL scaffolds possess carboxyl groups on the surface that may attract the positive charge of the cationic polymer $PTMAEMA_{33}$-b-$PHPMA_{180}$ by electrostatic interaction which has been reported previously by (Li et al., 2011, Santos et al., 2017). In addition, PCL-b-PEG/PCL scaffolds may interact with the cationic polymer through the hydrogen bond interactions between oxyethylene units in the PEG chains and the protonated amines on the cationic polymer (Verbaan et al., 2004). PCL scaffolds also present some hydrophobic interactions with the polymethacrylate backbone of the cationic polymer; however, these are lower in magnitude compared to the H-bonding interactions.

In order to improve the absorption of protein onto PCL, H-PCL and PCL-b-PEG/PCL scaffolds to be used as platforms for controlled protein release, cationic polymer $PTMAEMA_{33}$-b-$PHPMA_{180}$ was loaded on the surface of these scaffolds. In the next section the loading efficiency will be evaluate and it will be compared without cationically modified scaffolds.

6.3.4 Loading of avidin-rhodamine (AVI-RB) on the cationically modified surface of PCL, H-PCL and PCL-b-PEG/PCL scaffolds

Figure 6.7-A) shows fluorescence images of avidin-rhodamine absorbed on cationically modified PCL, H-PCL and PCL-b-PEG/PCL scaffolds after 24 h of incubation. From Figure 6.7-B) it observed that the cationically modified H-PCL scaffolds loaded significantly higher percentage of AVI-RB (43%)($P<0.0001$) than cationically modified PCL scaffolds (34%). No statistically significant differences were found between the percentages of AVI-RB loaded on cationically modified H-PCL and PCL-b-PEG/PCL scaffolds and between cationically modified PCL-b-PEG/PCL and PCL (ns) (Figure 6.7-B)). As discussed in section 5.5.2, greater quantity of cationic polymer was loaded on H-PCL and PCL-b-PEG/PCL scaffold compared to PCL. These results seemed to correlate with the percentage of avidin loaded on the surface of cationically modified PCL, H-PCL and PCL-b-PEG/PCL scaffolds. In general, it can be seen that cationically modified H-PCL scaffolds, loaded greater percentage of cationic polymer, also loaded greater percentage of avidin compared to cationically modified PCL polymer scaffold (Figure 6.7-B)). Comparing avidin loaded on scaffolds with and without cationic polymer (Figure 6.7-C)), it observed that more protein is loaded on H-PCL scaffolds without cationic polymer. H-PCL without cationic polymer had a significantly higher percentage ($p<0.0001$) of loading (60%) of avidin compared with cationically modified H-PCL scaffolds, which loaded 43% of avidin. PCL and PCL-b-PEG/PCL with and

without cationic polymer showed similar results of avidin loading percentage (~40%) (ns).

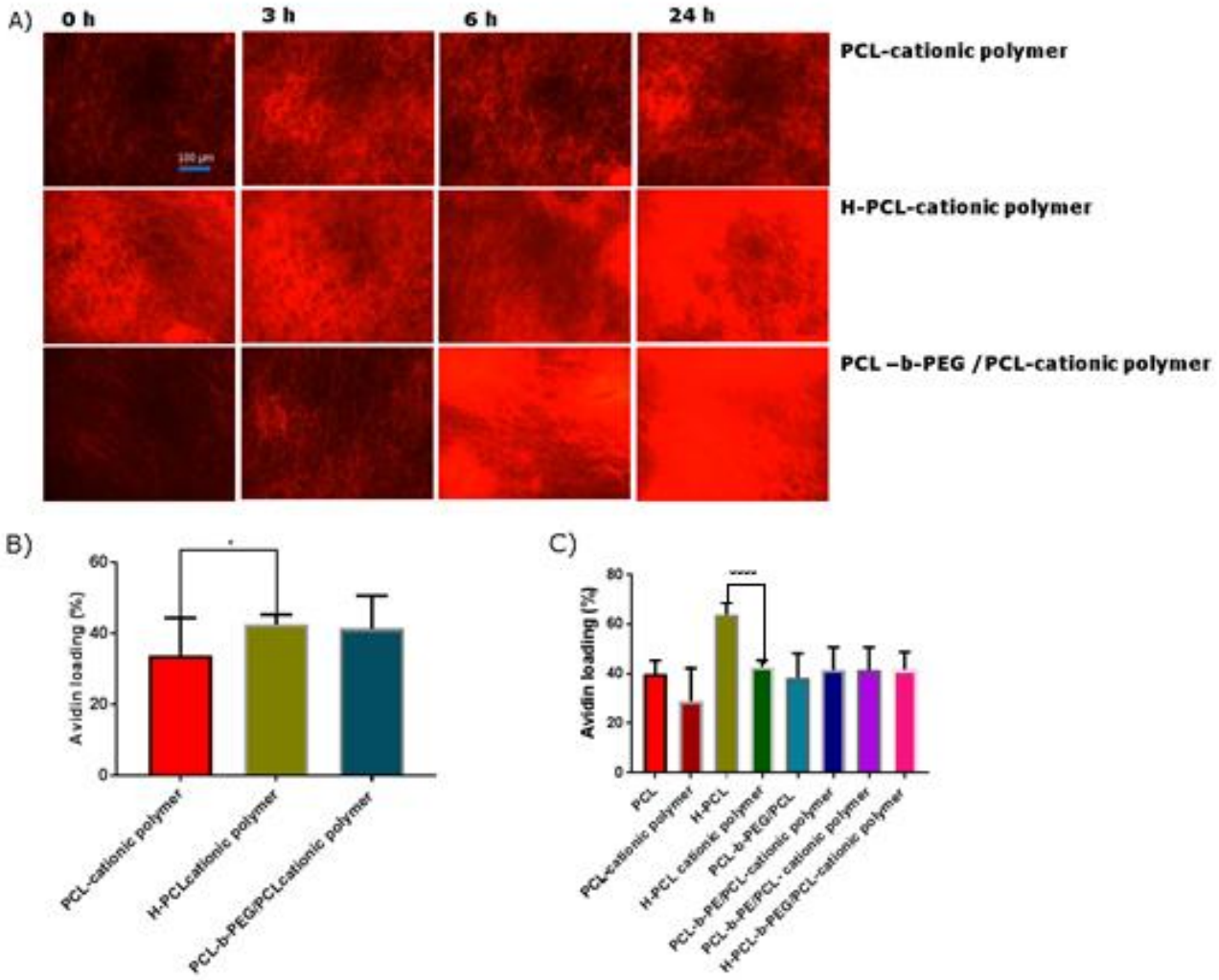


Figure 6.7 - A) Fluorescent microscopy images of avidin-rhodamine protein (AVI-RB) absorbed into PCL, H-PCL and PCL-b-PEG/PCL scaffolds. Magnification 10x, scale bar 100 microns. **B)** Percentage of avidin-rhodamine loaded on cationically modified PCL, H-PCL and PCL-b-PEG/PCL scaffolds in PBS pH 7.4 at 37°C. **C)** comparison of percentage of avidin-rhodamine loaded on PCL, H-PCL and PCL-b-PEG/PCL scaffolds with and without cationic polymer. Two way-ANOVA, Tukey's multiple comparison test. Three independent experiments carried out in triplicate (means±SD).

(Wang et al., 2009b) pointed out that enzyme loading is lower on hydrophobic surfaces, like PCL scaffolds, due to the limited accessibility of the enzyme to the surface of the scaffold. Consistently, the findings presented in this revealed a similar loading trend of different proteins, which were found to be lower on PCL scaffolds. On the other hands, the electrostatic interactions between negative surfaces of H-PCL scaffolds and positive charge of avidin permitted higher absorption of avidin to the scaffolds surface compared to cationically modified H-PCL scaffolds. The repulsive force of positive charges of cationic polymer and positive charge of avidin may limit the absorption of avidin to the scaffold. However, it has been reported that cationic polymers may interact with proteins that possess a positive net charge by interacting electrostatically (attraction forces) with the negative amino residues present in the protein (Ganguli et al., 2009). This phenomenon could explain the reason why avidin had a lower load on cationically modified H-PCL scaffolds than on H-PCL scaffolds.

6.3.5 Avidin (AVI-RB) release from the cationically modified surface of PCL, H-PCL and PCL-b-PEG/PCL scaffolds

Figure 6.8-A) shows fluorescence images of the cationically modified surface of PCL, H-PCL and PCL-b-PEG/PCL scaffolds after 21 days of release. It can be seen that in all the samples, the fluorescence remains and continues emitting, which is an indication that AVI-RB has not been released completely over that time. Figure 6.8-B) shows the release profile of AVI-RB (over two phases) from PCL, H-PCL and PCL-PCL-b-PEG/PCL cationically modified scaffolds. In statistical terms, no significant differences were found between avidin cumulative percentages among the 3 materials (cationically modified PCL, H-PCL and PCL-b-PEG/PCL scaffolds) in the first 24 hours nor over 21 days of release.

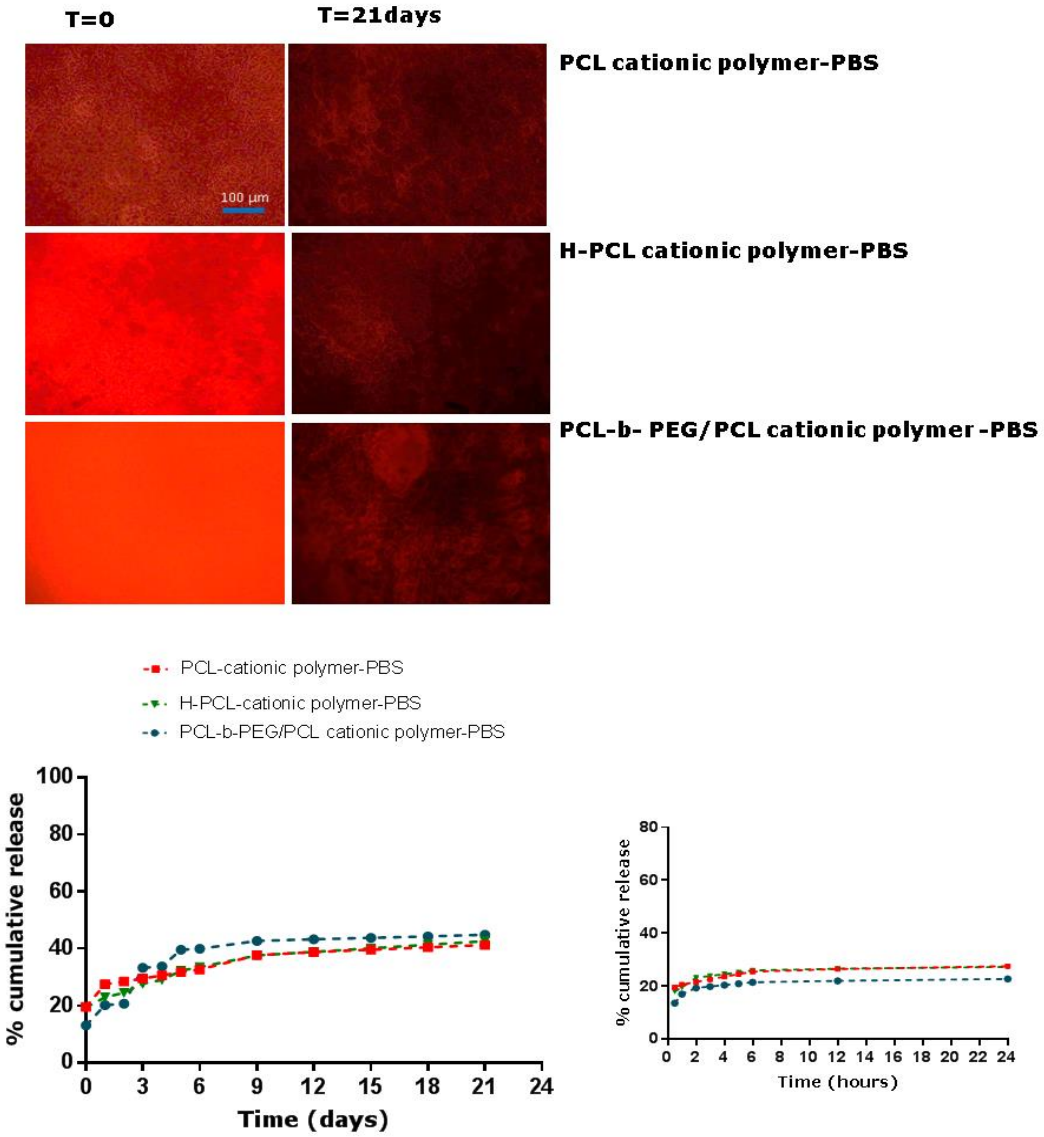


Figure 6.8 - A) Representative fluorescent microscopy images of Avidin-rhodamine on PCL, H-PCL and PCL-b-PEG/PCL scaffolds. Magnification 10x, scale bar 100 microns. **B)** Avidin-rhodamine release profiles from PCL, H-PCL and PCL-b-PEG/PCL scaffolds in PBS pH 7.4 at 37°C. Three independent experiments carried out in triplicate.

The release profile of avidin from PCL, H-PCL and PCL-b-PEG/PCL scaffolds with and without cationic polymer treatment showed (Figure 6.9) that avidin released from cationically modified scaffolds tend to be more of zero order kinetics; the release of avidin from cationically modified scaffolds was not dependent on time. While scaffolds without cationic treatment showed a remarkable burst release, first order kinetic release, characterized by an increment of the avidin concentration depended on time (during the first 6 h of incubation). From day 6 onwards, the release profiles of avidin from treated or untreated scaffolds were similar. In addition, it was found that after 24 h PCL modified with cationic polymer released higher quantities of avidin (27%) compared with avidin released from plain PCL (20%) ($P<0.0001$). Also, cationically modified H-PCL scaffolds released higher quantity (27%) of avidin than H-PCL scaffold (20%) ($P<0.0001$). In contrast, PCL-b-PEG/PCL scaffolds released higher percentage of avidin (27%) compared with PCL-b-PEG/PCL scaffolds modified with cationic polymer (23%) (P 0.0160). After 21 days of release of avidin, were similar from the different scaffolds (ns), reaching values between 41-47% of cumulative percentage. While for PCL-b-PEG/PCL avidin cumulative percentage was higher than 58% ($P<0.0001$) compared with PCL-b-PEG/PCL with cationic polymer treatment (45%).

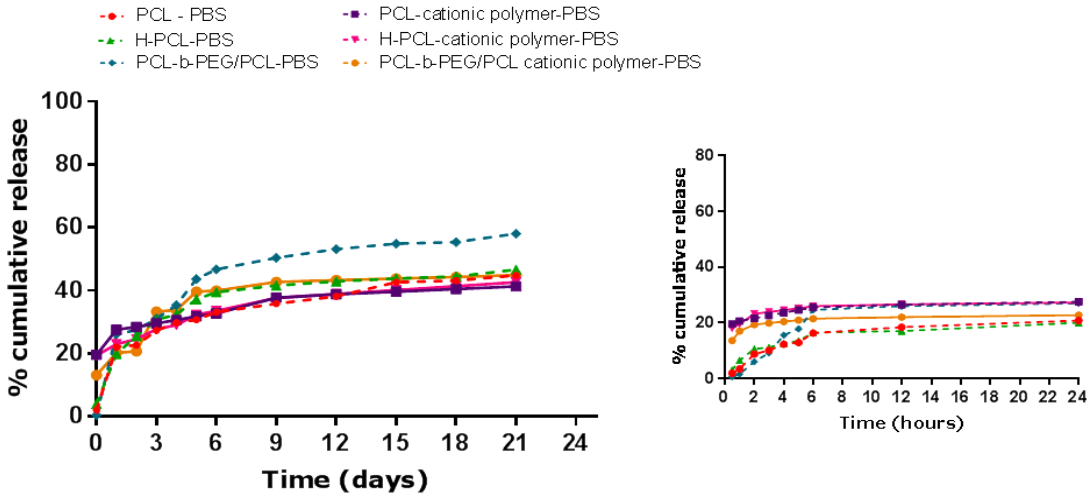


Figure 6.9 - Comparison between AVI-RB release profile from PCL, H-PCL scaffolds and PCL-b-PEG/PCL with and witout ationic polymer treament. Three independent experiments carried out in triplicate.

These results showed a correlation between the quantity of protein loaded and quantity of protein released. A higher quantity of avidin was loaded on scaffolds without cationic treatment and a greater quantity of avidin was released from the same scaffolds. These findings were in agreement with other authors who indicated that at higher s of metronidazole (MNA) loaded on PCL fibrous scaffolds, the burst release is meant to be higher (He et al., 2015). Also, (Zilberman and Kraitzer, 2008) pointed out that the increment on encapsulated drug concentration leads to a higher diffusion force, and thus, higher drug release was observed.

6.3.6 Loading of Lysozyme-rhodamine B (LYZ-RB) on the cationically modified surface of PCL, H-PCL and PCL-b-PEG/PCL scaffolds

Figure 6.10-A) shows Lysozyme-rhodamine (LYZ-RB) absorbed on cationically modified PCL, H-PCL and PCL-b-PEG/PCL scaffolds after 24 hours of incubation. Figure 7.10-B) shows the percentage of Lysozyme-rhodamine (LYZ-RB) loaded on cationically modified PCL, H-PCL and PCL-b-PEG/PCL scaffolds after 24 h of incubation. In general, cationically modified H-PCL and PCL-b-PEG/PCL scaffolds loaded significantly higher percentages of LYS-RB than PCL scaffolds. H-PCL scaffolds loaded 64% of LYZ-RB, which was significantly higher (P 0.0317) than LYZ-RB loaded on PCL scaffolds (53%). The cationically modified PCL-b-PEG/PCL scaffolds loaded higher percentage of LYZ-RB with 61% compared with PCL (53%) (P 0.0158). No statistically significant differences were found between the percentage of LYZ-RB loaded on cationically modified H-PCL and PCL-b-PEG/PCL scaffolds. These results are in agreement with the findings shown for avidin loaded on the same scaffolds (section 5.5.2). Comparing the percentage of LYZ-RB loaded on scaffolds with and without cationic polymer modification (Figure 7.10-C), it seemed that PCL, H-PCL and PCL-b-PEG/PCL scaffolds with and without treatment with cationic polymer did not show any significant differences in terms of loading % of LYZ.

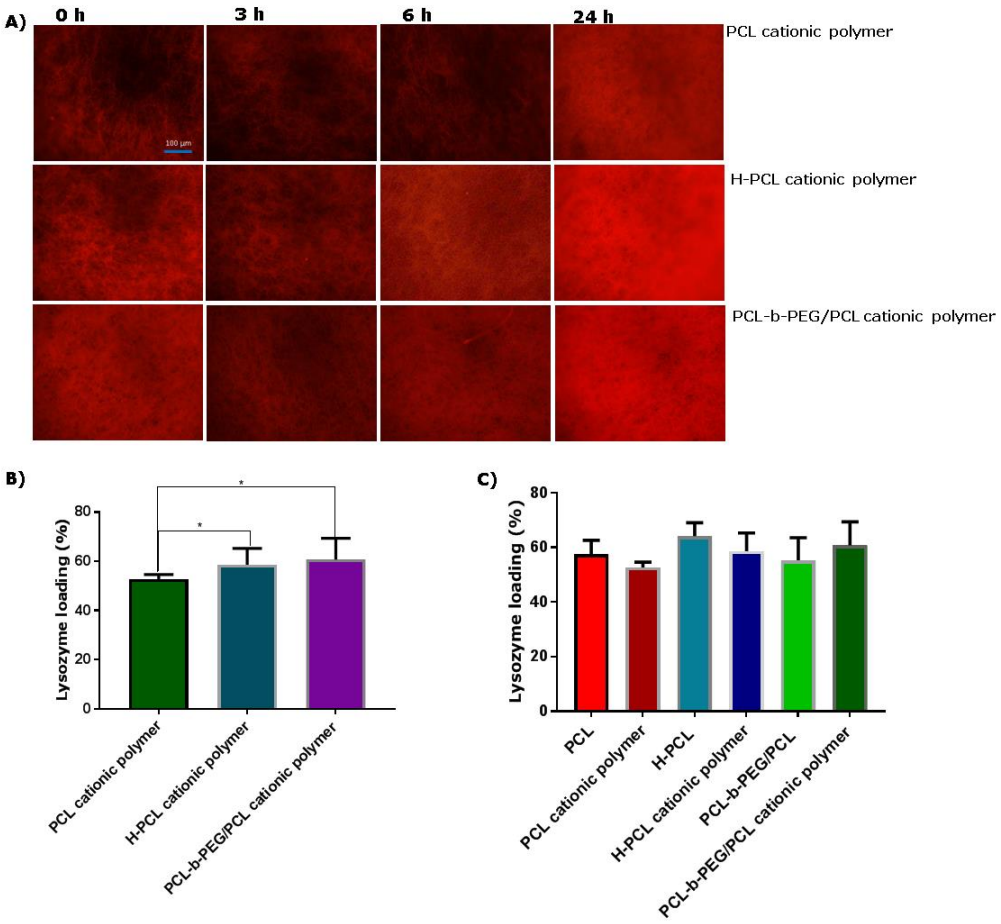


Figure 6.10 - A) Fluorescence microscopy images of lysozyme-rhodamine B conjugate protein (LYZ-RB) absorbed on cationically modified PCL, H-PCL and PCL-b-PEG/PCL scaffolds. Magnification 10x, scale bar 100 microns. **B)** Percentage of LYZ-RB loaded onto cationically modified PCL, H-PCL and PCL-b-PEG/PCL scaffolds in PBS pH 7.4 at 37°C. Two way-ANOVA, Tukey's multiple comparison test. Three independent experiments carried out in triplicate (means±SD).

Even though avidin was loaded significantly higher in cationically modified H-PCL and PCL-b-PEG/PCL scaffolds than on cationically modified PCL scaffolds, the quantity of protein loaded was greater for lysozyme than avidin. This may suggest that the differences in terms of the percentage of loading of these two positive proteins (avidin and lysozyme) can be attribute to the higher molecular weight of avidin (66kDa) when compared with lysozyme (14 kDa). Also, there are differential architectural features (the shape of avidin is more complex), that may cause an hindrance effect (for example glycosylation patterns in vivo) (Schillemans et al., 2011) and thereby may cause an anti-cooperative effect on other molecules binding to the same surface (Zhao et al., 2010). In general, it can be seen that H-PCL and PCL-b-PEG/PCL scaffolds, which loaded more cationic polymer, also loaded greater percentage of LYZ-RB compared with cationically modified PCL scaffolds. Lysozyme possesses a positive net charge, but also has negative amino acid residues that allow electrostatic interactions with cationic polymers (Ganguli et al., 2009).

Findings presented here revel that the addition of cationic polymers onto the surface of electrospun scaffolds did not significantly improved lysozyme absorption onto catatonically modified scaffolds.

6.3.7 Release of Lysozyme-rhodamine B (LYZ-RB) from the cationically modified surface of PCL, H-PCL and PCL-b-PEG/PCL scaffolds

Figure 6.11-A) shows the fluorescence qualitative analysis for all the samples. It can be seen that after 21 days of release, fluorescence can still be detected, which perhaps, is an indication that LYZ-RB has not been released completely over that time. From a quantitative point of view, Figure 6.11-B) shows the release profile of LYZ-RB from cationically modified PCL, H-PCL and PCL-PCL-b-PEG/PCL scaffolds. LYZ-RB release profiles from cationically modified PCL and H-PCL are very similar. A short burst release of LYZ-RB from scaffolds cationically modified PCL and H-PCL was observed from 30 min to 2 hours, reaching values of LYZ-RB cumulative release ~ 40% from PCL and H-PCL after 2 hours (ns). After the burst phase, LYZ-RB release from cationically modified PCL and H-PCL reached a plateau. From the first hour to 4 hours of incubation, LYZ-RB cumulative release from cationically modified PCL-b-PEG/PCL scaffolds showed a significantly lower LYZ-RB cumulative release compared with cationically modified PCL. At 4 h of incubation, the cumulative release reached values of 30% from PCL-b-PEG/PCL scaffolds which was significantly lower than LZ-RB released from PCL scaffolds (40% of LZ-RB cumulative release) (p 0.0388). The burst release of LYZ-RB from cationically modified PCL-b-PEG/PCL was extended to 6 hours, reaching values of LYZ-RB cumulative release of 40% (after 6 hours); no significant difference was observed between cumulative release of LZ-RB from cationically modified PCL, H-PCL and PCL-b-PEG/PCL

scaffolds after 6 hours. LYZ-RB release from cationically modified PCL-b-PEG/PCL slowed down after 6 hours and LYZ –RB continued progressively and was time- dependent until day 9. After that time, LYZ-RB release reached a plateau. No statistical differences of LYZ release were found between samples. Cationically modified PCL, H-PCL and PCL-b-PEG/PCL scaffolds released around 60% of LYZ-RB after 21 days (ns).

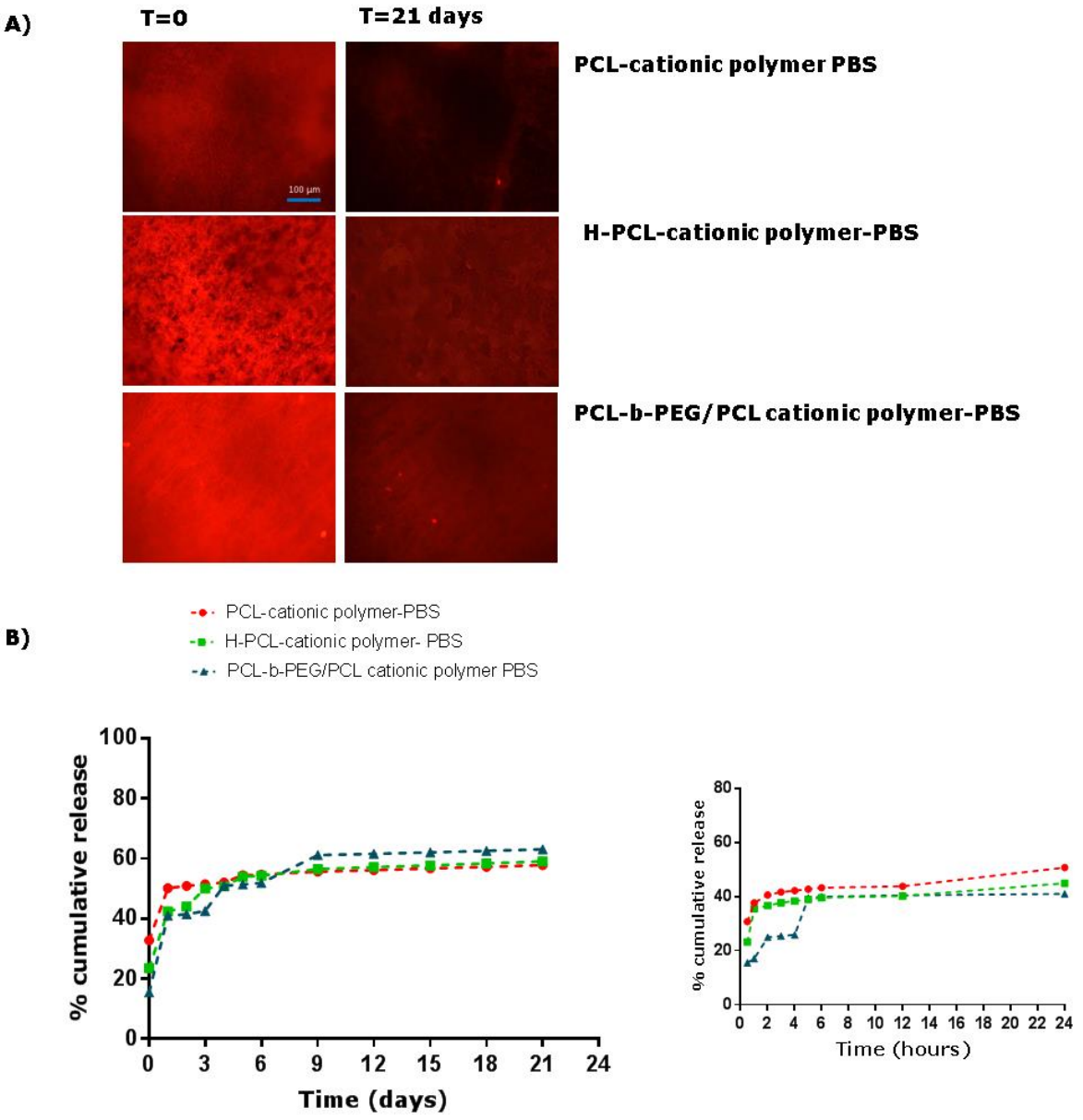


Figure 6.11 - A) Representative fluorescent microscopy images of lysozyme-rhodamine on PCL, H-PCL and PCL-b-PEG/PCL scaffolds. Magnification 10x, scale bar 100 microns. **B)** Lysozyme-rhodamine release profiles from PCL, H-PCL and PCL-b-PEG/PCL scaffolds in PBS pH 7.4 at 37°C. Three independent experiments carried out in triplicate.

In addition, the release profile of LYZ-RB released from PCL, H-PCL and PCL-b-PEG/PCL scaffolds with and without out cationic polymer treatment was compared (Figure 6.12). In general, it can be seen that non-modified scaffolds released higher concentrations of Lysozyme to the media than cationically charged scaffolds. It was found that the release profile of lysozyme was similar (ns) in PCL and cationically PCL scaffolds for 18 days. At day 21, PCL scaffolds released 84% of the lysozyme, while cationically modified PCL scaffolds released 60% of the total loaded lysozyme (p 0.0001). In addition, in the first 30 min, lysozyme released from H-PCL was significantly higher (40%) (P 0.00206) compared with cationically modified scaffolds H-PCL (23%). After 6 days, H-PCL released a significantly higher quantity of lysozyme (78%) (P 0.0018) compared with cationically modified H-PCL scaffold (54%). At the end of the 21 days, the cationically modified H-PCL-scaffolds released a total of 59% of lysozyme, which was significantly lower than release from H-PCL scaffolds, which released 80% of the total loaded lysozyme (P 0.0027). In addition, it was compared to the lysozyme release profile from PCL-b-PEG/PCL and the cationically modified PCL-b-PEG/PCL scaffolds. The lysozyme released from cationically modified PCL-b-PEG/PCL scaffolds, presented a significantly lower release, reaching values of 15% (P <0.0001) compared with PCL-PEG/PCL with a cumulative release of 44% after 30 min. From 1 hour onwards, a plateau of LYZ-RB cumulative released from PCL-b-PEG/PCL was observed, reaching values of LYZ-RB cumulative release of 48% in the first 4 hours. While LYZ-RB release from cationically modified

PCL-b-PEG/PCL scaffold showed a significantly lower burst release (30%) in the first 4 h (p 0.0008). After 24 h, the LYZ-RB cumulative release from cationically modified PCL-b-PEG/PCL and PCL-b-PEG/PCL scaffolds was no significantly different. At the end of the 21 days, amount of LYZ-RB released from cationically modified PCL-b-PEG/PCL scaffold reached cumulative values of 63%, the same as PCL-b-PEG/PCL without cationic polymer treatment (ns).

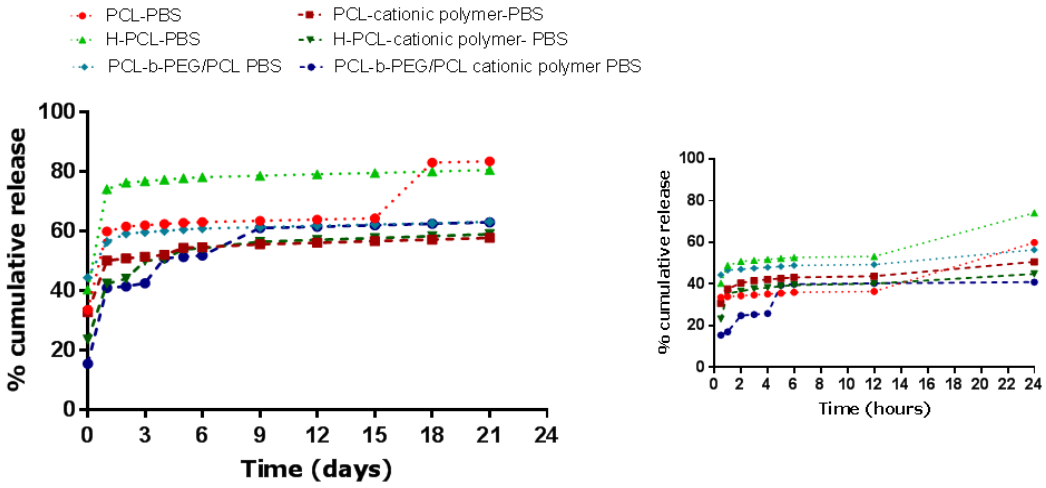


Figure 6.12 - Comparison between LZ-RB release profile from PCL, H-PCL scaffolds and PCL-b-PEG/PCL with and witout ationic polymer treament. Three independent experiments carried out in triplicate.

Loading and release of avidin and lysozyme presented in the current study have been reported before and can be explained by "wrong side interaction" between protein/polymer (Salmaso and Caliceti, 2013). This type of interaction is an unexpected behaviour and can be explain by the heterogeneity of protein charge, which can present positive or negative domains on the protein surface. This can cause the fluctuation of dipole-dipole charge orientation. Additionally, hydrophobic domains on the protein surface can interact with the polymer though hydrogen bonds and hydrophobic interactions, enabling protein /polymer association (da Silva et al., 2006, Salmaso and Caliceti, 2013).

In addition, avidin and lysozyme release from scaffolds can be related to the diffusion of protein determined by protein-fibre interactions and stearic effect caused by the size and molecular weight of proteins and the charge of the proteins (Gelain et al., 2010). (Gelain et al., 2010) evaluated cytokines on RADA16-I nanofiber system and found that the diffusion of cytokines was strongly dependent to the charge, the electrostatic interaction with the nanofibers, and the hindrance effect.

6.3.8 The bioactivity of Lysozyme-rhodamine B (LYZ-RB) after its release from the scaffolds

Figure 6.13 shows the bioactivity of lysozyme at the end of the release studies and after all lysozyme fractions were pooled and concentrated by using ultrafiltration devices (vivaspin GE healthcare Bio-Science AB, Sweden). It was found that the bioactivity of lysozyme was in general maintained after being released from all the scaffolds (with and without treatment). No statistically significant differences were found between materials. Lysozyme released from the scaffolds with and without cationically modification maintained an activity between 75- 80% when to the initial bioactivity of lysozyme (during loading).

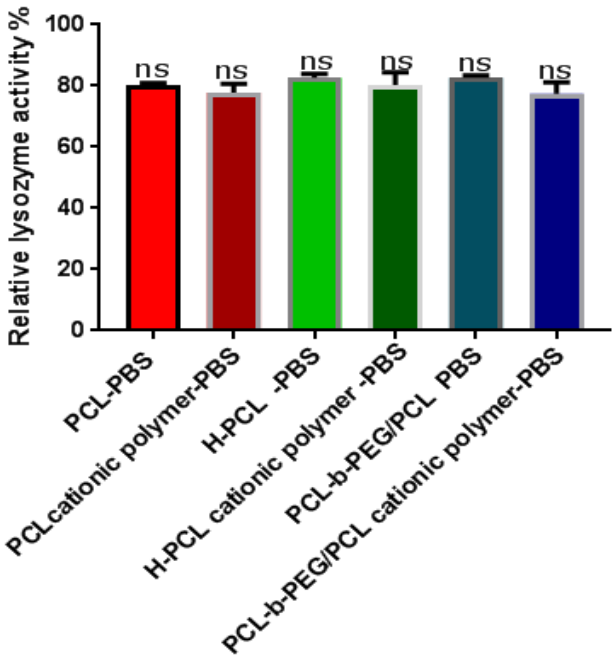


Figure 6.13 - Relative lysozyme activity. Lysozymes release pooled fraction from cationically modified PCL, H-PCL and PCL-b-PEG/PCL scaffolds were analysed through EnzChek® Lysozyme assay. Three independent experiments carried out in triplicate (means±SD).

(Ganguli et al., 2009) reported that the addition (10 mg/mL) of cationic polymer (polycation PEAMA-g-PEG) caused the complete inactivation of lysozyme activity without changing the secondary structure of the enzyme. Positive charges of this cationic polymer strongly interact with the negative residues (glutamic acids and 6 asparagine acids) on lysozyme that are part of the active site. However, the concentration of the cationic polymer was substantially higher (100 x) in the study conducted by (Ganguli et al., 2009) compared to the concentration used in the present study. Consequently, the electrostatic interactions were stronger and greater in number, which caused inactivation in the study conducted by (Ganguli et al., 2009).

One of the important factors to consider in a protein or enzyme release process, is the stability of the proteins during these processes (Wang et al., 2009a). The enzymatic activity of lysozyme released from the three different scaffolds (cationically modified PCL, H-PCL and PCL-b-PEG/PCL) did not show any significant detrimental effect on the released fraction of lysozyme from the different scaffolds.

6.3.9 The loading of *Lucilia sericata* maggot excretion/secretion on the cationic polymeric modified surface of PCL, H-PCL and PCL-b-PEG/PCL scaffolds

Figure 6.14-A) shows fluorescent images of *L. sericata* maggot E/S labelled with rhodamine absorbed into the scaffolds. From Figure 6.14-B) it observed that cationically modified PCL scaffolds did not show any significant differences between materials in term of loading percentage. On comparing loading percentages of *L. sericata* maggot E/S on scaffolds with and without cationic polymer treatment (Figure 6.14-C), it was found that the loading of *L. sericata* maggot E/S was similar for both materials (ns). Cationically modified H-PCL and H-PCL scaffolds loaded ~55% of *L. sericata* maggot E/S (ns). In addition, cationically modified PCL and PCL scaffolds loaded similar percentage of *L. sericata* maggot E/S (~50%) (ns). In contrast, cationically modified PCL-b-PEG/PCL scaffolds loaded significantly higher *L. sericata* maggot E/S (57%) (P 0.00057) compared with PCL-b-PEG/PCL (52%).

L. sericata maggot E/S is a complex mixture of proteins (Cesta, 2011) that possess different amino acid sequences, with different PI and thus different net charge (appendix). It is probable that the negative net charge of proteins interacts by electrostatic forces with positive charge of quaternary ammonium groups of $PTMAEMA_{33}$-b-$PHPMA_{180}$. The loading of *L. sericata* maggot E/S was more efficient and highly significant on cationically modified PCL-b-PEG/PCL scaffolds.

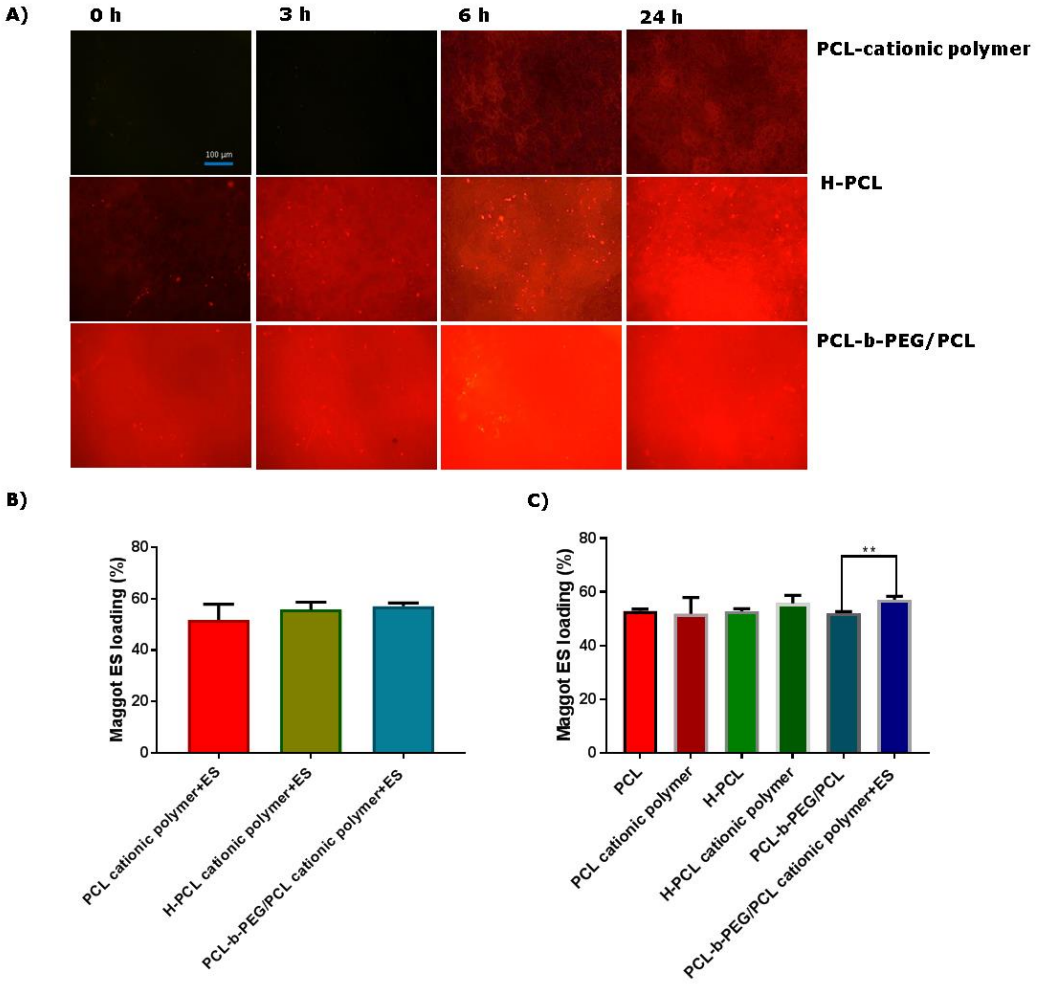


Figure 6.14 - A) Representative fluorescence microscopy images of *L. sericata* maggot E/S-NHS Rho fluorescein conjugate protein absorbed into cationically modified PCL, H-PCL and PCL-b-PEG/PCL scaffolds. Magnification 10x, scale bar 100 microns. **B)** *L. sericata* maggot E/S loading percentage on treated scaffolds. Determinations of protein was done by Bradford assay. **C)** Comparison of percentage of *L. sericata* maggot E/S loaded on PCL, H-PCL and PCL-b-PEG/PCL scaffolds with and without cationic polymer. Two way-ANOVA, Tukey's multiple comparison test. Two independent experiments carried out in duplicate (means±SD).

6.3.10 The release of *Lucilia sericata* maggot excretion/secretion from the cationically modified PCL, H-PCL and PCL-b-PEG/PCL scaffolds

From Figure 6.15 it can be seen that similar results were obtained for the release profile of *L. sericata* maggot E/S from the cationically modified PCL, H-PCL and PCL-b-PEG/PCL scaffolds. *L. sericata* maggot E/S released from all of these scaffolds presented an initial burst release within the first 6 hours and then a slowdown phase, with a progressive increment of *L. sericata* maggot E/S quantity released into the media on a time dependent basis. Thirty minutes after the immersion of the cationically modified PCL, H-PCL and PCL-b-PEG/PCL scaffolds into the media, cumulative release of *L. sericata* maggot E/S reached 3% (ns). For *L. sericata* maggot E/S release from cationically modified PCL scaffolds, the cumulative release values reached lower values (17%) compared with cationically modified H-PCL (22%) (p 0.092) and PCL-b-PEG/PCL (%) (p 0.077) scaffolds after 6 hours. After that (24 h post incubation), the release of *L. sericata* maggot E/S from scaffolds slowed down and the values of cumulative release reached 23% for cationic modified PCL; significantly lower compared with the release of *L. sericata* maggot E/S from cationically modified PCL-b-PEG/PCL (28%) (p 0.0017) and H-PCL (28%) (p 0.031). After 21 days, *L. sericata* maggot E/S cumulative release reached values ~ 60% from cationically modified PCL-b-PEG/PCL, H-PCL and PCL scaffolds (ns).

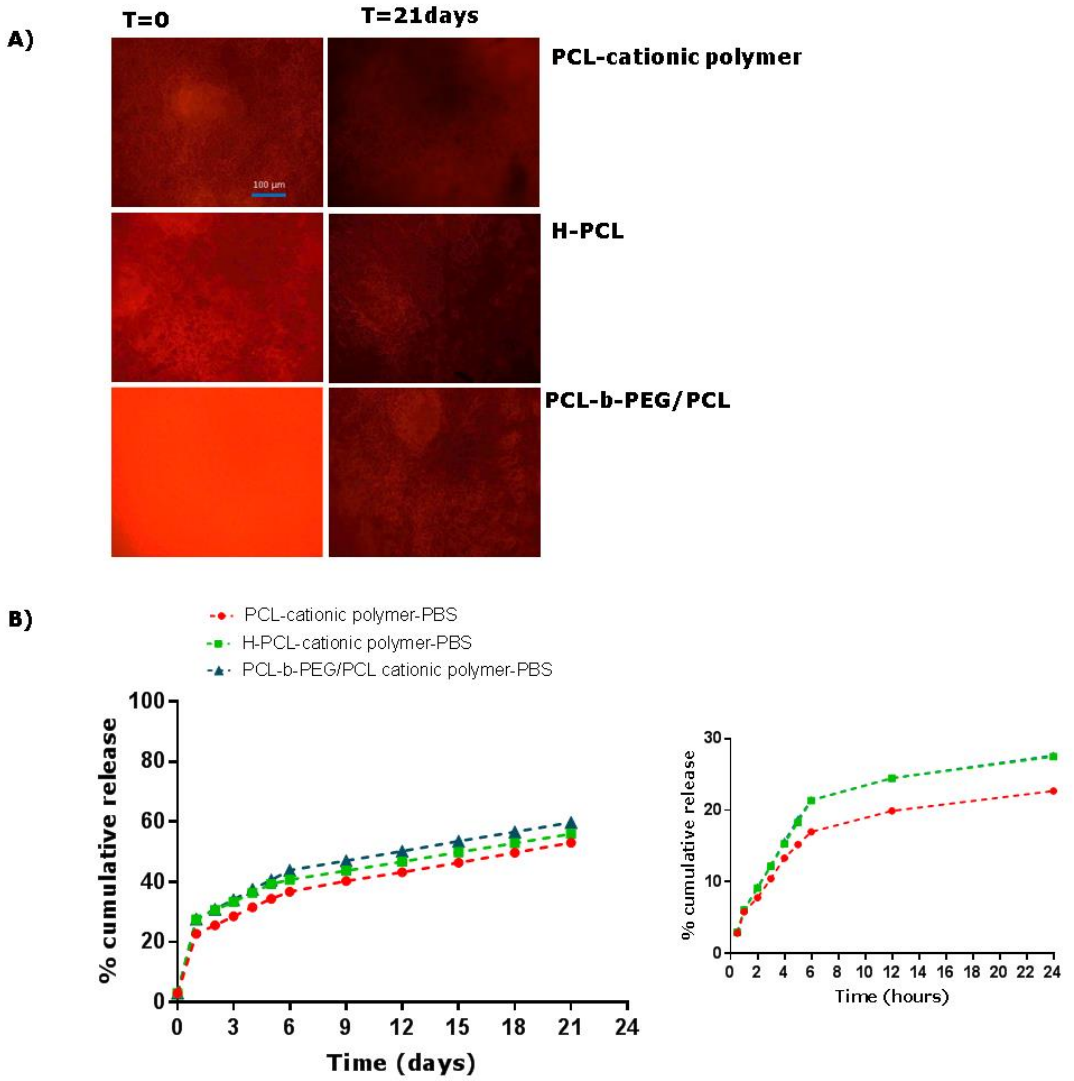


Figure 6.15 - Representative fluorescent microscopy images of *L. sericata* maggot E/S -rhodamine on PCL, H-PCL and PCL-b-PEG/PCL scaffolds. Magnification 10x, scale bar 100 microns. B) *L. sericata* maggot E/S -rhodamine release profiles from PCL, H-PCL and PCL-b-PEG/PCL scaffolds in PBS pH 7.4 at 37°C. Two independent experiments carried out in duplicate (means±SD).

In addition, the effect of the cationic polymer modification on the surface of the scaffolds with respect to the release of *L. sericata* maggot E/S was analysed. From Figure 6.16 it can be seen that the release of *L. sericata* maggot E/S was greater in scaffolds without cationic polymer modification. PCL scaffolds showed a significant higher cumulative release of *L. sericata* maggot E/S (25%) ($P < 0.0001$) compared with cationic modified PCL scaffolds (20%) after 12 hours of release. H-PCL scaffolds (with and without cationic polymer) did not reveal any significant differences in terms of cumulative release of *L. sericata* maggot E/S, reaching values of ~25%. While PCL-b-PEG/PCL scaffolds showed a significantly higher cumulative release of 30% (P 0.0050) compared with *L. sericata* maggot E/S released (25%) from cationic modified PCL-b-PEG/PCL scaffolds. No statistical differences were found from at the end of 21 days of maggot released from the different scaffolds. These results are controversial, because the loading capacity of *L. sericata* maggot E/S on the scaffolds increased with the addition of cationic polymer.

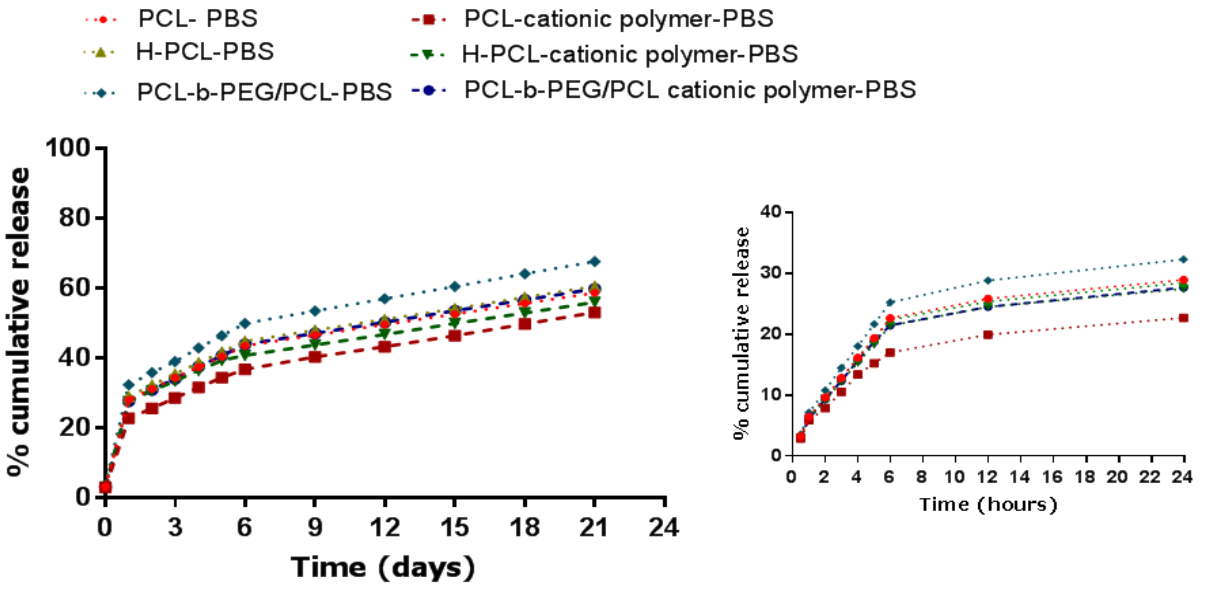


Figure 6.16 – Comparision of L. sericata maggot E/S-rhodamine release profiles from PCL, H-PCL and PCL-b-PEG/PCL scaffolds with and without cationic polymeric treatment, in PBS pH 7.4 at 37°C. Two independent experiments carried out in duplicate

A higher maggot release was expected from the scaffold that had higher loaded proteins. However, (Srikar et al., 2008) reported that PMMA (poly methyl methacrylate) nanofibers controlled the release of proteins, and an increment of PMMA decelerated the release compared with PCL mats. In addition, the results presented here were in agreement with Schillemans et al. (2011), who reported that the release of cytochrome C protein (positively charged) from polymer dextran methacrylate (negatively charged) hydrogel was slow and in a time-dependent manner due to a limited diffusion distance caused by steric hindrance. Also, they concluded that increasing charge density led to the decrease in the amount of released protein.

The findings presented in this study may be explained by the fact that *L. sericata* maggot E/S is a complex mixture of proteins with different charges, some of them positive, others neutral and others negative.

Also, the molecular weight of the protein widely varies between 25-50 KDa (Schmidtchen et al., 2003). Therefore, it may be that negative proteins are bonded through attracting forces to the cationic polymer while repulsing force positive proteins weakly associated to the cationic polymer allow the release of this molecules to the media. In order to study the electrostatic interactions between proteins of *L. sericata* maggot E/S and cationic polymer, it was necessary to calculate the isoelectric points of the main *L. sericata* maggot E/S proteins. Isoelectric points (PI) of *L. sericata* maggot E/S proteins such as lucifencin, trypsin, and chymotrypsin were calculated theoretically and based on the amino-acid sequences of *L. sericata* maggot E/S proteins. The calculation of PI was performed by using an online tool, ExPASy Bioinformation Resource Portal, which calculates PI and Mw for a list of UNIProt Knowledgebase (Swiss-Prot or TrEMBL)(Walker, 2005). Theoretical analysis showed that lucifecin possesses a molecular weight of 13 KDa, with a PI of 8.27 and positive charge at pH 7.4 (Kozlowski, 2016). Chymotrypsin possesses a PI of 7.73 and a molecular weight of 26 kDa and a neutral to positive charge of pH 7.4. Finally, trypsin PI was estimated to be 5.28 and molecular weight at 27 kDa, thus negatively charge at pH 7.4. In accordance with these results, it can be hypothesised that trypsin will be strongly loaded to the cationic polymer through attractive forces. Chymotrypsin will probably interact weakly through negative amino acid residues, and lucifencin will be released faster due to the repulsive force between the cationic polymers and the positive charge of the protein. Lucifencin has been reported to have an antimicrobial

action. As a result, a fast release will be beneficial to wound healing treatment, and a sustainable release of chymotrypsin and trypsin favour enhancement of tissue granulation formation.

In terms of cumulative amount of released *L. sericata* maggot E/S, ~5 µg of *L. sericata* maggot E/S were measured from cationicallly modified scaffolds after 24 h and no significant differences were found in terms of *L. sericata* maggot E/S cumulative release between materials. After 21 days, cumulative amount of released *L. sericata* maggot E/S ~14 µg from cationicallly modified scaffolds and no significant differences were found in terms of *L. sericata* maggot E/S cumulative release between materials. The cumulative amount of *L. sericata* maggot E/S released from cationicallly modified scaffolds over 21 days (14 µg/mL) can be further compared with values presented by (Horobin et al., 2006). They showed that the amount of *L. sericata* maggot E/S of 1 µg/mL exerted a significant enhancement on fibroblast migration over 48 h. Whereas the total amount measured in the current study was 10x higher. In addition (Smith et al., 2006) reported the incorporation of *L. sericata* maggot E/S into a prototype hydrogel, with a maximum release of 50 µg/mL over 12 h. They confirmed that *L. sericata* maggot E/S remarkable enhanced rate of closure. In the current study, preliminary assessment of released *L. sericata* maggot E/S on fibroblast migration did not show any enhancement on wound closure. This may be explained by the fact that (Horobin et al., 2006) used fresh aliquots of *L. sericata* maggot E/S and (Smith et al., 2006) conduced release studies of *L. sericata* maggot E/S in a shorter period of time (12 h)

while in the current study the activity of *L. sericata* maggot E/S was probably affected as consequence of sample aging, the length of realise studies, storage (Freeze-thaw cycles) and problems related with the sterility of *L. sericata* maggot E/S.

6.3.11 The activity of *Lucilia sericata* maggot excretion/secretion after release

Pooled aliquots of *L. sericata* maggot E/S were collected and measured for the final bioactivity as described in chapter 2 sections 2.5.10 and 2.5.15.

Figure 6.17 shows the comparative analysis of protease activity of *L. sericata* maggot E/S released from cationic modified PCL, H-PCL and PCL-b-PEG/PCL scaffolds. In general, no statistical differences were found between protease activities of *L. sericata* maggot E/S flowing release from scaffolds. However, a reduction of biological activity was observed in all samples following release from scaffolds with cationically modified polymer (relative to the initial aliquot activity). To confirm this trend a greater number of samples need to be tested. Protease activity was significantly higher (80%) from PCL-b-PEG/PCL scaffolds than the activity of *L. sericata* maggot E/S from cationically modified H-PCL scaffolds (32%) (p 0.0326).

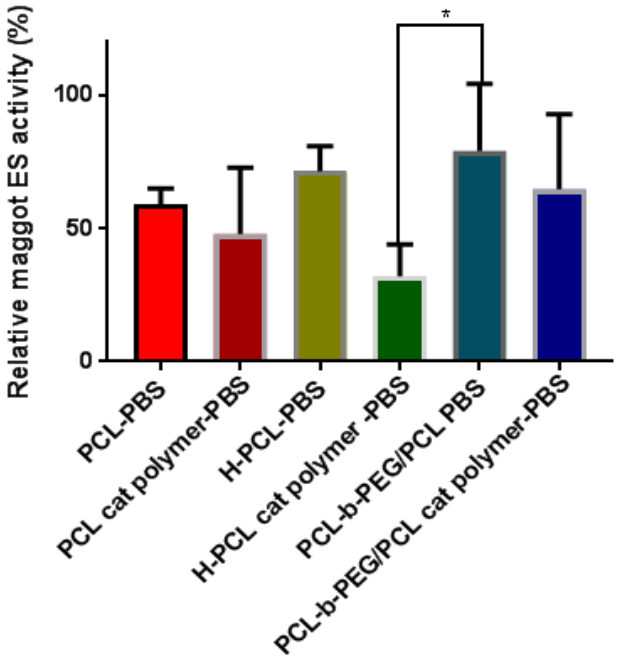


Figure 6.17 - Relative protease activity from *L. sericata* maggot E/S. *L. sericata* maggot E/S release pooled fraction from PCL, H-PCL and PCL-b-PEG/PCL scaffolds with and without cationic treatment. Enzymatic activity was analysed through protease assay. Two independent experiments carried out in triplicate (means±SD).

6.4 Conclusions

Cationic polymer $PTMAEMA_{33}$-b-$PHPMA_{180}$ was successfully synthesized through RAFT polymerization and was biocompatible with fibroblasts up to a concentration of 500 μg/mL.

$PTMAEMA_{33}$-b-$PHPMA_{180}$ was successfully loaded on electrospun scaffolds. PCL-b-PEG/PCL loaded significantly higher percentage of cationic polymer (~18%) on the surface compared with PCL (14%).

Avidin and Lysozyme were two hydrophilic proteins with a positive net charge used as model proteins, which presumably interacted through 'wrong side' interaction with the cationic polymer, loading higher quantity on the surface of the scaffolds compared with protein loading % on scaffolds without cationic polymer modification.

The comparison of the release profiles of avidin from PCL, H-PCL and PCL-b-PEG/PCL scaffolds with and without out cationic polymer treatment showed that release of avidin from cationically modified scaffolds, tends to be more of zero order kinetics and not time dependent. On the other hand, scaffolds without cationic treatment showed a burst release characterized by a time dependent increment of the avidin (during the first 6 h of incubation). From day 6 onwards, the release profiles of avidin from treated or not treated scaffolds were similar.

It was found that the bioactivity of lysozyme was no significantly reduced (compared with scaffolds without cationic modification) by the modification of the scaffold surfaces with cationic polymer ($PTMAEMA_{30}$-b-$PHPMA_{180}$).

It was hypothesized that *L. sericata* maggot E/S may be incorporated more efficiently on electrospun H-PCL and PCL-b-PEG/PCL scaffolds modified by the incorporation of a cationic polymer $PTMAEMA_{33}$-b-$PHPMA_{180}$. From the results presented here, it was found that *L. sericata* maggot E/S was loaded more efficiently on scaffolds with cationic polymer modification than on scaffolds without cationic polymer. In general, the release of proteins within the first hours was also reduced when the scaffolds' surface was modified with $PTMAEMA_{33}$-b-$PHPMA_{180}$ cationic polymer.

The release profiles of *L. sericata* maggot E/S showed that the burst release and the cumulative release of maggot was significantly lower on cationically modified scaffolds. PCL scaffolds showed a significantly higher cumulative release of *L. sericata* maggot E/S (25%) ($P < 0.0001$) compared with cationically modified PCL scaffolds (20%) after 12 hours of release. H-PCL scaffolds (with and without cationic polymer) did not reveal any significant differences in terms of cumulative release of *L. sericata* maggot excretion/secretion, reaching values of ~25%. In the meantime, PCL-b-PEG/PCL scaffolds showed a significantly higher cumulative release of 30% (P 0.0050) compared with *L. sericata* maggot E/S released (25%) from cationically modified PCL-b-PEG/PCL scaffolds.

Cumulative amount of released *L. sericata* maggot E/S was ~14µg from cationicallly modified after 21 days. The cumulative amount of *L. sericata* maggot E/S released from cationicallly modified scaffolds over 21 days (14 µg/mL) which was 10x higher that the concentration used by (Horobin et al., 2006) for migration assays, but lower than

the released maggot concentration used by (Smith et al., 2006) (50 µg/mL).

For granulation tissue formation, a burst release followed by a sustained release is required, which is in agreement with the release profiles found in this study.

The activity of *L. sericata* maggot proteases was significantly reduced from cationically modified H-PCL compared the biological activity of *L. sericata* maggot E/S released from PCL-b-PEG/PCL In term of the loss of enzymatic activity, the literature indicated that non-specific interactions between enzyme and scaffold lead to undesired change on protein conformation and activity and in general all processing (freeze-thaw cycles, length of release studies, drying and washing procedures) (Wang et al., 2009b). Therefore, further investigations in the loss of protease activity from *L. sericata* maggot E/S after the released are suggested in order to determine which step causes a damaging effect on protease activity.

The release of *L. sericata* maggot E/S occurred in a sustained manner, which means that these scaffolds show suitable characteristics for wound healing.

It is the first time that this particular cationic polymer is used to absorbed *L. sericata* maggot E/S as a platform for the release of therapeutic molecules for wound healing. The modification of PCL-b-PEG/PCL scaffolds with cationic polymer improved the loading efficiency of a mixture of protein onto the surface and permitted the release bioactive molecules and preservation of biological activity of proteases from *L. sericata* maggot E/S.

CHAPTER 7 Conclusions and Future work

The aim of this current research project was to develop a bioactive electrospun scaffold with suitable properties for fibroblast proliferation and infiltration. The incorporation of therapeutic biomolecules from *L. sericata* maggot ES into these scaffolds was hypothesised to provide a potentially attractive and novel clinical solution to support skin wound healing. Such a bioactive scaffold would provide the structural environment for cells to grow, infiltrate and release active molecules for healing wounds.

The first part of this research focused on the investigation of biomolecules with therapeutic action on wound healing. In this sense, fibroblast metabolic activity was tested using AlamarBlue® assay and the *in vitro* wound model scratch assay was used to evaluate fibroblast migration following exposure to different concentrations of propolis and its main components. Previous research had not focused nor reported the effect of propolis on fibroblast migration for wound healing. Instead, research has mainly tested the anti-invasion capacity of propolis to prove its anticancer effect on malignant cells (Barbarić et al., 2011, Carvalho et al., 2014). On the other hand, propolis has been used for wound healing, in both *in vitro* and *in vivo* assays, significantly shortening the time of healing. Considering that fibroblast migration is a crucial step to consider in the election of bioactive molecules for wound healing, it was hypothesized that

propolis and its constituent compounds quercetin, rutin and artepillin C may have a beneficial effect on wound healing by enhancing granulation tissue formation. The cytotoxicity results revealed that propolis enhanced relative metabolic activity (%) at concentrations between 2.9-11.7 µg/mL, and at higher concentrations a cytotoxic effect was observed. Higher concentrations of quercetin, rutin and artepillin C (100-30 µM) showed the same dose-dependent cytotoxic effect. Additionally, no evidence was found that propolis and its compounds significantly enhanced NIH-3T3 fibroblast migration *in vitro*. The beneficial effect of propolis on wound healing may be attributed to the anti-inflammatory and antimicrobial effect (Drago et al., 2007, Dota et al., 2011). However, neither propolis nor its compounds influenced fibroblast migration. It was therefore decided to use *L. sericata* maggot excretion/secretion as a source of bioactive molecules because of the known beneficial effects of *L. sericata* maggot ES on wound healing by enhancing fibroblast migration and granulation tissue formation (Horobin et al., 2005, Sherman, 2014, Bexfield et al., 2010, Britland et al., 2011).

Next, scaffolds based on PCL and PCL-b-PEG/PCL with suitable mechanical, geometrical, and biological properties were developed. The aim was to enable fibroblast proliferation and infiltration, to support regeneration of the wound. Scaffolds were fabricated using electrospinning. The electrospinning set up, polymer concentration and solvents used were optimised to fabricate scaffolds with a random fibre arrangement. It was possible to electrospin poly (ε-

caprolactone) scaffolds with a fibre diameter ranging from 2 to 14 μm and PCL-b-PEG/PCL scaffolds with an average fibre diameter ranging from 1 to ~4μm. It was found that PCL scaffolds, having a fibre diameter ~4 μm, with a porosity between 60-80%, thickness ~60-144 microns, Young's modulus of ~6 MPa, supported fibroblasts as evidenced by measurement of their metabolic activity and infiltration compared with PCL scaffolds with a lower or higher average fibre diameter. Also, it was hypothesised that modification of the hydrophilicity of the PCL scaffolds may improve biocompatibility and also degradation rates of the material. For that reason, PCL was blended with PCL-b-PEG/PCL and it was found that PCL-b-PEG/PCL slightly improved the hydrophilicity of the scaffold surface. In addition, it was found that scaffolds fabricated from a ratio of PCL-b-PEG/PCL (40:60 15% *w/w*) significantly enhanced fibroblast metabolic activity and infiltration (60%) compared with scaffolds fabricated from PCL alone. Characterization of the PCL-b-PEG/PCL scaffolds showed an average pore size of ~40 μm and a porosity between 70%. The mechanical properties of the PCL-b-PEG/PCL scaffolds mimicked that of ECM (Young's modulus ~9 MPa). In addition, the degradation rate of PCL-b-PEG /PCL scaffolds was faster than those fabricated from PCL alone. In summary, the PCL-b-PEG/PCL scaffolds met the requirements of providing a supporting scaffold for skin fibroblasts and as such, it was hypothesised that they possessed a greater potential for skin wound regeneration applications.

Furthermore, *L. sericata* maggot ES was incorporated into PCL, H-PCL, and PCL-b-PEG/PCL electrospun scaffolds, with the aim that the bioactive molecules would be released in a sustained manner and enhance fibroblast migration (to promote wound closure). Avidin and lysozyme were used as model proteins to evaluate the loading (adsorption) and release from PCL, H-PCL and PCL-b-PEG/PCL electrospun scaffolds. It was found that lysozyme, a simple and small protein with a positive net charge was released faster and in greater quantities than avidin (a bigger and more complex protein). *L. sericata* maggot ES (a complex mixture of proteins) was released from PCL and PCL-b-PEG/PCL scaffolds over 21 days. PCL-b-PEG/PCL scaffolds provided a platform that allowed reduction of the burst release and allowed a sustained release of avidin which was also seen with *L. sericata* maggot ES. In the first instance, scaffolds were incubated with 1 mL of 40 µg/mL of *L. sericata* maggot ES (as determined by the Bradford assay). After 24 h incubation, 20 µg/mL of *L. sericata* maggot ES was loaded onto the scaffolds. The cumulative amount of *L. sericata* maggot ES released from PCL-b-PEG scaffolds showed that after 24 h, 13 µg/mL (32%) had been released in total into the media and after 21 days a total of 14 µg/mL (67%) had been released.

The loading and release of *L. sericata* maggot ES from electrospun scaffolds have not been reported before. The incorporation of *L. sericata* maggot ES into a scaffold system created a novel solution for improved wound healing because the scaffolds provided fibroblast support and infiltration.

Moreover, post electrospinning modification of PCL, H-PCL and PLC-b-PEG/PCL scaffolds using a cationic polymer PTMAEMA-PHPMA was used to improve the loading and release of proteins. It was hypothesized that *L. sericata* maggot ES may be incorporated more efficiently on electrospun H-PCL and PCL-b-PEG/PCL scaffolds modified by the incorporation of a cationic polymer $PTMAEMA_{30}$-b-$PHPMA_{180.}$ PTMAEMA-PHPMA was successfully synthesised by using RAFT polymerization, which was biocompatible with fibroblasts up to a concentration of 500 µg/mL. Avidin and lysozyme were used as model proteins (two hydrophilic proteins with a positive net charge), which presumably interacted through induced hydrophobic and ionic interactions with the cationic polymer. This resulted in higher loading of proteins on the surface of the scaffolds compared with protein loading on scaffolds without cationic polymer modification. A comparison study of the release profile of avidin from PCL, H-PCL and PCL-b-PEG/PCL scaffolds with and without cationic polymer treatment showed that avidin released from cation polymer modified scaffolds tended to follow more zero-order kinetics; i.e the release of avidin from cationic modified scaffolds was not time-dependent. While scaffolds without cationic treatment showed a burst release (first order kinetics), characterized by an increment of the avidin concentration in a time-dependent manner (during the first 6 h of incubation). The release of proteins was reduced when the scaffold surface was modified with $PTMAEMA_{30}$-b-$PHPMA_{180}$ cationic polymer. Moreover, *L. sericata* maggot ES was loaded more efficiently onto cationically modified PCL-b-PEG/PCL scaffolds compared with PCL-b-

PEG/PCL scaffolds (without cationic polymer). No statistically significant differences were found between PCL and H-PCL scaffolds with and without cationic polymer modification.

Release profiles of *L. sericata* maggot ES showed that the burst and cumulative release of *L. sericata* maggot ES were significantly lower when cationic polymer was incorporated into the scaffolds. PCL scaffolds showed a significantly higher cumulative release of *L. sericata* maggot ES (25%) ($P < 0.0001$) compared with cationic modified PCL scaffolds (20%) after 12 hours of release. H-PCL scaffolds (with and without a cationic polymer) did not reveal any significant differences in terms of cumulative release of *L. sericata* maggot ES; values reached ~25%. While PCL-b-PEG/PCL scaffolds showed a significant higher cumulative release of 30% (P 0.0050) compared with *L. sericata* maggot ES released (25%) from cationic modified PCL-b-PEG/PCL scaffolds. Release profiles of *L. sericata* maggot ES released from cationically modified were similar. No statistical significant differences were found at the end of 21 days of *L. sericata* maggot ES released from the different scaffolds. Analysis of PCL-b-PEG/PCL scaffolds showed that after 21 days a total of 14 µg/mL (60%) had been released.

The release of *L. sericata* maggot ES occurred in a sustained manner, which according to (Leung et al., 2011) is a desirable characteristic of scaffolds for wound healing. It was hypothesised that a sustained release of a serine proteinase can provide the stimuli for fibroblast migration from the edges of the wound into the scaffold.

In addition, the protease activity of *L. sericata* maggot ES was preserved when PCL-b-PEG/PCL and cationically modified PCL-b-PEG/PCL scaffolds were used as the platform for release.

Contribution of this thesis to new knowledge:

This thesis has developed a 3-D PCL-b-PEG/PCL scaffold proposed for the enhancement of skin wound healing. The thesis revealed that it is possible to develop bioactive electrospun scaffolds based on PCL-b-PEG/PCL polymers with suitable properties for cell proliferation and infiltration. PCL-b-PEG/PCL scaffold offered a platform for loading and releases of bioactive molecules from *L. sericata* maggot ES that possess therapeutic properties to accelerate granulation tissue formation. In addition, PCL-b-PEG/CPL can be post modified with a cationic polymer to increase the loading efficiency of negatively charged proteins (by electrostatic interactions) and with proteins with a net positive charge but possess negative amino acid residues. Therefore, PCL-b-PEG/PCL scaffolds may provide a cost-effective solution for skin wound healing through the delivery of bioactive molecules.

Limitations of the current work

Some limitations have been set due to environmental restrictions for *L. sericata* maggot ES production. This may include the production of *L. sericata* maggot ES in a sterile environment to avoid contamination and possible loss of activity due to bacterial infections.

7.1 Future work

No evidence was found that propolis, quercetin rutin and artepillin C significantly enhanced NIH-3T3 fibroblast migration *in vitro*. Future work will need to consider fibroblast from other species and primary cell lines. Also, an *in vivo* investigation of the influence of propolis on fibroblast migration *in vivo* should also be considered.

Propolis or its compounds positively influence wound healing through different pathways. For example, propolis aids wound healing by controlling the inflammatory response and infection. It would be appropriate therefore to incorporate propolis onto scaffolds for release in a controlled manner subsequent assessment of the material *in vivo*.

In addition, this thesis has demonstrated the potential use of 3-D PCL-b-PEG/CPL scaffolds for the treatment of chronic skin wounds by offering a suitable environment for fibroblasts to proliferate and infiltrate. PCL-b-PEG/PCL electrospun scaffolds enhanced significantly fibroblast proliferation and cell infiltration. After comparing the chemical properties of PCL and PCL-b-PEG/PCL scaffolds it was not clear why PCL-PEG/PCL improved fibroblast infiltration. Therefore, this will be considered in the future work, to further evaluate the effect of PCL-b-PEG/PCL on the wettability of a surface preparing the polymer on a slide as a film and extrapolating that data to the 3D scaffolds (due to the difficulties in making water contact measurements on the scaffolds due their surface roughness).

An electrospun scaffold should facilitate the wound healing and regenerative process which should and coincide with the degradation time of the scaffold. Therefore, this will be considered in the future work, to further explore alternative polymers or tuning the existing PCL-b-PEG co-polymer to increase the degradation rate to range from several weeks to 6 months.

In chapter 5 and 6, the loading and release of *L. sericata* maggot ES onto the electrospun scaffolds was conducted. In the future, it should be considered to explore other methods to incorporate *L. sericata* maggot ES onto the scaffolds to minimise the loss of activity during loading and release. In addition, this part of the research needs to further evaluate therapeutic effectiveness of the *L. sericata* maggot ES released from electrospun PCL-b-PEG/PCL scaffolds on fibroblast, endothelial and keratinocytes *in vitro and in vivo*. An *in vivo* model that allows the testing of the effect of *L. sericata* maggot ES for a long period of time (including histological assessment) will be necessary to evaluate any local effect on wound healing. In the case of *L. sericata* maggot ES released from cationically modified scaffolds, future work needs a cationic polymer structure that has less density charge.

In addition, it will be necessary to consider further characterization of the electrospun scaffolds containing *L. sericata* maggot ES to acquire information regarding protein structure and stability on/in the scaffolds. Preliminary FTIR and DSC analyses were conducted. It will be considered in the future work, to expand FTIR spectra to further

analysis of bands ~1650 and 1550 cm^{-1} (detection of amides I and II) to determine the presence of the proteins on the material

Finally, chronic wounds are characterized by the present of macrophages and other leukocytes that infiltrate the tissue and release an important number of cytokines, proteases and ROS. Here it is proposed to design a Reactive Oxygen species (ROS) responsive polymer to trigger *L. sericata* maggot ES for future work. ROS responsive polymers could be used as carriers of *L. sericata* maggot ES on the surface of the electrospun fibres surface such that the release of the proteins is triggered *in situ* on the wound bed.

References

ABDELRAHMAN, T. & NEWTON, H. 2011. Wound dressings: principles and practice. *Surgery (Oxford),* 29**,** 491-495.

AGARWAL, S., ZHANG, Y., MAJI, S. & GREINER, A. 2012. PDMAEMA based gene delivery materials. *Materials Today,* 15**,** 388-393.

AL-SHAMMARI, B., AL-FARISS, T., AL-SEWAILM, F. & ELLEITHY, R. 2011. The effect of polymer concentration and temperature on the rheological behavior of metallocene linear low density polyethylene (mLLDPE) solutions. *Journal of King Saud University-Engineering Sciences,* 23**,** 9-14.

AL-WAILI, N., SALOM, K. & AL-GHAMDI, A. A. 2011. Honey for wound healing, ulcers, and burns; data supporting its use in clinical practice. *The scientific world journal,* 11**,** 766-787.

ALRUBAIY, L. & AL-RUBAIY, K. K. 2009. Skin substitutes: a brief review of types and clinical applications. *Oman medical journal,* 24**,** 4.

AMOS, P. J., KAPUR, S. K., STAPOR, P. C., SHANG, H., BEKIRANOV, S., KHURGEL, M., RODEHEAVER, G. T., PEIRCE, S. M. & KATZ, A. J. 2010. Human adipose-derived stromal cells accelerate diabetic wound healing: impact of cell formulation and delivery. *Tissue Engineering Part A,* 16**,** 1595-1606.

ANDREWS, K. L., HOUDEK, M. T. & KIEMELE, L. J. 2015. Wound management of chronic diabetic foot ulcers: from the basics to regenerative medicine. *Prosthet Orthot Int,* 39**,** 29-39.

ARIMA, Y. & IWATA, H. 2007. Effect of wettability and surface functional groups on protein adsorption and cell adhesion using well-defined mixed self-assembled monolayers. *Biomaterials,* 28**,** 3074-3082.

ARMENTANO, I., DOTTORI, M., FORTUNATI, E., MATTIOLI, S. & KENNY, J. 2010. Biodegradable polymer matrix nanocomposites for tissue engineering: a review. *Polymer degradation and stability,* 95**,** 2126-2146.

AUGUSTINE, R., DOMINIC, E. A., REJU, I., KAIMAL, B., KALARIKKAL, N. & THOMAS, S. 2015. Electrospun poly (ε-caprolactone)-based skin substitutes: In vivo evaluation of wound healing and the mechanism of cell proliferation. *Journal of Biomedical Materials Research Part B: Applied Biomaterials,* 103**,** 1445-1454.

BADROSSAMAY, M. R., MCILWEE, H. A., GOSS, J. A. & PARKER, K. K. 2010. Nanofiber assembly by rotary jet-spinning. *Nano letters,* 10**,** 2257.

BAJI, A., MAI, Y.-W., WONG, S.-C., ABTAHI, M. & CHEN, P. 2010. Electrospinning of polymer nanofibers: effects on oriented morphology, structures and tensile properties. *Composites science and technology,* 70**,** 703-718.

BAKER, S. C., ROHMAN, G., SOUTHGATE, J. & CAMERON, N. R. 2009. The relationship between the mechanical properties and cell behaviour on PLGA and PCL scaffolds for bladder tissue engineering. *Biomaterials,* 30**,** 1321-1328.

BALASUNDARAM, G. & WEBSTER, T. J. 2006. A perspective on nanophase materials for orthopedic implant applications. *Journal of Materials Chemistry,* 16**,** 3737-3745.

BALDWIN, A. D. & KIICK, K. L. 2010. Polysaccharide-modified synthetic polymeric biomaterials. *Peptide Science,* 94**,** 128-140.

BALGUID, A., MOL, A., VAN MARION, M. H., BANK, R. A., BOUTEN, C. V. & BAAIJENS, F. P. 2008. Tailoring fiber diameter in electrospun poly (ε-caprolactone) scaffolds for optimal cellular infiltration in cardiovascular tissue engineering. *Tissue Engineering Part A,* 15**,** 437-444.

BANKOVA, V. 2005. Chemical diversity of propolis and the problem of standardization. *Journal of ethnopharmacology,* 100**,** 114-117.

BARBARIĆ, M., MIŠKOVIĆ, K., BOJIĆ, M., LONČAR, M. B., SMOLČIĆ-BUBALO, A., DEBELJAK, Ž. & MEDIĆ-ŠARIĆ, M. 2011. Chemical composition of the ethanolic propolis extracts and its effect on HeLa cells. *Journal of ethnopharmacology,* 135**,** 772-778.

BARONI, A., BUOMMINO, E., DE GREGORIO, V., RUOCCO, E., RUOCCO, V. & WOLF, R. 2012. Structure and function of the epidermis related to barrier properties. *Clinics in Dermatology,* 30**,** 257-262.

BARRIENTOS, S., BREM, H., STOJADINOVIC, O. & TOMIC-CANIC, M. 2014. Clinical application of growth factors and cytokines in wound healing. *Wound Repair and Regeneration,* 22**,** 569-578.

BARROSO, P. R., LOPES-ROCHA, R., PEREIRA, E. M. F., MARINHO, S. A., DE MIRANDA, J. L., LIMA, N. L. & VERLI, F. D. 2012. Effect of propolis on mast cells in wound healing. *Inflammopharmacology,* 20**,** 289-294.

BAUER, S. M., BAUER, R. J. & VELAZQUEZ, O. C. 2005. Angiogenesis, vasculogenesis, and induction of healing in chronic wounds. *Vascular and endovascular surgery,* 39**,** 293-306.

BAUM, C. L. & ARPEY, C. J. 2005. Normal cutaneous wound healing: clinical correlation with cellular and molecular events. *Dermatologic surgery,* 31**,** 674-686.

BAUTISTA, E. B., BERMÚDEZ-MORALES, V. H. & BALTAZAR, E. H. 2011. MATERIALES POLIMÉRICOS DE APLICACIÓN EN TERAPIA GÉNICA. *Revista Iberoamericana de Polímeros,* 12**,** 1.

BEANES, S. R., DANG, C., SOO, C. & TING, K. 2003. Skin repair and scar formation: the central role of TGF-[beta]. *Expert reviews in molecular medicine,* 5**,** 1-22.

BEHM, B., BABILAS, P., LANDTHALER, M. & SCHREML, S. 2012. Cytokines, chemokines and growth factors in wound healing. *Journal of the European Academy of Dermatology and Venereology,* 26**,** 812-820.

BEN-SHALOM, N., NEVO, Z., PATCHORNIK, A. & ROBINSON, D. 2012. Novel injectable chitosan mixtures forming hydrogels. Google Patents.

BEN SGHAIER, M., PAGANO, A., MOUSSLIM, M., AMMARI, Y., KOVACIC, H. & LUIS, J. 2016. Rutin inhibits proliferation, attenuates superoxide production and decreases adhesion and migration of human cancerous cells. *Biomedicine & Pharmacotherapy,* 84**,** 1972-1978.

BERLANGA-ACOSTA, J., SCHULTZ, G. S., LÓPEZ-MOLA, E., GUILLEN-NIETO, G., GARCÍA-SIVERIO, M. & HERRERA-MARTÍNEZ, L. 2012. Glucose toxic effects on granulation tissue productive cells: the diabetics' impaired healing. *BioMed research international,* 2013.

BERRETTA, A. A., NASCIMENTO, A. P., BUENO, P., VAZ, M. & MARCHETTI, J. M. 2012a. Propolis standardized extract (EPP-AF), an innovative chemically and biologically reproducible pharmaceutical compound for treating wounds. *International journal of biological sciences,* 8**,** 512-521.

BERRETTA, A. A., NASCIMENTO, A. P., BUENO, P. C. P. & LEITE, M. M. D. O. L. 2012b. Propolis standardized extract (EPP-AF®), an innovative chemically and biologically reproducible pharmaceutical compound for treating wounds. *International journal of biological sciences,* 8**,** 512.

BEXFIELD, A., BOND, A., MORGAN, C., WAGSTAFF, J., NEWTON, R., RATCLIFFE, N., DUDLEY, E. & NIGAM, Y. 2010. Amino acid derivatives from Lucilia sericata excretions/secretions may contribute to the beneficial effects of maggot therapy via increased angiogenesis. *British Journal of Dermatology,* 162**,** 554-562.

BEZEMER, J., RADERSMA, R., GRIJPMA, D., DIJKSTRA, P., FEIJEN, J. & VAN BLITTERSWIJK, C. 2000. Zero-order release of lysozyme from poly (ethylene glycol)/poly (butylene terephthalate) matrices. *Journal of Controlled Release,* 64**,** 179-192.

BHARDWAJ, N. & KUNDU, S. C. 2010. Electrospinning: a fascinating fiber fabrication technique. *Biotechnology advances,* 28**,** 325-347.

BHATTARAI, P., THAPA, K. B., BASNET, R. B. & SHARMA, S. 2014. Electrospinning: how to produce nanofibers using most inexpensive technique? An insight into the real challenges of electrospinning such nanofibers and its application areas. *International Journal of Biomedical and Advance Research,* 5**,** 401-405.

BISHAYEE, K., GHOSH, S., MUKHERJEE, A., SADHUKHAN, R., MONDAL, J. & KHUDA-BUKHSH, A. 2013. Quercetin induces cytochrome-c release and ROS accumulation to promote apoptosis and arrest the cell cycle in G2/M, in cervical carcinoma: signal cascade and drug-DNA interaction. *Cell proliferation,* 46**,** 153-163.

BOATENG, J. S., MATTHEWS, K. H., STEVENS, H. N. & ECCLESTON, G. M. 2008. Wound healing dressings and drug delivery systems: a review. *Journal of pharmaceutical sciences,* 97**,** 2892-2923.

BONVEHÍ, J. S. & GUTIÉRREZ, A. L. 2012. The antimicrobial effects of propolis collected in different regions in the Basque Country (Northern Spain). *World Journal of Microbiology and Biotechnology,* 28**,** 1351-1358.

BORSKA, S., CHMIELEWSKA, M., WYSOCKA, T., DRAG-ZALESINSKA, M., ZABEL, M. & DZIEGIEL, P. 2012. < i> In vitro</i> effect of quercetin on human gastric carcinoma: Targeting cancer cells death and MDR. *Food and Chemical Toxicology,* 50**,** 3375-3383.

BOUGHTON, E. & MCLENNAN, S. 2013. Biomimetic scaffolds for skin tissue and wound repair. *Biomimetic Biomaterials: Structure and Applications***,** 153.

BRADFORD, M. M. 1976. A rapid and sensitive method for the quantitation of microgram quantities of protein utilizing the principle of protein-dye binding. *Analytical biochemistry,* 72**,** 248-254.

BRAGHIROLLI, D. I., STEFFENS, D. & PRANKE, P. 2014. Electrospinning for regenerative medicine: a review of the main topics. *Drug discovery today,* 19**,** 743-753.

BREM, H. & TOMIC-CANIC, M. 2007. Cellular and molecular basis of wound healing in diabetes. *The Journal of clinical investigation,* 117**,** 1219-1222.

BRIGGS, T. & ARINZEH, T. L. 2014. Examining the formulation of emulsion electrospinning for improving the release of bioactive proteins from electrospun fibers. *Journal of Biomedical Materials Research Part A,* 102**,** 674-684.

BRITLAND, S., SMITH, A., FINTER, W., EAGLAND, D., VOWDEN, K., VOWDEN, P., TELFORD, G., BROWN, A. & PRITCHARD, D. 2011. Recombinant Lucilia sericata chymotrypsin in a topical hydrogel formulation degrades human wound eschar ex vivo. *Biotechnology progress,* 27**,** 870-874.

BROWN, A., HOROBIN, A., BLOUNT, D., HILL, P., ENGLISH, J., RICH, A., WILLIAMS, P. & PRITCHARD, D. 2012. Blow fly Lucilia sericata nuclease digests DNA associated with wound slough/eschar and with Pseudomonas aeruginosa biofilm. *Medical and veterinary entomology,* 26**,** 432-439.

BÚFALO, M. C., BORDON-GRACIANI, A. P., CONTI, B. J., ASSIS GOLIM, M. & SFORCIN, J. M. 2014. The immunomodulatory effect of propolis on receptors expression, cytokine production and fungicidal activity of human monocytes. *Journal of Pharmacy and Pharmacology,* 66**,** 1497-1504.

BUFALO, M. C., CANDEIAS, J. M. & SFORCIN, J. M. 2009. In vitro cytotoxic effect of Brazilian green propolis on human laryngeal epidermoid carcinoma (HEp-2) cells. *Evidence-Based Complementary and Alternative Medicine,* 6**,** 483-487.

BÚFALO, M. C., FERREIRA, I., COSTA, G., FRANCISCO, V., LIBERAL, J., CRUZ, M. T., LOPES, M. C., BATISTA, M. T. & SFORCIN, J. M. 2013. Propolis and its constituent caffeic acid suppress LPS-stimulated pro-inflammatory response by blocking NF-κB and MAPK activation in macrophages. *Journal of ethnopharmacology,* 149**,** 84-92.

BULZOMI, P., GALLUZZO, P., BOLLI, A., LEONE, S., ACCONCIA, F. & MARINO, M. 2012. The pro-apoptotic effect of quercetin in cancer cell lines requires ERβ-dependent signals. *Journal of cellular physiology,* 227**,** 1891-1898.

BUSCHLE-DILLER, G., COOPER, J., XIE, Z., WU, Y., WALDRUP, J. & REN, X. 2007. Release of antibiotics from electrospun bicomponent fibers. *Cellulose,* 14**,** 553-562.

BYE, F. J., BULLOCK, A. J., SINGH, R., SEFAT, F., ROMAN, S. & MACNEIL, S. 2014. Development of a basement membrane substitute incorporated into an electrospun scaffold for 3D skin tissue engineering. *Journal of Biomaterials and Tissue Engineering,* 4**,** 686-692.

CAI, J., YUE, Y., RUI, D., ZHANG, Y., LIU, S. & WU, C. 2011. Effect of chain length on cytotoxicity and endocytosis of cationic polymers. *Macromolecules,* 44**,** 2050-2057.

CAI, S., XU, H., JIANG, Q. & YANG, Y. 2013. Novel 3D electrospun scaffolds with fibers oriented randomly and evenly in three dimensions to closely mimic the unique architectures of extracellular matrices in soft tissues: fabrication and mechanism study. *Langmuir,* 29**,** 2311-2318.

CAIADO, F., CARVALHO, T., SILVA, F., CASTRO, C., CLODE, N., DYE, J. F. & DIAS, S. 2011. The role of fibrin E on the modulation of endothelial progenitors adhesion, differentiation and angiogenic growth factor production and the promotion of wound healing. *Biomaterials,* 32**,** 7096-7105.

CARMONA-RIBEIRO, A. M. & DE MELO CARRASCO, L. D. 2013. Cationic antimicrobial polymers and their assemblies. *International journal of molecular sciences,* 14**,** 9906-9946.

CARVALHO, R. S., GONÇALVES, V. M. M., FERREIRA, A. M., CARDOSO, S. M., SOBRAL, A. J., AGUIAR, C. A. & BALTAZAR, F. 2014. Antitumoral and antiangiogenic activity of Portuguese propolis in in vitro and in vivo models.
CASTRO, C., MURA, F., VALENZUELA, G., FIGUEROA, C., SALINAS, R., ZUÑIGA, M. C., TORRES, J. L., FUGUET, E. & DELPORTE, C. 2014. Identification of phenolic compounds by HPLC-ESI-MS/MS and antioxidant activity from Chilean propolis. *Food Research International,* 64**,** 873-879.
CAZANDER, G., PRITCHARD, D. I., NIGAM, Y., JUNG, W. & NIBBERING, P. H. 2013. Multiple actions of Lucilia sericata larvae in hard-to-heal wounds. *BioEssays,* 35**,** 1083-1092.
CESTA, D. 2011. The effect of salivary gland extract of Lucillia sericata maggots on the human dermal fibroblasts proliferation. *OnLine Journal of Biological Sciences,* 11**,** 96-100.
CHAMBERS, L., WOODROW, S., BROWN, A., HARRIS, P., PHILLIPS, D., HALL, M., CHURCH, J. & PRITCHARD, D. 2003. Degradation of extracellular matrix components by defined proteinases from the greenbottle larva Lucilia sericata used for the clinical debridement of non-healing wounds. *British Journal of Dermatology,* 148**,** 14-23.
CHAN, D. C., FONG, D. H., LEUNG, J. Y., PATIL, N. & LEUNG, G. K. 2007. Maggot debridement therapy in chronic wound care. *Hong Kong medical journal*.
CHAN, G. C.-F., CHEUNG, K.-W. & SZE, D. M.-Y. 2013. The immunomodulatory and anticancer properties of propolis. *Clinical reviews in allergy & immunology,* 44**,** 262-273.
CHANG, H.-I. & WANG, Y. 2011. *Cell responses to surface and architecture of tissue engineering scaffolds*, INTECH Open Access Publisher.
CHEN, F.-M., ZHANG, M. & WU, Z.-F. 2010. Toward delivery of multiple growth factors in tissue engineering. *Biomaterials,* 31**,** 6279-6308.
CHEN, M., PATRA, P. K., LOVETT, M. L., KAPLAN, D. L. & BHOWMICK, S. 2009. Role of electrospun fibre diameter and corresponding specific surface area (SSA) on cell attachment. *Journal of tissue engineering and regenerative medicine,* 3**,** 269-279.
CHEN, M., PATRA, P. K., WARNER, S. B. & BHOWMICK, S. 2007. Role of fiber diameter in adhesion and proliferation of NIH 3T3 fibroblast on electrospun polycaprolactone scaffolds. *Tissue Engineering,* 13**,** 579-587.
CHENG, H., QIN, Z. H., GUO, X. F., HU, X. S. & WU, J. H. 2013. Geographical origin identification of propolis using GC–MS and electronic nose combined with principal component analysis. *Food Research International,* 51**,** 813-822.
CHEUNG, K.-W., SZE, D. M.-Y., CHAN, W. K., DENG, R.-X., TU, W. & CHAN, G. C.-F. 2011. Brazilian green propolis and its constituent, Artepillin C inhibits allogeneic activated human CD4 T cells expansion and activation. *Journal of Ethnopharmacology,* 138**,** 463-471.
CHISCA, S., BARZIC, A. I., SAVA, I., OLARU, N. & BRUMA, M. 2012. Morphological and rheological insights on polyimide chain entanglements for electrospinning produced fibers. *The Journal of Physical Chemistry B,* 116**,** 9082-9088.
CHO LEE, A.-R., LEEM, H., LEE, J. & CHAN PARK, K. 2005. Reversal of silver sulfadiazine-impaired wound healing by epidermal growth factor. *Biomaterials,* 26**,** 4670-4676.
CHO, S. J., JUNG, S. M., KANG, M., SHIN, H. S. & YOUK, J. H. 2015. Preparation of hydrophilic PCL nanofiber scaffolds via electrospinning of PCL/PVP-b-PCL block copolymers for enhanced cell biocompatibility. *Polymer,* 69**,** 95-102.
CHOI, J. S., LEONG, K. W. & YOO, H. S. 2008. In vivo wound healing of diabetic ulcers using electrospun nanofibers immobilized with human epidermal growth factor (EGF). *Biomaterials,* 29**,** 587-596.
CHOI, S. M., KANG, H. Y., MIN, H.-J., LEE, R., IKRAM, M., SUBHAN, F., JIN, S. W., JEONG, Y. H., KWAK, J.-Y. & YOON, S. 2015. Bioactive fish collagen/polycaprolactone composite nanofibrous scaffolds fabricated by electrospinning for 3D cell culture. *Journal of biotechnology,* 205**,** 47-58.
CHONG, E., PHAN, T., LIM, I., ZHANG, Y., BAY, B., RAMAKRISHNA, S. & LIM, C. 2007a. Evaluation of electrospun PCL/gelatin nanofibrous scaffold for wound healing and layered dermal reconstitution. *Acta biomaterialia,* 3**,** 321-330.
CHONG, E. J., PHAN, T. T., LIM, I. J., ZHANG, Y. Z., BAY, B. H., RAMAKRISHNA, S. & LIM, C. T. 2007b. Evaluation of electrospun PCL/gelatin nanofibrous

scaffold for wound healing and layered dermal reconstitution. *Acta Biomaterialia,* 3**,** 321-330.
CHOW, J.-M., SHEN, S.-C., HUAN, S. K., LIN, H.-Y. & CHEN, Y.-C. 2005. Quercetin, but not rutin and quercitrin, prevention of H 2 O 2-induced apoptosis via anti-oxidant activity and heme oxygenase 1 gene expression in macrophages. *Biochemical pharmacology,* 69**,** 1839-1851.
CHU, Y., YU, D., WANG, P., XU, J., LI, D. & DING, M. 2010. Nanotechnology promotes the full-thickness diabetic wound healing effect of recombinant human epidermal growth factor in diabetic rats. *Wound Repair and Regeneration,* 18**,** 499-505.
CHUA, L. S. 2013. A review on plant-based rutin extraction methods and its pharmacological activities. *Journal of ethnopharmacology,* 150**,** 805-817.
CIPITRIA, A., SKELTON, A., DARGAVILLE, T., DALTON, P. & HUTMACHER, D. 2011. Design, fabrication and characterization of PCL electrospun scaffolds—a review. *Journal of Materials Chemistry,* 21**,** 9419-9453.
CRAMARIUC, B., CRAMARIUC, R., SCARLET, R., MANEA, L. R., LUPU, I. G. & CRAMARIUC, O. 2013. Fiber diameter in electrospinning process. *Journal of Electrostatics,* 71**,** 189-198.
CUSHNIE, T. & LAMB, A. J. 2005. Antimicrobial activity of flavonoids. *International journal of antimicrobial agents,* 26**,** 343-356.
DA SILVA, F. L. B., LUND, M., JÖNSSON, B. & ÅKESSON, T. 2006. On the complexation of proteins and polyelectrolytes. *The Journal of Physical Chemistry B,* 110**,** 4459-4464.
DA SILVA FROZZA, C. O., GARCIA, C. S. C., GAMBATO, G., DE SOUZA, M. D. O., SALVADOR, M., MOURA, S., PADILHA, F. F., SEIXAS, F. K., COLLARES, T. & BORSUK, S. 2013a. Chemical characterization, antioxidant and cytotoxic activities of Brazilian red propolis. *Food and Chemical Toxicology,* 52**,** 137-142.
DA SILVA FROZZA, C. O., GARCIA, C. S. C., GAMBATO, G., DE SOUZA, M. D. O., SALVADOR, M., MOURA, S., PADILHA, F. F., SEIXAS, F. K., COLLARES, T., BORSUK, S., DELLAGOSTIN, O. A., HENRIQUES, J. A. P. & ROESCH-ELY, M. 2013b. Chemical characterization, antioxidant and cytotoxic activities of Brazilian red propolis. *Food and Chemical Toxicology,* 52**,** 137-142.
DALEPRANE, J. B. & ABDALLA, D. S. 2013. Emerging Roles of Propolis: Antioxidant, Cardioprotective, and Antiangiogenic Actions. *Evidence-Based Complementary and Alternative Medicine,* 2013.
DARLENSKI, R., KAZANDJIEVA, J. & TSANKOV, N. 2011. Skin barrier function: morphological basis and regulatory mechanisms. *J. Clin. Med,* 4**,** 36-45.
DASH, T. K. & KONKIMALLA, V. B. 2012. Polymeric modification and its implication in drug delivery: poly-ε-caprolactone (PCL) as a model polymer. *Molecular pharmaceutics,* 9**,** 2365-2379.
DAVYDOV, L. 2011. Maggot therapy in wound management in modern era and a review of published literature. *Journal of pharmacy practice,* 24**,** 89-93.
DE ALMEIDA, E. B., CORDEIRO CARDOSO, J., KARLA DE LIMA, A., DE OLIVEIRA, N. L., DE PONTES-FILHO, N. T., OLIVEIRA LIMA, S., LEAL SOUZA, I. C. & DE ALBUQUERQUE-JÚNIOR, R. L. C. 2013. The incorporation of Brazilian propolis into collagen-based dressing films improves dermal burn healing. *Journal of Ethnopharmacology,* 147**,** 419-425.
DE CASTRO, P. A., SAVOLDI, M., BONATTO, D., BARROS, M. H., GOLDMAN, M. H. S., BERRETTA, A. A. & GOLDMAN, G. H. 2011. Molecular characterization of propolis-induced cell death in Saccharomyces cerevisiae. *Eukaryotic Cell,* 10**,** 398-411.
DE FUNARI, C. S., DE OLIVEIRA FERRO, V. & MATHOR, M. B. 2007. Analysis of propolis from< i> Baccharis dracunculifolia</i> DC.(Compositae) and its effects on mouse fibroblasts. *Journal of ethnopharmacology,* 111**,** 206-212.
DEL GAUDIO, C., BIANCO, A., FOLIN, M., BAIGUERA, S. & GRIGIONI, M. 2009. Structural characterization and cell response evaluation of electrospun PCL membranes: micrometric versus submicrometric fibers. *Journal of Biomedical Materials Research Part A,* 89**,** 1028-1039.
DELAVARY, B. M., VAN DER VEER, W. M., VAN EGMOND, M., NIESSEN, F. B. & BEELEN, R. H. 2011. Macrophages in skin injury and repair. *Immunobiology,* 216**,** 753-762.

DEMIDOVA-RICE, T. N., HAMBLIN, M. R. & HERMAN, I. M. 2012a. Acute and impaired wound healing: pathophysiology and current methods for drug delivery, part 1: normal and chronic wounds: biology, causes, and approaches to care. *Advances in skin & wound care,* 25**,** 304.

DEMIDOVA-RICE, T. N., HAMBLIN, M. R. & HERMAN, I. M. 2012b. Acute and impaired wound healing: pathophysiology and current methods for drug delivery, part 2: role of growth factors in normal and pathological wound healing: therapeutic potential and methods of delivery. *Advances in skin & wound care,* 25**,** 349.

DHAR, S., GU, F. X., LANGER, R., FAROKHZAD, O. C. & LIPPARD, S. J. 2008. Targeted delivery of cisplatin to prostate cancer cells by aptamer functionalized Pt (IV) prodrug-PLGA–PEG nanoparticles. *Proceedings of the National Academy of Sciences,* 105**,** 17356-17361.

DIASA, J. R., ANTUNESB, F. E. & BÁRTOLOA, P. J. 2013. Influence of the rheological behaviour in electrospun PCL nanofibres production for tissue engineering applications. *CHEMICAL ENGINEERING,* 32.

DIEGELMANN, R. F. & EVANS, M. C. 2004. Wound healing: an overview of acute, fibrotic and delayed healing. *Front Biosci,* 9**,** 283-289.

DOMINGOS, M., INTRANUOVO, F., GLORIA, A., GRISTINA, R., AMBROSIO, L., BÁRTOLO, P. & FAVIA, P. 2013. Improved osteoblast cell affinity on plasma-modified 3-D extruded PCL scaffolds. *Acta biomaterialia,* 9**,** 5997-6005.

DOTA, K. F. D., CONSOLARO, M. E. L., SVIDZINSKI, T. I. E. & BRUSCHI, M. L. 2011. Antifungal activity of Brazilian propolis microparticles against yeasts isolated from vulvovaginal candidiasis. *Evidence-Based Complementary and Alternative Medicine,* 2011.

DRAGO, L., DE VECCHI, E., NICOLA, L. & GISMONDO, M. 2007. In vitro antimicrobial activity of a novel propolis formulation (Actichelated propolis). *Journal of applied microbiology,* 103**,** 1914-1921.

DRIVER, V. R., FABBI, M., LAVERY, L. A. & GIBBONS, G. 2010. The costs of diabetic foot: the economic case for the limb salvage team. *Journal of vascular surgery,* 52**,** 17S-22S.

DUMVILLE, J. C., WORTHY, G., BLAND, J. M., CULLUM, N., DOWSON, C., IGLESIAS, C., MITCHELL, J. L., NELSON, E. A., SOARES, M. O. & TORGERSON, D. J. 2009. Larval therapy for leg ulcers (VenUS II): randomised controlled trial. *Bmj,* 338**,** b773.

DURAN, V., MATIC, M., JOVANOVĆ, M., MIMICA, N., GAJINOV, Z., POLJACKI, M. & BOZA, P. 2004. Results of the clinical examination of an ointment with marigold (Calendula officinalis) extract in the treatment of venous leg ulcers. *International journal of tissue reactions,* 27**,** 101-106.

DURMAZ, Y. Y., LIN, Y. L. & ELSAYED, M. E. 2013. Development of Degradable, pH-Sensitive Star Vectors for Enhancing the Cytoplasmic Delivery of Nucleic Acids. *Advanced Functional Materials,* 23**,** 3885-3895.

ELAMURUGAN, T., JAGDISH, S., KATE, V. & CHANDRA PARIJA, S. 2011. Role of bone biopsy specimen culture in the management of diabetic foot osteomyelitis. *International Journal of Surgery,* 9**,** 214-216.

EMING, S. A., KRIEG, T. & DAVIDSON, J. M. 2007. Inflammation in wound repair: molecular and cellular mechanisms. *Journal of Investigative Dermatology,* 127**,** 514-525.

ERAL, H. & OH, J. 2013. Contact angle hysteresis: a review of fundamentals and applications. *Colloid and polymer science,* 291**,** 247-260.

ERENCIA, M., CANO, F., TORNERO, J. A., MACANAS, J. & CARRILLO, F. 2014. Resolving the electrospinnability zones and diameter prediction for the electrospinning of the gelatin/water/acetic acid system. *Langmuir,* 30**,** 7198-7205.

ERNST, O. & ZOR, T. 2010. Linearization of the bradford protein assay. *JoVE (Journal of Visualized Experiments)***,** e1918-e1918.

EVANS, N. D., OREFFO, R. O. C., HEALY, E., THURNER, P. J. & MAN, Y. H. 2013. Epithelial mechanobiology, skin wound healing, and the stem cell niche. *Journal of the Mechanical Behavior of Biomedical Materials,* 28**,** 397-409.

FAIRBANKS, B. D., GUNATILLAKE, P. A. & MEAGHER, L. 2015. Biomedical applications of polymers derived by reversible addition – fragmentation chain-transfer (RAFT). *Advanced Drug Delivery Reviews,* 91**,** 141-152.

FALANGA, V. 2005. Wound healing and its impairment in the diabetic foot. *The Lancet,* 366**,** 1736-1743.
FAROOQUI, T. & FAROOQUI, A. A. 2012. Beneficial effects of propolis on human health and neurological diseases. *Front Biosci (Elite Ed),* 4**,** 779-793.
FARRUGIA, B. L., BROWN, T. D., UPTON, Z., HUTMACHER, D. W., DALTON, P. D. & DARGAVILLE, T. R. 2013. Dermal fibroblast infiltration of poly (ε-caprolactone) scaffolds fabricated by melt electrospinning in a direct writing mode. *Biofabrication,* 5**,** 025001.
FONG, J. & WOOD, F. 2006. Nanocrystalline silver dressings in wound management: a review. *international Journal of Nanomedicine,* 1**,** 441.
FRANCINI, N., PURDIE, L., ALEXANDER, C., MANTOVANI, G. & SPAIN, S. G. 2015. Multifunctional poly [N-(2-hydroxypropyl) methacrylamide] copolymers via postpolymerization modification and sequential thiol–ene chemistry. *Macromolecules,* 48**,** 2857-2863.
FRANCIS, L., MENG, D., KNOWLES, J. C., ROY, I. & BOCCACCINI, A. R. 2010. Multi-functional P(3HB) microsphere/45S5 Bioglass®-based composite scaffolds for bone tissue engineering. *Acta Biomaterialia,* 6**,** 2773-2786.
GADKARI, S. B. 2014. Scaling analysis for electrospinning. *SpringerPlus,* 3**,** 705.
GANGULI, S., YOSHIMOTO, K., TOMITA, S., SAKUMA, H., MATSUOKA, T., SHIRAKI, K. & NAGASAKI, Y. 2009. Regulation of lysozyme activity based on thermotolerant protein/smart polymer complex formation. *Journal of the American Chemical Society,* 131**,** 6549-6553.
GAUTAM, S., DINDA, A. K. & MISHRA, N. C. 2013. Fabrication and characterization of PCL/gelatin composite nanofibrous scaffold for tissue engineering applications by electrospinning method. *Materials Science and Engineering: C,* 33**,** 1228-1235.
GAZZARRI, M., BARTOLI, C., MOTA, C., PUPPI, D., DINUCCI, D., VOLPI, S. & CHIELLINI, F. 2013. Fibrous star poly (ε-caprolactone) melt-electrospun scaffolds for wound healing applications. *Journal of Bioactive and Compatible Polymers,* 28**,** 492-507.
GELAIN, F., UNSWORTH, L. D. & ZHANG, S. 2010. Slow and sustained release of active cytokines from self-assembling peptide scaffolds. *Journal of Controlled Release,* 145**,** 231-239.
GHASEMI-MOBARAKEH, L., MORSHED, M., KARBALAIE, K., FESHARAKI, M.-A., NEMATALLAHI, M., NASR-ESFAHANI, M.-H. & BAHARVAND, H. 2009. The thickness of electrospun poly (epsilon-caprolactone) nanofibrous scaffolds influences cell proliferation. *Int J Artif Organs,* 32**,** 150-8.
GIGLIOBIANCO, G., CHONG, C. K. & MACNEIL, S. 2015. Simple surface coating of electrospun poly-L-lactic acid scaffolds to induce angiogenesis. *Journal of biomaterials applications,* 30**,** 50-60.
GOLEBIEWSKA, E. M. & POOLE, A. W. 2014. Platelet secretion: From haemostasis to wound healing and beyond. *Blood Reviews*.
GONG, C., WU, Q., WANG, Y., ZHANG, D., LUO, F., ZHAO, X., WEI, Y. & QIAN, Z. 2013. A biodegradable hydrogel system containing curcumin encapsulated in micelles for cutaneous wound healing. *Biomaterials,* 34**,** 6377-6387.
GOU, M., MEN, K., SHI, H., XIANG, M., ZHANG, J., SONG, J., LONG, J., WAN, Y., LUO, F. & ZHAO, X. 2011. Curcumin-loaded biodegradable polymeric micelles for colon cancer therapy in vitro and in vivo. *Nanoscale,* 3**,** 1558-1567.
GOU, M. L., HUANG, M. J., GOU, M. L., HUANG, M. J., QIAN, Z. Y., GOU, M. L., HUANG, M. J., QIAN, Z. Y., YANG, L. & GOU, M. L. 2007. Preparation of anionic poly (ε-caprolactone)-poly (ethylene glycol)-poly (ε-caprolactone) copolymeric nanoparticles as basic protein antigen carrier. *Growth Factors,* 25**,** 202-208.
GOWDA, S., WEINSTEIN, D. A., BLALOCK, T. D., GANDHI, K., MAST, B. A., CHIN, G. & SCHULTZ, G. S. 2013. Topical application of recombinant platelet-derived growth factor increases the rate of healing and the level of proteins that regulate this response. *International wound journal*.
GRAY, D., ACTON, C., CHADWICK, P., FUMAROLA, S., LEAPER, D., MORRIS, C., STANG, D., VOWDEN, K., VOWDEN, P. & YOUNG, T. 2011. Consensus guidance for the use of debridement techniques in the UK. *Wounds UK,* 7**,** 77-84.
GREAVES, N. S., ASHCROFT, K. J., BAGUNEID, M. & BAYAT, A. 2013. Current understanding of molecular and cellular mechanisms in fibroplasia and

angiogenesis during acute wound healing. *Journal of dermatological science,* 72**,** 206-217.
GRIEB, G., STEFFENS, G., PALLUA, N., BERNHAGEN, J. & BUCALA, R. 2011. Circulating fibrocytes–biology and mechanisms in wound healing and scar formation. *Int Rev Cell Mol Biol,* 291**,** 1-19.
GUO, S. & DIPIETRO, L. A. 2010a. Factors affecting wound healing. *Journal of dental research,* 89**,** 219-229.
GUO, S. A. & DIPIETRO, L. A. 2010b. Factors affecting wound healing. *Journal of dental research,* 89**,** 219-229.
GUPTA, B., AGARWAL, R. & ALAM, M. 2010. Textile-based smart wound dressings.
GUPTA, R. K. 2000. *Polymer and composite rheology*, CRC Press.
HAN, X., CHEN, B. & CHEN, P. 2014. Self/co-assembling, cell penetrating peptides—a promising siRNAdelivery system. *Austin J Nanomed Nanotechnol,* 2**,** 1008.
HARPER, D., YOUNG, A. & MCNAUGHT, C.-E. 2014. The physiology of wound healing. *Surgery (Oxford)*.
HARRIS, J. M. 2013. *Poly (ethylene glycol) chemistry: biotechnical and biomedical applications*, Springer Science & Business Media.
HARRIS, L. G., BEXFIELD, A., NIGAM, Y., ROHDE, H., RATCLIFFE, N. A. & MACK, D. 2009. Disruption of Staphylococcus epidermidis biofilms by medicinal maggot Lucilia sericata excretions/secretions. *The International journal of artificial organs,* 32**,** 555-564.
HE, M., XUE, J., GENG, H., GU, H., CHEN, D., SHI, R. & ZHANG, L. 2015. Fibrous guided tissue regeneration membrane loaded with anti-inflammatory agent prepared by coaxial electrospinning for the purpose of controlled release. *Applied Surface Science,* 335**,** 121-129.
HENSHAW, F., BOLTON, T., NUBE, V., HOOD, A., VELDHOEN, D., PFRUNDER, L., MCKEW, G., MACLEOD, C., MCLENNAN, S. & TWIGG, S. 2014. Topical application of the bee hive protectant propolis is well tolerated and improves human diabetic foot ulcer healing in a prospective feasibility study. *Journal of diabetes and its complications*.
HILE, C. & VEVES, A. 2005. Microcirculation of the diabetic foot. *Diabetes and Cardiovascular Disease.* Springer.
HOCKING, A. M. & GIBRAN, N. S. 2010. Mesenchymal stem cells: paracrine signaling and differentiation during cutaneous wound repair. *Experimental cell research,* 316**,** 2213-2219.
HOQUE, M. E., MENG, T. T. H., CHUAN, Y. L., CHOWDHURY, M. & PRASAD, R. 2014. Fabrication and characterization of hybrid PCL/PEG 3D scaffolds for potential tissue engineering applications. *Materials Letters,* 131**,** 255-258.
HORI, J. I., ZAMBONI, D. S., CARRÃO, D. B., GOLDMAN, G. H. & BERRETTA, A. A. 2013. The Inhibition of Inflammasome by Brazilian Propolis (EPP-AF). *Evidence-Based Complementary and Alternative Medicine,* 2013.
HOROBIN, A., SHAKESHEFF, K., WOODROW, S., ROBINSON, C. & PRITCHARD, D. 2003. Maggots and wound healing: an investigation of the effects of secretions from Lucilia sericata larvae upon interactions between human dermal fibroblasts and extracellular matrix components. *British Journal of Dermatology,* 148**,** 923-933.
HOROBIN, A. J., SHAKESHEFF, K. M. & PRITCHARD, D. I. 2005. Maggots and wound healing: an investigation of the effects of secretions from Lucilia sericata larvae upon the migration of human dermal fibroblasts over a fibronectin-coated surface. *Wound repair and regeneration,* 13**,** 422-433.
HOROBIN, A. J., SHAKESHEFF, K. M. & PRITCHARD, D. I. 2006. Promotion of human dermal fibroblast migration, matrix remodelling and modification of fibroblast morphology within a novel 3D model by Lucilia sericata larval secretions. *Journal of Investigative Dermatology,* 126**,** 1410-1418.
HUANG, C., CHEN, R., KE, Q., MORSI, Y., ZHANG, K. & MO, X. 2011. Electrospun collagen–chitosan–TPU nanofibrous scaffolds for tissue engineered tubular grafts. *Colloids and Surfaces B: Biointerfaces,* 82**,** 307-315.
HUANG, M. H., LI, S., HUTMACHER, D. W., SCHANTZ, J. T., VACANTI, C. A., BRAUD, C. & VERT, M. 2004. Degradation and cell culture studies on block copolymers prepared by ring opening polymerization of ϵ-caprolactone in the presence of poly (ethylene glycol). *Journal of Biomedical Materials Research Part A,* 69**,** 417-427.

IIZAKA, S., SUGAMA, J., NAKAGAMI, G., KAITANI, T., NAITO, A., KOYANAGI, H., MATSUO, J., KADONO, T., KONYA, C. & SANADA, H. 2011. Concurrent validation and reliability of digital image analysis of granulation tissue color for clinical pressure ulcers. *Wound Repair and Regeneration,* 19**,** 455-463.

INPANYA, P., FAIKRUA, A., OUNAROON, A., SITTICHOKECHAIWUT, A. & VIYOCH, J. 2012. Effects of the blended fibroin/aloe gel film on wound healing in streptozotocin-induced diabetic rats. *Biomedical Materials,* 7**,** 035008.

IORIO, M. L., GOLDSTEIN, J., ADAMS, M., STEINBERG, J. & ATTINGER, C. 2011. Functional limb salvage in the diabetic patient: the use of a collagen bilayer matrix and risk factors for amputation. *Plastic and reconstructive surgery,* 127**,** 260-267.

ISIDOROV, V. A., SZCZEPANIAK, L. & BAKIER, S. 2014. Rapid GC/MS determination of botanical precursors of Eurasian propolis. *Food Chemistry,* 142**,** 101-106.

JACKSON, W. M., NESTI, L. J. & TUAN, R. S. 2012. Concise review: clinical translation of wound healing therapies based on mesenchymal stem cells. *Stem cells translational medicine,* 1**,** 44-50.

JAEGER, W., BOHRISCH, J. & LASCHEWSKY, A. 2010. Synthetic polymers with quaternary nitrogen atoms—Synthesis and structure of the most used type of cationic polyelectrolytes. *Progress in Polymer Science,* 35**,** 511-577.

JAMNONGKAN, T., SHIROTA, R., SUKUMARAN, S. K., SUGIMOTO, M. & KOYAMA, K. 2014. Effect of ZnO nanoparticles on the electrospinning of poly (vinyl alcohol) from aqueous solution: influence of particle size. *Polymer Engineering & Science,* 54**,** 1969-1975.

JEFFCOATE, W., PRICE, P., PHILLIPS, C., GAME, F., MUDGE, E., DAVIES, S., AMERY, C., EDMONDS, M., GIBBY, O. & JOHNSON, A. 2009. *Randomised controlled trial of the use of three dressing preparations in the management of chronic ulceration of the foot in diabetes*, Prepress Projects Limited.

JEONG, J. H., LIM, D. W., HAN, D. K. & PARK, T. G. 2000. Synthesis, characterization and protein adsorption behaviors of PLGA/PEG di-block co-polymer blend films. *Colloids and Surfaces B: Biointerfaces,* 18**,** 371-379.

JEONG SOON, J., SO YEON, K., SANG BONG, L., KYUNG OK, K., JOONG SOO, H. & YOUNG MOO, L. 2006. Poly(ethylene glycol)/poly(ε-caprolactone) diblock copolymeric nanoparticles for non-viral gene delivery: The role of charge group and molecular weight in particle formation, cytotoxicity and transfection. *Journal of Controlled Release,* 113**,** 173-182.

JI, W., YANG, F., VAN DEN BEUCKEN, J. J. J. P., BIAN, Z., FAN, M., CHEN, Z. & JANSEN, J. A. 2010. Fibrous scaffolds loaded with protein prepared by blend or coaxial electrospinning. *Acta Biomaterialia,* 6**,** 4199-4207.

JIANG, C.-P., HUANG, J.-R. & HSIEH, M.-F. 2011. Fabrication of synthesized PCL-PEG-PCL tissue engineering scaffolds using an air pressure-aided deposition system. *Rapid Prototyping Journal,* 17**,** 288-297.

JIANG, Y.-C., JIANG, L., HUANG, A., WANG, X.-F., LI, Q. & TURNG, L.-S. 2017. Electrospun polycaprolactone/gelatin composites with enhanced cell–matrix interactions as blood vessel endothelial layer scaffolds. *Materials Science and Engineering: C,* 71**,** 901-908.

JIN, G., PRABHAKARAN, M. P., KAI, D. & RAMAKRISHNA, S. 2013. Controlled release of multiple epidermal induction factors through core–shell nanofibers for skin regeneration. *European Journal of Pharmaceutics and Biopharmaceutics,* 85**,** 689-698.

JONES, J. 2005. Winter's concept of moist wound healing: a review of the evidence and impact on clinical practice. *Journal of wound care,* 14**,** 273-276.

KAMBUROGLU, K. & ÖZEN, T. 2011. Analgesic effect of Anatolian propolis in mice. *Ağrı: Ağrı (Algoloji) Derneği'nin Yayın organıdır= The journal of the Turkish Society of Algology,* 23**,** 47.

KANT, V., GOPAL, A., PATHAK, N. N., KUMAR, P., TANDAN, S. K. & KUMAR, D. 2014. Antioxidant and anti-inflammatory potential of curcumin accelerated the cutaneous wound healing in streptozotocin-induced diabetic rats. *International Immunopharmacology,* 20**,** 322-330.

KARAHALILOĞLU, Z., ERCAN, B., CHUNG, S., TAYLOR, E., DENKBAŞ, E. B. & WEBSTER, T. J. 2014. Nanostructured anti-bacterial poly-lactic-co-glycolic acid films for skin tissue engineering applications. *Journal of Biomedical Materials Research Part A,* 102**,** 4598-4608.

KATARIA, K., GUPTA, A., RATH, G., MATHUR, R. & DHAKATE, S. 2014. In vivo wound healing performance of drug loaded electrospun composite nanofibers transdermal patch. *International journal of pharmaceutics,* 469**,** 102-110.
KEMPF, M., MIYAMURA, Y., LIU, P.-Y., CHEN, A. C.-H., NAKAMURA, H., SHIMIZU, H., TABATA, Y., KIMBLE, R. M. & MCMILLAN, J. R. 2011. A denatured collagen microfiber scaffold seeded with human fibroblasts and keratinocytes for skin grafting. *Biomaterials,* 32**,** 4782-4792.
KERR, M. 2012. Foot care for people with diabetes: the economic case for change. *NHS Diabetes*.
KHORSHIDI, S., SOLOUK, A., MIRZADEH, H., MAZINANI, S., LAGARON, J. M., SHARIFI, S. & RAMAKRISHNA, S. 2016. A review of key challenges of electrospun scaffolds for tissue-engineering applications. *Journal of tissue engineering and regenerative medicine,* 10**,** 715-738.
KI, C. S., BAEK, D. H., GANG, K. D., LEE, K. H., UM, I. C. & PARK, Y. H. 2005. Characterization of gelatin nanofiber prepared from gelatin–formic acid solution. *Polymer,* 46**,** 5094-5102.
KIM, J. I., PANT, H. R., SIM, H.-J., LEE, K. M. & KIM, C. S. 2014a. Electrospun propolis/polyurethane composite nanofibers for biomedical applications. *Materials Science and Engineering: C*.
KIM, M. S., PARK, S. J., GU, B. K. & KIM, C.-H. 2012. Polycaprolactone-chitin nanofibrous mats as potential scaffolds for tissue engineering. *Journal of Nanomaterials,* 2012**,** 10.
KIM, S. E., YUN, Y.-P., HAN, Y.-K., LEE, D.-W., OHE, J.-Y., LEE, B.-S., SONG, H.-R., PARK, K. & CHOI, B.-J. 2014b. Osteogenesis induction of periodontal ligament cells onto bone morphogenic protein-2 immobilized PCL fibers. *Carbohydrate polymers,* 99**,** 700-709.
KIM, T. G., LEE, D. S. & PARK, T. G. 2007. Controlled protein release from electrospun biodegradable fiber mesh composed of poly (ε-caprolactone) and poly (ethylene oxide). *International journal of pharmaceutics,* 338**,** 276-283.
KOŁBUK, D., SAJKIEWICZ, P., MANIURA-WEBER, K. & FORTUNATO, G. 2013. Structure and morphology of electrospun polycaprolactone/gelatine nanofibres. *European Polymer Journal,* 49**,** 2052-2061.
KORHONEN, J. T., HUHTAMÄKI, T., IKKALA, O. & RAS, R. H. 2013. Reliable measurement of the receding contact angle. *Langmuir,* 29**,** 3858-3863.
KOZLOWSKI, L. P. 2016. IPC–Isoelectric Point Calculator. *Biology direct,* 11**,** 55.
KOZMA, E. M. 2013. Propolis induces chondroitin/dermatan sulphate and hyaluronic acid accumulation in the skin of burned wound. *Evidence-Based Complementary and Alternative Medicine,* 2013.
KRAFT, R., HERNDON, D. N., FINNERTY, C. C., COX, R. A., SONG, J. & JESCHKE, M. G. 2014. Predictive Value of IL-8 for Sepsis and Severe Infections After Burn Injury-A Clinical Study. *Shock*.
KRAMER, N., WALZL, A., UNGER, C., ROSNER, M., KRUPITZA, G., HENGSTSCHLÄGER, M. & DOLZNIG, H. 2013. In vitro cell migration and invasion assays. *Mutation Research/Reviews in Mutation Research,* 752**,** 10-24.
KROEZE, K. L., BOINK, M. A., SAMPAT-SARDJOEPERSAD, S. C., WAAIJMAN, T., SCHEPER, R. J. & GIBBS, S. 2011. Autocrine regulation of re-epithelialization after wounding by chemokine receptors CCR1, CCR10, CXCR1, CXCR2, and CXCR3. *Journal of Investigative Dermatology,* 132**,** 216-225.
KUCHARZEWSKI, M., KUBACKA, S., URBANEK, T., WILEMSKA-KUCHARZEWSKA, K. & MORAWIEC, T. 2013. Stan Scheller: the forerunner of clinical studies on using propolis for poor and chronic nonhealing wounds. *Evidence-Based Complementary and Alternative Medicine,* 2013.
KÜHN, J., SHAFFER, E., MENA, J., BRETON, B., PARENT, J., RAPPAZ, B., CHAMBON, M., EMERY, Y., MAGISTRETTI, P. & DEPEURSINGE, C. 2013. Label-free cytotoxicity screening assay by digital holographic microscopy. *Assay and drug development technologies,* 11**,** 101-107.
KUMAZAKI, M., SHINOHARA, H., TANIGUCHI, K., YAMADA, N., OHTA, S., ICHIHARA, K. & AKAO, Y. 2014. Propolis cinnamic acid derivatives induce apoptosis through both extrinsic and intrinsic apoptosis signaling pathways and modulate of miRNA expression. *Phytomedicine,* 21**,** 1070-1077.

KUROPATNICKI, A. K., SZLISZKA, E. & KROL, W. 2013. Historical aspects of propolis research in modern times. *Evidence-Based Complementary and Alternative Medicine,* 2013.
KURPINSKI, K. T., STEPHENSON, J. T., JANAIRO, R. R. R., LEE, H. & LI, S. 2010. The effect of fiber alignment and heparin coating on cell infiltration into nanofibrous PLLA scaffolds. *Biomaterials,* 31**,** 3536-3542.
KUZELOVA KOSTAKOVA, E., MESZAROS, L., MASKOVA, G., BLAZKOVA, L., TURCSAN, T. & LUKAS, D. 2017. Crystallinity of Electrospun and Centrifugal Spun Polycaprolactone Fibers: A Comparative Study. *Journal of Nanomaterials,* 2017.
LA FONTAINE, J., BHAVAN, K., TALAL, T. K. & LAVERY, L. A. 2014. Current concepts in the surgical management of acute diabetic foot infections. *The Foot,* 24**,** 123-127.
LAM, C. X., TEOH, S. H. & HUTMACHER, D. W. 2007. Comparison of the degradation of polycaprolactone and polycaprolactone–(β-tricalcium phosphate) scaffolds in alkaline medium. *Polymer international,* 56**,** 718-728.
LEAPER, D. 2011. Debridement methods of non-viable tissue in wounds. *Advanced wound repair therapies***,** 606.
LEE, K., SILVA, E. A. & MOONEY, D. J. 2011. Growth factor delivery-based tissue engineering: general approaches and a review of recent developments. *Journal of The Royal Society Interface,* 8**,** 153-170.
LEE, M., CHEN, T. T., IRUELA-ARISPE, M. L., WU, B. M. & DUNN, J. C. Y. 2007. Modulation of protein delivery from modular polymer scaffolds. *Biomaterials,* 28**,** 1862-1870.
LEPPINIEMI, J. & HYTÖNEN, V. 2016. Therapeutic proteins in bioactive materials for wound healing. *Bioinspired Materials for Medical Applications***,** 273.
LEUNG, V., HARTWELL, R., YANG, H., GHAHARY, A. & KO, F. 2011. Bioactive nanofibres for wound healing applications. *J Fiber Bioeng Informat,* 4**,** 1-14.
LEVERE, M. E., PASCUAL, S., MONTEMBAULT, V., CASSE, N., CARUSO, A. & FONTAINE, L. 2013. Thermoresponsive block copolymers containing reactive azlactone groups and their bioconjugation with lysozyme. *Polymer Chemistry,* 4**,** 675-685.
LI, C., YUAN, W., JIANG, H., LI, J., XU, F., YANG, W. & MA, J. 2011. PCL film surfaces conjugated with P (DMAEMA)/gelatin complexes for improving cell immobilization and gene transfection. *Bioconjugate chemistry,* 22**,** 1842-1851.
LI, D., WU, T., HE, N., WANG, J., CHEN, W., HE, L., HUANG, C., EI-HAMSHARY, H. A., AL-DEYAB, S. S. & KE, Q. 2014. Three-dimensional polycaprolactone scaffold via needleless electrospinning promotes cell proliferation and infiltration. *Colloids and Surfaces B: Biointerfaces,* 121**,** 432-443.
LIAO, H., ZAKHALEVA, J. & CHEN, W. 2009. Cells and tissue interactions with glycated collagen and their relevance to delayed diabetic wound healing. *Biomaterials,* 30**,** 1689-1696.
LIAO, I.-C., WAN, A. C., YIM, E. K. & LEONG, K. W. 2005. Controlled release from fibers of polyelectrolyte complexes. *Journal of Controlled Release,* 104**,** 347-358.
LIM, T. C., CHIAN, K. S. & LEONG, K. F. 2010. Cryogenic prototyping of chitosan scaffolds with controlled micro and macro architecture and their effect on in vivo neo-vascularization and cellular infiltration. *Journal of Biomedical Materials Research Part A,* 94**,** 1303-1311.
LIN-GIBSON, S., COOPER, J. A., LANDIS, F. A. & CICERONE, M. T. 2007. Systematic investigation of porogen size and content on scaffold morphometric parameters and properties. *Biomacromolecules,* 8**,** 1511-1518.
LIN, C.-C. & ANSETH, K. S. 2009. PEG hydrogels for the controlled release of biomolecules in regenerative medicine. *Pharmaceutical research,* 26**,** 631-643.
LIN, Y.-C., GRAHOVAC, T., OH, S. J., IERACI, M., RUBIN, J. P. & MARRA, K. G. 2013. Evaluation of a multi-layer adipose-derived stem cell sheet in a full-thickness wound healing model. *Acta Biomaterialia,* 9**,** 5243-5250.
LINDBLAD, W. J. 2008. Review Paper: Considerations for Determining if a Natural Product Is an Effective Wound-Healing Agent. *The international journal of lower extremity wounds,* 7**,** 75-81.

LIU, X., LIN, T., FANG, J., YAO, G., ZHAO, H., DODSON, M. & WANG, X. 2010. In vivo wound healing and antibacterial performances of electrospun nanofibre membranes. *Journal of biomedical materials research Part A,* 94**,** 499-508.
LOH, Q. L. & CHOONG, C. 2013. Three-dimensional scaffolds for tissue engineering applications: role of porosity and pore size. *Tissue Engineering Part B: Reviews,* 19**,** 485-502.
LÓPEZ, B. G.-C., SCHMIDT, E. M., EBERLIN, M. N. & SAWAYA, A. C. H. F. 2014. Phytochemical markers of different types of red propolis. *Food Chemistry,* 146**,** 174-180.
LOTFY, M. 2006. Biological activity of bee propolis in health and disease. *Asian Pac J Cancer Prev,* 7**,** 22-31.
LOWERY, J. L., DATTA, N. & RUTLEDGE, G. C. 2010. Effect of fiber diameter, pore size and seeding method on growth of human dermal fibroblasts in electrospun poly (ε-caprolactone) fibrous mats. *Biomaterials,* 31**,** 491-504.
LU, C., GUO, S. R., ZHANG, Y. & YIN, M. 2006. Synthesis and aggregation behavior of four types of different shaped PCL-PEG block copolymers. *Polymer international,* 55**,** 694-700.
LUO, C., STRIDE, E. & EDIRISINGHE, M. 2012. Mapping the influence of solubility and dielectric constant on electrospinning polycaprolactone solutions. *Macromolecules,* 45**,** 4669-4680.
MAEDA, T., KIMURA, C., TAKAHASHI, K. & ICHIMURA, K. 2014. Increase in skin perfusion pressure after maggot debridement therapy for critical limb ischaemia. *Clinical and experimental dermatology,* 39**,** 911-914.
MAENTHAISONG, R., CHAIYAKUNAPRUK, N., NIRUNTRAPORN, S. & KONGKAEW, C. 2007. The efficacy of aloe vera used for burn wound healing: A systematic review. *Burns,* 33**,** 713-718.
MAGHDOURI-WHITE, Y., BOWLIN, G. L., LEMMON, C. A. & DRÉAU, D. 2014. Mammary epithelial cell adhesion, viability, and infiltration on blended or coated silk fibroin–collagen type I electrospun scaffolds. *Materials Science and Engineering: C,* 43**,** 37-44.
MALAFAYA, P. B., SILVA, G. A. & REIS, R. L. 2007. Natural–origin polymers as carriers and scaffolds for biomolecules and cell delivery in tissue engineering applications. *Advanced drug delivery reviews,* 59**,** 207-233.
MANDAL, M. D. & MANDAL, S. 2011. Honey: its medicinal property and antibacterial activity. *Asian Pacific Journal of Tropical Biomedicine,* 1**,** 154-160.
MANO, J., SILVA, G., AZEVEDO, H. S., MALAFAYA, P., SOUSA, R., SILVA, S., BOESEL, L., OLIVEIRA, J. M., SANTOS, T. & MARQUES, A. 2007. Natural origin biodegradable systems in tissue engineering and regenerative medicine: present status and some moving trends. *Journal of the Royal Society Interface,* 4**,** 999-1030.
MARMUR, A. 2012. Hydro-hygro-oleo-omni-phobic? Terminology of wettability classification. *Soft Matter,* 8**,** 6867-6870.
MARTTILA, A. T., AIRENNE, K. J., LAITINEN, O. H., KULIK, T., BAYER, E. A., WILCHEK, M. & KULOMAA, M. S. 1998. Engineering of chicken avidin: a progressive series of reduced charge mutants. *FEBS Letters,* 441**,** 313-317.
MATEO, J. N., KULKARNI, S. S., DAS, L., BANDYOPADHYAY, S., TEPPER, G. C., WYNNE, K. J. & BANDYOPADHYAY, S. 2010. Wetting behavior of polymer coated nanoporous anodic alumina films: transition from super-hydrophilicity to super-hydrophobicity. *Nanotechnology,* 22**,** 035703.
MATSUMOTO, Y. & KUROYANAGI, Y. 2010. Development of a wound dressing composed of hyaluronic acid sponge containing arginine and epidermal growth factor. *Journal of Biomaterials Science, Polymer Edition,* 21**,** 715-726.
MCLENNAN, S., YUE, D. & TWIGG, S. 2006. Molecular aspects of wound healing in diabetes. *Primary Intention: The Australian Journal of Wound Management,* 14**,** 8.
MCLENNAN, S. V., BONNER, J., MILNE, S., LO, L., CHARLTON, A., KURUP, S., JIA, J., YUE, D. K. & TWIGG, S. M. 2008. The anti-inflammatory agent Propolis improves wound healing in a rodent model of experimental diabetes. *Wound Repair and Regeneration,* 16**,** 706-713.
MERRELL, J. G., MCLAUGHLIN, S. W., TIE, L., LAURENCIN, C. T., CHEN, A. F. & NAIR, L. S. 2009. Curcumin-loaded poly (ε-caprolactone) nanofibres: Diabetic wound dressing with anti-oxidant and anti-inflammatory properties. *Clinical and Experimental Pharmacology and Physiology,* 36**,** 1149-1156.

MESSERLI, S. M., AHN, M.-R., KUNIMASA, K., YANAGIHARA, M., TATEFUJI, T., HASHIMOTO, K., MAUTNER, V., UTO, Y., HORI, H. & KUMAZAWA, S. 2009. Artepillin C (ARC) in Brazilian green propolis selectively blocks oncogenic PAK1 signaling and suppresses the growth of NF tumors in mice. *Phytother Res,* 23**,** 423-427.

METCALFE, A. D. & FERGUSON, M. W. 2007. Tissue engineering of replacement skin: the crossroads of biomaterials, wound healing, embryonic development, stem cells and regeneration. *Journal of the Royal Society Interface,* 4**,** 413-437.

MILLERET, V., SIMONA, B., NEUENSCHWANDER, P. & HALL, H. 2011. Tuning electrospinning parameters for production of 3D-fiber-fleeces with increased porosity for soft tissue engineering applications. *Eur Cell Mater,* 21**,** 286-303.

MOHAMMADIAN, F. & EATEMADI, A. 2016. Drug loading and delivery using nanofibers scaffolds. *Artificial cells, nanomedicine, and biotechnology***,** 1-8.

MOLAN, P. C. 2006. The evidence supporting the use of honey as a wound dressing. *The International Journal of Lower Extremity Wounds,* 5**,** 40-54.

MOROZ, A. & DEFFUNE, E. 2013. Platelet-rich plasma and chronic wounds: remaining fibronectin may influence matrix remodeling and regeneration success. *Cytotherapy,* 15**,** 1436-1439.

MOURA, L. I., DIAS, A., CARVALHO, E. & DE SOUSA, H. C. 2013. Recent advances on the development of wound dressings for diabetic foot ulcer treatment—A review. *Acta biomaterialia,* 9**,** 7093-7114.

MOURA, L. I. F., DIAS, A. M. A., LEAL, E. C., CARVALHO, L., DE SOUSA, H. C. & CARVALHO, E. 2014. Chitosan-based dressings loaded with neurotensin—an efficient strategy to improve early diabetic wound healing. *Acta Biomaterialia,* 10**,** 843-857.

MOURA, S. A. L. D., FERREIRA, M. A. N. D., ANDRADE, S. P., REIS, M. L. C., NOVIELLO, M. D. L. & CARA, D. C. 2011. Brazilian green propolis inhibits inflammatory angiogenesis in a murine sponge model. *Evidence-Based Complementary and Alternative Medicine,* 2011.

MPHANDE, A., KILLOWE, C., PHALIRA, S., WYNN JONES, H. & HARRISON, W. 2007. Effects of honey and sugar dressings on wound healing. *Journal of wound care,* 16**,** 317-319.

MUMCUOGLU, K. 2012. The use of maggot debridement therapy in the treatment of chronic wounds in hospitalised and ambulatory patients. *J. Wound Care,* 21**,** 78-85.

MUNIR, M. M., SURYAMAS, A. B., ISKANDAR, F. & OKUYAMA, K. 2009. Scaling law on particle-to-fiber formation during electrospinning. *Polymer,* 50**,** 4935-4943.

NANJWADE, B., BECHRA, H., NANJWADE, V., DERKAR, G. & MANVI, F. 2011. Formulation and characterization of hydralazine hydrochloride biodegraded microspheres for intramuscular administration. *J. Bioanal. Biomed,* 3**,** 32-37.

NG, M. F. 2010. The role of mast cells in wound healing. *International wound journal,* 7**,** 55-61.

NISBET, D., YU, L., ZAHIR, T., FORSYTHE, J. S. & SHOICHET, M. 2008. Characterization of neural stem cells on electrospun poly (ε-caprolactone) submicron scaffolds: evaluating their potential in neural tissue engineering. *Journal of Biomaterials Science, Polymer Edition,* 19**,** 623-634.

NITANAN, T., AKKARAMONGKOLPORN, P., ROJANARATA, T., NGAWHIRUNPAT, T. & OPANASOPIT, P. 2013. Neomycin-loaded poly(styrene sulfonic acid-co-maleic acid) (PSSA-MA)/polyvinyl alcohol (PVA) ion exchange nanofibers for wound dressing materials. *International Journal of Pharmaceutics,* 448**,** 71-78.

NOVAK, E. M., SILVA, M. S. E. C., MARCUCCI, M. C., SAWAYA, A. C. H. F., GIMÉNEZ-CASSINA LÓPEZ, B., FORTES, M. A. H. Z., GIORGI, R. R., MARUMO, K. T., RODRIGUES, R. F. & MARIA, D. A. 2014. Antitumoural activity of Brazilian red propolis fraction enriched with xanthochymol and formononetin: An in vitro and in vivo study. *Journal of Functional Foods,* 11**,** 91-102.

NYAME, T. T., CHIANG, H. A. & ORGILL, D. P. 2014. Clinical Applications of Skin Substitutes. *Surgical Clinics of North America,* 94**,** 839-850.

OLCZYK, P., KOMOSINSKA-VASSEV, K., WINSZ-SZCZOTKA, K., STOJKO, J., KLIMEK, K. & KOZMA, E. M. 2013a. Propolis induces chondroitin/dermatan sulphate and hyaluronic acid accumulation in the skin of burned wound. *Evidence-Based Complementary and Alternative Medicine,* 2013.

OLCZYK, P., WISOWSKI, G., KOMOSINSKA-VASSEV, K., STOJKO, J., KLIMEK, K., OLCZYK, M. & KOZMA, E. M. 2013b. Propolis modifies collagen types I and III accumulation in the matrix of burnt tissue. *Evidence-Based Complementary and Alternative Medicine,* 2013.

OLIVEIRA, R. N., MCGUINNESS, G. B., RAMOS, M. E. T., KAJIYAMA, C. E. & THIRÉ, R. M. Properties of PVA Hydrogel Wound-Care Dressings Containing UK Propolis. Macromolecular Symposia, 2016. Wiley Online Library, 122-127.

ÖLSCHLÄGER, V., SCHRADER, A. & HOCKERTZ, S. 2009. Comparison of primary human fibroblasts and keratinocytes with immortalized cell lines regarding their sensitivity to sodium dodecyl sulfate in a neutral red uptake cytotoxicity assay. *Arzneimittelforschung,* 59**,** 146-152.

ORSI, R., FERNANDES, A., BANKOVA, V. & SFORCIN, J. 2012. The effects of Brazilian and Bulgarian propolis in vitro against Salmonella Typhi and their synergism with antibiotics acting on the ribosome. *Natural product research,* 26**,** 430-437.

ORYAN, A., NAEINI, A. T., NIKAHVAL, B. & GORJIAN, E. 2010. Effect of aqueous extract of Aloe vera on experimental cutaneous wound healing in rat. *Veterinarski arhiv,* 80**,** 509-522.

PANEVA, D., MESPOUILLE, L., MANOLOVA, N., DEGÉE, P., RASHKOV, I. & DUBOIS, P. 2006. Comprehensive study on the formation of polyelectrolyte complexes from (quaternized) poly [2-(dimethylamino) ethyl methacrylate] and poly (2-acrylamido-2-methylpropane sodium sulfonate). *Journal of Polymer Science Part A: Polymer Chemistry,* 44**,** 5468-5479.

PAPKOV, D., ZOU, Y., ANDALIB, M. N., GOPONENKO, A., CHENG, S. Z. & DZENIS, Y. A. 2013. Simultaneously strong and tough ultrafine continuous nanofibers. *ACS nano,* 7**,** 3324-3331.

PARENTE, L. M. L., JÚNIOR, L., DE SOUZA, R., TRESVENZOL, L. M. F., VINAUD, M. C., DE PAULA, J. R. & PAULO, N. M. 2012. Wound healing and anti-inflammatory effect in animal models of Calendula officinalis L. growing in Brazil. *Evidence-Based Complementary and Alternative Medicine,* 2012.

PAULINO, N., ABREU, S. R. L., UTO, Y., KOYAMA, D., NAGASAWA, H., HORI, H., DIRSCH, V. M., VOLLMAR, A. M., SCREMIN, A. & BRETZ, W. A. 2008. Anti-inflammatory effects of a bioavailable compound, Artepillin C, in Brazilian propolis. *European Journal of Pharmacology,* 587**,** 296-301.

PHAM, Q. P., SHARMA, U. & MIKOS, A. G. 2006. Electrospun poly (ε-caprolactone) microfiber and multilayer nanofiber/microfiber scaffolds: characterization of scaffolds and measurement of cellular infiltration. *Biomacromolecules,* 7**,** 2796-2805.

POPOVA, M. P., GRAIKOU, K., CHINOU, I. & BANKOVA, V. S. 2010. GC-MS profiling of diterpene compounds in Mediterranean propolis from Greece. *Journal of agricultural and food chemistry,* 58**,** 3167-3176.

POSNETT, J., GOTTRUP, F., LUNDGREN, H. & SAAL, G. 2009. The resource impact of wounds on health-care providers in Europe. *Journal of Wound care,* 18**,** 154.

POWELL, H. M. & BOYCE, S. T. 2009. Engineered human skin fabricated using electrospun collagen–PCL blends: morphogenesis and mechanical properties. *Tissue Engineering Part A,* 15**,** 2177-2187.

PRETE, P. E. 1997. Growth effects of Phaenicia sericata larval extracts on fibroblasts: mechanism for wound healing by maggot therapy. *Life sciences,* 60**,** 505-510.

PRITCHARD, D. I. & BROWN, A. P. 2015. Degradation of MSCRAMM target macromolecules in VLU slough by Lucilia sericata chymotrypsin 1 (ISP) persists in the presence of tissue gelatinase activity. *International wound journal,* 12**,** 414-421.

PUHL, S., LI, L., MEINEL, L. & GERMERSHAUS, O. 2014. Controlled protein delivery from electrospun non-wovens: novel combination of protein crystals and a biodegradable release matrix. *Molecular pharmaceutics,* 11**,** 2372-2380.

QI, Y. & CHILKOTI, A. 2015. Protein–polymer conjugation—moving beyond PEGylation. *Current Opinion in Chemical Biology,* 28**,** 181-193.

QIN, X. & WU, D. 2011. Effect of different solvents on poly (caprolactone)(PCL) electrospun nonwoven membranes. *Journal of thermal analysis and calorimetry,* 107**,** 1007-1013.

QIN, X. & WU, D. 2012. Effect of different solvents on poly (caprolactone)(PCL) electrospun nonwoven membranes. *Journal of thermal analysis and calorimetry,* 107**,** 1007-1013.
QIN, Y., WANG, H.-W., KARUPPANAPANDIAN, T. & KIM, W. 2010. Chitosan green tea polyphenol complex as a released control compound for wound healing. *Chinese Journal of Traumatology (English Edition),* 13**,** 91-95.
RAHMAN, C. V., BEN-DAVID, D., DHILLON, A., KUHN, G., GOULD, T. W., MÜLLER, R., ROSE, F. R., SHAKESHEFF, K. M. & LIVNE, E. 2014. Controlled release of BMP-2 from a sintered polymer scaffold enhances bone repair in a mouse calvarial defect model. *Journal of tissue engineering and regenerative medicine,* 8**,** 59-66.
REINKE, J. & SORG, H. 2012. Wound repair and regeneration. *European Surgical Research,* 49**,** 35-43.
RIGHI, A., NEGRI, G. & SALATINO, A. 2013. Comparative chemistry of propolis from eight brazilian localities. *Evidence-based Complementary and Alternative Medicine,* 2013.
RNJAK-KOVACINA, J. & WEISS, A. S. 2011. Increasing the pore size of electrospun scaffolds. *Tissue Engineering Part B: Reviews,* 17**,** 365-372.
RNJAK-KOVACINA, J., WISE, S. G., LI, Z., MAITZ, P. K. M., YOUNG, C. J., WANG, Y. & WEISS, A. S. 2011. Tailoring the porosity and pore size of electrospun synthetic human elastin scaffolds for dermal tissue engineering. *Biomaterials,* 32**,** 6729-6736.
ROŠIC, R., PELIPENKO, J., KOCBEK, P., BAUMGARTNER, S., BEŠTER-ROGAČ, M. & KRISTL, J. 2012. The role of rheology of polymer solutions in predicting nanofiber formation by electrospinning. *European Polymer Journal,* 48**,** 1374-1384.
RUSSO, A., CARDILE, V., SANCHEZ, F., TRONCOSO, N., VANELLA, A. & GARBARINO, J. 2004. Chilean propolis: antioxidant activity and antiproliferative action in human tumor cell lines. *Life sciences,* 76**,** 545-558.
SAHOO, S., ANG, L. T., GOH, J. C. H. & TOH, S. L. 2010. Growth factor delivery through electrospun nanofibers in scaffolds for tissue engineering applications. *Journal of biomedical materials research Part A,* 93**,** 1539-1550.
SAKTHIVEL, K. & GURUVAYOORAPPAN, C. 2013. Amentoflavone inhibits iNOS, COX-2 expression and modulates cytokine profile, NF-κB signal transduction pathways in rats with ulcerative colitis. *International immunopharmacology,* 17**,** 907-916.
SALMASO, S. & CALICETI, P. 2013. Self assembling nanocomposites for protein delivery: supramolecular interactions of soluble polymers with protein drugs. *International journal of pharmaceutics,* 440**,** 111-123.
SANDERS, L. M. & HENDREN, R. W. 1997. *Protein delivery: physical systems*, Springer Science & Business Media.
SANTOS, F. G., BONKOVOSKI, L. C., GARCIA, F. P., CELLET, T. S., WITT, M. A., NAKAMURA, C. V., RUBIRA, A. F. & MUNIZ, E. C. 2017. Antibacterial Performance of a PCL–PDMAEMA Blend Nanofiber-Based Scaffold Enhanced with Immobilized Silver Nanoparticles. *ACS Applied Materials & Interfaces,* 9**,** 9304-9314.
SARHAN, W. A. & AZZAZY, H. M. 2017. Apitherapeutics and phage-loaded nanofibers as wound dressings with enhanced wound healing and antibacterial activity.
SARKAR, A. & KELLOGG, G. E. 2010. Hydrophobicity-shake flasks, protein folding and drug discovery. *Current topics in medicinal chemistry,* 10**,** 67-83.
SAWAYA, A., DA SILVA CUNHA, I. B. & MARCUCCI, M. C. 2011. Analytical methods applied to diverse types of Brazilian propolis. *Chemistry Central Journal,* 5**,** 27.
SCHIFFMAN, J. D., WANG, Y., GIANNELIS, E. P. & ELIMELECH, M. 2011. Biocidal activity of plasma modified electrospun polysulfone mats functionalized with polyethyleneimine-capped silver nanoparticles. *Langmuir,* 27**,** 13159-13164.
SCHILLEMANS, J. P., VERHEYEN, E., BARENDREGT, A., HENNINK, W. E. & VAN NOSTRUM, C. F. 2011. Anionic and cationic dextran hydrogels for post-loading and release of proteins. *Journal of controlled release,* 150**,** 266-271.
SCHMIDTCHEN, A., WOLFF, H., RYDENGARD, V. & HANSSON, C. 2003. Detection of serine proteases secreted by Lucilia sericata in vitro and during treatment of a chronic leg ulcer. *Acta dermato-venereologica,* 83**,** 310-311.

SCHMITZ, M., EBERLEIN, T. & ANDRIESSEN, A. 2014. Wound treatment costs comparing a bio-cellulose dressing with moist wound healing dressings and conventional dressings. *Wound Medicine,* 6**,** 11-14.
SCHREML, S., SZEIMIES, R.-M., PRANTL, L., LANDTHALER, M. & BABILAS, P. 2010. Wound healing in the 21st century. *Journal of the American Academy of Dermatology,* 63**,** 866-881.
SEHN, E., HERNANDES, L., FRANCO, S., GONÇALVES, C. & BAESSO, M. 2009. Dynamics of reepithelialisation and penetration rate of a bee propolis formulation during cutaneous wounds healing. *Analytica Chimica Acta,* 635**,** 115-120.
SELL, S. A., WOLFE, P. S., GARG, K., MCCOOL, J. M., RODRIGUEZ, I. A. & BOWLIN, G. L. 2010. The use of natural polymers in tissue engineering: a focus on electrospun extracellular matrix analogues. *Polymers,* 2**,** 522-553.
SEN, C. K., GORDILLO, G. M., ROY, S., KIRSNER, R., LAMBERT, L., HUNT, T. K., GOTTRUP, F., GURTNER, G. C. & LONGAKER, M. T. 2009. Human skin wounds: a major and snowballing threat to public health and the economy. *Wound Repair and Regeneration,* 17**,** 763-771.
SEOL, Y.-J., KANG, T.-Y. & CHO, D.-W. 2012. Solid freeform fabrication technology applied to tissue engineering with various biomaterials. *Soft Matter,* 8**,** 1730-1735.
SERAFICA, G., MORMINO, R., OSTER, G. A., LENTZ, K. E. & KOEHLER, K. P. 2010. Microbial cellulose wound dressing for treating chronic wounds. Google Patents.
SHALUMON, K., CHENNAZHI, K., TAMURA, H., KAWAHARA, K., NAIR, S. & JAYAKUMAR, R. 2012. Fabrication of three-dimensional nano, micro and micro/nano scaffolds of porous poly (lactic acid) by electrospinning and comparison of cell infiltration by Z-stacking/three-dimensional projection technique. *IET nanobiotechnology,* 6**,** 16-25.
SHEIKH, F. A., JU, H. W., LEE, J. M., MOON, B. M., PARK, H. J., LEE, O. J., KIM, J.-H., KIM, D.-K. & PARK, C. H. 2014. 3D electrospun silk fibroin nanofibers for fabrication of artificial skin. *Nanomedicine: Nanotechnology, Biology and Medicine*.
SHENOY, S. L., BATES, W. D., FRISCH, H. L. & WNEK, G. E. 2005. Role of chain entanglements on fiber formation during electrospinning of polymer solutions: good solvent, non-specific polymer–polymer interaction limit. *Polymer,* 46**,** 3372-3384.
SHERMAN, R. A. 2014. Mechanisms of maggot-induced wound healing: what do we know, and where do we go from here? *Evidence-Based Complementary and Alternative Medicine,* 2014.
SHIMIZU, K., ASHIDA, H., MATSUURA, Y. & KANAZAWA, K. 2004. Antioxidative bioavailability of artepillin C in Brazilian propolis. *Archives of biochemistry and biophysics,* 424**,** 181-188.
SHIMIZU, K., DAS, S. K., HASHIMOTO, T., SOWA, Y., YOSHIDA, T., SAKAI, T., MATSUURA, Y. & KANAZAWA, K. 2005. Artepillin C in Brazilian propolis induces G0/G1 arrest via stimulation of Cip1/p21 expression in human colon cancer cells. *Molecular carcinogenesis,* 44**,** 293-299.
SILL, T. J. & VON RECUM, H. A. 2008. Electrospinning: applications in drug delivery and tissue engineering. *Biomaterials,* 29**,** 1989-2006.
SILVA, J. C., RODRIGUES, S., FEÁS, X. & ESTEVINHO, L. M. 2012. Antimicrobial activity, phenolic profile and role in the inflammation of propolis. *Food and Chemical Toxicology,* 50**,** 1790-1795.
SKÓRKOWSKA-TELICHOWSKA, K., CZEMPLIK, M., KULMA, A. & SZOPA, J. 2013. The local treatment and available dressings designed for chronic wounds. *Journal of the American Academy of Dermatology,* 68**,** e117-e126.
SKOTAK, M., RAGUSA, J., GONZALEZ, D. & SUBRAMANIAN, A. 2011. Improved cellular infiltration into nanofibrous electrospun cross-linked gelatin scaffolds templated with micrometer-sized polyethylene glycol fibers. *Biomedical Materials,* 6**,** 055012.
SMITH, A. G., POWIS, R. A., PRITCHARD, D. I. & BRITLAND, S. T. 2006. Greenbottle (Lucilia sericata) larval secretions delivered from a prototype hydrogel wound dressing accelerate the closure of model wounds. *Biotechnology progress,* 22**,** 1690-1696.
SOHRABI, S. & RUSSELL, D. 2014. Diabetic foot and foot debridement technique. *Surgery (Oxford),* 32**,** 491-495.

SOMBOONWONG, J., THANAMITTRAMANEE, S., JARIYAPONGSKUL, A. & PATUMRAJ, S. 2000. Therapeutic effects of Aloe vera on cutaneous microcirculation and wound healing in second degree burn model in rats. *Journal of the Medical Association of Thailand= Chotmaihet thangphaet,* 83**,** 417.

SOMERS, P., NARINE, K., DE SOMER, F., VOS, F. D. & V. NOOTEN, G. 2008. Sustained release and activation of the growth factor basic fibroblast growth factor from loaded scaffolds in heart valve tissue engineering. *Growth Factors,* 26**,** 293-299.

SONNEMANN, K. J. & BEMENT, W. M. 2011. Wound repair: toward understanding and integration of single-cell and multicellular wound responses. *Annual review of cell and developmental biology,* 27**,** 237-263.

SOUZA, E. A. D., INOUE, H. T., FERNANDES JÚNIOR, A., VEIGA, N. & ORSI, R. D. O. 2014. Influence of seasonality and production method on the antibacterial activity of propolis. *Acta Scientiarum. Animal Sciences,* 36**,** 49-53.

SRIKAR, R., YARIN, A. L., MEGARIDIS, C., BAZILEVSKY, A. & KELLEY, E. 2008. Desorption-limited mechanism of release from polymer nanofibers. *Langmuir,* 24**,** 965-974.

SUK CHOI, J. & SANG YOO, H. 2007. Electrospun nanofibers surface-modified with fluorescent proteins. *Journal of Bioactive and Compatible Polymers,* 22**,** 508-524.

SUMAN, K., RAO, V. K. & BHANUKIRAN, K. 2011. Study of rheological and mechanical properties of biodegradable polylactide and polycaprolactone blends. *International Journal of Engineering Science and Technology***,** 6259-6265.

SZENTIVANYI, A., CHAKRADEO, T., ZERNETSCH, H. & GLASMACHER, B. 2011. Electrospun cellular microenvironments: understanding controlled release and scaffold structure. *Advanced drug delivery reviews,* 63**,** 209-220.

TAFANI, M., SANSONE, L., LIMANA, F., ARCANGELI, T., DE SANTIS, E., POLESE, M., FINI, M. & RUSSO, M. A. 2016. The interplay of reactive oxygen species, hypoxia, inflammation, and sirtuins in cancer initiation and progression. *Oxidative medicine and cellular longevity,* 2016.

TAKZARE, N., HOSSEINI, M.-J., HASANZADEH, G., MORTAZAVI, H., TAKZARE, A. & HABIBI, P. 2009. Influence of Aloe vera gel on dermal wound healing process in rat. *Toxicology mechanisms and methods,* 19**,** 73-77.

TAM, S. K., DUSSEAULT, J., BILODEAU, S., LANGLOIS, G., HALLÉ, J. P. & YAHIA, L. H. 2011. Factors influencing alginate gel biocompatibility. *Journal of biomedical materials research Part A,* 98**,** 40-52.

TANAKA, A., NAGATE, T. & MATSUDA, H. 2005. Acceleration of wound healing by gelatin film dressings with epidermal growth factor. *The Journal of veterinary medical science/the Japanese Society of Veterinary Science,* 67**,** 909-913.

TECILAZICH, F., DINH, T. & VEVES, A. 2012. Role of Peripheral Neuropathy in the Development of Foot Ulceration and Impaired Wound Healing in Diabetes Mellitus. *IN Nutritional and Therapeutic Interventions for Diabetes and Metabolic Syndrome*.

TELFORD, G., BROWN, A., KIND, A., ENGLISH, J. & PRITCHARD, D. 2011. Maggot chymotrypsin I from Lucilia sericata is resistant to endogenous wound protease inhibitors. *British Journal of Dermatology,* 164**,** 192-196.

TELFORD, G., BROWN, A., SEABRA, R., HOROBIN, A., RICH, A., ENGLISH, J. & PRITCHARD, D. 2010. Degradation of eschar from venous leg ulcers using a recombinant chymotrypsin from Lucilia sericata. *British Journal of Dermatology,* 163**,** 523-531.

TENENHAUS, M., RENNEKAMPFF, H. & MULDER, G. 2016. Living cell products as wound healing biomaterials: current and future modalities. *Wound Healing Biomaterials-Volume 1: Therapies and Regeneration***,** 201.

TESFAYE, S. & SELVARAJAH, D. 2012. Advances in the epidemiology, pathogenesis and management of diabetic peripheral neuropathy. *Diabetes/metabolism research and reviews,* 28**,** 8-14.

TIWARI, S., PRATYUSH, D. D., GUPTA, S. K. & SINGH, S. K. 2014. Chapter 15 - Significance of Surgical Intervention in the Management of Diabetic Foot Infections. *In:* RAI, K. K. (ed.) *Microbiology for Surgical Infections.* Amsterdam: Academic Press.

TOMIZAWA, A., KANNO, S.-I., OSANAI, Y., GOTO, A., SATO, C., YOMOGIDA, S. & ISHIKAWA, M. 2013. Induction of apoptosis by a potent caffeic acid derivative, caffeic acid undecyl ester, is mediated by mitochondrial damage in NALM-6 human B cell leukemia cells. *Oncology reports,* 29**,** 425-429.

TONG, Z. & DENG, Y. 2013. The formation of asymmetric polystyrene/saponite composite nanoparticles via miniemulsion polymerization. *Journal of Applied Polymer Science,* 127**,** 3916-3922.
TORETI, V. C., SATO, H. H., PASTORE, G. M. & PARK, Y. K. 2013. Recent progress of propolis for its biological and chemical compositions and its botanical origin. *Evidence-Based Complementary and Alternative Medicine,* 2013.
TRAN, N. Q., JOUNG, Y. K., LIH, E. & PARK, K. D. 2011. In situ forming and rutin-releasing chitosan hydrogels as injectable dressings for dermal wound healing. *Biomacromolecules,* 12**,** 2872-2880.
TWINING, S. S. 1984. Fluorescein isothiocyanate-labeled casein assay for proteolytic enzymes. *Analytical biochemistry,* 143**,** 30-34.
UMTHONG, S., PHUWAPRAISIRISAN, P., PUTHONG, S. & CHANCHAO, C. 2011. In vitro antiproliferative activity of partially purified Trigona laeviceps propolis from Thailand on human cancer cell lines. *BMC complementary and alternative medicine,* 11**,** 37.
VALENTE, M. J., BALTAZAR, A. F., HENRIQUE, R., ESTEVINHO, L. & CARVALHO, M. 2011. Biological activities of Portuguese propolis: Protection against free radical-induced erythrocyte damage and inhibition of human renal cancer cell growth< i> in vitro</i>. *Food and Chemical Toxicology,* 49**,** 86-92.
VARDAR-ÜNLÜ, G., SILICI, S. & ÜNLÜ, M. 2008. Composition and in vitro antimicrobial activity of Populus buds and poplar-type propolis. *World Journal of Microbiology and Biotechnology,* 24**,** 1011-1017.
VELEIRINHO, B., REI, M. F. & LOPES-DA-SILVA, J. 2008. Solvent and concentration effects on the properties of electrospun poly (ethylene terephthalate) nanofiber mats. *Journal of Polymer Science Part B: Polymer Physics,* 46**,** 460-471.
VERBAAN, F., OUSSOREN, C., SNEL, C., CROMMELIN, D., HENNINK, W. & STORM, G. 2004. Steric stabilization of poly (2-(dimethylamino) ethyl methacrylate)-based polyplexes mediates prolonged circulation and tumor targeting in mice. *The journal of gene medicine,* 6**,** 64-75.
VERBELEN, J., HOEKSEMA, H., HEYNEMAN, A., PIRAYESH, A. & MONSTREY, S. 2014. Aquacel® Ag dressing versus Acticoat™ dressing in partial thickness burns: a prospective, randomized, controlled study in 100 patients. Part 1: Burn wound healing. *Burns,* 40**,** 416-427.
VIJAYKUMAR, H., PAI, S. A., PANDEY, V. & KAMBLE, P. 2011. Comparative study of collagenase and papain-urea based preparations in the management of chronic nonhealing limb ulcers. *Indian Journal of Science and Technology,* 4**,** 1096-1100.
VISAVADIA, B. G., HONEYSETT, J. & DANFORD, M. H. 2008. Manuka honey dressing: An effective treatment for chronic wound infections. *British Journal of Oral and Maxillofacial Surgery,* 46**,** 55-56.
WADHWA, R., NIGAM, N., BHARGAVA, P., DHANJAL, J. K., GOYAL, S., GROVER, A., SUNDAR, D., ISHIDA, Y., TERAO, K. & KAUL, S. C. 2016. Molecular Characterization and Enhancement of Anticancer Activity of Caffeic Acid Phenethyl Ester by γ Cyclodextrin. *Journal of Cancer,* 7**,** 1755.
WALKER, J. M. 2005. *The proteomics protocols handbook*, Springer.
WANG, K., XU, M., ZHU, M., SU, H., WANG, H., KONG, D. & WANG, L. 2013. Creation of macropores in electrospun silk fibroin scaffolds using sacrificial PEO-microparticles to enhance cellular infiltration. *Journal of Biomedical Materials Research Part A,* 101**,** 3474-3481.
WANG, K., ZHANG, J., PING, S., MA, Q., CHEN, X., XUAN, H., SHI, J., ZHANG, C. & HU, F. 2014a. Anti-inflammatory effects of ethanol extracts of Chinese propolis and buds from poplar (Populus×canadensis). *Journal of Ethnopharmacology,* 155**,** 300-311.
WANG, Y., CHANG, H.-I., LI, X., ALPAR, O. & COOMBES, A. G. 2009a. Delivery of bioactive macromolecules from microporous polymer matrices: release and activity profiles of lysozyme, collagenase and catalase. *European Journal of Pharmaceutical Sciences,* 37**,** 387-394.
WANG, Z.-G., WAN, L.-S., LIU, Z.-M., HUANG, X.-J. & XU, Z.-K. 2009b. Enzyme immobilization on electrospun polymer nanofibers: An overview. *Journal of Molecular Catalysis B: Enzymatic,* 56**,** 189-195.
WANG, Z., CUI, Y., WANG, J., YANG, X., WU, Y., WANG, K., GAO, X., LI, D., LI, Y. & ZHENG, X.-L. 2014b. The effect of thick fibers and large pores of electrospun

poly (ε-caprolactone) vascular grafts on macrophage polarization and arterial regeneration. *Biomaterials,* 35**,** 5700-5710.
WARNES, G. 2016. The Multiplexing of Assays for the Measurement of Early Stages of Apoptosis by Polychromatic Flow Cytometry.
WEI, Q., BECHERER, T., ANGIOLETTI-UBERTI, S., DZUBIELLA, J., WISCHKE, C., NEFFE, A. T., LENDLEIN, A., BALLAUFF, M. & HAAG, R. 2014. Protein interactions with polymer coatings and biomaterials. *Angewandte Chemie International Edition,* 53**,** 8004-8031.
WISE, S. G., YEO, G. C., HIOB, M. A., RNJAK-KOVACINA, J., KAPLAN, D. L., NG, M. K. & WEISS, A. S. 2014. Tropoelastin: a versatile, bioactive assembly module. *Acta biomaterialia,* 10**,** 1532-1541.
WONG, S.-C., BAJI, A. & LENG, S. 2008. Effect of fiber diameter on tensile properties of electrospun poly (ε-caprolactone). *Polymer,* 49**,** 4713-4722.
WU, J., ZHENG, Y., SONG, W., LUAN, J., WEN, X., WU, Z., CHEN, X., WANG, Q. & GUO, S. 2014. In situ synthesis of silver-nanoparticles/bacterial cellulose composites for slow-released antimicrobial wound dressing. *Carbohydrate Polymers,* 102**,** 762-771.
WU, Y., CHEN, L., SCOTT, P. G. & TREDGET, E. E. 2007. Mesenchymal stem cells enhance wound healing through differentiation and angiogenesis. *Stem cells,* 25**,** 2648-2659.
XU, D., LIU, C.-Y. & CRAIG, S. L. 2011. Divergent shear thinning and shear thickening behavior of supramolecular polymer networks in semidilute entangled polymer solutions. *Macromolecules,* 44**,** 2343.
YANG, F., WOLKE, J. G. C. & JANSEN, J. A. 2008. Biomimetic calcium phosphate coating on electrospun poly(ε-caprolactone) scaffolds for bone tissue engineering. *Chemical Engineering Journal,* 137**,** 154-161.
YANG, L., LI, J., JIN, Y., LI, M. & GU, Z. 2015. In vitro enzymatic degradation of the cross-linked poly (ε-caprolactone) implants. *Polymer Degradation and Stability,* 112**,** 10-19.
YOLANDA, M.-M., MARIA, A.-V., AMAIA, F.-G., MARCOS, P.-B., SILVIA, P. L., DOLORES, E. & JESÚS, O.-H. 2014. Adult Stem Cell Therapy in Chronic Wound Healing. *J Stem Cell Res Ther,* 4**,** 2.
YOO, H. S., KIM, T. G. & PARK, T. G. 2009. Surface-functionalized electrospun nanofibers for tissue engineering and drug delivery. *Advanced drug delivery reviews,* 61**,** 1033-1042.
YORK, A. W., KIRKLAND, S. E. & MCCORMICK, C. L. 2008. Advances in the synthesis of amphiphilic block copolymers via RAFT polymerization: Stimuli-responsive drug and gene delivery. *Advanced Drug Delivery Reviews,* 60**,** 1018-1036.
YOUSEFZADEH, M. & RAMAKRISHNA, S. 2016. * Amirkabir University of Technology, Tehran, Iran,† National University of Singapore, Singapore, Singapore. *Electrospun Nanofibers***,** 303.
YUAN, Y. & LEE, T. R. 2013. Contact angle and wetting properties. *Surface science techniques.* Springer.
YUN, B.-W., YAN, Z., AMIR, R., HONG, S., JIN, Y.-W., LEE, E.-K. & LOAKE, G. J. 2012. Plant natural products: history, limitations and the potential of cambial meristematic cells. *Biotechnology and Genetic Engineering Reviews,* 28**,** 47-60.
ZAISS, S., BROWN, T. D., REICHERT, J. C. & BERNER, A. 2016. Poly (ε-caprolactone) Scaffolds Fabricated by Melt Electrospinning for Bone Tissue Engineering. *Materials,* 9**,** 232.
ZAMANI, M., PRABHAKARAN, M. P. & RAMAKRISHNA, S. 2013. Advances in drug delivery via electrospun and electrosprayed nanomaterials. *International journal of nanomedicine,* 8**,** 2997.
ZANDER, N. E., ORLICKI, J. A., RAWLETT, A. M. & BEEBE JR, T. P. 2013. Electrospun polycaprolactone scaffolds with tailored porosity using two approaches for enhanced cellular infiltration. *Journal of Materials Science: Materials in Medicine,* 24**,** 179-187.
ZHANG, C., YUAN, X., WU, L., HAN, Y. & SHENG, J. 2005a. Study on morphology of electrospun poly (vinyl alcohol) mats. *European polymer journal,* 41**,** 423-432.
ZHANG, H. 2011. Effects of electrospinning parameters on morphology and diameter of electrospun PLGA/MWNTs fibers and cytocompatibility in vitro. *Journal of Bioactive and Compatible Polymers,* 26**,** 590-606.

ZHANG, Q., JIANG, Y., ZHANG, Y., YE, Z., TAN, W. & LANG, M. 2013. Effect of porosity on long-term degradation of poly (ε-caprolactone) scaffolds and their cellular response. *Polymer degradation and stability,* 98**,** 209-218.
ZHANG, T., OMAR, R., SIHERI, W., AL MUTAIRI, S., CLEMENTS, C., FEARNLEY, J., EDRADA-EBEL, R. & WATSON, D. 2014. Chromatographic analysis with different detectors in the chemical characterisation and dereplication of African propolis. *Talanta,* 120**,** 181-190.
ZHANG, X., MENG, L., LU, Q., FEI, Z. & DYSON, P. J. 2009. Targeted delivery and controlled release of doxorubicin to cancer cells using modified single wall carbon nanotubes. *Biomaterials,* 30**,** 6041-6047.
ZHANG, Y., OUYANG, H., LIM, C. T., RAMAKRISHNA, S. & HUANG, Z. M. 2005b. Electrospinning of gelatin fibers and gelatin/PCL composite fibrous scaffolds. *Journal of Biomedical Materials Research Part B: Applied Biomaterials,* 72**,** 156-165.
ZHAO, Y., TANAKA, M., KINOSHITA, T., HIGUCHI, M. & TAN, T. 2010. Self-assembling peptide nanofiber scaffolds for controlled release governed by gelator design and guest size. *Journal of Controlled Release,* 147**,** 392-399.
ZHONG, S., ZHANG, Y. & LIM, C. 2010. Tissue scaffolds for skin wound healing and dermal reconstruction. *Wiley Interdisciplinary Reviews: Nanomedicine and Nanobiotechnology,* 2**,** 510-525.
ZHU, X., CUI, W., LI, X. & JIN, Y. 2008. Electrospun fibrous mats with high porosity as potential scaffolds for skin tissue engineering. *Biomacromolecules,* 9**,** 1795-1801.
ZILBERMAN, M. & KRAITZER, A. 2008. Paclitaxel-eluting composite fibers: Drug release and tensile mechanical properties. *Journal of Biomedical Materials Research Part A,* 84**,** 313-323.

Appendix

APIS FLORA®

www.apisflora.com.br · 0800 94 04 800

Apis Flora Industrial e Comercial Ltda.
Laboratório de Controle de Qualidade
R: Triunfo, 945 • CEP: 14020 670
Ribeirão Preto • SP • Brasil
Tel.: 16 3514-4444

CERTIFICATE OF ANALYSIS

Product: 100% Water Soluble Extra-Green Propolis Powder
Code: 00905 **Manufacturing Date:** May, 2012
Batch Nº: 13990112 **Expiration Date:** May, 2015

Physical-Chemical Assay	Results	Specifications
Character	according	Brownish yellow or other colors, with a clear aromatic smell, bitter feeling, no impurities
Density	0.318	Informative
pH	8.47	7.5-8.5
Moisture	1.0	Max. 5.0% w/w
Solubility in Ethanol	71.1	Min. 70.0% w/w
Total flavonoids (as quercetin)	43.1	Min. 40 mg/g
Artepillin C	44.1	Min 30.0 mg/g
Total Phenol (as tannic acid)	167.4	Min. 170 mg/g

Microbiological Assay	Results	Specifications
cfu/g	< 10	≤ 1000 cfu/g
Mold	< 10	≤ 500 cfu/g
Yeast	< 10	≤ 500 cfu/g
Pathogenic bacteria *(Salmonella, Shigella, Staphyloccus aureus, Hemolityc streptococcus)*	according	Not found

Product approved by:

Quality Assurance
Aline Utino Higa - CRF-SP: 28.882

Responsible Pharmacist
Andresa A. Berretta - CRF-SP: 26.257

Store product closed, protected from light, heat and humidity

chemical characterization of Propolis Water soluble extract using HPLC methodology

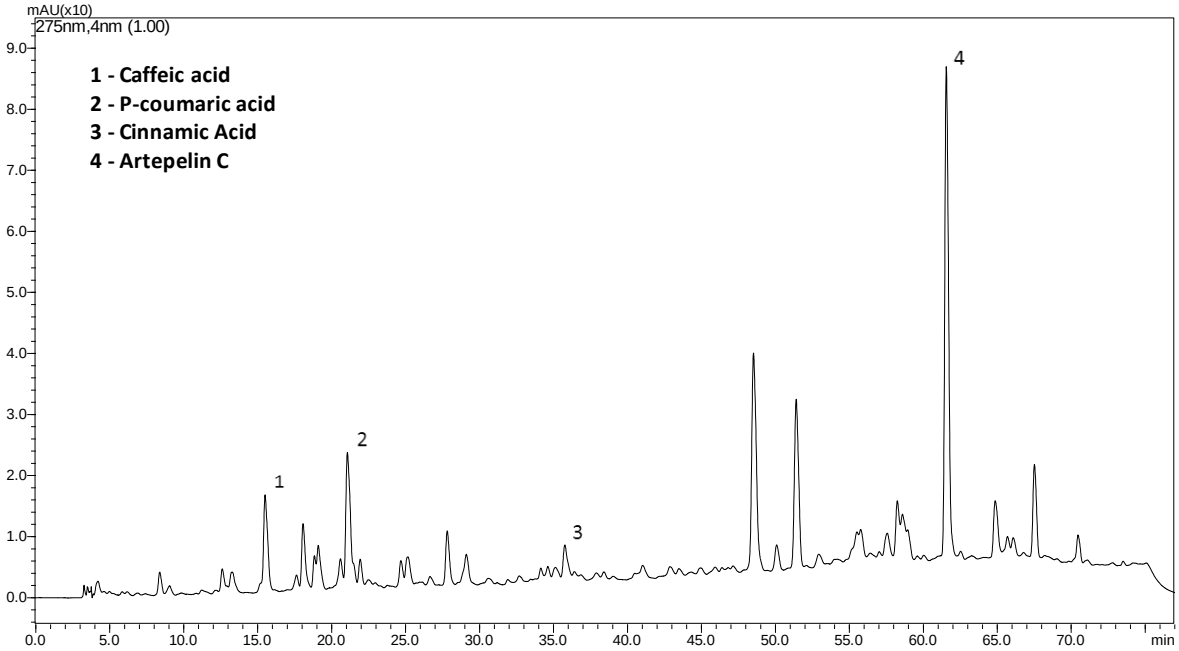


Figure 1 – Chromatography profile of Propolis Water Soluble Extract. (1) Caffeic acid; (2)p-coumaric acid; (3) cinnamic acid and (4) artepellin C. The chromatograms were plotted at 275 nm, using RP-HPLC, C18 (Shim-pack, CLC-ODS (M), 25 cm x 4.6) column and gradient elution with methanol and acidic water (formic acid pH=2.7).

Table a) Chemical characterization of Propolis Water Soluble Extract, using HPLC methodology according Berretta et al. (2012).

Compounds	**mg/g**
Caffeic acid	4.836
p-coumaric acid	4.476
Cinnamic acid	0.451
Artepellin C	44.078

Calibration curves for 3T3, GFP-3T3 and Bj6 cells

The graph shows a representative calibration curve for the range of cell densities (60,000 - 240,000 cells/mL). A linear relationship was observed between 60,000 cells/mL and 240,000 cell/mL where linear regression was equal (R^2 was 0.99).

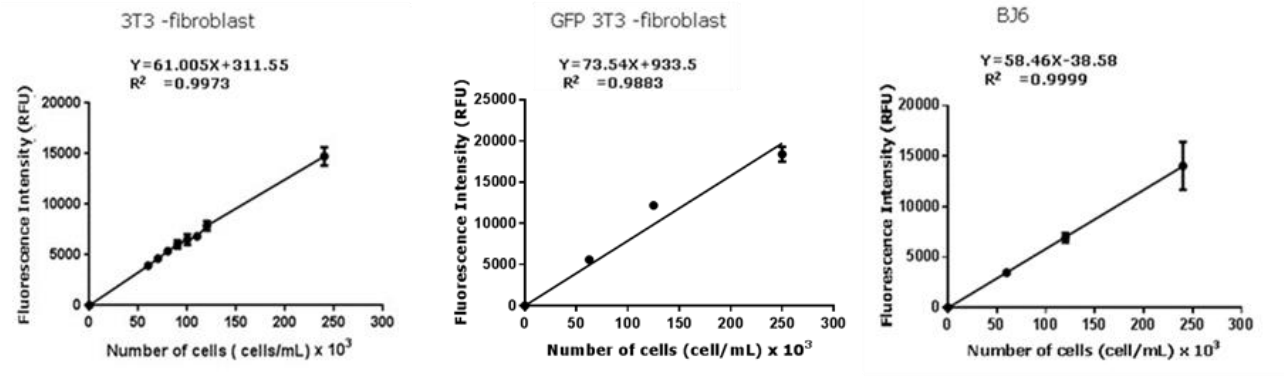
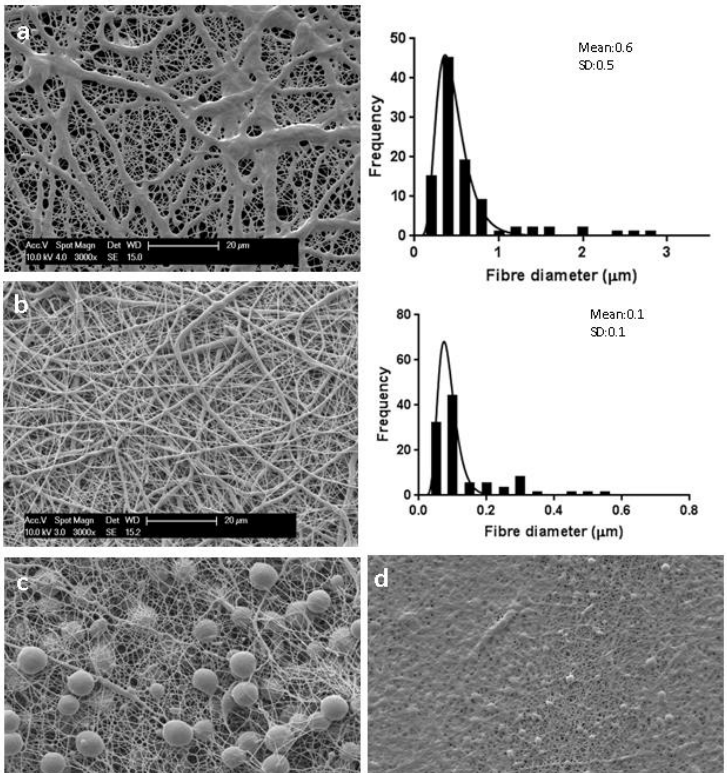


Figure Shows a representative calibration curve. Fluorescent intensity (nm) versus NHI-3T3 Fibroblast concentration (cells/mL) of a set of standard solution. Three independent experiments

Electrospinning of PCL-b-PEG polymers



Electrospinning of PCL-b-PEG polymers SEM micrographs (at x3000). Scale bar 20 µm and log –normal distribution of the size and frequency of their respective fibres

Electrospinning parameters for PCL-b-PEG scaffold production

PCL-PEG Concentration (w/w %)	PCL–PEG Molar mass.	Solvent	Collector distance (cm)	Voltage (kV)	Flow Rate (mL/h)	Motion (rpm)	Needle Inner diameter mm	Collector	Sample	Fibre diameter (mean±SD)
15	57.000	chloroform	17	12	2	50	0.6	RTC	Fig a	0.6±0.5
15	57.000	chloroform	20.5	20	2	50	0.6	RTC	Fig b	0.1±0.1
11	57.000	chloroform	20.5	14	2	2	0.6	RTC	Fig c	
15	57.000	DCM	17	25	0.8	50	0.6	RTC	Fig d	

Biological evaluation of electrospun fibre scaffolds of PCL-b PEG/PCL blends

Figure 5.4 reveals the metabolic activity of GFP expressing murine fibroblasts when cultured on PCL-b-PEG/PCL scaffolds. In general, fibroblasts on PCL-b-PEG/PCL 40:60 scaffolds showed, from an early stage, to exhibit greater metabolic activity than scaffolds made with a higher content of PCL-b-PEG (PCL-b-PEG/PCL ratios 50:50 and 60:40) and compared to PCL alone scaffolds (chapter 4). For this experiment, the fibre diameter of the tested scaffolds was maintained in the microscale, ranging between 2 and 3 μm. Since the PCL-b-PEG fibres had a diameter of 0.1±0.1 μm and were not uniform, these fibres were not tested further.

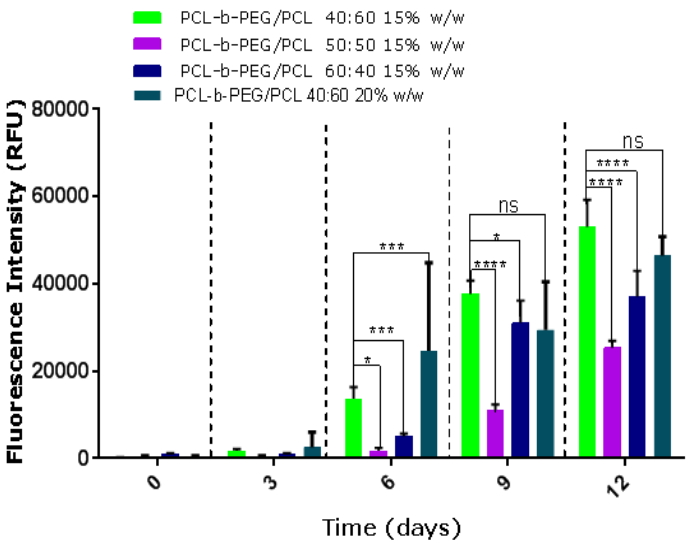


Figure - Fluorescence readings of metabolic activity of 3T3 GFP fibroblasts cultured on PCL-b-PEG/PCL scaffolds over 12 days. 3T3 metabolic activity was assessed using Alamar Blue®. Two way-ANOVA, Tukey's multiple comparison test. Three independent experiments carried out in triplicate (means±SD).

Statistical analysis of *L. sericata* maggot E/S, LYZ-Rho and AVi-FITC loading % on PCL, H-PCL and PCL-b-PEG/PCL scaffolds.

Tukey's multiple comparisons test	Mean Diff.	95.00% CI of diff.	Significant?	Summary	Adjusted P Value
30 min					
LZ PCL-PBS vs. LZ H-PCL-PBS	-6.787	-16.12 to 2.543	No	ns	0.3647
LZ PCL-PBS vs. LZ PCL-b-PEG/PCL PBS	-10.83	-20.16 to -1.496	Yes	**	0.0099
LZ PCL-PBS vs. AVI PCL- PBS	31.55	22.22 to 40.88	Yes	****	<0.0001
LZ PCL-PBS vs. AVI H-PCL PBS	30.4	21.07 to 39.73	Yes	****	<0.0001
LZ PCL-PBS vs. AVI PCL-b-PEG/PCL-PBS	25.67	16.34 to 35	Yes	****	<0.0001
LZ PCL-PBS vs. Maggot ES PCL	30.41	19.78 to 41.05	Yes	****	<0.0001
LZ PCL-PBS vs. Maggot ES H-PCL	30.29	19.65 to 40.93	Yes	****	<0.0001
LZ PCL-PBS vs. Maggot ES PCL-b-PEG/PCL	30.06	19.42 to 40.69	Yes	****	<0.0001
LZ H-PCL-PBS vs. LZ PCL-b-PEG/PCL PBS	-4.039	-13.37 to 5.291	No	ns	0.9158
LZ H-PCL-PBS vs. AVI PCL- PBS	38.34	29.01 to 47.67	Yes	****	<0.0001
LZ H-PCL-PBS vs. AVI H-PCL PBS	37.19	27.86 to 46.52	Yes	****	<0.0001
LZ H-PCL-PBS vs. AVI PCL-b-PEG/PCL-PBS	32.46	23.12 to 41.78	Yes	****	<0.0001
LZ H-PCL-PBS vs. Maggot ES PCL	37.2	26.56 to 47.84	Yes	****	<0.0001
LZ H-PCL-PBS vs. Maggot ES H-PCL	37.08	26.44 to 47.71	Yes	****	<0.0001
LZ H-PCL-PBS vs. Maggot ES PCL-b-PEG/PCL	36.84	26.21 to 47.48	Yes	****	<0.0001
LZ PCL-b-PEG/PCL PBS vs. AVI PCL- PBS	42.38	33.05 to 51.71	Yes	****	<0.0001
LZ PCL-b-PEG/PCL PBS vs. AVI H-PCL PBS	41.23	31.9 to 50.56	Yes	****	<0.0001
LZ PCL-b-PEG/PCL PBS vs. AVI PCL-b-PEG/PCL-PBS	36.49	27.16 to 45.82	Yes	****	<0.0001
LZ PCL-b-PEG/PCL PBS vs. Maggot ES PCL	41.24	30.6 to 51.88	Yes	****	<0.0001
LZ PCL-b-PEG/PCL PBS vs. Maggot ES H-PCL	41.12	30.48 to 51.75	Yes	****	<0.0001
LZ PCL-b-PEG/PCL PBS vs. Maggot ES PCL-b-PEG/PCL	40.88	30.24 to 51.52	Yes	****	<0.0001
AVI PCL- PBS vs. AVI H-PCL PBS	-1.151	-10.48 to 8.179	No	ns	>0.9999
AVI PCL- PBS vs. AVI PCL-b-PEG/PCL-PBS	-5.886	-15.22 to 3.443	No	ns	0.5681
AVI PCL- PBS vs. Maggot ES PCL	-1.14	-11.78 to 9.498	No	ns	>0.9999
AVI PCL- PBS vs. Maggot ES H-PCL	-1.264	-11.9 to 9.374	No	ns	>0.9999
AVI PCL- PBS vs. Maggot ES PCL-b-PEG/PCL	-1.498	-12.14 to 9.14	No	ns	>0.9999
AVI H-PCL PBS vs. AVI PCL-b-PEG/PCL-PBS	-4.736	-14.07 to 4.594	No	ns	0.8147
AVI H-PCL PBS vs. Maggot ES PCL	0.01102	-10.63 to 10.65	No	ns	>0.9999
AVI H-PCL PBS vs. Maggot ES H-PCL	-0.1132	-10.75 to 10.52	No	ns	>0.9999
AVI H-PCL PBS vs. Maggot ES PCL-b-PEG/PCL	-0.3469	-10.98 to 10.29	No	ns	>0.9999
AVI PCL-b-PEG/PCL-PBS vs. Maggot ES PCL	4.747	-5.891 to 15.38	No	ns	0.9013
AVI PCL-b-PEG/PCL-PBS vs. Maggot ES H-PCL	4.622	-6.015 to 15.26	No	ns	0.9142
AVI PCL-b-PEG/PCL-PBS vs. Maggot ES PCL-b-PEG/PCL	4.389	-6.249 to 15.03	No	ns	0.9353
Maggot ES PCL vs. Maggot ES H-PCL	-0.1242	-11.93 to 11.68	No	ns	>0.9999
Maggot ES PCL vs. Maggot ES PCL-b-PEG/PCL	-0.3579	-12.16 to 11.44	No	ns	>0.9999
Maggot ES H-PCL vs. Maggot ES PCL-b-PEG/PCL	-0.2337	-12.04 to 11.57	No	ns	>0.9999
6 h					
LZ PCL-PBS vs. LZ H-PCL-PBS	-16.77	-26.1 to -7.441	Yes	****	<0.0001
LZ PCL-PBS vs. LZ PCL-b-PEG/PCL PBS	-12.93	-22.26 to -3.599	Yes	***	0.0006
LZ PCL-PBS vs. AVI PCL- PBS	18.7	9.372 to 28.03	Yes	****	<0.0001
LZ PCL-PBS vs. AVI H-PCL PBS	18.11	8.784 to 27.44	Yes	****	<0.0001
LZ PCL-PBS vs. AVI PCL-b-PEG/PCL-PBS	14.46	5.127 to 23.79	Yes	****	<0.0001
LZ PCL-PBS vs. Maggot ES PCL	13.39	2.748 to 24.02	Yes	**	0.0032
LZ PCL-PBS vs. Maggot ES H-PCL	13.69	3.056 to 24.33	Yes	**	0.0023
LZ PCL-PBS vs. Maggot ES PCL-b-PEG/PCL	10.8	0.1615 to 21.44	Yes	*	0.0435
LZ H-PCL-PBS vs. LZ PCL-b-PEG/PCL PBS	3.843	-5.487 to 13.17	No	ns	0.9359
LZ H-PCL-PBS vs. AVI PCL- PBS	35.47	26.14 to 44.8	Yes	****	<0.0001
LZ H-PCL-PBS vs. AVI H-PCL PBS	34.89	25.56 to 44.21	Yes	****	<0.0001
LZ H-PCL-PBS vs. AVI PCL-b-PEG/PCL-PBS	31.23	21.9 to 40.56	Yes	****	<0.0001
LZ H-PCL-PBS vs. Maggot ES PCL	30.16	19.52 to 40.79	Yes	****	<0.0001
LZ H-PCL-PBS vs. Maggot ES H-PCL	30.47	19.83 to 41.1	Yes	****	<0.0001
LZ H-PCL-PBS vs. Maggot ES PCL-b-PEG/PCL	27.57	16.93 to 38.21	Yes	****	<0.0001
LZ PCL-b-PEG/PCL PBS vs. AVI PCL- PBS	31.63	22.3 to 40.96	Yes	****	<0.0001
LZ PCL-b-PEG/PCL PBS vs. AVI H-PCL PBS	31.04	21.71 to 40.37	Yes	****	<0.0001
LZ PCL-b-PEG/PCL PBS vs. AVI PCL-b-PEG/PCL-PBS	27.39	18.06 to 36.72	Yes	****	<0.0001
LZ PCL-b-PEG/PCL PBS vs. Maggot ES PCL	26.31	15.68 to 36.95	Yes	****	<0.0001
LZ PCL-b-PEG/PCL PBS vs. Maggot ES H-PCL	26.62	15.98 to 37.26	Yes	****	<0.0001
LZ PCL-b-PEG/PCL PBS vs. Maggot ES PCL-b-PEG/PCL	23.73	13.09 to 34.37	Yes	****	<0.0001
AVI PCL- PBS vs. AVI H-PCL PBS	-0.5882	-9.918 to 8.742	No	ns	>0.9999
AVI PCL- PBS vs. AVI PCL-b-PEG/PCL-PBS	-4.246	-13.58 to 5.085	No	ns	0.8908
AVI PCL- PBS vs. Maggot ES PCL	-5.316	-15.95 to 5.321	No	ns	0.8274
AVI PCL- PBS vs. Maggot ES H-PCL	-5.008	-15.65 to 5.63	No	ns	0.8703
AVI PCL- PBS vs. Maggot ES PCL-b-PEG/PCL	-7.903	-18.54 to 2.735	No	ns	0.3352
AVI H-PCL PBS vs. AVI PCL-b-PEG/PCL-PBS	-3.657	-12.99 to 5.673	No	ns	0.9516
AVI H-PCL PBS vs. Maggot ES PCL	-4.728	-15.37 to 5.91	No	ns	0.9033
AVI H-PCL PBS vs. Maggot ES H-PCL	-4.42	-15.06 to 6.218	No	ns	0.9327
AVI H-PCL PBS vs. Maggot ES PCL-b-PEG/PCL	-7.314	-17.95 to 3.323	No	ns	0.4456
AVI PCL-b-PEG/PCL-PBS vs. Maggot ES PCL	-1.071	-11.71 to 9.567	No	ns	>0.9999
AVI PCL-b-PEG/PCL-PBS vs. Maggot ES H-PCL	-0.7627	-11.4 to 9.875	No	ns	>0.9999
AVI PCL-b-PEG/PCL-PBS vs. Maggot ES PCL-b-PEG/PCL	-3.657	-14.29 to 6.981	No	ns	0.9780
Maggot ES PCL vs. Maggot ES H-PCL	0.3082	-11.49 to 12.11	No	ns	>0.9999
Maggot ES PCL vs. Maggot ES PCL-b-PEG/PCL	-2.586	-14.39 to 9.215	No	ns	0.9990
Maggot ES H-PCL vs. Maggot ES PCL-b-PEG/PCL	-2.894	-14.7 to 8.907	No	ns	0.9977

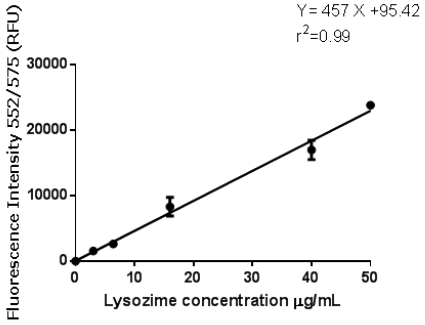
24 h

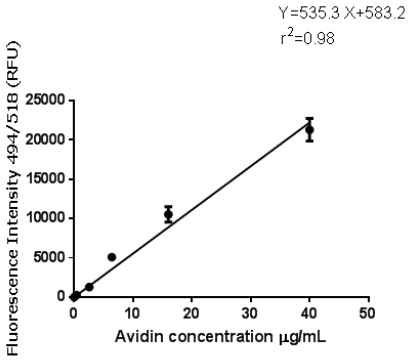
LZ PCL-PBS vs. LZ H-PCL-PBS	-14.27	-29.89 to 1.349	No	ns	0.1050
LZ PCL-PBS vs. LZ PCL-b-PEG/PCL PBS	3.48	-12.14 to 19.1	No	ns	0.9989
LZ PCL-PBS vs. AM PCL- PBS	37.94	22.32 to 53.56	Yes	****	<0.0001
LZ PCL-PBS vs. AM-H-PCL-PBS	40.04	24.43 to 55.66	Yes	****	<0.0001
LZ PCL-PBS vs. AM PCL-b-PEG/PCU-PBS	33.82	18.2 to 49.44	Yes	****	<0.0001
LZ PCL-PBS vs. MAggot ES PCL	31.99	14.18 to 49.8	Yes	****	<0.0001
LZ PCL-PBS vs. MAggot ES H-PCL	30.24	11.11 to 49.37	Yes	****	<0.0001
LZ PCL-PBS vs. Maggot ES PCL-b-PEG/PCL	27.68	9.87 to 45.48	Yes	****	<0.0001
LZ H-PCL-PBS vs. LZ PCL-b-PEG/PCL PBS	17.75	2.132 to 33.37	Yes	*	0.0128
LZ H-PCL-PBS vs. AM PCL- PBS	52.21	36.59 to 67.82	Yes	****	<0.0001
LZ H-PCL-PBS vs. AM-H-PCL-PBS	54.31	38.69 to 69.93	Yes	****	<0.0001
LZ H-PCL-PBS vs. AM PCL-b-PEG/PCU-PBS	48.09	32.47 to 63.7	Yes	****	<0.0001
LZ H-PCL-PBS vs. MAggot ES PCL	46.26	28.45 to 64.07	Yes	****	<0.0001
LZ H-PCL-PBS vs. MAggot ES H-PCL	44.51	25.38 to 63.63	Yes	****	<0.0001
LZ H-PCL-PBS vs. Maggot ES PCL-b-PEG/PCL	41.95	24.14 to 59.75	Yes	****	<0.0001
LZ PCL-b-PEG/PCL PBS vs. AM PCL- PBS	34.46	18.84 to 50.07	Yes	****	<0.0001
LZ PCL-b-PEG/PCL PBS vs. AM-H-PCL-PBS	36.56	20.95 to 52.18	Yes	****	<0.0001
LZ PCL-b-PEG/PCL PBS vs. AM PCL-b-PEG/PCU-PBS	30.34	14.72 to 45.96	Yes	****	<0.0001
LZ PCL-b-PEG/PCL PBS vs. MAggot ES PCL	28.51	10.7 to 46.32	Yes	****	<0.0001
LZ PCL-b-PEG/PCL PBS vs. MAggot ES H-PCL	26.76	7.63 to 45.89	Yes	***	0.0005
LZ PCL-b-PEG/PCL PBS vs. Maggot ES PCL-b-PEG/PCL	24.2	6.39 to 42	Yes	***	0.0009
AM PCL- PBS vs. AM-H-PCL-PBS	2.106	-13.51 to 17.72	No	ns	>0.9999
AM PCL- PBS vs. AM PCL-b-PEG/PCU-PBS	-4.119	-19.74 to 11.5	No	ns	0.9962
AM PCL- PBS vs. MAggot ES PCL	-5.946	-23.75 to 11.86	No	ns	0.9819
AM PCL- PBS vs. MAggot ES H-PCL	-7.7	-26.83 to 11.43	No	ns	0.9441
AM PCL- PBS vs. Maggot ES PCL-b-PEG/PCL	-10.26	-28.07 to 7.546	No	ns	0.6866
AM-H-PCL-PBS vs. AM PCL-b-PEG/PCU-PBS	-6.225	-21.84 to 9.392	No	ns	0.9472
AM-H-PCL-PBS vs. MAggot ES PCL	-8.052	-25.86 to 9.754	No	ns	0.8949
AM-H-PCL-PBS vs. MAggot ES H-PCL	-9.805	-28.93 to 9.322	No	ns	0.8072
AM-H-PCL-PBS vs. Maggot ES PCL-b-PEG/PCL	-12.37	-30.17 to 5.44	No	ns	0.4323
AM PCL-b-PEG/PCU-PBS vs. MAggot ES PCL	-1.827	-19.63 to 15.98	No	ns	>0.9999
AM PCL-b-PEG/PCU-PBS vs. MAggot ES H-PCL	-3.58	-22.71 to 15.55	No	ns	0.9997
AM PCL-b-PEG/PCU-PBS vs. Maggot ES PCL-b-PEG/PCL	-6.142	-23.95 to 11.66	No	ns	0.9778
MAggot ES PCL vs. MAggot ES H-PCL	-1.753	-22.71 to 19.2	No	ns	>0.9999
MAggot ES PCL vs. Maggot ES PCL-b-PEG/PCL	-4.315	-24.07 to 15.44	No	ns	0.9990
MAggot ES H-PCL vs. Maggot ES PCL-b-PEG/PCL	-2.561	-23.51 to 18.39	No	ns	>0.9999

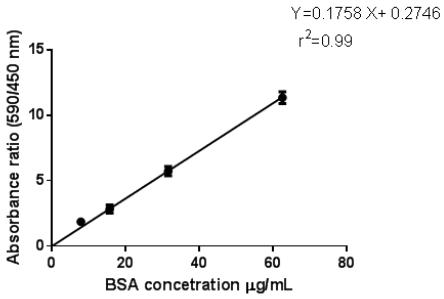
21 days

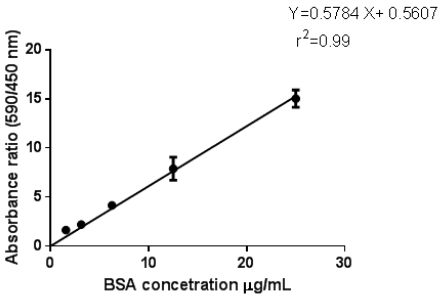
LZ PCL-PBS vs. LZ H-PCL-PBS	2.92	-12.7 to 18.54	No	ns	0.9997
LZ PCL-PBS vs. LZ PCL-b-PEG/PCL PBS	20.34	4.722 to 35.96	Yes	**	0.0018
LZ PCL-PBS vs. AM PCL- PBS	38.79	23.17 to 54.41	Yes	****	<0.0001
LZ PCL-PBS vs. AM-H-PCL-PBS	36.94	21.33 to 52.56	Yes	****	<0.0001
LZ PCL-PBS vs. AM PCL-b-PEG/PCU-PBS	25.53	9.908 to 41.14	Yes	****	<0.0001
LZ PCL-PBS vs. MAggot ES PCL	24.88	7.078 to 42.69	Yes	***	0.0005
LZ PCL-PBS vs. MAggot ES H-PCL	21.48	2.352 to 40.61	Yes	*	0.0148
LZ PCL-PBS vs. Maggot ES PCL-b-PEG/PCL	15.91	-1.899 to 33.71	No	ns	0.1231
LZ H-PCL-PBS vs. LZ PCL-b-PEG/PCL PBS	17.42	1.803 to 33.04	Yes	*	0.0160
LZ H-PCL-PBS vs. AM PCL- PBS	35.87	20.25 to 51.49	Yes	****	<0.0001
LZ H-PCL-PBS vs. AM-H-PCL-PBS	34.03	18.41 to 49.64	Yes	****	<0.0001
LZ H-PCL-PBS vs. AM PCL-b-PEG/PCU-PBS	22.61	6.988 to 38.22	Yes	***	0.0003
LZ H-PCL-PBS vs. MAggot ES PCL	21.96	4.158 to 39.77	Yes	**	0.0043
LZ H-PCL-PBS vs. MAggot ES H-PCL	18.56	-0.5673 to 37.69	No	ns	0.0652
LZ H-PCL-PBS vs. Maggot ES PCL-b-PEG/PCL	12.99	-4.818 to 30.79	No	ns	0.3619
LZ PCL-b-PEG/PCL PBS vs. AM PCL- PBS	18.45	2.831 to 34.07	Yes	**	0.0078
LZ PCL-b-PEG/PCL PBS vs. AM-H-PCL-PBS	16.61	0.9877 to 32.22	Yes	*	0.0274
LZ PCL-b-PEG/PCL PBS vs. AM PCL-b-PEG/PCU-PBS	5.185	-10.43 to 20.8	No	ns	0.9825
LZ PCL-b-PEG/PCL PBS vs. MAggot ES PCL	4.545	-13.26 to 22.35	No	ns	0.9970
LZ PCL-b-PEG/PCL PBS vs. MAggot ES H-PCL	1.14	-17.99 to 20.27	No	ns	>0.9999
LZ PCL-b-PEG/PCL PBS vs. Maggot ES PCL-b-PEG/PCL	-4.432	-22.24 to 13.37	No	ns	0.9975
AM PCL- PBS vs. AM-H-PCL-PBS	-1.844	-17.46 to 13.77	No	ns	>0.9999
AM PCL- PBS vs. AM PCL-b-PEG/PCU-PBS	-13.26	-28.88 to 2.354	No	ns	0.1709
AM PCL- PBS vs. MAggot ES PCL	-13.9	-31.71 to 3.902	No	ns	0.2692
AM PCL- PBS vs. MAggot ES H-PCL	-17.31	-36.44 to 1.818	No	ns	0.1125
AM PCL- PBS vs. Maggot ES PCL-b-PEG/PCL	-22.88	-40.69 to -5.074	Yes	**	0.0023
AM-H-PCL-PBS vs. AM PCL-b-PEG/PCU-PBS	-11.42	-27.04 to 4.198	No	ns	0.3584
AM-H-PCL-PBS vs. MAggot ES PCL	-12.06	-29.87 to 5.746	No	ns	0.4686
AM-H-PCL-PBS vs. MAggot ES H-PCL	-15.47	-34.59 to 3.662	No	ns	0.2259
AM-H-PCL-PBS vs. Maggot ES PCL-b-PEG/PCL	-21.04	-38.84 to -3.23	Yes	**	0.0078
AM PCL-b-PEG/PCU-PBS vs. MAggot ES PCL	-0.6406	-18.45 to 17.17	No	ns	>0.9999
AM PCL-b-PEG/PCU-PBS vs. MAggot ES H-PCL	-4.045	-23.17 to 15.08	No	ns	0.9992
AM PCL-b-PEG/PCU-PBS vs. Maggot ES PCL-b-PEG/PCL	-9.617	-27.42 to 8.19	No	ns	0.7581
MAggot ES PCL vs. MAggot ES H-PCL	-3.405	-24.36 to 17.55	No	ns	0.9999
MAggot ES PCL vs. Maggot ES PCL-b-PEG/PCL	-8.977	-28.73 to 10.78	No	ns	0.8923
MAggot ES H-PCL vs. Maggot ES PCL-b-PEG/PCL	-5.572	-26.52 to 15.38	No	ns	0.9960

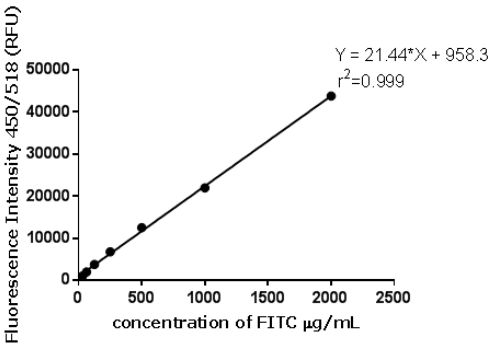
Calibration curves

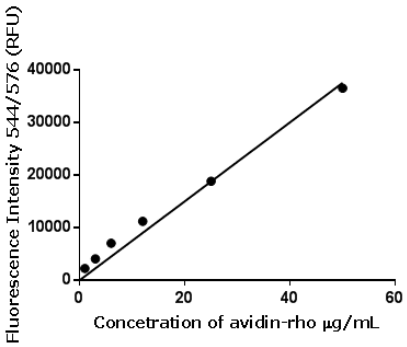






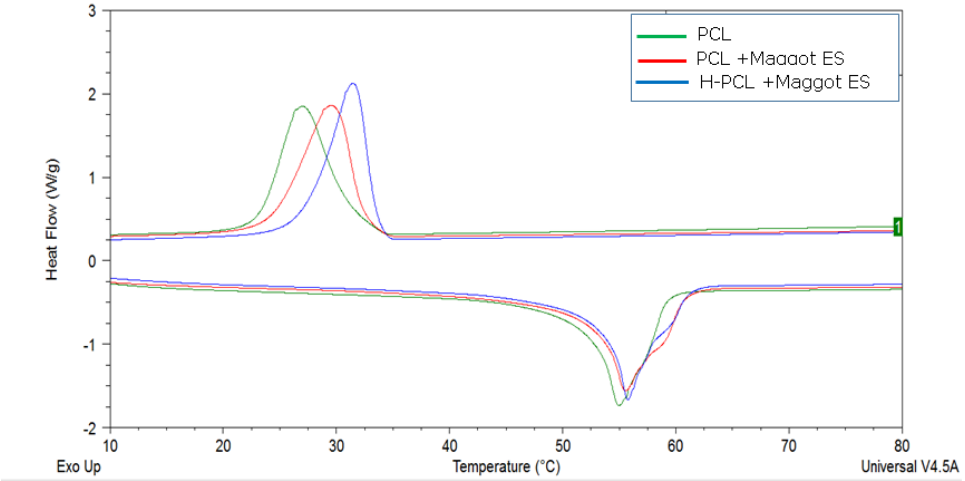




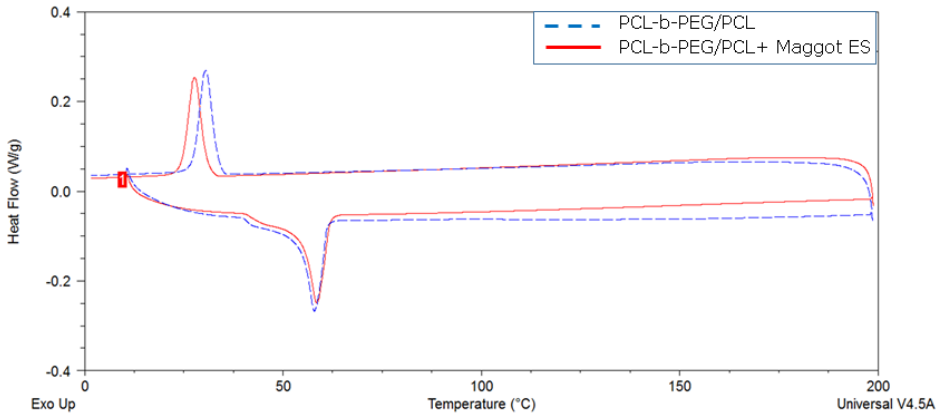


Y=685.3 X+2248
r^2=0.99

DSC thermograms of A) PCL electrospun scaffolds with and without *L. sericata* maggot E/S and B) PCL-b-PEG/PCL electrospun scaffolds with and without *L. sericata* maggot E/S.



Polymer	Tm(°C)	ΔHm(J/g)	Tc(°C)	ΔHc(J/g)
PCL	55.1	48.5	27.0	51.0
PCL+ES	55.6	54.9	29.5	53.3
H-PCL+ES	55.7	50.5	31.5	50.9



Polymer	Tm(°C)	ΔHm(J/g)	Tc(°C)	ΔHc(J/g)
PEG-b-PCL/PCL	54.2	61.0	30.5	59.0
PEG-b-PCL/PCL+ES	53.8	53.0	27.7	55.0

Legend:

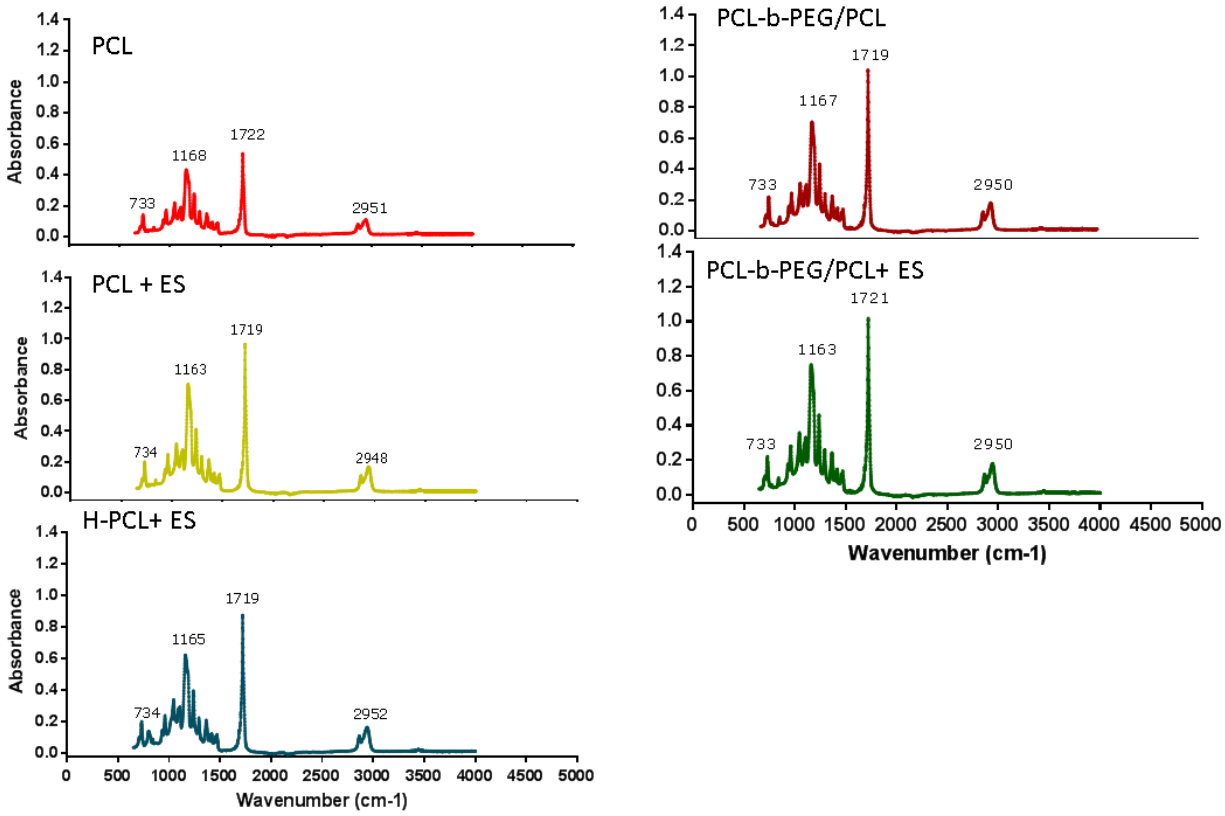
Tm (melting point)

Tc (crystallization point)

ΔHm (enthalpy of fusion)

ΔHc (enthalpy of crystallization)

Fourier-transform infrared spectra of PCL, H-PCL and PCL-b-PEG/PCL electrospun scaffolds coverage with L. sericata maggot E/S.



Amino acid sequences of lucifencin, chymiotrypsin and trypsin from maggot ES.

Lucifencin:

H_2N-Ala-Thr-Cys-Asp-Leu-Leu-Ser-Gly-Thr-Gly-Val-Lys-His-Ser-Ala-Cys-Ala-Ala-His-Cys-Leu-Leu-Arg-Gly-Asn-Arg-Gly-Gly-Tyr-Cys-Asn-Gly-Arg-Ala-Ile-Cys-Val-Cys-Arg-Asn-COOH. (Kozlowski, 2016).

Chymiotrpsin:

RITNGQDAVMGQFPYQVGLSLKLDNFKSSWCGGSLIGNEWVLTAAHCTDG
VKAVTVYLGATVRTQAEVKYTVKYTVKPSDILIHPGWNNKTLKNDISLVRIP
ETAYTALIQPVELPALASSYPSFAGDEVIASGWGRISDSVTGVTNYLQWARL
EVISNAACARTYGGTITTSSSNLCVKTPGGVSTCKGDSGGPLVLASSGVQV
GLTSFGSILGCEKGYPAAFTRVTSYLEWINEHTGISY. (Pritchard et al., 2016)

Trypsin:

RITNGELAKPGQFPYQAGLSLSLVFGNKGAWCGGTLISNRWVLTAAHCTDG
ADGVTVYLGATDIKNDNEKGQQRIYSSKANIVVHANWDASTLSNDISLIKL
PVAVEENELIQPATLPKMDGKISTLEGDMVVASGWGRDSDAATSVSQFLR
YIEVPVLKQSTCKTYYLGSVTDKMICIKSVDDKKSTCNGDSGGPLVYKDGG
VNYVIGATSFGIALGCEKGWPGVFTRVTSYLDWIEEEVSGVVNK.

(Pritchard et al., 2016).